

FINAL REPORT

Investigating Electrocatalytic and Catalytic Approaches for in situ
Treatment of Perfluoroalkyl Contaminants in Groundwater

SERDP Project ER-2424

FEBRUARY 2020

Charles Schaefer, Ph.D.
CDM Smith

Christopher Higgins
Timothy Strathmann
Colorado School of Mines

Lee Ferguson
Duke University

Christina Andaya
APTIM (formerly CB&I)

Distribution Statement A

This document has been cleared for public release



Page Intentionally Left Blank

This report was prepared under contract to the Department of Defense Strategic Environmental Research and Development Program (SERDP). The publication of this report does not indicate endorsement by the Department of Defense, nor should the contents be construed as reflecting the official policy or position of the Department of Defense. Reference herein to any specific commercial product, process, or service by trade name, trademark, manufacturer, or otherwise, does not necessarily constitute or imply its endorsement, recommendation, or favoring by the Department of Defense.

Page Intentionally Left Blank

REPORT DOCUMENTATION PAGE

Form Approved
OMB No. 0704-0188

Public reporting burden for this collection of information is estimated to average 1 hour per response, including the time for reviewing instructions, searching existing data sources, gathering and maintaining the data needed, and completing and reviewing this collection of information. Send comments regarding this burden estimate or any other aspect of this collection of information, including suggestions for reducing this burden to Department of Defense, Washington Headquarters Services, Directorate for Information Operations and Reports (0704-0188), 1215 Jefferson Davis Highway, Suite 1204, Arlington, VA 22202-4302. Respondents should be aware that notwithstanding any other provision of law, no person shall be subject to any penalty for failing to comply with a collection of information if it does not display a currently valid OMB control number. **PLEASE DO NOT RETURN YOUR FORM TO THE ABOVE ADDRESS.**

1. REPORT DATE (DD-MM-YYYY) 4-2-2020		2. REPORT TYPE SERDP Final Report		3. DATES COVERED (From - To) Sept. 2014 to Sept. 2019	
4. TITLE AND SUBTITLE Investigating Electrocatalytic and Catalytic Approaches for in situ Treatment of Perfluoroalkyl Contaminants in Groundwater				5a. CONTRACT NUMBER W912HQ-14-C-0058	
				5b. GRANT NUMBER N/A	
				5c. PROGRAM ELEMENT NUMBER N/A	
6. AUTHOR(S) Schaefer, Charles E., Ph.D. (CDM Smith) Higgins, Christopher P., Ph.D. (Colorado School of Mines) Strathmann, Timothy J., Ph.D. (Colorado School of Mines) Ferguson, P. Lee, Ph.D. (Duke University) Andaya, Christina (APTIM Federal Services)				5d. PROJECT NUMBER ER-2424	
				5e. TASK NUMBER N/A	
				5f. WORK UNIT NUMBER N/A	
7. PERFORMING ORGANIZATION NAME(S) AND ADDRESS(ES) APTIM Federal Services, LLC. 17 Princess Road Lawrenceville, NJ 08648				8. PERFORMING ORGANIZATION REPORT NUMBER ER-2424	
9. SPONSORING / MONITORING AGENCY NAME(S) AND ADDRESS(ES) Strategic Environmental Research and Development Program 4800 Mark Center Drive, Suite 17D03 Alexandria, VA 22350-3605				10. SPONSOR/MONITOR'S ACRONYM(S) SERDP	
				11. SPONSOR/MONITOR'S REPORT NUMBER(S) ER-2424	
12. DISTRIBUTION / AVAILABILITY STATEMENT Distribution Statement A: Approved for Public Release, Distribution is Unlimited					
13. SUPPLEMENTARY NOTES None					
14. ABSTRACT The overall goal of this research was to develop and assess oxidative electrocatalytic and reductive catalytic approaches for treatment of per- and polyfluoroalkyl substances (PFAS) associated with aqueous film-forming foams (AFFFs) in groundwater. Results of the electrochemical (EC) experiments showed that defluorination of perfluoroalkyl acids (PFAAs) PFAAs occurred in AFFF-impacted waters. and resulted in substantial defluorination. The generation of perchlorate, though treatable with subsequent biological reduction, was a notable unwanted reaction product. Results from Vitamin B12 catalyzed experiments showed that both a biogenic cobalt-corrin complex (B ₁₂) and an artificial cobalt-porphyrin complex (Co-PP) catalytically defluorinated multiple C-F bonds in branched PFAS, but were unreactive with linear PFAS structures. Results of the UV-sulfite experiments demonstrated that a wide range of PFAS in AFFF were transformed upon generation of hydrated electrons, but that apparent reaction rates were heavily dependent upon PFAS structure.					
15. SUBJECT TERMS Electrocatalytic, Catalytic Approaches, in situ Treatment, Perfluoroalkyl Contaminants, Groundwater					
16. SECURITY CLASSIFICATION OF:			17. LIMITATION OF ABSTRACT	18. NUMBER OF PAGES	19a. NAME OF RESPONSIBLE PERSON
a. REPORT	b. ABSTRACT	c. THIS PAGE			Dr. Charles Schaefer
U	U	U	UU	204	19b. TELEPHONE NUMBER (include area code) 732-590-4633

Page Intentionally Left Blank

Contents

LIST OF FIGURES	iii
LIST OF TABLES	vii
LIST OF ACRONYMS	viii
ABSTRACT	1
Objectives.....	1
Technical Approach	1
Results	1
Benefits	1
EXECUTIVE SUMMARY	2
1. OBJECTIVES	11
2. BACKGROUND	13
2.1 PFAS at DoD Facilities.....	13
2.2 PFAS Chemistry Sources.....	14
2.3 Treatment Challenges and Emerging Approaches.....	16
2.4 Electrochemical Oxidation.....	16
2.5 Vitamin B-12 Catalyzed Defluorination	17
2.6 UV-Sulfite.....	17
3. MATERIALS AND METHODS.....	19
3.1 Overall Approach and Rationale.....	19
3.2 Anode Screening	20
3.3 Electrochemical Experiments using Boron-Doped Diamond (BDD) Anodes.....	22
3.4 B-12 Catalyzed Reduction Sites	32
3.5 UV-Sulfite Treatment Studies.....	37
3.6 PFAS Analytical and Development of PFAS Libraries.....	48
4. RESULTS AND DISCUSSION.....	55
4.1 Screening of Commercially Available Anodes for Treatment of PFOA and PFOS.....	55
4.2 Electrochemical Experiments using Boron-Doped Diamond (BDD) Anodes.....	57
4.3 B12-Catalyzed Reduction	90
4.4 UV-Sulfite Reduction	98
4.5 PFAS Analytical Libraries	126
5. CONCLUSIONS AND IMPLICATIONS FOR FUTURE RESEARCH/IMPLEMENTATION.....	127
6. LITERATURE CITED	130
APPENDIX A: SUPPORTING DATA	139
APPENDIX B: LIST OF PUBLICATIONS	154

LIST OF FIGURES

Figure 1. Representative structures of PFAS present in AFFF and at AFFF-impacted sites	
Figure 2. Electrochemical treatment of PFOA in 1500 mg/L Na ₂ SO ₄ , and (when added) 167 mg/L NaCl	
Figure 3. Proposed transformation pathway based on electrochemical treatment of 3m AFFF.....	
Figure 4. Degradation of perfluoro-3,7-dimethyloctanoic acid and the corresponding defluorination data catalyzed by B12 and CoPP complexes	
Figure 5. Reaction timecourse data for UV-sulfite treatment of PFAS detected in AFFF by targeted analysis.....	
Figure 2.1. Representative structures of PFASs present in AFFF and at AFFF-impacted sites.....	
Figure 2.2. Spatial distribution of the total molar concentration of perfluorocarboxylates produced from precursors upon oxidation	
Figure 2.3. Structure of Vitamin B12, shown to catalyze defluorination of PFAS	
Figure 2.4. UV excitation of selected chemical sensitizers can generate strongly reducing hydrated electron, transient species that have been shown to degrade individual perfluoroalkyl carboxylates and sulfonates.....	
Figure 3.1. Experimental approach, segregated into Tasks	
Figure 3.2. Electrochemical system (electrochemical cell and electrodes from Advanced Diamond Technologies) used for evaluating PFOA and PFOS oxidation using BDD anodes	
Figure 3.3. Electrochemical system using the Microflow Cell with BDD anodes produced by Condias	
Figure 3.4. Representative IC chromatograms showing all peaks detected during the full elution period (70 min), and zoomed-in area (1.4–20.2 min) containing the F ⁻ peak at 8.9 min.....	
Figure 3.5. Extracted MS-detected ion chromatograms of analyte compounds and internal standard compounds	
Figure 3.6. Photograph of photoreactor setup with 18 W UV LP Hg lamp	
Figure 3.7. Example of I ₃ ⁻ generation during UV254 irradiation of the KI/KIO ₃ actinometer.....	
Figure 3.8. Example of the photolysis of H ₂ O ₂ throughout UV254 irradiation	
Figure 3.9. Comparison of sodium fluoride added and fluoride release measured	
Figure 3.10. ¹⁹ F NMR spectra for PFOA. The peak for the internal standard sodium trifluoroacetate is labeled for reference (NaCO ₂ CF ₃)	
Figure 3.11. ¹⁹ F NMR spectra for a AFFF diluted 1-to-5.....	
Figure 3.12. Screenshot of spectrum viewing and verification in SCIEX Explorer during acquisition process.....	

Figure 3.13. Screenshot of LibraryView spectrum entry for an example compound, 4:2 FTSO-PrAd-DiMePrS (4:2 fluorotelomer sulfinyl ethyl amide trimethyl sulfonic acid 1,1-dimethyl ethyl sulfonate)

Figure 3.14. Suspect screening workflow to identify XIC and HRMS Library matches in sample data acquired via QToF-MS SWATH®

Figure 4.1.1. PFOS removal during electrochemical treatment using a Ti/RuO₂ (Grade 1) anode.

Figure 4.1.2. Fluoride generation from 20 mg/L PFOA in an undivided EC cell using Ti/SnO₂-F anodes prepared at the commercial electrode facility.....

Figure 4.2.1. PFOA removal and fluoride generation versus time as a function of applied current density and with/without chloride present

Figure 4.2.2. PFOA and PFOS removal at 3 mA/cm² and 50 mA/cm² in chloride-containing electrolyte.....

Figure 4.2.3. Oxidant generation, measured via the DPD method, during the electrochemical experiments at different applied current densities, and in the presence of chloride (sodium sulfate present in all experiments)

Figure 4.2.4. Biological treatment system to treat perchlorate in electrochemically treated water. DAP = diammonium phosphate.....

Figure 4.2.5. Influent and effluent perchlorate concentrations to the biological treatment column.

Figure 4.2.6. Degradation rate constants for PFOA and chloride during electrochemical treatment in electrolyte (1500 mg/L Na₂SO₄, 167 mg/L NaCl) as a function of the applied current density.

Figure 4.2.7. Semi-quantitative HRMS analysis used to estimate the fluorine in the predominant precursor compounds in W1 and W2.....

Figure 4.2.8. Total oxidizable precursor (TOP) assay results for W1 and W2.....

Figure 4.2.9. PFAS removal during electrochemical oxidation in W1.....

Figure 4.2.10. PFAS formation followed by removal during electrochemical oxidation in W1.....

Figure 4.2.11. Fraction of the molar F concentration in the indicated PFAS relative to t=0 in PFCAs and PFSAs in W1 during electrochemical treatment.....

Figure 4.2.12. Oxidation pathway observed during electrochemical treatment of W1

Figure 4.2.13. PFAS removal during electrochemical oxidation in W2.....

Figure 4.2.14. PFAS formation followed by removal during electrochemical oxidation in W2.....

Figure 4.2.15. Proposed transformation pathway based on electrochemical treatment of W1

Figure 4.2.16. Fraction of the molar F concentration in the indicated PFAS relative to t=0 in PFCAs and PFSAs in W1 during electrochemical treatment.....

Figure 4.2.17. F generation as fluoride and in PFAAs during electrochemical treatment of W1 and W2.....

Figure 4.2.18. PFCAs and PFSAs concentrations relative to the initial PFAS concentration measured at the end of each 24-hour EC batch treatment time

Figure 4.2.19. Removal of PFAAs at Day 1 compared to Day 14

Figure 4.2.20. F removed as fluoride from PFAS.....

Figure 4.4.21. The decrease in the first order rate constant describing chloride removal (via electrochemical oxidation) relative to the chloride oxidation rate constant observed on day 1

Figure 4.2.22. Using groundwater W2, PFOA concentrations in a divided electrochemical cell using sequential cathodic-anodic treatment

Figure 4.2.23. Using groundwater W2, PFOS concentrations in a divided electrochemical cell using sequential cathodic-anodic treatment

Figure 4.2.24. Using groundwater synthetic groundwater spiked with 3M AFFF, perfluorinated carboxylate concentrations showed no indication of formation or removal during cathodic treatment, but did show indications of formation (from oxidation of PFAA precursors) during anodic treatment.....

Figure 4.2.25. Using groundwater synthetic groundwater spiked with 3M AFFF, perfluorinated sulfonate concentrations showed no indication of formation or removal during cathodic treatment, but did show indications of removal during anodic treatment.....

Figure 4.3.1. Defluorination of 1 under different conditions.....

Figure 4.3.2. Defluorination of 1 at room temperature ($21 \pm 2^\circ\text{C}$)

Figure 4.3.3. Degradation and defluorination for each PFAS with cobalt catalysts shown in (e) ...

Figure 4.3.4 Calculated bond dissociation energies (in kJ mol^{-1}) at B3LYP/6-311+G(2d,2p)/SMD level of theory (BDEs) of C–F bonds in the PFASs shown in Figure 2.....

Figure 4.3.5 Examples of branched PFASs detected in the environment.....

Figure 4.3.6 Change of individual C–F bond BDEs (in kJ mol^{-1}) upon the weakest C–F being replaced by a C–H

Figure 4.4.1. Reaction timecourses observed during UV-sulfite treatment of the targeted list PFAS within AFFF.....

Figure 4.4.2. Observed defluorination of PFAS within AFFF during UV-sulfite treatment.....

Figure 4.4.3. Influence of SO_3^{2-} concentration on fluoride release, PFAS degradation (%), and PFAS generation (C·C0-1) after reaction for 11 hours.....

Figure 4.4.2. “Bubble” plots of PFAS in AFFF before UV-sulfite treatment and after 49 h of UV-sulfite reaction.....

Figure 4.4.3. Degradation of the PFSA derivative FOSAA by UV-sulfite treatment, and formation of PFOS, PFOA, and perfluorooctane sulfonamide (FOSA)

Figure 4.4.4. Analysis of volatile reaction products during UV-sulfite treatment of AFFF solutions. (GC-MS/MS total ion chromatograms)

Figure 4.4.5. Changes in relative concentration of PFOS, PFH_xS , and PFOA measured in AFFF mixtures and in single-solute experiments. Observed pseudo first-order degradation rate constants (kobs)

Figure 4.4.6. Chromatogram for the PFOS analyte in untreated ($t = 0$ h) sample of UV-sulfite treatment of diluted AFFF

Figure 4.4.7. Observed rate constants for degradation of linear PFAS isomers: PFSAs, PFCAs, and FTSs in diluted AFFF during UV-sulfite treatment.....

Figure 4.4.8. First-order degradation rate constants for targeted PFAS measured in Ellsworth Air Force Base groundwater

Figure 4.4.9. Concentration of 6:2 FTCA during UV-sulfite treatment

Figure 4.4.10. First-order degradation rate constants for targeted PFAS measured in Peterson Air Force Base groundwater from well MW 1-8

Figure 4.4.11. First-order degradation rate constants for targeted PFAS measured in Peterson Air Force Base groundwater from well MW 2-3

Figure 4.4.12. First-order degradation rate constants for targeted PFAS measured in Fountain groundwater

Figure 4.4.13. Comparison of observed first-order degradation rate constants (k_{obs} , h⁻¹) for PFASs in Ellsworth Air Force base groundwater (EAFB), Fountain groundwater (FGW), and Peterson Air Force base groundwater from two wells (MW 1-8, MW 2-3)

Figure 4.4.14. First-order degradation rate constants of PFOS, PFHxS, and PFOA in matrices varying in complexity, including: Ellsworth Air Force Base groundwater (EAFB), Fountain groundwater (FGW), Peterson Air Force Base groundwaters from two wells (MW 1-8, MW 2-3), dilute AFFF experiments (AFFF), and single solute experiments.....

LIST OF TABLES

- Table 3.3.1. Characteristics of groundwater used for the initial PFOA/PFOS testing using boron-doped diamond anodes
- Table 3.3.2. Characteristics of the unfiltered groundwaters used for assessing treatment of a wide-range of PFASs using BDD anodes.
- Table 3.4.1. Information of PFASs and Co Species Used in this Study.
- Table 3.4.2. QTOF-MS parameters for the detection of analyte and internal standard compounds.
- Table 3.4.3. Summary of LC-QToF calibration regressions.
- Table 3.4.4. List of targeted compounds and mass-labeled internal standards used for PFAS analysis and quantification.
- Table 3.6.1. Examples of consistent structure names for XIC list.
- Table 3.6.2. Literature source and type of sample analyzed for HRMS Library additions
- Table 4.2.1. First order transformation rate constants determined during electrochemical testing of PFOA and PFOS using a BDD anode. PFHpS and PFHxS were present as low level impurities in the PFOS solution.
- Table 4.2.2. Current-normalized pseudo first order rate constants as defined by Eq. 2. \pm values indicate the 95% confidence intervals from duplicate experiments; R² values are provided in parenthesis. A rate constant for PFOA in W1 is not provided due to the observed transient increase in PFOA.
- Table 4.3. Applied energy and percentage removal of PFAAs in W1 and W2. For PFHxA, PFPeA, and PFBA in W1, concentrations at the end of the experiment were greater than at the beginning due to precursor transformations.
- Table 4.4.1. Measured concentrations of PFAS from the target analyte list of 44 compounds after dilution 1-to-60,000, and following application of the TOP assay.
- Table 4.4.2. PFAS detected by suspect screening analysis.
- Table 4.4.3 Optical properties of sulfite-containing solutions.
- Table 4.4.4. Results of UV-only control reaction.^a
- Table 4.4.5. Observed first-order degradation rate constants for PFAS on the target list.
- Table 4.4.6. Observed first-order degradation rate constants for PFAS on the suspect screening list.
- Table 4.4.7. Water quality parameters in filtered groundwater samples.
- Table 4.5.1. PFAS XIC list and HRMS library summary statistics

LIST OF ACRONYMS

AFB	Air Force Base
AFFF	aqueous film-forming foam
BDD	boron doped diamond (electrode)
BTEX	benzene, toluene, ethylbenzene, and xylenes
CE	Coulombic efficiency
CSM	Colorado School of Mines
DCE	<i>cis</i> -1,2-dichloroethene
DHC	<i>Dehalococcoides</i> sp.
DNAPL	dense non-aqueous phase liquid
DO	dissolved oxygen
DOC	dissolved organic carbon
DOM	dissolved organic matter
DoD	Department of Defense
e_{aq-}	hydrated electron
EDB	ethylene dibromide
EELS	electron energy loss spectroscopy
EPA	Environmental Protection Agency
ERSON	Environmental Restoration Statement of Need
ESTCP	Environmental Security Technology Certification Program
FID	flame ionization detector
ft bgs	feet below ground surface
FTOH	fluorotelomer alcohol
FTSA	fluorotelomer sulfonate
GC	gas chromatograph
GC-ECD	gas chromatography with electron capture detection
GC-FID	gas chromatography with flame ionization detection
GC-MS/MS	gas chromatography with tandem mass spectrometry detection
gpm	gallons per minute
HPLC	high-performance liquid chromatography
HRMS	high resolution mass spectrometry
IC	ion chromatography
ICP-AES	inductively coupled plasma-atomic emissions spectrophotometry
IPR	In-Progress Review

ISCO	<i>in situ</i> chemical oxidation
LC-QToF-MS	liquid chromatography with quantitative time-of-flight mass spectrometry detection
MMO	mixed metal oxide (electrode)
MNA	monitored natural attenuation
NAWC	Naval Air Warfare Center
NCBC	Naval Construction Battalion Center
NOD	natural oxidant demand
PCE	tetrachloroethene
PFAAs	perfluoroalkyl acids
PFASs	per- and polyfluoroalkyl substances
PFBA	perfluorobutanoic acid
PFBS	perfluorobutane sulfonate
PFCAs	perfluorocarboxylic acids
PFDoA	perfluorododecanoic acid
PFDS	perfluorodecane sulfonate
PFHpA	perfluoroheptanoic acid
PFHxA	perfluorohexanoic acid
PFHxS	perfluorohexane sulfonate
PFNA	perfluorononanoic acid
PFOA	perfluorooctanoic acid
PFOS	perfluorooctane sulfonate
PFOSA	perfluorooctane sulfonamide
PFPeA	perfluoropentanoic acid
PFSA	perfluoroalkyl sulfonic acids
PFTeA	perfluorotetradecanoic acid
PFTTrA	perfluorotridecanoic acid
PFUnA	perfluoroundecanoic acid
RPM	Remedial Project Manager
SEM-EDS	scanning electron microscopy with energy dispersive spectroscopy
SERDP	Strategic Environmental Research and Development Program
SGW	synthetic groundwater
SEM	scanning electron microscopy
SON	Statement of Need
TBA	tert-butyl alcohol
TCE	trichloroethene
TOC	total organic carbon
TDS	total dissolved solids
TN	total nitrogen analysis

TOP Assay	total oxidizable precursor assay
VC	vinyl chloride
VOC	volatile organic compound
VOCCs	volatile organic co-contaminants
XIC	extracted ion chromatogram
XPS	x-ray photoelectron spectroscopy
XRD	x-ray diffraction

Abstract

Introduction and Objectives

The overall goal of this research was to develop and assess oxidative electrocatalytic and reductive catalytic approaches for treatment of per- and polyfluoroalkyl substances (PFAS) associated with aqueous film-forming foams (AFFFs) in groundwater. Initial testing of the reductive approach indicated that treatment with supported metal catalysts were ineffective for defluorination of the perfluoroalkyl acids (PFAAs), thus the reductive approach was modified to focus on reduction via: (1) application of vitamin B12 and related cobalt complexes as homogeneous catalysts, and (2) application of UV-sulfite for generation of hydrated electrons (e_{aq}^-).

Technical Approach

Electrochemical (EC) experiments were performed using boron-doped diamond (BDD) anodes to assess the oxidation of both individual PFAAs and the wide range of potential PFAA precursors commonly found in AFFF. Experiments focused on identifying the extent of defluorination in both “fresh” AFFF solutions, and in groundwater collected from historically AFFF-impacted sites. Both target and suspect (including several classes of potential PFAA precursors) analyses, as well as fluoride generation, were used to evaluate results.

Reductive transformation of PFAS via cobalt complexes and hydrated electrons generated via the UV-sulfite process were performed in a series of batch experiments. Similar to the approach used for the EC experiments, treatment of individual PFAAs in simple electrolytes as well as treatment of a wider range of PFAS in AFFF-spiked solutions and AFFF-impacted groundwater were evaluated with respect to parent chemical degradation and extent of defluorination. The influences of PFAS structure and geochemical conditions on reaction rates was examined.

Results

Results of the EC experiments showed that defluorination of PFAAs occurred in AFFF-impacted waters. EC treatment of PFAA precursors showed an oxidation pathway that in some cases resulted in formation of PFAAs, but in all waters studied resulted in substantial defluorination. The generation of perchlorate, though treatable with subsequent biological reduction, was a notable unwanted reaction product. Results from Vitamin B12 catalyzed experiments showed that both a biogenic cobalt-corrin complex (B_{12}) and an artificial cobalt-porphyrin complex ($Co-PP$) catalytically defluorinate multiple C–F bonds in branched PFAS, but were unreactive with linear PFAS structures. Results of the UV-sulfite experiments demonstrated that a wide range of PFAS in AFFF were transformed upon generation of hydrated electrons, but that apparent reaction rates were heavily dependent upon PFAS structure. Analysis indicates that up to 50 percent of the organic fluorine in AFFF was liberated as fluoride ion during treatment. Finally, experiments demonstrated that the same PFAS present in contaminated groundwater obtained from DoD facilities can also be treated by UV-sulfite, with similar structure-reactivity trends observed among PFAS.

Benefits

Results from these studies have shown that both EC, B12, and UV-sulfite treatment can defluorinate a wide range of PFAS, and offer potential solutions to the DoD for AFFF-impacted waters. Additional longer-term and larger scale testing is recommended to further evaluate these technologies and demonstrate their potential effectiveness under field conditions.

Executive Summary

Introduction

PFAS Chemistry and Sources

Per- and polyfluoroalkyl substances (PFAS) include a wide range of fluorine-containing compounds. Of particular importance is the perfluorinated subclass of PFAS, referred to as perfluoroalkyl acids (PFAAs) which include perfluorocarboxylates and perfluorosulfonates (Figure 1). Under appropriate chemical or biological conditions, poly-fluorinated PFAS (i.e., not completely perfluorinated) can be converted to much more recalcitrant PFAAs, and thus are often referred to as PFAA precursors. Both PFAAs and PFAA precursors have been used in various formulations of AFFF used by the DoD for fire-fighting and fire training (Moody and Field, 1999; Moody et al., 2003; Place and Field, 2012). PFAAs are characterized by an alkane backbone, a terminal functional group, and fluorine atoms at all remaining available positions on the alkane backbone. Some PFAAs, particularly perfluorooctanoic acid (PFOA), are known to originate from the biodegradation of fluorotelomer-based precursors, some of which are present in AFFF (Place and Field, 2012).

While some attention has recently been focused on the remediation of PFAAs such as perfluorooctane sulfonate (PFOS) and PFOA, considerably less attention has been given to PFAA precursors. Evidence from our site investigation at Ellsworth AFB, which included analysis of PFAA in soil and groundwater as well as direct measurement of specific PFAA precursors and oxidizable PFAA precursors (measured through the formation of perfluorocarboxylates in the laboratory using persulfate; Houtz and Sedlak, 2012), suggests that *in situ*

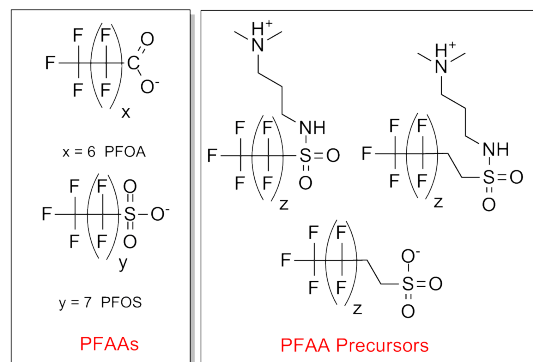


Figure 1. Representative structures of PFAS present in AFFF and at AFFF-impacted sites.

transformation of PFAA precursors to PFAAs is likely, and may be facilitated by processes such as air biosparging (McGuire et al., 2014). In our investigation of the site, samples collected from locations outside the zone of influence of these remedial activities showed much higher levels of PFAA precursors. *With respect to remediation, these data suggest that any in situ treatment for PFAAs must also be capable of treating the PFAA precursors, as these chemicals may be an important source of PFAAs at AFFF-impacted sites.*

Electrochemical Oxidation

An alternative and particularly promising approach for treatment of PFOS, PFOA, and other PFAS is via electrocatalytic oxidation at mixed metal oxide (MMO) or boron-doped diamond (BDD) anodes (Carter and Farrell, 2008; Ochiai et al., 2011, Zhuo et al., 2011). Of particular note are the results of Zhou et al. (2011), who demonstrated the use of MMO on titanium anodes for treatment of PFOA in electrolyte solution. These reactions occur via an initial step of direct electron transfer

at the anode; electrochemically generated oxidants may also facilitate the oxidation of fluorinated daughter products or precursor compounds. The generation of oxidants provides added benefit, as these oxidants (i.e., hydroxyl radical, chlorine) can be effective for removal of hydrocarbon or chlorinated solvent co-contaminants that often are co-mingled with PFASs, such as the plume observed during our investigation at Ellsworth AFB. When using BDD anodes, substantial quantities of perchlorate were also formed from chloride present in the groundwater being treated.

Reductive Catalytic and Photocatalytic Treatment

As highly halogenated chemicals, PFAS may also be subject to reductive transformation in the presence of suitably strong reducing agents or catalysts. Recently, Ochoa-Herrera *et al.* observed >70% fluoride ion (F^-) release from a mixture of branched PFOS isomers by reaction with Vitamin B₁₂ (a corrin-Co^{III} complex, catalyst precursor) and Ti^{III} citrate (reductant) (Ochoa-Herrera *et al.*, 2008). While B12 is a naturally occurring enzyme co-factor, this finding also suggests a strategy for synthetic catalysts based upon Co-corrin complexes that may be effective in promoting reductive transformation of PFAS. A second approach to achieve reductive transformation of PFAS involved UV generation of strongly reducing hydrated electrons (e_{aq}^- , NHE = -2.9 V), which have been shown to be effective in degrading individual PFAA structures, including PFOS and PFOA (Buxton *et al.*, 1988; Gu *et al.*, 2017, 2016; Herbert and Coons, 2017; Park *et al.*, 2011, 2009; Qu *et al.*, 2016, 2010; Song *et al.*, 2013). These short-lived reactive species can be generated via UV excitation of an appropriate sensitizer species (e.g., iodide, 3-indole acetic acid, nitrilotriacetic acid, sulfite) (Park *et al.*, 2009; Song *et al.*, 2013; Sun *et al.*, 2018; Tian *et al.*, 2016). Here, we focus on use of sulfite. While the UV-sulfite process has been demonstrated to be effective in transforming individual PFAS compounds, the efficacy of this process for treatment of the broader range of PFAS mixtures present in AFFF-impacted waters is unknown. Most importantly, little is known about the effectiveness of UV-sulfite treatment for structures beyond the PFCAs and PFSA for which reference standards are available to quantify directly.

Objectives

The overall goal of this research was to develop and assess the use of electrocatalytic and catalytic/photocatalytic approaches for treatment of PFAS in groundwater. For this effort, our focus was initially on two parallel treatment approaches that rely on catalytic metals. The first approach relied on the use of mixed metal oxide (MMO) and boron-doped diamond (BDD) anodes for the catalytic oxidation of PFAS in electrochemical (EC) systems. The second approach involved the use of supported rhodium (Rh)-based catalysts to facilitate reductive hydrodefluorination of PFAS; this second approach had potential for treatment as a permeable reactive barrier, or as an *in situ* source area treatment technology. Initial testing of this second reductive approach indicated that treatment would not be effective, so the reductive approach was modified to focus on two approaches that showed early promise for reductive transformation of PFAS: (1) application of B12 and related cobalt corrin complexes as homogeneous catalysts, and (2) application of UV-sulfite for generation of hydrated electrons (e_{aq}^-). Thus, this study focused on PFAS treatment via:

1. Electrochemical oxidation
2. Reduction using B12-catalyzed reaction
3. Reduction using the UV-sulfite process

To attain the overall project goal, the following specific objectives were developed:

- Measure the degradation kinetics of representative PFASs during EC oxidation treatment and B12-catalyzed and UV-sulfite reductive treatment processes;
- Identify PFAS transformation products and elucidate the controlling reaction mechanisms;
- Determine the optimal anode formulations for treatment;
- Determine the influence of current density on electrochemical treatment performance;
- Evaluate the impacts of co-contaminants and groundwater geochemistry on treatment effectiveness and anode longevity;
- Demonstrate that the wide range of PFAS, including perfluoroalkyl acid precursors, can be effectively treated using the proposed strategies; and
- Evaluate the overall potential for treatment using both the oxidative and reductive technologies.

Technical Approach

Electrochemical Oxidation Experiments

Electrochemical oxidation experiments were performed using a small bench-scale system. Various commercially available anode materials were evaluated (i.e., MMO and BDD anodes from multiple vendors) and both undivided and divided cell configurations were evaluated. Experiments were performed over a range of applied current densities in both simple electrolytes (e.g., sodium sulfate, sodium chloride) and in natural groundwater. In addition, both individual PFAA compounds were evaluated, as well as complex PFAS mixtures associated with AFFF-impacted groundwaters and diluted 3M AFFF solutions. PFAS treatment was evaluated with respect to transformation of suspected PFAA precursors (when present), removal of PFAAs, fluoride generation, and overall energy demand. Generation of perchlorate, as well as the ability to subsequently biologically reduce the generated perchlorate, was also evaluated as part of this study.

Reductive Catalytic and UV Photocatalytic Treatment Experiments

Experiments evaluating PFAS reduction catalyzed by B12 and structurally related corrin complexes were conducted in batch experiments performed under strict anaerobic conditions in a glovebox environment. Replicate batch reactors were prepared with individual perfluorocarboxylate structures together with cobalt catalyst, bulk reducing agent (Ti^{III} -citrate), and pH buffer. Reactions were monitored for a period of 15 days, monitoring both fluoride ion release (by ion chromatography) and degradation of the parent PFAS structures (by high resolution LC-QToF-MS analysis). Experimental results were complemented with Density Functional Theory (DFT) to calculate molecular descriptors that would be predictive of PFAS reactivity with the cobalt complexes.

UV-sulfite treatment experiments were performed using a quartz immersion well photoreactor incorporating an 18 W low pressure Hg UV lamp that irradiates at 254 nm. Sodium sulfite was provided as a UV sensitizer to generate hydrated electrons (e_{aq}^-) upon irradiation. Solution pH was typically buffered at 9.5 using 5 mM NaHCO_3 . Experiments examined the treatment of individual PFAA structures (PFOS, PFOA, PFHXS), treatment of AFFF diluted in pH buffered solution (typically diluted 1-to-60,000 fold to mimic groundwater PFAS concentrations), and treatment of AFFF-impacted groundwater collected from DoD facilities. High resolution LC-QToF-MS analysis was used to monitor degradation of individual PFAS in the different mixtures. In selected experiments, fluoride ion release was monitored using ion selective electrode measurements. UV-only and dark control reactions were included to verify that transformation results principally from UV generation of hydrated electrons. Experiments also examined reactivity of suspected precursors that generate PFAAs as reaction byproducts during treatment.

Results & Discussion

Electrochemical Oxidation Experiments

Initial electrode screening experiments indicated that BDD anodes, as opposed to a wide variety of MMO anodes, were the most effective for treating PFOS and PFOA. Subsequent experiments showed that substantial removal and defluorination of PFOA (Figure 2) and PFOS occurred, and overall treatment was a function of the applied current density. Treatment in electrolyte was similar to that observed in natural groundwater. Although substantial generation of perchlorate and chlorate occurred due to the oxidation of chloride, subsequent biotic treatment (via addition of electron donor) facilitated the reductive treatment of the electrochemically generated perchlorate.

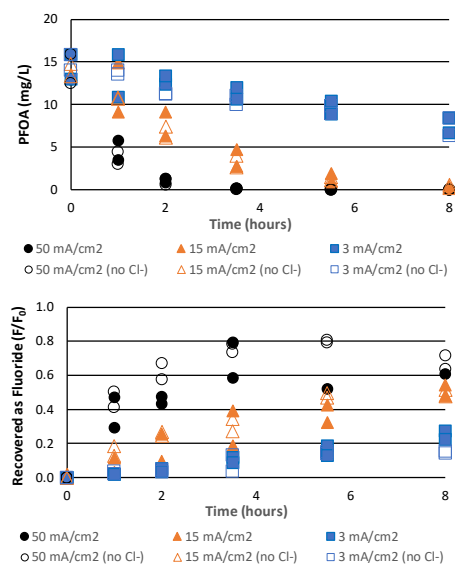


Figure 2. Electrochemical treatment of PFOA in 1500 mg/L Na_2SO_4 , and (when added) 167 mg/L NaCl .

Additional EC experiments using 3M AFFF-spiked water provided insight into the complex oxidation pathway for the suspected PFAA precursors (Figure 3).

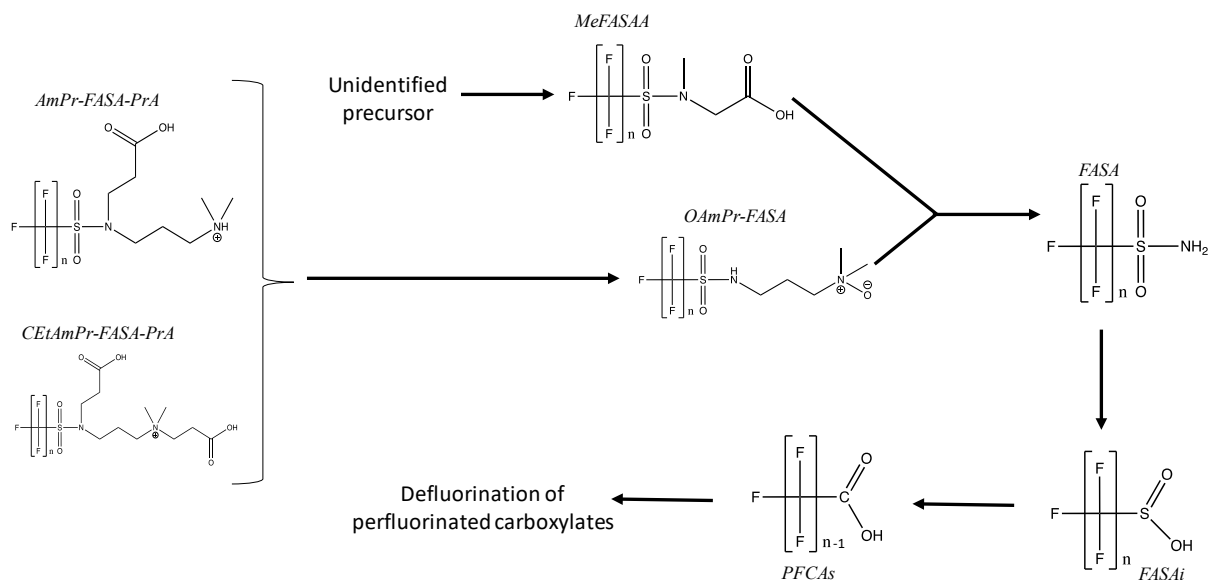


Figure 3. Proposed transformation pathway based on electrochemical treatment of 3m AFFF. Solid lines point to compounds that showed a transient increase during electrochemical treatment.

Interestingly, the oxidation pathway observed in historically AFFF-impacted groundwater did not result in the transient generation of PFAAs as observed in Figure 3, despite the fact that abundant PFAA precursors were present and the fact that fluoride generation indicated that substantial defluorination of precursors occurred. These results highlight the complexity of understanding oxidation pathways and fluorine mass balances when performing EC oxidation on AFFF-impacted waters.

B12-Catalyzed Reduction

Experiments demonstrated reductive transformation of branched PFAS catalyzed by B12 and structurally related cobalt-corrin complexes (Figure 4). Experimental results and theoretical calculations revealed correlations between the extent of PFAS defluorination, the local C–F bonding environment, and calculated bond dissociation energies (BDEs). In general, BDEs for tertiary C–F bonds < secondary C–F bonds < primary C–F bonds. A tertiary C–F bond adjacent to three fluorinated carbons (or two fluorinated carbons and one carboxyl group) had a relatively low BDE that permits an initial defluorination to occur. Neither B12 or CoPP complexes induced significant defluorination in linear perfluorooctanoic acid (PFOA; no tertiary C–F bond) or a perfluoroalkyl ether carboxylic acid (tertiary C–F BDEs too high). Thus, the current complexes have limited utility in treating legacy mixtures of PFAS that are predominantly linear in nature. That said, these results do open new lines of research, including (1) designing branched PFAS and cobalt complexes

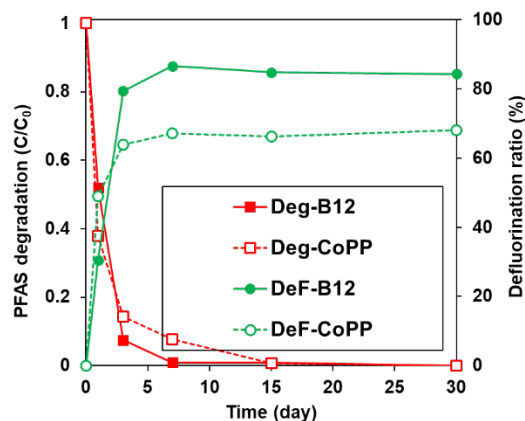


Figure 4. Degradation of perfluoro-3,7-dimethyloctanoic acid and the corresponding defluorination data catalyzed by B12 and CoPP complexes. Reaction conditions: PFAS (0.1 mM), Co catalyst (0.25 mM), Ti^{III} citrate (~36 mM), and carbonate buffer (~40 mM) pH 9.0; 70°C.

that promote complete defluorination in natural and engineered systems, and (2) evaluating potential impacts of branched PFAS in biological systems where B₁₂ is present.

Reductive Treatment by UV-Sulfite

Here, UV-sulfite treatment was applied to an AFFF mixture diluted in buffered electrolyte matrix to characterize reactions between hydrated electrons (e_{aq}^-) and different PFAS structures (>40) identified by high resolution LC-QTOF-MS analysis. Results of these experiments show that individual PFAA structures (PFOS, PFOA, and PFHXS) present in the AFFF mixture are degraded at measured reaction rates similar to rates measured in individual-solute experiments, validating that the rate constants we measured for diverse structures in the AFFF mixture are representative of rates that would occur in isolation. Results show that PFAS reactivity varies widely among PFAS structures present in AFFF. Whereas some structures, including perfluoroalkyl carboxylic acids (PFCAs) like PFOA, long-chain perfluoroalkyl sulfonates (PFSAs) like PFOS and some precursor species of PFAAs are readily broken down upon UV sulfite treatment, some other structures, most notably the short-chain PFSAs like perfluorobutane sulfonate and fluorotelomer acid species (FTAs) are much less reactive during UV-sulfite treatment (Figure 5). These trends are consistent with results from fluoride release measurements where the extent of fluoride ion release from the PFAS was incomplete (up to 53% of the F content of the AFFF during reactions).

In addition, temporal data indicates that selected PFSA, PFCAs, and FTAs can form as intermediates or stable end-products due to UV-sulfite treatment of PFAA precursors. Thus, these results indicate that while treatment with UV-sulfite can be effective for treating PFOS and PFOA down to the USEPA's recently release lifetime HALs, remediation of the wider diversity of PFAS identified at DOD sites will be more challenging. UV-sulfite treatment experiments were also conducted with AFFF-impacted groundwater collected from DoD facilities. Results of this work confirms successful PFAS treatment in a variety of groundwater matrices. Rates of individual PFAS destruction in groundwater are similar or greater than those observed in lab-spiked solutions, suggesting promise for remedial applications. Structure-reactivity trends also reveal mechanistic insights that can be applied to predict reactivity with a wider range of potential undiscovered PFAS structures.

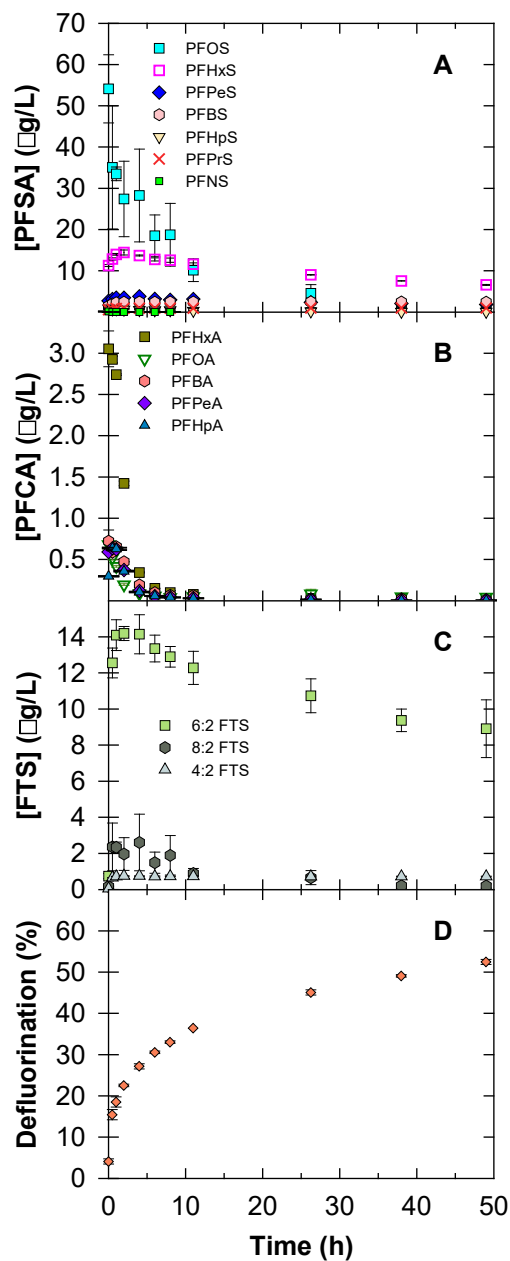


Figure 5. Reaction timecourse data for UV-sulfite treatment of PFAS detected in AFFF by targeted analysis. (A) PFOS and related PFSA, (B) PFOA and related PFCAs, and (C) FTSs. Panel (D) Shows the percent of total fluorine released as F^- during treatment with UV-sulfite. Reaction conditions: AFFF (1-to-60,000 dilution), 10 mM Na_2SO_3 , 5 mM NaHCO_3 ($\text{pH}_0 = 9.5$).

Implications for Future Research and Benefits

Together, results from the EC oxidation, B12, and UV-sulfite studies suggest that these technologies show promise, but have challenges, for remedial application. EC oxidation is

effective for the wide range of PFAS typically present in AFFF formulations, even in the presence of other organic contaminants. However, substantial energy is expended related to the oxidation of suspected PFAA precursors. Approaches to develop more energy efficient and cost-effective approaches for these initial oxidation steps would likely benefit the EC approach. In addition, BDD anodes are expensive compared to other anodes typically used in the industry, so development of more inexpensive anodes, or methods to increase the effective surface area of BDD anodes, are likely needed to promote widespread application of this technology. Finally, perchlorate generation is problematic from both a Coulombic efficiency perspective, as well as a health/regulatory perspective. While applications in the absence of chloride (e.g., treatment of PFAS in chloride-free ion exchange regeneration solutions) may provide an excellent opportunity for EC oxidation of PFASs, methods to effectively eliminate this problematic reaction or to readily reduce the perchlorate once formed (e.g., via biotic treatment) require further demonstration

UV-sulfite treatment is effective for some classes of PFAS, but others, most notably short-chain sulfonic acid and fluorotelomer acid structures, are found to be unreactive with hydrated electrons. Fortunately, short chain analogues that appear most recalcitrant are also considered to pose much less health risks than long-chain analogues. Still, this process is much more effective than the more commonly applied persulfate-based oxidation technologies that are only effective at oxidizing perfluorocarboxylic acid structures and PFAA precursors. One potential strategy worth investigating in the future is a sequential persulfate-UV-sulfite treatment where a wide range of PFAA precursors can first be oxidized to perfluorocarboxylate structures, which should then be amenable to rapid reduction by UV-sulfite treatment (results presented here show that perfluorocarboxylates are highly reactive regardless of chain length. Like EC treatment, UV-sulfite treatment with conventional low pressure Hg lamps is energy intensive, likely limiting applications to concentrate stream management applications. That said, the technology will also benefit from ongoing research into more efficient light sources (e.g., UV LEDs) that direct a larger fraction of input energy to UV photons (and not lost as heat) and identification of sensitizers that produce hydrated electrons with greater quantum efficiencies (i.e., fraction of UV photons resulting in generation of hydrated electrons).

1.0 Objectives

This SERDP Proposal was submitted in response to the SERDP Statement of Need ERSON-14-02 that addressed the need to develop cost-effective remediation approaches for poly- and perfluoroalkyl substances (PFAS) in groundwater. Perfluorooctane sulfonate (PFOS) and perfluorooctanoic acid (PFOA) were noted as compounds of particular importance.

The overall goal of this research was to develop and assess the use of electrocatalytic and catalytic approaches for treatment of PFAS in groundwater. For this effort, our focus was initially on two parallel treatment approaches that rely on catalytic metals. The first approach relied on the use of mixed metal oxide (MMO) and boron-doped diamond (BDD) anodes for the catalytic oxidation of PFAS in electrochemical (EC) systems. The second approach involved the use of supported Rh-based catalysts to facilitate reductive hydrodefluorination of PFASs; this second approach had potential for treatment as a permeable reactive barrier, or as an *in situ* source area treatment technology. Initial testing of this second reductive approach indicated that treatment would not be effective, so the reductive approach was modified to focus on two approaches that showed early promise for reductive transformation of PFAS: (1) application of B12 and related cobalt corrin complexes as homogeneous catalysts, and (2) application of UV-sulfite for generation of hydrated electrons (e_{aq}^-). Thus, this study focused on PFAS treatment via:

1. Electrochemical oxidation
2. Reduction using B12-catalyzed reaction
3. Reduction using the UV-sulfite process

To attain the overall project goal, the following specific objectives were developed:

- Measure the degradation kinetics of representative PFAS during EC oxidation and B12-catalyzed and UV-sulfite reductive treatment;
- Identify PFAS transformation products and elucidate the controlling reaction mechanisms;
- Determine the optimal anode formulations for treatment;
- Determine the influence of current density on electrochemical treatment performance;
- Evaluate the impacts of co-contaminants and groundwater geochemistry on treatment effectiveness and anode longevity;
- Demonstrate that the wide range of PFAS, including perfluoroalkyl acid precursors, can be effectively treated using the proposed strategies; and
- Evaluate the overall potential for treatment using both the oxidative and reductive technologies.

This project primarily consisted of a series of bench scale batch experiments using BDD anodes, B12 and related cobalt catalysts and UV-sulfite reactors. Key fundamental and design questions that were addressed as part of this research focused on the reaction kinetics, F mass balances, energy consumption, secondary products (and mitigation of those products), and understanding how environmental factors (e.g., co-contaminants, groundwater geochemistry, PFAS mixture) impacted treatment.

2.0 Background

2.1 PFAS at DoD Facilities

PFAS soil and groundwater contamination is becoming the leading environmental concern at many DoD facilities. Contamination is often detected at or near fire training areas where aqueous film-forming foams (AFFFs), which are known to contain PFAS, have been used (Schultz et al., 2004). Porter et al. (2011) note that >200 fire training sites in use after 1970 at Air Force facilities alone could contain PFASs that exceed current health advisory levels. More recent work (Anderson et al., 2019) present data from 324 DoD sites across 56 installations. Indeed, investigations completed by members of this project team indicated significant levels (up to mg/kg in soil and hundreds of $\mu\text{g/L}$ in groundwater) of PFASs at a former fire training area at Ellsworth AFB (McGuire et al., 2014). Moreover, this study indicated that partially-degraded components in AFFFs may be a primary source for many of the perfluoroalkyl compounds in soils and groundwater (McGuire et al., 2014), particularly the perfluorocarboxylates. ***Once formed in situ from AFFF components or released directly, perfluoroalkyl acids (e.g., PFOA and PFOS) are extremely persistent in the environment, and studies show that PFOS and PFOA are recalcitrant to biodegradation and natural abiotic degradation processes occurring in subsurface environments (Key et al., 1997; Houde et al., 2006; Parsons et al., 2008).*** Coupled with their persistence are very low regulatory levels; the USEPA has set health advisory levels for the sum of PFOA and PFOS in drinking water at 70 ng/L, respectively. These concentrations are exceeded by several orders of magnitude at many DoD sites. Many states of currently enacted or pending regulations for PFOA, PFOS, and/or other PFAAs in drinking water at concentrations substantially lower than the 70 ng/L health advisory level established by the USEPA.

PFAS have been detected in groundwater impacted by fire-fighting activities at Fallon Naval Air Station (NV) and Tyndall Air Force Base (FL) with concentrations ranging from 125 to 7,096 $\mu\text{g/L}$ (Moody and Field, 1999). A groundwater plume at Wurtsmith Air Force Base (MI) was identified with perfluorocarboxylate and perfluorosulfonate compound concentrations ranging from 3 to 125 $\mu\text{g/L}$ (Moody et al., 2003). As mentioned above, shallow groundwater sampling at Ellsworth AFB has identified PFOA and PFOS groundwater concentrations in excess of 250 and 100 $\mu\text{g/L}$, respectively. PFOS levels measured in shallow groundwater at Joint Base MDL as part of SERDP Project ER18-1204 were approximately 100 $\mu\text{g/L}$, with overlying PFOS vadose zone soil concentrations in the 10s of $\mu\text{g/kg}$. Migration of PFASs from fire training sites has led to dilute groundwater plumes of substantial size. Thus, natural attenuation is not a viable strategy at most sites, and PFAS concentrations in groundwater will likely remain well above action levels in groundwater for a sustained duration. ***Without a demonstrated cost-effective and energy efficient technology to treat PFASs in groundwater, this issue is one of significant urgency and liability to the DoD. Cost effective approaches to contain the highly mobile PFASs and mitigate their downgradient migration are therefore of high value.*** The approaches proposed herein, which utilize oxidative electrochemical and reductive (UV-sulfite) technologies for PFAS treatment, provide evidence that these technologies may provide viable strategies for addressing PFAS in groundwater.

2.2 PFAS Chemistry and Sources

PFAS include both poly and perfluorinated substances. Of particular importance are the perfluorinated subclass of PFAS, referred to as perfluoroalkyl acids (PFAAs) which include perfluorocarboxylates and perfluorosulfonates (Figure 2.1). Under appropriate chemical or biological conditions, poly-fluorinated PFASs (i.e., not completely perfluorinated) can be converted to PFAAs, and thus are often referred to as PFAA precursors. Both PFAAs themselves as well as PFAA precursors have been used in various formulations of AFFF used by the DoD for fire-fighting and fire training (Moody and Field, 1999; Moody et al., 2003; Place and Field, 2012). PFAAs are characterized by an alkane backbone, a terminal functional group, and fluorine atoms at all remaining available positions on the alkane backbone. Some PFAAs, particularly PFOA, are known to originate from the biodegradation of fluorotelomer-based precursors, some of which are present in AFFF (Place and Field, 2012).

While attention has recently been focused on the remediation of PFAAs such as PFOS and PFOA, considerably less attention has been given to PFAA precursors. Evidence from our site investigation at Ellsworth AFB, which included analysis of PFAAs in soil and groundwater as well as direct measurement of specific PFAA precursors and oxidizable PFAA precursors (measured through the formation of perfluorocarboxylates in the laboratory using persulfate; Houtz and Sedlak, 2012), suggests that *in situ* transformation of PFAA precursors to PFAAs is likely. However, there is also evidence to suggest that remediation technologies designed to remove co-contaminants such as benzene (i.e., air biosparging)

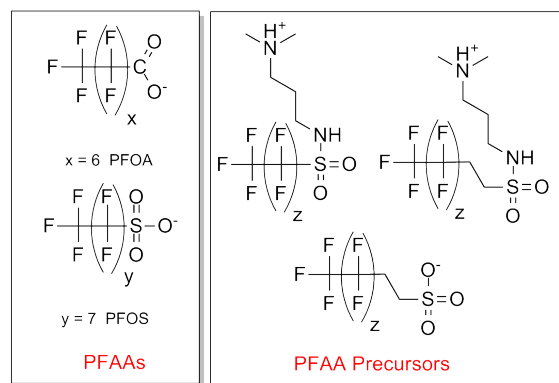


Figure 2.1. Representative structures of PFASs present in AFFF and at AFFF-impacted sites.

may have already facilitated this transformation (McGuire et al., 2014). In our investigation of the site (Figure 2.2), samples collected from locations outside the zone of influence of these remedial activities showed much higher levels of PFAA precursors. ***With respect to remediation, these data suggest that any in situ treatment for PFAAs must also be capable of treating the PFAA precursors, as these chemicals may be an important source of PFAAs at AFFF-impacted sites.***

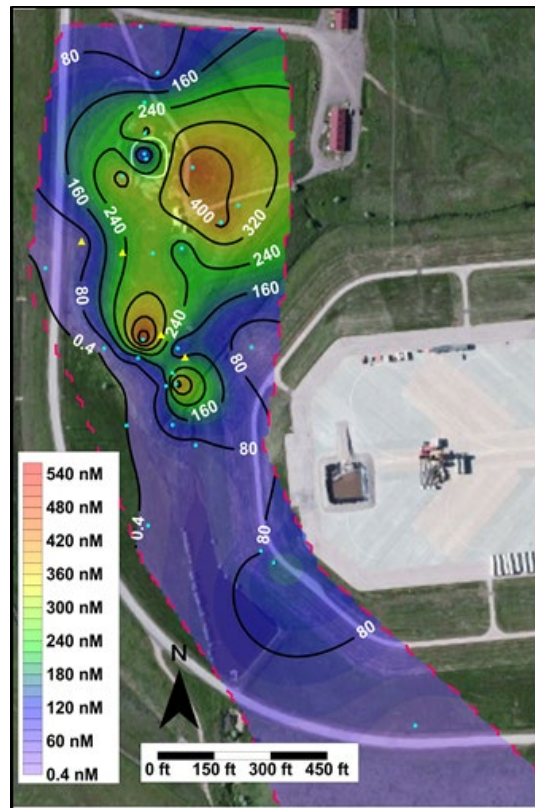


Figure 2.2. Spatial distribution of the total molar concentration of perfluorocarboxylates produced from precursors upon oxidation. These data were obtained from a fire training area at Ellsworth AFB as part of an ongoing research project.

Many AFFF sites suspected of PFAS contamination are likely also contaminated with other chemicals of concern. In particular, fuel hydrocarbons were intentionally applied and ignited at many sites and extinguished with PFAS-bearing AFFF products (Levine et al., 1997). Other possible co-contaminants, such as chlorinated solvents, have been detected at sites associated with fire-training facilities (e.g., McCray and Brusseau, 1998a; McCray and Brusseau, 1998b; McCray et al., 2010). ***The presence of these co-contaminants can influence selection of potential remedial technologies.***

2.3 Treatment Challenges and Emerging Approaches

Due to their low Henry's law constants, PFAS are not amenable to air sparging technologies. Likewise, due to their relatively low affinity for activated carbon adsorbents, as well as their low adsorption rates, treatment with activated carbon is not an efficient remedial option (Yu et al., 2009; Zhao et al., 2011). Anion exchange resins have been shown to outperform granular activated carbon, but removal of the shorter-chained perfluorinated carboxylates is still relatively poor (Zaggia et al., 2016; Woodard et al., 2017). The presence of high levels of co-contaminants that compete for available adsorption sites further diminishes the effectiveness of activated carbon. With little naturally occurring attenuation mechanisms, PFASs persist and migrate extensively in the subsurface, creating large dissolved plumes.

While there have been some reports of the biodegradation of PFAAs (Parsons et al., 2008), most studies suggest that these compounds are not susceptible to biodegradation, and no methods for stimulating their biodegradation *in situ* have been demonstrated (Remde and Debus, 1996; Houde et al., 2006, Liou et al., 2010; Ferrey et al., 2012). Recently, oxidation of PFASs (including PFOS and PFOA) has been demonstrated using persulfate, but only after applying significant energy (e.g., heat, microwave, or ultrasonic irradiation) to generate sulfate radicals (Lee et al., 2009; Liu et al., 2011; Hori et al., 2012), thereby casting doubt on the promise of these approaches as cost-effective *in situ* remedial options. Bruton and Sedlak (2017) demonstrated that perfluorinated carboxylates, but not perfluorinated sulfonates are amendable to persulfate oxidation at elevated temperature and low pH conditions. Sonication has also been shown to defluorinate PFAS, and recent studies have demonstrated the use of plasma for PFAS destruction. Chemical reduction of PFAAs by zerovalent iron has only been shown to be effective at elevated temperatures (e.g., 350 °C) (Hori et al., 2006; Hori et al., 2008). Rhodium-based catalysts are effective in defluorinating aromatic C-F bonds (Baumgartner and McNeill, 2012), but are ineffective in defluorinating aliphatic C-F bonds that are more representative of PFAS structures.

2.4 Electrochemical Oxidation

Several recent studies have demonstrated the potential for electrochemical (EC) oxidation of PFAS-impacted waters. These studies have generally focused on the use of titanium-based anodes (Zhou et al. 2011, Schaefer et al. 2015, Yang et al. 2015, Liang et al. 2018) or boron-doped diamond (BDD) anodes (Carter and Farrell 2008, Ochiai et al. 2011, Urtiaga et al. 2015, Schaefer et al. 2017). BDD anodes have received much attention due to their strong oxidizing potential, longevity, and the fact that they are commercially produced in high surface area (> 1 m²) systems. Studies using BDD anodes have shown that the PFAS oxidation mechanism consists of an initial controlling direct electron transfer step at the anode (Ochiai et al., 2011, Zhuo et al. 2012, Schaefer et al., 2017), followed by an “unzipping” mechanism of the perfluorinated chain that sequentially forms shorter-chained perfluorinated carboxylic acids (PFCAs) as complete defluorination occurs. Prior to the research performed herein, much less attention has been given to oxidation of the PFAA precursors, treatment in groundwater systems at environmentally relevant concentrations, and longevity of PFAS treatment.

2.5 Vitamin B12-Catalyzed Defluorination

The recalcitrance of PFASs to biological and chemical degradation is attributed to the high stability of C–F bonds (Merina et al., 2016). However, Ochoa-Herrera *et al.* observed >70% fluoride ion (F⁻) release from a mixture of branched PFOS isomers by reaction with B₁₂ (a corrin-Co^{III} complex, catalyst precursor, Figure 2.3) and Ti^{III} citrate (reductant) (Ochoa-Herrera, 2008). More recently, Park *et al.* reported cleavage of multiple *sp*³ C–F bonds from analytical standards of mono-branched PFOS with a –CF₃ at the 3-, 4-, 5-, or 6-position using B₁₂ and nanosized Zn⁰ as an alternative reductant (Park et al., 2017). Since B₁₂ is an essential component for microorganisms and animals, these findings suggest that reductive defluorination of branched PFASs could occur in natural environments or biological systems. Furthermore, if the initial defluorination replaces one or more F atoms with H atoms, additional defluorination mechanisms could be triggered. For example, HF elimination from fluorotelomers (i.e., –CH₂–CF₂– into –CH=CF–) has been observed both *in vivo* and abiotically in the environment, and such a transformation could significantly alter the toxicity of the PFASs (Liu and Mejia Avedaño, 2013; Phillips et al., 2007). Hence, it is both scientifically intriguing and practically imperative to further investigate critical structural factors determining Co-mediated defluorination of branched PFASs. Particularly lacking is information on the influence of PFAS structure and cobalt corrin structure on reaction rates. Further understanding of these factors will be critical to development of practical treatment technologies to address complex mixtures of PFAS like AFFF-impacted water.

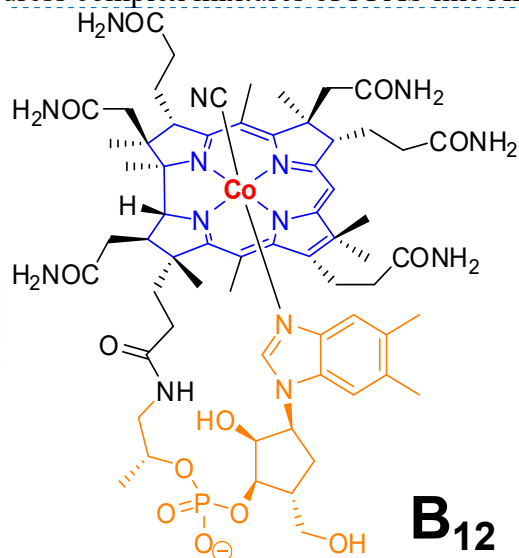


Figure 2.3. Structure of Vitamin B12, shown to catalyze defluorination of PFAS

2.6 UV-Sulfite

Ultraviolet light (UV) photochemical processes leading to generation of hydrated electrons (e_{aq}⁻) has recently gained attention for their effectiveness in degrading both perfluoroalkyl carboxylates like PFOA and perfluoroalkyl sulfonates like PFOS (Buxton et al., 1988; Gu et al., 2017, 2016; Herbert and Coons, 2017; Park et al., 2011, 2009; Qu et al., 2016, 2010; Song et al.,

2013). Hydrated electrons are short-lived transient reactive species that are very strong reducing agents (standard electrode potential of -2.9 V). They can be generated by UV light excitation of an appropriate sensitizer species (e.g., sulfite, iodide, nitrilotriacetic acid, and 3-indole acetic acid) (Figure 2.4) (Park et al., 2009; Song et al., 2013; Sun et al., 2018; Tian et al., 2016). Practical technology development has recently been focusing on the application of UV together with sulfite since sulfite is a relatively inexpensive bulk chemical already widely used as a food preservative and used widely in wastewater treatment plants to dechlorinate disinfected wastewater prior to discharge. In addition, the sulfate decomposition byproduct of sulfite is naturally occurring and not considered to be harmful to human health or ecosystems (Li et al., 2012; MacCrehan et al., 1998; Song et al., 2013).

While a number of earlier reports demonstrate that the UV-sulfite process is able to degrade individual PFAS compounds (Gu et al., 2017, 2016; Song et al., 2013), reactivity of the broader range of PFAS present in complex mixtures like AFFF remains unclear. Thus, further investigation is necessary to fully characterize the reactivity and persistence of diverse PFAS structures that possess different polar head groups, chain lengths, branching, degree of fluorination (i.e., perfluoro- versus polyfluoroalkyl structures), and derivative precursor structures identified by high resolution mass spectrometry analyses that have made it possible to quantify PFAS down to $< 1 \text{ ng}\cdot\text{L}^{-1}$ (Hu et al., 2016; Krauss et al., 2010). In addition, these methods are powerful tools for identifying new PFAS (Barzen-Hanson et al., 2017). These techniques can now be applied to characterize UV-sulfite reactions with a variety of AFFF-impacted waters, ultimately enabling us to relate PFAS reactivity to specific molecular properties and structural characteristics. This will ultimately allow us to obtain insights into the potential of UV-sulfite processes for remediation of AFFF-impacted groundwater at DOD facilities.

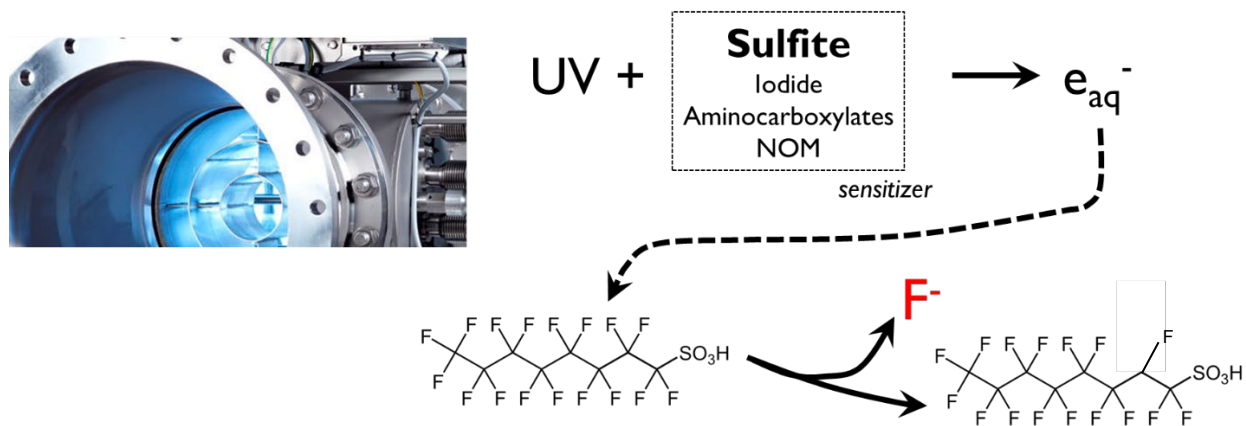


Figure 2.4. UV excitation of selected chemical sensitizers can generate strongly reducing hydrated electron, transient species that have been shown to degrade individual perfluoroalkyl carboxylates and sulfonates.

3.0 Materials and Methods

3.1 Overall Approach and Rationale

The overall experimental approach used for evaluating both the oxidative (electrochemical) and reductive (catalytic and UV-sulfite) approaches are summarized in Figure 3.1. For evaluating PFAS electrochemical treatment, a commercially-available bench-scale system was used to perform a wide range of experiments. Initial testing began with screening of commercially available anodes, focusing on removal of both PFOA and PFOS. Our rationale for selecting only anodes that were commercially available was that this would facilitate scale-up of electrochemical systems and avert concerns with both the longevity and production capabilities/costs associated with newly developed or emerging electrode types.

As discussed in Section 3.2, BDD anodes were selected for advanced testing of EC oxidation of PFASs (Task 2). Experiments to attain improved insight into PFOA and PFOS (along with other PFAAs) defluorination were carried out in various matrices. Testing also provided insight into treatment mechanisms, including potential impacts of organic co-contaminants. Task 2 also investigated perchlorate generation, and the use of biotic reduction of electrochemically generated perchlorate as a potential means of mitigation.

EC treatment of PFAS was studied further by evaluating treatment of diluted AFFF and by evaluating treatment of AFFF-impacted groundwater collected from a former fire-fighting training area (Task 3). These experiments focused on the fate of suspected PFAA precursors, the fluorine mass balance, energy requirements, and on the oxidation pathways. The final EC tasks focused on evaluating divided EC cell configurations, and on longer-term testing to assess anode longevity.

Reductive PFAS treatment initially focused on the use of supported metal catalysts (e.g., Rh/C) (Task 6). Based on our initial findings, reductive treatment using supported metal catalysts was discontinued, and focus was placed on the use of B12 and related cobalt corrin complexes for catalytic reduction. Experiments with B12 and related cobalt catalysts evaluated a range of individual PFAS structures to identify structure-activity relationships. In addition, the majority of our research efforts related to PFAS reduction were redirected to UV-sulfite treatment for generation of hydrated electrons (Tasks 7-8). Initial UV-sulfite testing was also performed using PFAAs in electrolyte. Subsequent testing using diluted AFFF and groundwater systems impacted by AFFF contamination provided insight into treatment kinetics and energy requirements.

As part of the ongoing effort to identify and (semi)-quantify the broad range of suspect analytes that serve as both potential PFAA precursors and intermediate products of oxidative or reductive treatment, analytical libraries were developed for LC-QToF-MS analysis (Task 9).

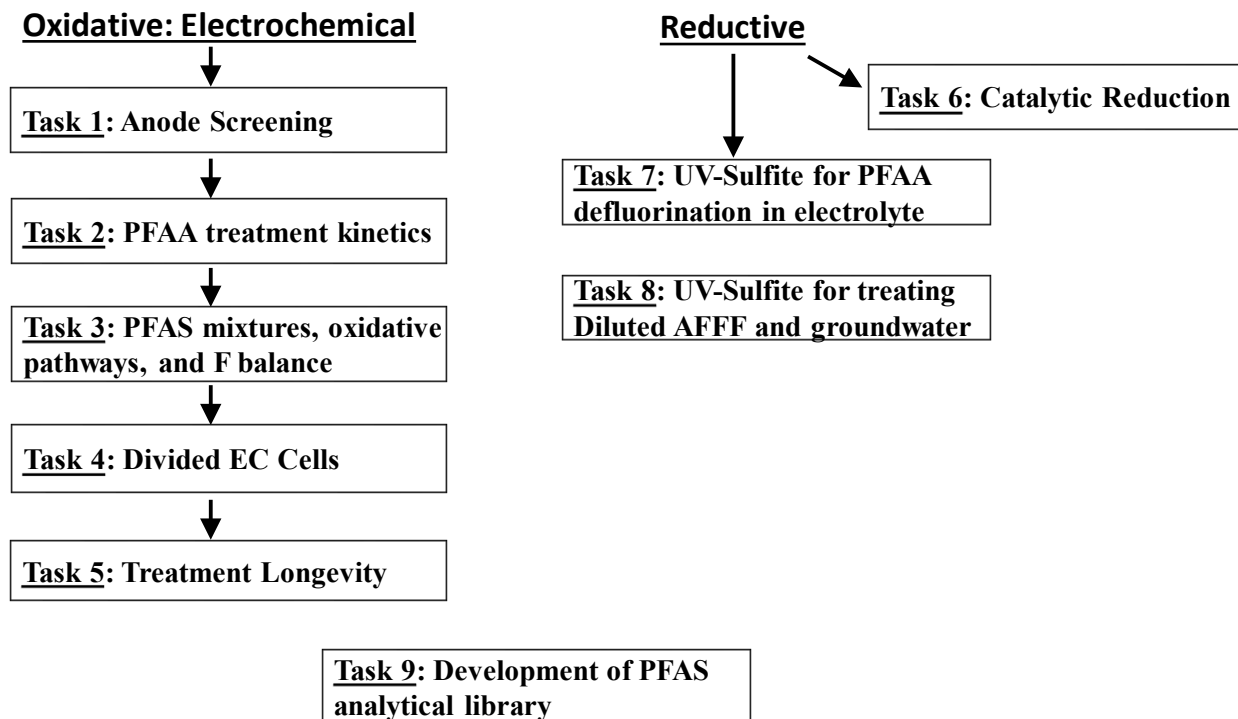


Figure 3.1. Experimental approach, segregated into Tasks.

3.2 Anode Screening

Materials and Electrochemical System

Initial experiments were performed to determine which commercially available anodes were most effective for defluorinating PFAAs. PFOA and PFOS were selected as the model PFAAs for testing. The following anode materials were obtained from Electrochem Technologies & Materials, Inc. (Montreal, Canada):

- Ti/IrO₂ (Grade 1 Ti)
- Ti/IrO₂ (Grade 7 Ti)
- Nb/IrO₂
- Ta/IrO₂
- Ti/RuO₂ (Grade 1 Ti)
- Ti/RuO₂ (Grade 7 Ti)
- Ti/IrO₂/RuO₂ (Grade 7 Ti)

In addition, a study performed by Yang et al. (2015) using synthesized Ti/SnO₂-F anodes was shown to be effective for treating PFOA. Results also suggested that these Ti/SnO₂-F anodes

would have substantially longer activity with respect to PFOA defluorination than other mixed metal oxide (MMO) anode materials. Following the procedures described in Yang et al. (2015), we synthesized several Ti/SnO₂-F anodes (synthesized at the Colorado School of Mines (CSM). Ti/SnO₂-F anodes were also purchased from a commercial electrode company; one of the purchased Ti/SnO₂-F anodes also was doped with palladium.

Electrochemical experiments were performed using a Micro-Flow Cell (Electrocell North America, Inc., Amherst, NY). The cathode material was stainless steel (316) in all experiments, and the anode material was varied using the mixed metal oxide (MMO) materials described above. The active surface area of each electrode was 10 cm². The distance between electrodes was 8 mm. Two flow cells were constructed to expedite testing. The flow cells were operated in both undivided and divided configurations. When operating as a divided cell, a Nafion 117 cation exchange membrane was used to separate the anolyte and catholyte (ElectroCell North America, Inc).

All experiments were performed in batch mode, where 0.5 L polypropylene vessels contained the anolyte and catholyte, or the combined electrolyte solution for undivided electrochemical cells (Figure 1). Electrolyte solution (200 mL) was recirculated through the electrochemical cell at 0.1 L/min using a peristaltic pump; for divided cells, the recirculation was performed for both the anolyte and catholyte. Flow rates were verified using flow meters. The electrolyte solution consisted of 750 mg/L sodium perchlorate. For the catholyte in the divided electrochemical cell, the electrolyte consisted of a 500 mg/L Na₂SO₄ solution. We note that sodium perchlorate was selected because perchlorate does not become further oxidized by the MMO anodes, and is not expected to compete with PFOS or PFOA at the anode surface.

All experiments were performed under constant current conditions, while monitoring voltage. Power was supplied using an E3646A 60W dual power supply (Agilent). Current densities of 0 mA/cm² (serving as no-current controls) and 10 mA/cm² were examined. All experiments were performed at room temperature. No-current controls were performed with and without vigorous sparging, and experiments were performed for both divided and undivided electrochemical cell configurations. Electrolyte solution for control also were prepared at a pH of 2 (using perchloric acid) to mimic the decrease in pH observed in the anolyte under applied current conditions. In addition, a base trap was constructed by fabricating an air-tight cap used to cover a 0.5L polypropylene wide-mouth bottle. The cap was fitted with three ports for the influent, effluent, and base trap. The influent outlet held tubing (Tygon) that allowed electrolyte to leave the reservoir and enter the electrochemical cell, while the effluent outlet held tubing that allowed “treated” electrolyte to circulate back into the reservoir. The base trap outlet was made up of a valve that allowed gases to escape the closed reservoir into a small tube connected to a 16 ½ gauge needle enclosed in tubing, which was immersed in 50mL of a 1,000 mg/L sodium bicarbonate solution in a 100 mL graduated cylinder.

The 200 mL electrolyte solutions (or, just the anolyte solution for divided flow cell configurations) were amended with PFOS and/or PFOA. Target PFOS and PFOA of 20 mg/L were desired for these experiments to 1) enable analysis using a conductivity detector and 2) to facilitate identification of fluoride daughter products. A 40% acid solution of perfluorooctane sulfonic acid

(77283-10ML) was purchased from Sigma-Aldrich. 6 μ L of this solution was added to 200 mL of 750 mg/L perchlorate solution for an initial concentration of 20mg/L. PFOA (171468-5G) was also purchased from Sigma-Aldrich, but in powder form. 4 mg of PFOA was added to 750mg/L perchlorate solution to obtain an initial concentration of 20mg/L.

System Monitoring and Analyses

The electrolyte (or, anolyte in divided flow cells) solution was monitored as a function of time during the duration of each experiment, which typically lasted 6 hours. Aqueous samples were collected hourly for pH, PFOA/PFOS, and fluoride analyses. Voltage also was monitored through each experiment. Periodic monitoring for pH, fluoride, and PFOS/PFOA also were performed in both the base trap and catholyte.

The pH of each sample was determined by BDH pH test strips (VWR, Cat. No. BDH35309.606). Fluoride was analyzed via ion chromatography using EPA Method 300.0. PFOS and PFOA screening analysis was performed using reverse-phase HPLC with a conductivity detector with an acetonitrile/borate buffer eluent and chemical conductivity suppression. PFOS and PFOA quantification to 0.50 and 0.20 mg/L, respectively, was attained.

3.3 Electrochemical Experiments using Boron-Doped Diamond (BDD) Anodes

3.3.1 Initial Testing Using PFOA and PFOS

Materials

PFOA (96% purity) and PFOS (~40% in H₂O) were purchased from Sigma Aldrich. Reagent grade *tert*-Butyl alcohol (TBA) was purchased from Spectrum Chemical. NaCl and Na₂SO₄ were purchased from JT Baker and Macron Fine Chemicals, respectively. Deionized water (Nanopure system) was used to make the electrolyte solutions. Characteristics of the natural groundwater used for this initial testing is provided in Table 3.3.1.

Table 3.3.1. Characteristics of groundwater used for the initial PFOA/PFOS testing using boron-doped diamond anodes.

Analyte	Concentration
Fluoride (mg/L)	<0.2*
Chloride (mg/L)	18
Sulfate (mg/L)	25
Nitrate (mg/L)	5.5
Nitrite (mg/L)	<0.2*
Total Organic Carbon (mg/L)	11
Turbidity (NTU)	1.83
Perchlorate (mg/L)	0.15
Alkalinity (mg/L CaCO ₃)	352
Conductivity (µmho/cm)	769
pH	6.7
Hardness (mg/L CaCO ₃)	363

*Compound below the practical quantitation limit.

Electrochemical Experiments

The electrochemical system employed for the boron-doped diamond (BDD) experiments using PFOA/PFOS only (as opposed to the wider ranges of PFAS examined in the BDD experiments described in Section 3.3.2) is shown in Figure 3.2. Electrochemical experiments were performed using a single compartment electrochemical cell and electrodes purchased from Advanced Diamond Technologies (Romeoville, IL). The BDD anode consisted of an ultrananocrystalline diamond coating (2 µm) on niobium; the cathode was tungsten. The available surface area of each rectangular electrode was 38 cm², and the electrode spacing was 0.4 cm.

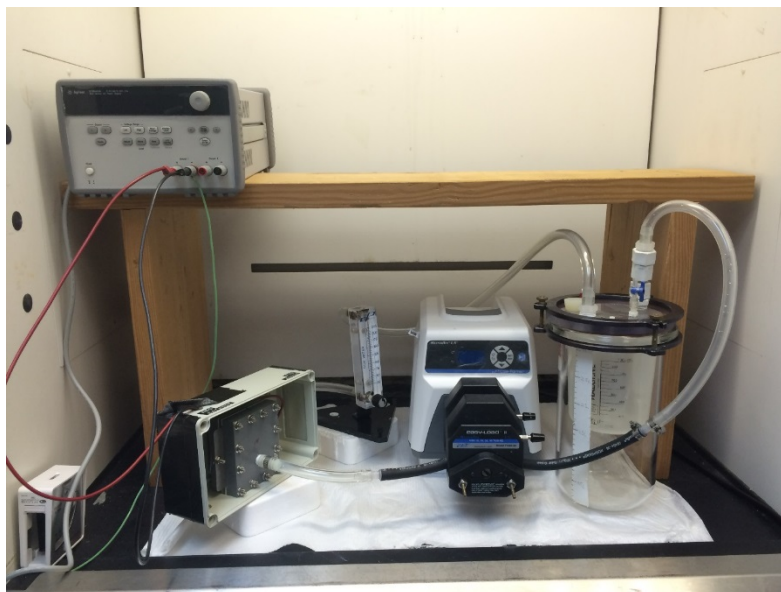


Figure 3.2. Electrochemical system (electrochemical cell and electrodes from Advanced Diamond Technologies) used for evaluating PFOA and PFOS oxidation using BDD anodes. Shown are the power source, recirculation pump and flowmeter, reaction vessel, and the BDD electrochemical cell.

Batch experiments were performed in duplicate using a polypropylene vessel containing 250 mL of deionized water. The deionized water was spiked to attain the target level of PFOA or PFOS and amended electrolyte (either 1500 mg/L Na_2SO_4 or 1500 mg/L Na_2SO_4 + 167 mg/L NaCl). Urtiaga et al. (Chiu and Reinhard, 1995) demonstrated that the presence of sulfate had only a minor impact on PFOA treatment, thus sulfate was not expected to impact assessment of PFOA and PFOS treatment. Thus, sodium sulfate was used instead of perchlorate as electrolyte; this facilitated evaluation of perchlorate generation (in experiments amended with NaCl) during testing. A parallel experiment was also performed in electrolyte solution (containing NaCl) amended with 100 mg/L TBA, a known scavenger of hydroxyl radicals [25]. The TBA-amended experiments were used to assess the role of hydroxyl radicals on PFOS and PFOA defluorination, as well as the potential role of co-mingled organic contaminants (e.g., petroleum hydrocarbons or chlorinated solvents) on PFOA/PFOS treatment. Experiments conducted with natural groundwater (250 mL) were amended with Na_2SO_4 (final concentration increased to 525 mg/L sulfate) to increase the electrical conductivity so that the voltage applied to the electrodes for a given current density was similar ($\pm 1\text{V}$) to that employed in the electrolyte experiments.

Initial experiments were performed with elevated PFAS concentrations (15 mg/L PFOA, 10 mg/L PFOS) to facilitate detection of transformation products, including fluoride and any transient formation of shorter-chained PFAAs. Subsequent experiments with low concentrations (0.3 mg/L PFOA, 0.6 mg/L PFOS) were performed to better mimic conditions observed in PFAS-contaminated groundwater (Hu, et al., 2016; Im, et al., 2014; Kissa, 2001; Klassen et al., 1994).

All experiments were performed under constant current conditions at room temperature (approximately 20°C). Power was supplied using an E3646A 60W Dual Output Power Supply (Agilent). Current densities of 50, 15, and 3 mA/cm² were examined. Experiments were performed at galvanostatic conditions and the cell voltage was measured directly on the power supply that was connected to the electrochemical cell. The 250 mL solution was re-circulated from the polypropylene vessel through the electrochemical cell at 250 mL/min using a peristaltic pump and 0.5 inch tygon tubing. After initiating the experiment, aqueous samples were collected for analysis as a function of electrochemical treatment time. Initially, duplicate samples were collected at each timepoint and immediately quenched by mixing with 20 µl of a sterile 1.5 g/L sodium thiosulfate solution to scavenge any residual oxidant species remaining in the sample (Langlois and Oehme, 2006). Comparison of quenched and non-quenched samples showed that addition of the quenching agent did not influence the extent of PFOA or PFOS oxidation (or any of the transformation products), so this preservation step was discontinued. Control experiments also were performed without applied current to account for any PFOS/PFOA losses not attributable to electrochemical treatment (e.g., sorption).

Biological Reduction of Electrochemically Generated Perchlorate

A screening level biological treatment column experiment was performed to determine if perchlorate generated by the anodic oxidation of Cl⁻ during the electrochemical treatment of PFOA and PFOS could be re-reduced to Cl⁻ by subsequent biological treatment. Using methods similar to those employed previously for biologically- enhanced perchlorate reduction (Gu, et al., 2016), two stainless steel columns (7.2 cm diameter and 30 cm long) were placed in series and packed with 2,400 g of a medium fine sand. The ends of the columns were sealed using Lexan plates with machined grooves to accept Viton O-rings to seal the column. Column ends were fitted with stainless steel two-way control valves to facilitate water sampling. Electrochemically treated water was introduced upflow through the columns using a peristaltic pump at 3.6 mL/h. Water entering the columns was amended with sodium lactate, diammonium phosphate, yeast extract, and molybdenum at target influent concentrations of 900, 10, 100, and 0.1 mg/L, respectively. The total residence time in the columns was approximately 9 days. Influent and effluent samples were periodically collected, filtered, and analyzed for perchlorate, chlorate, and chloride. After 155 days, the downgradient column was further bioaugmented with 50 mL of a suspension (optical density at 550 nm ~1.0) of perchlorate-degrading bacterium *Azospira suillum* JPLRND (Gu, et al., 2017; Langlois and Oehme, 2006).

Analytical

Treated solutions were monitored for residual oxidants, pH, anions, and perfluorinated carboxylates and sulfonates. The N,N-diethyl-p-phenylene diamine (DPD) method (Spectronic 20D+, ThermoScientific) was used to determine residual oxidants, including active chlorine species and H₂O₂ (Krauss, et al., 2010). An Oakton probe (Part no. WD-35634-14) was used to measure sample pH. Anions were analyzed via ion chromatography using EPA Methods 300.0

(most anions) and 314.2 (perchlorate analysis). Detection limits for most anions were 200 µg/L; the detection limit for the perchlorate method was 0.25 µg/L. TBA was analyzed by Chemtech (Mountainside, NJ) using gas chromatograph/mass spectrometry (GC/MS) following EPA Method 8260C (0.5 µg/L detection limit).

PFAS were analyzed using methods reported previously (Schaefer et al., 2015). Briefly, samples were collected in 20 mL polypropylene vials and were pH neutralized (as needed) to a final pH between pH 5-9. A 50 µL aliquot of each sample was then diluted in 10 mL of Optima Water (Fisher Scientific) because of the high initial PFOA and PFOS concentrations. This sample was then further diluted for analysis. An aliquot of the diluted sample was transferred to a microcentrifuge tube containing Optima water, Optima methanol (Fisher Scientific), a small aliquot of basic water (0.01% ammonium hydroxide in water), and mass labelled surrogate (at a concentration of 230 ng/L), to obtain a volume of 1500 µL (80 vol% water and 20 vol% methanol). This ratio was found to minimize surrogate loss and improve chromatography during analysis. The samples were centrifuged at 17,000 relative centrifugal force (rcf) for 10 min, and then 1350 µL of the solution was transferred to an auto-sampler vial for analysis by liquid chromatography with tandem mass spectrometry (LC-MS/MS). Chromatography was performed using 10 mM ammonium acetate in water, and 10 mM ammonium acetate in methanol. Eluents were delivered initially at a flow rate of 0.6 mL/min by a Shimadzu LC-20AD LC system. The flow rate was decreased to 0.4 mL/min at 4.5 minutes, and then ramped up again to 0.6 mL/min at 9.5 minutes. A CTC Analytics Leap Technologies autosampler injected 1 mL of the sample on a 50 mm x 4.6 mm Gemini C₁₈ column with a 3 µm particle size, with a C₁₈ guard column. Initial eluent conditions were 90% water, and 10% methanol. The methanol percentage was ramped to 85% over 1.5 minutes, then to 95% by 9 minutes, and by 9.5 minutes before decreasing to 10% over the final 0.5 minutes. The PFASs were analyzed by an MDS Sciex Applied Biosystems API 3200 in negative electrospray ionization mode under multiple reaction monitoring, and two transitions were monitored for each PFAS. A list of PFASs are found in the supplementary information (Table S1). Blanks and quality controls were included every eight to ten samples and carry over was minimal. Quality assurance criteria included signal/noise >10 and above the limit of quantitation (LOQ; see Supplementary data section for definition); LOQs were analyte, matrix, and run dependent, but were generally 6 - 21 ng/L in an undiluted sample. Depending on the degree of dilution necessary to enable accurate quantitation of the PFAS spiked experiments (i.e., 75 – 7500-fold dilutions), the dilution-adjusted LOQs ranged between 0.45 – 157.5 µg/L. Surrogate recoveries were generally >60%, and relative standard deviations for replicate analyses of the same sample were generally <25%.

3.3.2 Testing to Assess Treatment in the Presence of a Wide Range of PFAS

Materials

Two natural groundwaters, designated W1 and W2, were used for all the electrochemical experiments in this section. W1 was collected from a DoD facility with no known AFFF impacts. W2 was collected from a DoD facility in the vicinity of a fire training area where AFFF was used,

and where elevated PFAS levels had been previously observed (McGuire et al., 2014). 3M AFFF was likely one of the products used at this location, as suggested by an empty drum of this solution identified at the site. Basic water quality parameters and dominant PFAA levels (in the case of W1, after spiking with 3M AFFF) are provided in Table 3.3.2. The AFFF solution used for spiking W1 was manufactured by 3M (2001), and was previously characterized and provided by Dr. Jennifer Field (Baduel, et al., 2017).

Table 3.3.2. Characteristics of the unfiltered groundwaters used for assessing treatment of a wide-range of PFASs using BDD anodes.

	W1 Concentration (natural groundwater spiked with 3M AFFF)	W2 Concentration (AFFF-impacted groundwater collected from Ellsworth AFB)
Fluoride (mg/L)	<0.2*	0.9**
Chloride (mg/L)	18	160
Sulfate (mg/L as SO ₄)	25	14
Nitrate (mg/L as N)	5.5	<0.2*
Total Organic Carbon (mg/L)	11	51 (5.1**)
Turbidity (NTU)	1.8	250 (6.3**)
Alkalinity (mg/L CaCO ₃)	352	890
Conductivity (µmhos/cm)	769	2120
pH	6.7	7.1
Hardness (mg/L CaCO ₃)	363	1,030
<i>PFAAs (µg/L) ***</i>		
PFBA	<0.074*	25
PFPeA	4.0	61
PFHxA	9.0	130
PFHpA	2.6	12
PFOA	15	58
PFBS	33	45
PFHxS	76	160
PFHpS	11	26
PFOS	300	22

* Compound not detected above method quantitation limit

** Measured after passing through a 20 micron filter

*** For W1, PFAA concentrations listed were after the groundwater was spiked with AFFF. PFAA concentrations were measured in both groundwaters after passing through a 20 micron filter. (PFBA= perfluorobutanoic acid, PFHxA=perfluorohexanoic acid, PFHpA = perfluoroheptanoic acid, PFOA=perfluorooctanoic acid. PFBS = perfluorobutane sulfonate, PFHxS = perfluorohexane sulfonate, PFHpS = perfluoroheptane sulfonate, PFOS = perfluorooctane sulfonate)

Electrochemical System

Electrochemical experiments were performed using a single compartment Microflow Cell (ElectroCell North America, Inc.) similarly to those described in Section 3.3.1. The cathode material was stainless steel, and the anode material was boron-doped diamond on niobium support (Condias, GmbH, Germany). The active surface area of each electrode was 10 cm². The distance between electrodes was 4 mm. *It is noted that the electrochemical cell and electrodes from Advanced Diamond Technologies (ADT), which were used for the experiments described in Section 3.3.1, were not used for the electrochemical experiments performed on the AFFF-impacted waters because initial testing showed that the ADT BDD anodes did not effectively treat the PFAAs present in the water.*

The experimental system using the Microflow Cell electrochemical system is shown in Figure 3.3. All experiments were performed in batch mode, where a polypropylene vessel served as the groundwater reservoir (Figure S1). Groundwater (0.25 L) was recirculated through the electrochemical cell at 0.10 L/min using a peristaltic pump. Flow rates were verified using a flowmeter. All experiments were performed under constant current conditions, while monitoring voltage. Power was supplied using an E3633A 200W power supply (Agilent). Current densities of 0 (no current controls) and 25 mA/cm² were used; one additional test at a current density of 200 mA/cm² also was used. All experiments were performed at room temperature (approximately 25 degrees C).

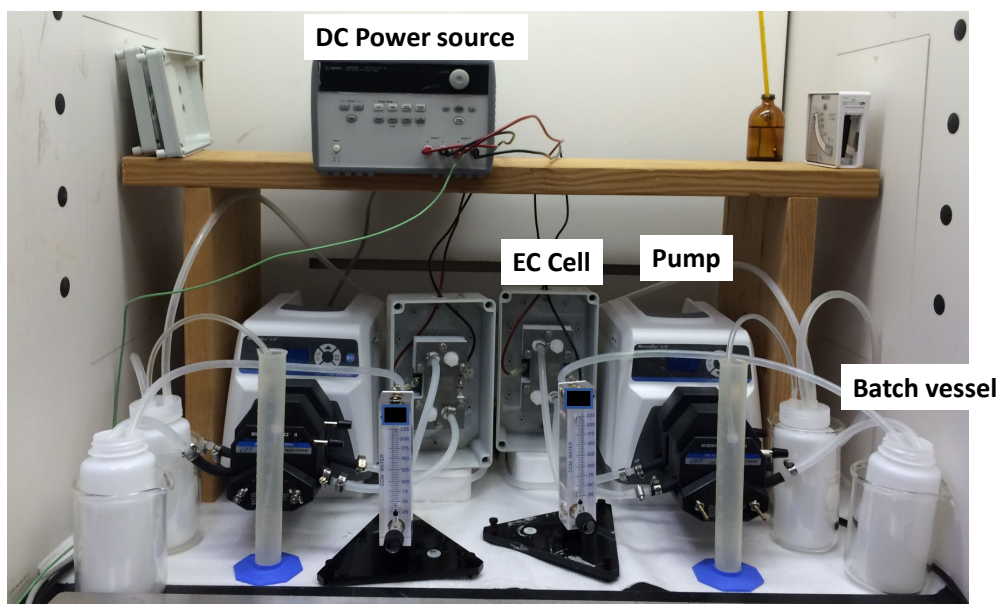


Figure 3.3. Electrochemical system using the Microflow Cell with BDD anodes produced by Condias. Two systems are shown.

For experiments performed using groundwater W1, the groundwater was amended with Na₂SO₄ so that the sulfate concentration in the groundwater increased by 500 mg/L sulfate. This sulfate addition was performed to increase the conductivity of the water so that the desired current density could be attained at an applied voltage similar to that in the W2 electrochemical experiments. In addition, as mentioned above, W1 was amended with 3M AFFF solution (0.02 mL AFFF solution to 250 mL of W1 groundwater). Thus, the AFFF-spiked W1 groundwater served as the “fresh” AFFF-impacted groundwater, while the W2 groundwater served as the “aged” AFFF-impacted groundwater. All groundwater was passed through a 20 µm filter prior to initiating the electrochemical experiments to prevent any particulates from entering the electrochemical cell.

The groundwater solution in each experiment was monitored as a function of time throughout the duration of each experiment, which typically lasted 8 hours. Samples were collected for determination of pH, anions, and PFAS. Temperature of the recirculated groundwater also was monitored.

Initially, duplicate samples were collected at select timepoints and immediately quenched by mixing with 20 µL of a sterile 1.5 g/L sodium thiosulfate solution to scavenge any residual oxidant species remaining in the sample (Herbert and Coons, 2017). Preliminary tests (data not shown) indicated that addition of the quenching agent did not impact the levels of PFASs detected in the electrochemically treated samples, so this preservation step was discontinued in later experiments. Control experiments were also performed without applied current to account for any PFAS losses, such as sorption or volatilization, not attributable to electrochemical treatment.

An additional experiment was performed in duplicate using PFOA (initial concentration of 20 mg/L) in 150 cm³ of 1480 mg/L sodium sulfate; the current density was 25 mA/cm². This PFOA experiment served to compare PFOA transformation rates to the more complex W1 and W2 groundwater systems, which contained a mixture of PFAS.

Analytical Methods

The pH was measured using an Oakton probe (Part no. WD-35634-14). Anions (except perchlorate) were analyzed via ion chromatography using EPA Method 300.0, with a detection limit of 200 µg/L. Perchlorate was analyzed via ion chromatography using EPA Method 314.2, with a detection limit of 0.25 µg/L. Descriptions of the quantitative analyses for PFAAs and the semi-quantitative analyses for potential PFAA precursors are provided in Appendix A1. Total oxidizable precursor analysis, based on the previously developed methods (Houtz and Sedlak, 2012), were performed on W1 and W2 by SGS Axys Analytical Services Ltd. (BC, Canada). Total organic fluorine was determined via combustion ion chromatography by Dr. Leo Yeung at Orebro University (Sweden).

3.3.3 Long-Term Electrochemical Testing

Bench-scale experiments were performed using the Microflow Cell electrochemical cell and BDD anode system described in Section 3.3.2 and shown in Figure 3.3. The W2 groundwater described in Section 3.3.2 was used for the long-term experiments described in this Section.

The long-term electrochemical experiments were performed at a constant applied current density of 20 mA/cm² (selected based on results of the testing described in Sections 3.3.1 and 3.3.2). In these long-term experiments, 0.25 L of AFFF-impacted groundwater was recirculated through the electrochemical cell at 0.1 L/min for 24 hour batch cycles. These 24-hour batch cycles were repeated for 21 days. At the end of each 24-hour batch cycle, the system was operated in reverse polarity for approximately 10 minutes to mitigate calcium scaling, the batch reservoir was then replaced with fresh untreated water. Water samples were collected at t=0 and t=24 hours during each 24-hour batch cycle during the 21 day study for analysis of PFAAs (via liquid chromatography with tandem mass spectrometry, with levels of quantification between 0.1 and 10 ng/L) and anions (chloride, fluoride, nitrate, chlorate, perchlorate, and sulfate via ion chromatography) as previously described in Section 3.3.2. Samples were not collected on days 16 through 18, as changes in PFAS treatment rates were expected to be minimal during this time interval (as discussed in the Results). Temperature, pH, and applied voltage also were monitored at the beginning and end of each 24-hour batch cycle. The electrochemical experiment was performed in duplicate.

3.3.4 Testing Evaluating alternate Anode Materials and Electrochemical Cell Configurations

Results from the testing described in Sections 3.3.2 and 3.3.3 showed that the majority of the organic fluorine present in AFFF-impacted waters exists as potential PFAA precursor compounds. These precursor compounds are likely oxidized under milder conditions than the strong oxidizing conditions that occur at the surface of the BDD anodes. To assess the extent to which potential PFAA precursor transformation may occur prior to anodic treatment using BDD anodes, experiments were performed using a divided compartment electrochemical cell (Microflow Cell). BDD electrodes (Condias) were used as both anodes and cathodes. Treatment of AFFF-impacted waters first included cathodic treatment, followed by anodic treatment. It is recognized that cathodic treatment could involve both reductive transformation of the PFAA precursors (via direct electron transfer at the cathode) or oxidative transformation via generation of peroxide. To assess the latter, parallel experiments were performed using air-sparged catholyte to increase the rate of peroxide generation in the catholyte, and thereby assess the role of peroxide on PFAA precursor transformation.

Experiments were performed using the AFFF-impacted water designated W2 (Section 3.3.2), and synthetic groundwater (18 mg/L chloride, 525mg/L sulfate, 5mg/L nitrate, 350 mg/L bicarbonate) amended with diluted 3M AFFF. The current density was 25 mA/cm², and the applied

voltage ranged from 13 to 20 V. The active surface area of each electrode was 10 cm². The distance between electrodes was approximately 4 mm, and the catholyte and anolyte volumes were 0.25 L. The anode and cathode compartments of the electrochemical cell were divided by a Nafion 117 membrane. Water was recirculated in each compartment of the cell at 0.1 L/min. An electrolyte solution (1,000 mg/L sodium sulfate) was used as the counter solution when testing either the cathodic or anodic treatment of the AFFF-impacted waters. Both PFAA and potential PFAA precursors were analyzed as described in Section 3.3.2.

In addition to evaluating treatment in divided electrochemical cells, nitrogen-doped tetrahedral amorphous carbon (ta-C:N) electrodes manufactured by Fraunhofer were evaluated. Preliminary testing by Fraunhofer showed that these electrodes were unstable when used as anodes, so electrochemical testing was performed using the ta-C:N electrodes as cathodes to determine if any reductive defluorination occurred. Ir/RuO₂ electrodes were used as the anodes, with 25 mA/cm² applied current. The electrochemical cell (Microflow Cell) was operated in an undivided configuration. The W2 groundwater was used in the testing. Experimental methodology and analyses were performed similarly to that described in Section 3.3.2.

3.4 B12-Catalyzed Reduction Studies

Chemicals and solution preparation

PFASs (SynQuest Laboratories), B₁₂ (Alfa Aesar) and other cobalt species (Sigma-Aldrich), 12% TiCl₃ solution (Acros Organics), and other chemicals (Fisher Chemical) were used as received. Information on PFASs and Co species used in this study is listed in Table 3.4.1. Stock solutions were prepared with degassed solvents in an anaerobic glove bag (95% N₂ and 5% H₂ atmosphere; Coy Laboratories). PFASs were dissolved in methanol as 15 mM stock solutions. Cobalt species were dissolved (B₁₂ and CoCl₂) or suspended (Co₃O₄ nanopowder) in DI water or dissolved in methanol (Co-PP and Co-*salen*) as 5 mM stock solutions. To prepare the Ti^{III} citrate stock solution, in a 500 mL glass bottle 11.76 g of sodium citrate tribasic dihydrate was dissolved in 200 mL of DI water (Vecitis et al., 2009). Then 25 mL of TiCl₃ solution was added with magnetic stirring, followed by adding saturated Na₂CO₃ solution until the pH reached 9.0. DI water was further added to make the final volume 500 mL.

Table 3.4.1. Information of PFASs and Co Species Used in this Study.

Symbol used in paper	Name	Purity grade	CAS#
1	Perfluoro-3,7-dimethyloctanoic acid	97%	172155-07-6
2	4-(Trifluoromethyl)hexafluoropent-2-enoic acid	97%	239795-58-5
3	Perfluorocyclohexylcarboxylic acid	90%	374-88-9
4	4,5,5,5-Tetrafluoro-4-(trifluoromethyl)pentanoic acid	97%	243139-62-0
5	Perfluoro(2,5-dimethyl-3,6-dioxanonanoic acid)	95%	13252-14-7
6	Perfluoro-N-methylpiperidine	99%	359-71-7
7	Perfluoro- <i>n</i> -octanoic acid	98%	335-67-1
8	Perfluoro-3,7-dimethyloctan-1-ol	97%	232587-50-7
9	1H,1H,2H,2H-Perfluoro(9-methyldecan)-1-ol	98%	31200-98-3
10	(Perfluorocyclohexyl)methanol	88%	28788-68-3
B₁₂	Cyanocob(III)alamin	98%	68-19-9
Co-PP	Protoporphyrin IX cobalt chloride	NA	102601-60-5
Co-salen	N,N'-Bis(salicylidene)ethylenediaminocobalt(II)	99%	14167-18-1
Co₃O₄	Cobalt(II,III) oxide nanopowder, <50 nm particle size	99.5%	1308-06-1
CoCl₂	Cobalt(II) chloride hexahydrate	98%	7791-13-1

The experimental procedure for batch reactions was modified from Ochoa-Herrera *et al* (Ochoa-Herrera et al., 2008). In an anaerobic glove bag, a series of 9-mL serum bottles were loaded with 4 mL of solution containing specific PFAS (0.1 mM), Ti^{III} citrate (~36 mM) with carbonate buffer (~40 mM), and cobalt catalyst (0.25 mM). The reaction mixture (~5 mL) thus contained 0.1 mM PFAS, 0.25 mM cobalt catalyst, ~36 mM Ti^{III}, and ~40 mM carbonate buffer. Each serum bottle was sealed with a rubber stopper and an aluminum crimp cap, wrapped with aluminum foil, and transferred to a 70°C oven. At designated reaction times, individual reactors were sacrificed for analysis. Each reactor was used for a single measurement, such that a typical reaction series of five time points (0, 1, 3, 7, and 15 days) began with five replicates of each reaction mixture. Each reaction series was repeated at least twice. The bottles were opened to the atmosphere after cooling, and a dark blue precipitate was observed at the bottom. The supernatant was collected and analyzed. Overnight exposure to air converted the dark blue precipitate mixture to a white precipitate (likely TiO₂ resulting from Ti^{III} oxidation) and a pink (B₁₂) or yellow-brown (Co-PP and Co-salen) aqueous supernatant. Due to the interference of Ti^{III} citrate matrix to the fluoride-selective electrode, F⁻ release was analyzed by ion chromatography. Degradation of parent PFAS was analyzed by liquid chromatography–quadrupole time-of-flight mass spectrometer (LC–QToF-MS). Details of instrumental analyses are described below.

Fluoride Ion Analysis

Fluoride concentration in each sample was analyzed by a Dionex ICS-5000 ion chromatography system with a conductivity detector (see Figure 3.4 for representative chromatograms). The reaction solution contains orders of magnitude higher concentrations of chloride, citrate, and carbonate (from Ti^{III} -citrate solution) than the fluoride released from PFASs. To eliminate the matrix effect on F^- quantification, NaF standards were also prepared in the reaction mixture containing Ti^{III} -citrate and B_{12} but no PFASs. Prior to IC analysis, both NaF standards and reaction samples were exposed to air and diluted with DI water for 100 fold. To separate the F^- peak from the known ions and unknown species in the reaction matrix, the following parameters were used:

Column: Dionex IonPac AS11-HC Analytical 4×250mm. Temperature: 30°C.
Flow rate: 1 mL min⁻¹. Suppressor type and current: AERS_4mm; 50mA.

Eluent gradient was generated with the mixing of 20 mM NaOH with Milli-Q water:

0-1 min: 5% NaOH.
1-25 min: 5%-42.5% NaOH (slope=0.3125 mM/min).
25-28 min: 42.5%-65% NaOH (slope=0.375 mM/min)
28-40 min: 65% 20mM NaOH.
40-45 min: 65%-5% NaOH.
45-65 min: 5% NaOH.

LC-QToF-MS Analysis

[¹³C₂]perfluorohexanoic acid ([¹³C₂]PFHxA), [¹³C₄]perfluorooctanoic acid ([¹³C₄]PFOA), [¹³C₅]perfluorononanoic acid ([¹³C₅]PFNA), and [¹³C₂]perfluorodecanoic acid ([¹³C₂]PFDA) were purchased from Wellington Laboratories (Ontario, Canada). Ammonium acetate (Optima LC/MS grade), ammonium hydroxide (Optima grade), methanol (Optima LC/MS grade), isopropanol (Optima LC/MS grade) and water (Optima LC/MS grade) were obtained from Fisher Scientific (Hampton, New Hampshire). Prior to analysis, samples were diluted 100- to 10,000-fold with a solution containing internal standards, methanol, isopropanol, and dilute ammonium hydroxide. The prepared sample solutions were then vortexed, centrifuged at 4,000 rpm for 10 minutes, and the supernatant fractions were collected for analysis. Target analytes (Compounds 1, 2, 3, and 7) and internal standards ([¹³C₂]PFHxA, [¹³C₄]PFOA], and [¹³C₂]PFDA) were quantified by liquid chromatography-high resolution mass spectrometry with a Sciex (Framingham, MA) Exion LC coupled to a Sciex X500R QTOF-MS via an electrospray source with an applied voltage of -4500 V. The source temperature was 550 °C. Mass spectra were collected over 100–1200 *m/z*, the collision energy was -5 V, the spectra accumulation time was 0.2 s, and the scan time was 0.842 s. Details of analyte and internal standard detection by QTOF-MS are shown in Table 3.4.2.

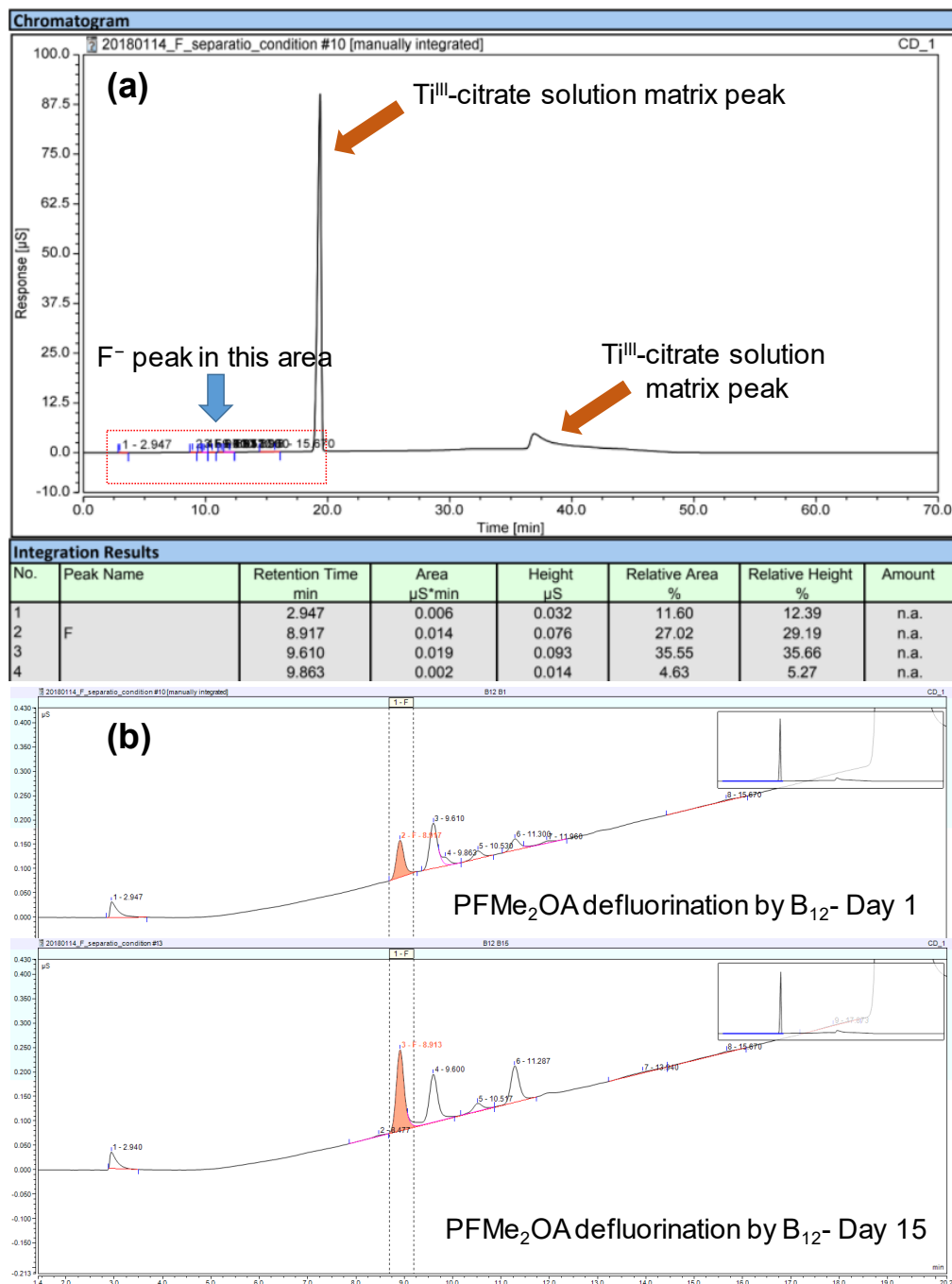


Figure 3.4. Representative IC chromatograms showing **(a)** all peaks detected during the full elution period (70 min), and **(b)** zoomed-in area (1.4–20.2 min) containing the F⁻ peak at 8.9 min.

Table 3.4.2. QTOF-MS parameters for the detection of analyte and internal standard compounds.

	1	2 (low range)	2	3	7
Formula:	C ₁₀ F ₁₉ O ₂ H	C ₆ F ₉ O ₂ H	C ₆ F ₉ O ₂ H	C ₇ F ₁₁ O ₂ H	C ₈ F ₁₅ O ₂ H
m/z:	512.96004	274.97601	274.97601	324.97281	412.96643
XIC width (Da):	0.00256	0.00137	0.00137	0.00162	0.00206
Average Retention Time (min):	10.30	7.38	7.38	7.92	9.29
Internal Standard:	[¹³ C ₂]PFDA	[¹³ C ₂]PFHxA	[¹³ C ₂]PFHxA	[¹³ C ₂]PFHxA	[¹³ C ₄]PFOA
Internal Standard m/z:	514.96675	314.97952	314.97952	314.97952	416.97984
Internal Standard XIC width (Da):	0.00131	0.00131	0.00131	0.00131	0.00131
Int. Std. Ave. Ret. Time (min):	10.44	7.81	7.81	7.81	9.30

Chromatographic separations were performed with a Phenomenex (Torrance, CA) Gemini C18 (100 x 3 mm, 5 μm) analytical column, which was preceded by a Phenomenex Gemini C18 guard column (4 x 2 mm) and two Agilent (Santa Clara, CA) Zorbax Diol guard columns (4.6 x 12.5 mm, 6 μm). Analytical and guard columns were maintained at 40°C during analysis. A binary gradient elution was used for separations with a 20 mM ammonium acetate aqueous phase (A) and a methanol solvent phase (B). The mobile phase flow rate was 600 μL / min and 1000 μL of prepared sample solution was injected with each run. Example extracted ion chromatograms of analyte and internal standard compounds are shown in Figure 3.5. External calibrations for analyte compound were determined as 1/x²-weighted linear regressions, with standards prepared in reaction matrix solutions (0.25 mM cobalt catalyst, ~32 mM Ti^{III}, and ~40 mM carbonate buffer at pH 9.0) that were diluted identically to samples. Calibrations were determined based on internal standard-corrected peak areas, and information about sample dilution and calibration regressions is shown in Table 3.4.3.

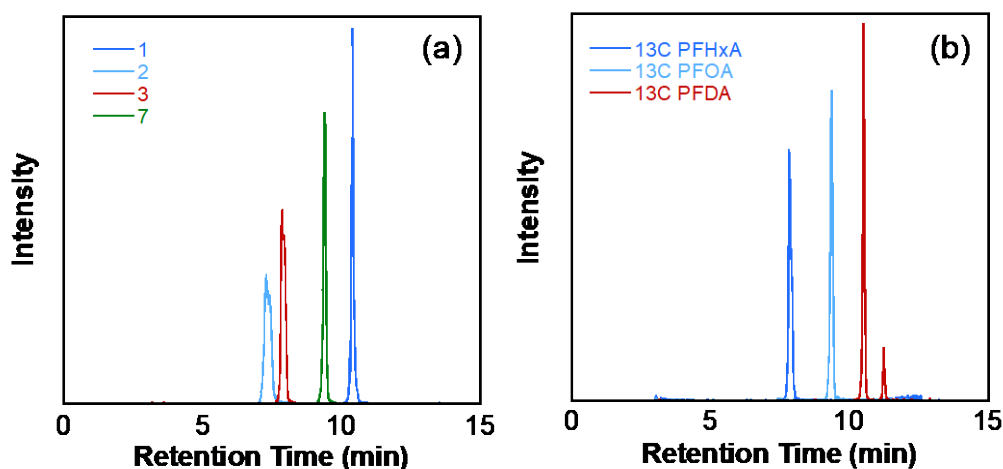


Figure 3.4.3. Extracted MS-detected ion chromatograms of (a) analyte compounds and (b) internal standard compounds.

Table 3.4.3. Summary of LC-QToF calibration regressions.

	Me ₂ PFOA	C=C (low range)	C=C	cyclo-COOH	n-PFOA
Sample Dilutions:	1000	10	10	10	1000
Linear Range (μM):	0.3 - 10	0.001 - 0.1	0.1 - 1.0	0.1 - 10	0.1 - 10
R²:	0.958	0.979	0.995	0.998	0.988

C–F bond dissociation energy (BDE) calculation

Bond dissociation energies (BDEs) of C–F bonds in PFAS structures (anion for carboxylic acids) were calculated using Grimme’s GD3-BJ empirical dispersion corrected hybrid density functional theory (DFT) at the B3LYP/6-311+G(2d,2p) level of theory (Becke 1993; Grimm et al., 2011; Lee et al., 1988; Stephens et al., 1994; Vosko et al., 1980). Truhlar’s SMD solvent model was chosen to implicitly model the aqueous environment (Marenich et al., 2009). The BDE for each bond was calculated through Eq. (1):

$$BDE = (H_{radical [PFAS\ minus\ F]}^* + H_{radical\ F}^*) - H_{parent\ PFAS}^* \quad (1)$$

where H^* represents the enthalpy of formation.

3.5 UV-Sulfite Treatment Studies

Chemicals.

All chemicals used for UV-sulfite experiments were reagent grade and were used as received from the vendors. An AFFF concentrate (labeled 1999 era 3M Lightwater Alcohol Resistant (AR)-AFFF) was obtained as a gift from CH2M Hill. Analysis shows it to be a mix of different AFFF source materials since PFAS structures consistent with both 3M-based and fluorotelomer-based industrial processes were detected in the mixture. Sodium sulfite (Sigma-Aldrich, ≥98%), sodium bicarbonate (Macron, ACS grade), sodium hydroxide (Fisher, 1N), hydrochloric acid (Fluka, 1N) sodium phosphate monobasic dihydrate (Sigma-Aldrich, ≥99%), 5,5'-Dithio-bis(2-nitrobenzoic acid) (Sigma-Aldrich, 99%), total ionic strength adjustment buffer concentrate (Fisher), potassium iodide (Alfa Aesar, 99%), sodium iodate (Fisher, certified), boric acid (Sigma Aldrich, 99.97%), hydrogen peroxide (Sigma Aldrich, 30 wt. %), ammonium molybdate tetrahydrate (Alfa Aesar, ACS grade), potassium hydrogen phthalate (Sigma Aldrich, ACS), sodium persulfate (Sigma Aldrich, ≥98%), deuterium oxide (Sigma Aldrich, 99.9 atom % D), sodium trifluoroacetate (Sigma Aldrich, 98%), sodium trifluoromethane sulfonate (Sigma Aldrich, 98%), sodium pentafluoropropionate (Sigma Aldrich, 98%), PFOS (Sigma Aldrich, ~40% in H₂O (T)), perfluorohexane sulfonate (PFHxS) (Wellington Laboratories, ≥98%), PFOA (Sigma Aldrich, 96%), sodium fluoride (Sigma Aldrich, ≥99%), perfluorooctanesulfonamidoacetic acid (FOSAA) (Wellington Laboratories, ≥98%), ammonium hydroxide (Fisher, Optima grade), ammonium acetate (Fisher, Optima grade), methanol (Fisher, Optima LC/MS grade), isopropanol (Fisher, Optima LC/MS grade). All solutions were prepared in the laboratory using DI water. Table

3.4.4. provides a list of PFAS standards and isotopically labeled standards used for PFAS quantification.

Table 3.4.4. List of targeted compounds and mass-labeled internal standards used for PFAS analysis and quantification.

PFAS native	Mass-labeled internal standard
2H-Perfluoro-2-octenoic acid (6:2)	2-Perfluorohexyl-[1,2- ¹³ C ₂]-ethanoic acid (6:2)
2H-Perfluoro-2-decenoic acid (8:2)	2-Perfluorooctyl-[1,2- ¹³ C ₂]-ethanoic acid (8:2)
2H-Perfluoro-2-dodecenoic acid (10:2)	2-Perfluorodecyl-[1,2- ¹³ C ₂]-ethanoic acid (10:2)
Perfluoro-n-butanoic acid	Perfluoro-n-[¹³ C ₄]butanoic acid
Perfluoro-n-pentanoic acid	Perfluoro-n-[¹³ C ₅]pentanoic acid
Perfluoro-n-hexanoic acid	Perfluoro-n-[1,2- ¹³ C ₂]hexanoic acid
Perfluoro-n-heptanoic acid	Perfluoro-n-[1,2,3,4- ¹³ C ₄]heptanoic acid
Perfluoro-n-octanoic acid	Perfluoro-n-[1,2,3,4- ¹³ C ₄]octanoic acid
Perfluoro-n-nonanoic acid	Perfluoro-n-[1,2,3,4,5- ¹³ C ₅]nonanoic acid
Perfluoro-n-decanoic acid	Perfluoro-n-[1,2- ¹³ C ₂]decanoic acid
Perfluoro-n-undecanoic acid	Perfluoro-n-[1,2- ¹³ C ₂]undecanoic acid
Perfluoro-n-dodecanoic acid	Perfluoro-n-[1,2- ¹³ C ₂]dodecanoic acid
Perfluoro-n-tridecanoic acid	Perfluoro-n-[1,2-¹³C₂]tetradecanoic acid
Perfluoro-n-tetradecanoic acid	Perfluoro-n-[1,2- ¹³ C ₂]tetradecanoic acid
3-Perfluoropropyl propanoic acid (3:3)	2-Perfluorohexyl-[1,2-¹³C₂]-ethanoic acid (6:2)
3-Perfluoropentyl propanoic acid (5:3)	2-Perfluorooctyl-[1,2-¹³C₂]-ethanoic acid (8:2)
3-Perfluoroheptyl propanoic acid (7:3)	2-Perfluorodecyl-[1,2-¹³C₂]-ethanoic acid (10:2)
Sodium 1H,1H,2H,2H-perfluorohexane sulfonate (4:2)	Sodium 1H,1H,2H,2H-perfluoro-1-[1,2- ¹³ C ₂]-hexane sulfonate (4:2)
Perfluoro-1-octanesulfonamide	Perfluoro-1-[¹³ C ₈]octanesulfonamide (in isopropanol)
N-methylperfluoro-1-octanesulfonamide	N-methyl-d ₃ -perfluoro-1-octanesulfonamide
N-ethylperfluoro-1-octanesulfonamide	N-ethyl-d ₅ -perfluoro-1-octanesulfonamide
Perfluoro-1-octanesulfonamidoacetic acid	N-methyl-d₃-perfluoro-1-octanesulfonamidoacetic acid
Sodium 8-chloroperfluoro-1-octanesulfonate	Sodium perfluoro-1-[1,2,3,4-¹³C₄]octanesulfonate
Sodium 1H,1H,2H,2H-perfluorohexane sulfonate (6:2)	Perfluoro-n-[1,2,3,4-¹³C₄]octanoic acid (PFOA [M+4])
Sodium 1H,1H,2H,2H-perfluorohexane sulfonate (8:2)	Sodium 1H,1H,2H,2H-perfluoro-1-[1,2- ¹³ C ₂]-hexane sulfonate (8:2)
Perfluoro-n-hexadecanoic acid	Perfluoro-n-[1,2- ¹³ C ₂]hexadecanoic acid
Perfluoro-n-octadecanoic acid	Perfluoro-n-[1,2-¹³C₂]hexadecanoic acid
N-methylperfluoro-1-octanesulfonamidoacetic acid	N-methyl-d ₃ -perfluoro-1-octanesulfonamidoacetic acid
N-ethylperfluoro-1-octanesulfonamidoacetic acid	N-ethyl-d ₅ -perfluoro-1-octanesulfonamidoacetic acid
2H-Perfluoro-2-octenoic acid (6:2)	2H-Perfluoro-[1,2- ¹³ C ₂]-2-octenoic acid
2H-Perfluoro-2-decenoic acid (8:2)	2H-Perfluoro-[1,2- ¹³ C ₂]-2-decenoic acid
2H-Perfluoro-2-dodecenoic acid (10:2)	2H-Perfluoro-[1,2- ¹³ C ₂]-2-dodecenoic acid
Sodium 1H,1H,2H,2H-perfluorohexane sulfonate (10:2)	Sodium 1H,1H,2H,2H-perfluoro-1-[1,2-¹³C₃]-hexane sulfonate (8:2)
Sodium perfluoro-1-propanesulfonate	Sodium perfluoro-1-[2,3,4-¹³C₃]-butanesulfonate
Potassium perfluoro-1-butanesulfonate	Sodium perfluoro-1-[2,3,4- ¹³ C ₃]-butanesulfonate
L-PFHxS with branched isomers (Potassium Salt)	Sodium perfluoro-1-hexane[¹⁸ O ₂]sulfonate
Sodium perfluoro-1-heptanesulfonate	Sodium perfluoro-1-hexane[¹⁸O₂]sulfonate
Sodium perfluoro-1-nonanesulfonate	Sodium perfluoro-1-[1,2,3,4-¹³C₄]octanesulfonate
Sodium perfluoro-1-decanesulfonate	Sodium perfluoro-1-[1,2,3,4-¹³C₄]octanesulfonate
Sodium perfluoro-1-dodecanesulfonate	Sodium perfluoro-1-[1,2,3,4-¹³C₄]octanesulfonate
Sodium perfluoro-1-pentanesulfonate	Sodium perfluoro-1-[1,2,3,4-¹³C₄]octanesulfonate
Potassium perfluorooctanesulfonate (Technical Grade)	Sodium perfluoro-1-[1,2,3,4-¹³C₄]octanesulfonate
Potassium 9-chlorohexadecafluoro-3-oxanonane-1-sulfonate	NA
Potassium 11-chloroeicosafluoro-3-oxaundecane-1-sulfonate	NA

Photoreactor. A glass photoreactor (7864-10, Ace Glass) with external cooling jacket and an internal jacketed lamp immersion well (quartz, 7874-38, Ace Glass) was filled with 575 mL reaction solution during each experiment (Figure 3.6). Irradiation of solution was accomplished using an 18 W low pressure Hg UV lamp (GPH212T5L/4P/HO, Norman Lamps) irradiating at 254 nm. Photon flux was measured to be $2.2 \pm 0.5 \times 10^{-6} \text{ E} \cdot \text{s}^{-1}$. The effective pathlength of the UV light was determined to be $2.85 \pm 0.03 \text{ cm}$. The average photon fluence rate was found to be $1.0 \times 10^{-8} \pm 3.3 \times 10^{-11} \text{ E} \cdot \text{s}^{-1} \cdot \text{cm}^{-2}$. These parameters were all determined using established methods (Li et al., 2012; Rahn, 1997). KI/KIO₃ actinometry was used to determine photon flux (Li et al., 2012). Eq. 3.1 was used to calculate photon flux.

$$I_0 = [I_3^-] \frac{1}{t} V \frac{1}{\Phi_{I_3^-}} \quad (3.1)$$

Where I_0 is the photon flux ($\text{E} \cdot \text{s}^{-1}$), $[I_3^-]$ = the triiodide concentration (M), t is the time in seconds, V is the reactor volume in liters, and $\Phi_{I_3^-}$ is the quantum yield for I_3^- formation (Rahn, 1997). The slope obtained from plotting $[I_3^-]$ versus time (i.e., slope = $I_0 \cdot V \cdot \Phi_{I_3^-}^{-1}$; Figure 3.7) was used to calculate the photon flux, I_0 . The photon flux for reactors used in this study was $2.2 \pm 0.5 \times 10^{-6} \text{ E} \cdot \text{s}^{-1}$.



Figure 3.6. Photograph of photoreactor setup with 18 W UV LP Hg lamp.

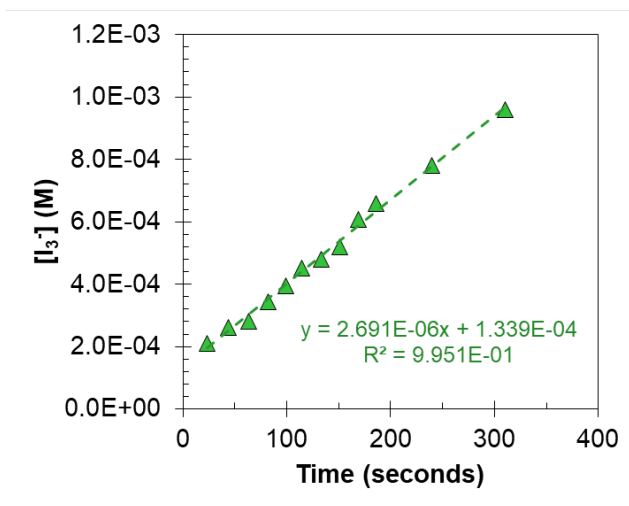


Figure 3.7. Example of I_3^- generation during UV_{254} irradiation of the KI/ KIO_3 actinometer.

The effective path length, an estimate of the path length that light takes that accounts for reactor geometry, was determined using H_2O_2 photolysis (Li et al., 2012). H_2O_2 was measured by

spectrophotometry using the I_3^- approach (Klassen et al., 1994). The I_3^- concentration was calculated using Beer-Lambert law (eq. 3.2).

$$A_{352} = \varepsilon_{I_3^-} l d [H_2O_2] \quad (3.2)$$

where A_{352} is the measured absorbance at 352 nm, ε is the molar extinction coefficient for I_3^- ($26,400 \text{ M}^{-1} \cdot \text{cm}^{-1}$), l is the path length of the cuvette (1 cm), d is the dilution factor, and $[H_2O_2]$ is the molar concentration of H_2O_2 . The concentration of H_2O_2 during UV_{254} irradiation is presented in Figure 3.8.

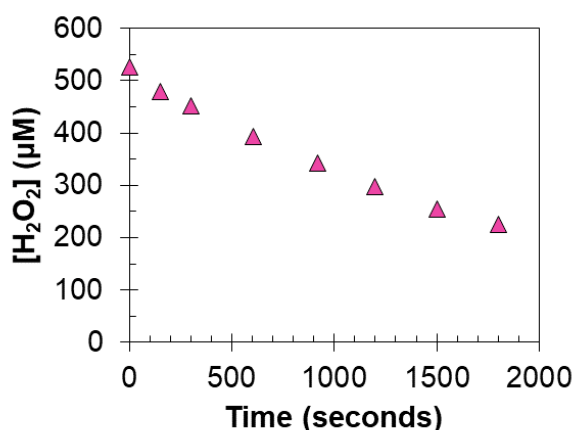


Figure 3.8. Example of the photolysis of H_2O_2 throughout UV_{254} irradiation. Reaction conditions: $[H_2O_2]_0 \sim 500 \mu\text{M}$, light source = 18 W UV LP Hg lamp.

At low H_2O_2 absorbance, photolysis follows first-order kinetics (Li et al., 2012).

$$\frac{d[H_2O_2]}{dt} = \left(\frac{-2.303 \varepsilon_{H_2O_2} z_{eff} I_0 \Phi_{H_2O_2}}{V} \right) [H_2O_2] \quad (3.3)$$

where $[H_2O_2]$ is the H_2O_2 concentration (M), $\varepsilon_{H_2O_2}$ is the H_2O_2 absorption coefficient ($\text{M}^{-1} \cdot \text{cm}^{-1}$), z_{eff} is the effective pathlength (cm), I_0 is the photon flux ($\text{E} \cdot \text{s}^{-1}$), V is the solution volume (L), and $\Phi_{H_2O_2}$ is the H_2O_2 photolysis quantum yield ($1 \text{ mol} \cdot \text{E}^{-1}$). After rearranging and integrating eq. 3.4:

$$\ln \frac{[H_2O_2]}{[H_2O_2]_0} = \left(\frac{-2.303 \varepsilon_{H_2O_2} z_{eff} I_0 \Phi_{H_2O_2}}{V} \right) t \quad (3.4)$$

By plotting $\ln[H_2O_2]/[H_2O_2]_0$ versus time, a slope can be obtained which is defined as follows.

$$\text{slope} = \left(\frac{-2.303 \varepsilon_{H_2O_2} z_{eff} I_0 \Phi_{H_2O_2}}{V} \right) \quad (3.5)$$

Solving for z_{eff} yields the effective path length value. An effective path length of 2.85 ± 0.03 was calculated for reactors used in this study.

As described in Li et al., 2012, the photolysis of H_2O_2 in a dilute solution can also be expressed as follows (Li et al., 2012).

$$\frac{d[\text{H}_2\text{O}_2]}{dt} = -2.303 \varepsilon_{\text{H}_2\text{O}_2} \Phi_{\text{H}_2\text{O}_2} [\text{H}_2\text{O}_2] I_s \quad (3.6)$$

where A_{irr} is the irradiated area (cm^2), L_{irr} is the path length (cm), V_{irr} is the volume of irradiated solution (L), $[\text{H}_2\text{O}_2]$ is the H_2O_2 molar concentration, $\varepsilon_{\text{H}_2\text{O}_2}$ is the molar absorption coefficient of H_2O_2 ($19.6 \text{ M}^{-1}\cdot\text{cm}^{-1}$), $\Phi_{\text{H}_2\text{O}_2}$ is the H_2O_2 photolysis quantum yield ($1 \text{ mol}\cdot\text{E}^{-1}$), and I_s is the apparent incident intensity ($\text{E}\cdot\text{s}^{-1}\cdot\text{cm}^{-2}$) and is defined as follows.

$$I_s = \frac{I_{\text{irr}} A_{\text{irr}} L_{\text{irr}}}{1000 V_{\text{irr}}} \quad (3.7)$$

where I_{irr} is the incident intensity ($\text{E}\cdot\text{s}^{-1}\cdot\text{cm}^{-2}$) and for a collimated beam, I_s is the I_{irr} ; for non-collimated beam conditions, and I_s is the apparent incident intensity. The average photon fluence rate measured for reactors used in this study was $1.0 \times 10^{-8} \pm 3.3 \times 10^{-11} \text{ E}\cdot\text{s}^{-1}\cdot\text{cm}^{-2}$.

Batch Photoreactions

Sodium sulfite (Na_2SO_3) was used as a photosensitizer to generate hydrated electrons in solutions. Sodium bicarbonate (5 mM) was used as a pH buffer (pH 9.5). The temperature of the reaction solutions were held constant at 20°C (circulating water bath; Isotemp, Fisher). Solutions were deoxygenated prior to initiating batch reactions by continuous sparging with $\text{N}_{2(\text{g})}$ (99%) for 1 h before spiking in the AFFF concentrate to initiate reactions. A low rate of $\text{N}_{2(\text{g})}$ flow was maintained throughout the experiment to eliminate oxygen intrusion into the reactor. Samples were taken at regular time intervals and refrigerated (4°C) prior to analysis. Duplicate experiments were performed for all conditions and uncertainties and min/max values observed are reported as the uncertainties. For most reactions, AFFF was diluted 60,000-fold into solutions to achieve initial PFAS concentrations similar to those measured in AFFF-impacted groundwater (on the order of 10^{-2} - $10^2 \mu\text{g}\cdot\text{L}^{-1}$) (Hu et al., 2016; Moody et al., 2003). A high level of dilution was also required because separate UV-only controls (i.e., no sulfite added) conducted with AFFF diluted 1-to-600 and 1-to-6,000 showed considerable self-photosensitization of reactive species (including e_{aq}^-) by AFFF itself. Such reactions are not expected to be important at environmentally relevant AFFF concentrations, so results discussed here are limited to experiments conducted at higher levels of AFFF dilution (i.e., 1-to-60,000).

Analytical

Optical UV-vis absorbance was measured for sulfite and diluted AFFF solutions using a DU 800 spectrophotometer (Beckman Coulter). Concentrations of sulfite were determined using

a modified spectrophotometric method, wherein sulfite reacts with 5,5'-dithiobis (2-nitrobenzoic acid) (DTNB) to form a thiol product with maximum absorbance at 412 nm. Fluoride concentrations were determined by ion selective electrode measurement using a fluoride ion-specific electrode (Fisher Accumet) coupled with a pH/ISE meter (Orion Versa Star). To verify fluoride concentrations, measurements of NaF spikes ranging of 0.1 - 1.5 mg-F·L⁻¹ were taken for a sample collected after 49 h of reaction (Figure 3.9). Matrix spikes validated measurement indicating that fluoride can be measured under these specific background matrix conditions. Dissolved oxygen (DO) concentrations were measured using a polarographic-type DO meter (SPER Scientific). These measurements indicated that sparging with nitrogen gas and addition of sulfite were sufficient to suppress DO concentrations <1 mg·L⁻¹.

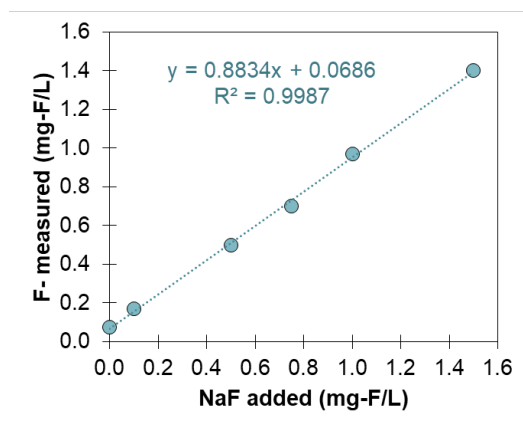


Figure 3.9. Comparison of sodium fluoride added and fluoride release measured.

Quantitative ¹⁹F NMR (500 MHz JEOL ECA-500 spectrometer) was used to estimate the total fluorine concentration in the AFFF mixture used in experiments (described above). A single pulse experiment was performed using automatic gain and deuterium oxide (D₂O) solvent. The acquisition parameters were set as follows: 0 ppm center frequency with a sweep width of 400 ppm, 16,384 data points, 32 scans, and 87.03 millisecond acquisition time. Pulse settings were as follows: 45° pulse, 7.4 μs pulse width, and 5 sec relaxation delay. Samples were processed using JEOL Delta NMR software (version 5.1.3). Sodium trifluoroacetate was used as an internal standard because initial test spectra showed that its chemical shift (-75.4 ppm) did not interfere with signals of chemicals in the AFFF sample. Amended samples contained water sample (50%, v/v), D₂O (50%, v/v), and sodium trifluoroacetate (0.025 mol-F·L⁻¹). A 0.7 mL aliquot of amended sample was transferred to NMR tubes (5 mm O.D., 7", Wilmad) for analysis. Total fluorine calculations were calculated using the eq. 3.8.

$$[Total F] = \frac{\sum Area_{sample}}{Area_{IS}} [IS] d \quad (3.8)$$

where [Total F] is the total molar fluorine concentration in sample, $\text{Area}_{\text{sample}}$ = sum of peak areas associated with fluorine from the sample, Area_{IS} = peak area associated with fluorine from the internal standard, [IS] = internal standard concentration ($\text{mol}\cdot\text{F}\cdot\text{L}^{-1}$), and d = dilution factor. To verify the quantitative method, the total fluorine concentrations of separately prepared solutions containing PFOA ($0.15 \text{ mol}\cdot\text{F}\cdot\text{L}^{-1}$), NaF ($0.5 \text{ mol}\cdot\text{F}\cdot\text{L}^{-1}$), and a PFAS mixture ($0.063 \text{ mol}\cdot\text{F}\cdot\text{L}^{-1}$ sodium trifluoromethane sulfonate, $0.063 \text{ mol}\cdot\text{F}\cdot\text{L}^{-1}$ sodium pentafluoropropionate, and $0.063 \text{ mol}\cdot\text{F}\cdot\text{L}^{-1}$ PFOA) were measured using sodium trifluoroacetate as an internal standard. An example of the ^{19}F NMR spectra for PFOA is shown in Figure 3.10.

To determine the total fluorine concentration in AFFF, AFFF was diluted 1-to-5 in DI water together with D_2O and sodium trifluoroacetate. 0.7 mL aliquots were then transferred to an NMR tube for analysis; the ^{19}F NMR spectra for the AFFF mixture used in this study is shown below (Figure 3.11).

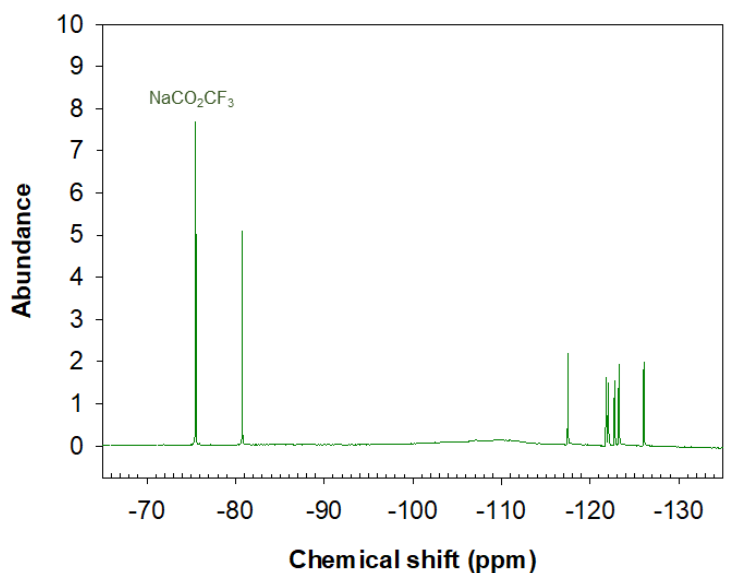


Figure 3.10. ^{19}F NMR spectra for PFOA. The peak for the internal standard sodium trifluoroacetate is labeled for reference (NaCO_2CF_3). In the NMR tube, 0.7 mL of amended sample contained: $0.05 \text{ mg}\cdot\text{F}\cdot\text{L}^{-1}$ PFOA and $0.025 \text{ mg}\cdot\text{F}\cdot\text{L}^{-1}$ sodium trifluoroacetate in water (50%, v/v) and D_2O (50%, v/v).

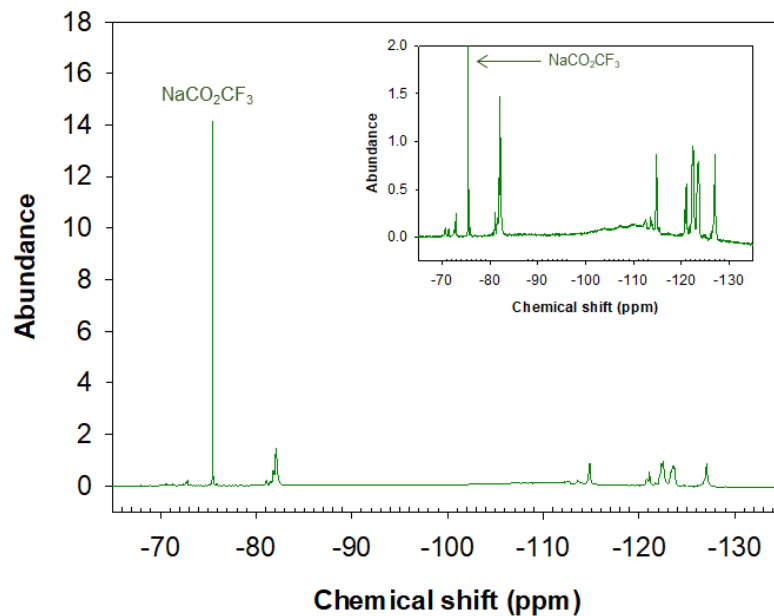


Figure 3.11. ^{19}F NMR spectra for a AFFF diluted 1-to-5. The peak for the internal standard sodium trifluoroacetate is labeled for reference (NaCO_2CF_3). In the NMR tube, 0.7 mL of amended sample contained: AFFF diluted 1-to-5 and $0.025 \text{ mg}\cdot\text{F}\cdot\text{L}^{-1}$ sodium trifluoroacetate in water (50%, v/v) and D_2O (50%, v/v). The insert shows the ^{19}F NMR spectra on a smaller y-axis scale.

Samples were also analyzed using the total oxidizable precursor (TOP) assay, modified from the method reported by Houtz and Sedlak, 2012 and Houtz et al., 2013 (Houtz et al., 2013; Houtz and Sedlak, 2012). Briefly, two solutions (100 mL) were prepared in duplicate (100 mL glass storage). One of the two solutions was subjected to the TOP assay reaction conditions and the other was prepared as a control. The solution undergoing the TOP assay was spiked with AFFF diluted 60,000-fold together with 60 mM sodium persulfate and 150 mM NaOH. The control solution contained AFFF 30 mM NaOH, but no sodium persulfate. The lower NaOH concentration in the control was added to yield the same final pH as the sample subjected to the TOP assay conditions ($\text{pH} > 12$). The TOP assay replicate was placed in a temperature controlled oven ($85 \pm 2 \text{ }^\circ\text{C}$) for 6 h, whereas the control solutions were covered in foil and placed on the benchtop for the same time period. After reaction, solutions were cooled to ambient temperature, and then samples were collected from both reactors and refrigerated at $4 \text{ }^\circ\text{C}$ until LC-QTOF-MS analysis. Samples were diluted to the applicable calibration range and neutralized to $\text{pH} 5 - 9$ before analysis.

Gas chromatography with tandem mass spectrometry analysis (GC-MS/MS) was used measure gaseous products (Thermo, TSQ 8000 EVO) that were recovered from reactor headspace on solid phase microextraction (SPME) fibers (polydimethylsiloxane/divinylbenzene, StableFlex, Sigma Aldrich). The SPME fiber holder (Sigma Aldrich) loaded with PDMS/DVB fiber was

inserted into the programmed temperature vaporizing injector (PTV) of the gas chromatograph (Thermo Scientific Trace 1310). The chromatographic method used He as carrier gas at 1.0 mL/min. The oven temperature was programmed to hold constant for the first 3 min at 60 °C before ramping up to 320 °C (15 °C/min) and then holding constant for 5 min. Splitless flow was used with a 5 mL/min purge flow rate. Gases from the GC column were transferred to the mass spectrometer (TSQ 8000 Evo triple quadrupole using electron impact ionization with source temperature set to 250 °C).

UV-Sulfite Treatment of AFFF-Impacted Groundwater

Groundwater samples were collected from Fountain, CO, Ellsworth Air Force Base (Rapid City, SD), and two wells in Peterson Air Force Base (Colorado Springs, CO). To prepare groundwaters for water quality analysis and UV-sulfite treatment experiments, pH was adjusted to pH = 11 with NaOH and left on the bench overnight to allow for precipitation and settling. Then samples were filtered using a 0.7 µm glass fiber filter. Filtrate was collected and adjusted to pH = 9.5 and stored at 4 °C before experiments. Groundwaters were characterized for total organic carbon (TOC) and total organic nitrogen (TON) by a TOC/TON analyzer, elemental analysis was performed by inductively coupled plasma atomic emission spectroscopy (ICP-AES), and anions were analyzed by ion chromatography (IC). UV-sulfite treatment of groundwaters was similar to experiments using dilute AFFF. 575 mL of groundwater was adjusted to pH = 9.5 prior to experiments due to pH drifting during storage. The groundwater was sparged for 1 h with nitrogen gas (N_{2(g)}) before spiking with sulfite. A sulfite dose of 10 mM was used in all groundwater experiments. Because groundwaters were impacted by AFFF, no AFFF spikes were added to groundwaters.

LC-QTOF-MS Analysis

LC-QToF-MS was used to measure concentrations of 44 PFAS (i.e., targeted analysis) and conduct suspect screening analysis of a larger XIC list. Individual samples were prepared in 15 mL centrifuge tubes. Samples were diluted to maintain concentrations within the calibration range (0.07 - 7,400 ng·L⁻¹ PFAS concentrations; 0.1 - 10,000 pg of analyte per 1.35 mL amended sample) and adjusted to pH = 5 - 9. Samples were amended with isotopically-labeled internal standards, NH₄OH, isopropanol and methanol. For any given volume in the centrifuge tube, the solutions were composed of: 0.638 (v/v) water, 0.033 (v/v) NH₄OH (1 mM), 0.096 (v/v) isopropanol, 0.037 (v/v) internal standards in methanol, and 0.196 (v/v) methanol. After sample amendments, centrifuge tubes were vortexed for 5 sec and then centrifuged at 4000 rpm for 10 min. Centrifuged aliquots were then transferred to HPLC vials containing 1.35 mL of volume composed of: 861 µL of water sample, 45 µL NH₄OH (1 mM), 130 µL of isopropanol, 50 µL of internal standards in methanol, and 264 µL of methanol. Samples were then refrigerated until analyzed.

One mL sample was injected (SCIEX ExionLC system) through a series of columns consisting of a guard column (SecurityGuard), two guard cartridges (6 μm , 4.6 \times 12.5 mm, ZORBAX Diol, Agilent), and a C18 analytical column (5 μm , 150 \times 4.6 mm, Gemini, Phenomenex). Analytes were separated using a gradient method with 0.6 mL \cdot min⁻¹ flow rate. The mobile phase was 90% 20 mM ammonium acetate (Fisher, Optima; mobile phase A) and 10% methanol (Fisher, Optima LC/MS; mobile phase B) from 0 - 0.5 min, 50% A and 50% B from 0.5 - 8 min, 1% A and 99% B from 8 - 13 min, and 90% A and 10% B from 13 - 20 min. The column temperature was 40 °C.

High resolution mass spectra were collected using a SCIEX X500R QToF in electrospray ionization (ESI) negative mode. The ion source was TurbolonSpray, the curtain gas was set to 35, ion source gas 1 was set to 60 psi, ion source gas 2 was set to 60 psi, and the source temperature was set to 550 °C. A SWATH acquisition method was used in LC-QTOF-MS analysis in negative ion mode with ionspray voltage set to -4500 V and collision-activated dissociation gas was set to 10. For targeted compound analysis, calibration data was prepared at the following concentrations: 0.1, 0.5, 1, 2, 5, 10, 20, 50, 100, 200, 500, 1000, 2000, 5000, 10,000 pg analyte per 1.35 mL. All calibration standards were amended with 100 pg of isotopically-labeled internal standards. The full list of analytes and mass-labeled internal standards used are listed in Table 3.4. A quality control standard (QC), laboratory blank (LB), and double blank (DB) were run every 10 samples. QCs contained a mid-range PFAS standard (300 pg of analyte in 1.35 mL) and mass-labeled internal standards. A negative ion mode autocalibration solution (SCIEX) was used to autocalibrate the instrument every 5 injections.

Data acquisition and processing was performed using SCIEX OS version 1.3. Targeted analytes were identified by comparing retention time, mass error, isotope ratios, and MS/MS information with internal standards. Only calibration curves with $R^2 \geq 0.97$ ($1 \cdot x^{-2}$ weighting) were used for quantification. Additionally, only samples with a 70 - 130% mass-labeled internal standard recovery were reported. SCIEX OS version 1.3 was used for data acquisition and processing to identify PFAS for which no standards were available by screening against an XIC list and MS/MS library. As an initial selection process, only samples before ($t = 0$ h) and after ($t = 49$ h) UV-sulfite reaction were screened for PFASs. Only PFASs with peak areas $> 1 \times 10^5$ were considered; Only PFASs with retention times > 5 min were considered. PFASs were then screened using the following criteria: mass error (ppm), isotope ratio difference, and library hit score. 48 PFASs were detected using this selection process.

3.6 PFAS Analytical and Development of PFAS Libraries

The prevalence of PFAS in the environment, coupled with their recalcitrance and potential toxicity, necessitates development of tools capable of identifying PFAS with speed and accuracy. While the majority of research has been focused on perfluoroalkyl sulfonates (PFASs, including PFOS) and perfluoroalkyl carboxylic acids (PFCAs, including PFOA), recent research has shown that AFFF formulations, a major source of PFASs, contain many other classes of these compounds (Barzen-Hanson et al., 2017; Place and Field, 2012). In recent years, more attention has been paid to these novel PFASs and their transformation products, comprising hundreds of fluorinated compounds with different functional groups. Many novel PFAS have not been extensively studied, as some have only been discovered in the past few years, and more are still in the process of being discovered through non-target analysis. The identification of novel PFAS is critical to further our understanding of the full extent of PFAS contamination at impacted sites, as well as the fate, transport, and transformation of PFASs in the environment. The objective of this task was to catalogue the large number of AFFF-associated novel PFASs being discovered in AFFF products and at AFFF-impacted sites, and to create an extensive extracted ion chromatogram (XIC) list and high-resolution mass spectrometry (HRMS) fragmentation library to enable the rapid identification of these compounds in environmental samples.

Methodology

Extracted Ion Chromatogram (XIC) List. An extensive literature review was conducted to develop a list of all AFFF-associated PFAS currently identified in AFFF products and AFFF-impacted environmental samples. Information catalogued for each compound included the compound name, acronym, chain length, neutral formula, neutral mass, expected ionization (positive or negative), any historical names and acronyms from literature, classes to which the compound belongs, and a list of papers where the compound class has been described. PFAS classes, or homologous series, reported in literature were extrapolated to include additional theoretical homologues within the appropriate carbon chain-length range (generally C2 – C12). Any theoretical homologues not observed in any samples were flagged as “inferred.” At the time of submission of this ER-2424 final report, details for compounds from over 30 peer-reviewed papers reporting discovery of novel PFAS classes have been compiled in an Excel spreadsheet. As new AFFF-associated PFAS were reported in literature or discovered through samples analysis, their formulae and masses were added to the XIC list. These additions will continue in the future to maintain a current list.

XIC Nomenclature. One of the difficulties in cataloging the large number of discovered AFFF-associated PFAS was developing a system to provide each compound with a unique, concise, and descriptive name while also following a consistent system of nomenclature. In the literature, there have been numerous inconsistencies in terminology used to name novel PFAS. This has led to compounds being classified with multiple names in different papers, or in some cases, the same name being used to describe different substances. Buck et al. aimed to unify terminology for PFAS used in science, regulation, industry by providing a framework for describing PFAS with IUPAC-like names (Buck et al., 2011). However, some of the papers used in this literature review were published prior to or shortly after 2011, and so did not use this consistent terminology.

Here, a new system of nomenclature was developed based on the naming system used by Barzen-Hanson et al. (2017) to describe 40 novel classes of AFFF-associated PFASs in 2017 (See examples in **Table 3.6.1**). The nomenclature used by Barzen-Hanson was drawn from IUPAC nomenclature and the framework provided in Buck et al. (2011). When necessary, changes were made to keep the naming system internally consistent and to ensure that each compound would have a unique name. For example, “propyl” and the “per” in “perfluoroalkyl” were both abbreviated as “P” by Barzen-Hanson et al., but propyl chains are abbreviated as “Pr” in the XIC list here to reduce ambiguity from acronyms. All formulae in the XIC list were standardized as $C_xH_yO_zSi_nP_nCl_oF_p$. The order in which fluorinated chains are described in naming was also standardized so that the connectivity of the molecule can be better understood from the name given.

Table 3.6.1. Examples of consistent structure names for XIC list.

Compound Name	Acronym	Structure
6:2 fluorotelomer thia carboxy propanoamido propyl dimethyl ammonium	6:2 FTTh-CPrAd-PrAm	
N-sulfo hydroxy propyl dimethyl ammonio propyl perfluorohexane sulfonamide hydroxy propyl sulfonate	S-OHPrAmPr-FHxSA-OHPrS	
N-carboxy ethyl dimethyl ammonio propyl perfluorohexane sulfonamide propanoic acid	CEtAmPr-FHxSA-PrA	
N-ethyl dimethyl ammonio propyl perfluorohexane N-ethyl sulfonamide	EtAmPr-FHx-N-EtSA	

High-Resolution Mass Spectrometry (HRMS) Fragmentation Library. Fragmentation spectra for 250 compounds not found in the SCIEX HRMS library were acquired via LC-QTOF-MS and added to an internal HRMS library. Data were collected from neat standards, commercial AFFF products, and environmental samples such as AFFF-impacted groundwater and industrial wastewater.

All compounds added to the XIC list were also considered for addition to the HRMS Library, in cases where the compound had actually been observed, and was not a theoretical homolog. For each of these compounds, a neat standard was used if possible. For most compounds, neat standards were not available. For compounds described in literature for which no neat standards exist, the authors who first discovered each compound were contacted and asked to provide the original samples from which novel compounds were elucidated. **Table 3.6.2** below details the sources of spectra other than neat standards.

Table 3.6.2. Literature source and type of sample analyzed for HRMS Library additions

Compound Originally Reported	Type of Sample Analyzed
Barzen-Hanson et al. 2017	AFFF, groundwater
D'Agostino & Mabury 2014	Commercial surfactants
Liu et al. 2015	Industrial wastewater

Acquisition of HRMS Fragmentation Data. Samples were prepared by dilution with Optima® HPLC-grade water and Optima® HPLC-grade methanol (Fisher Scientific, Fair Lawn, NJ). A 1 mL aliquot of each sample was injected using a SCIEX ExionLC™ liquid chromatography (LC; SCIEX, Framingham, MA) system. A delay column (Luna 5 µm C18 100 Å LC column, 30 x 3 mm; Phenomenex, Torrance, CA) was used to separate out any interferents in the eluents. Sample was injected onto an analytical column (Gemini C18, 3 mm x 100 mm x 5 µm; Phenomenex) preceded by two Zorbax DIOL guard columns (4.6 mm x 12.5 mm x 6 µm; Agilent, Santa Clara, CA) and a SecurityGuard™ C18 Guard Cartridge (4 mm x 2 mm I.D.; Phenomenex). The column oven was held at 40°C.

In general, samples of neat standards and mixtures were run using the same LC method as environmental samples, so that relevant retention time information could be acquired. The aqueous mobile phase (A) was 20 mM ammonium acetate (Fisher Scientific) in Optima® HPLC-grade water and the organic mobile phase (B) was 100% Optima® HPLC-grade methanol. Eluent flow rate was held at 0.60 mL/min, and composition was ramped from 90% A to 50% A over the first 0.5 minutes, then to 1.0% A at 8 minutes and held until 13 minutes, then ramped to 90% A at 13.5 minutes and held to 20 minutes. Some neat standard were run with no analytical column, as this allowed fragmentation data to be collected with a shorter analytical run. For these compounds, no retention time information was gathered.

Detection was done using a SCIEX X500R quadrupole time-of-flight-mass spectrometer (QTOF-MS) system with electrospray ionization (ESI). The mode of ESI used (positive or negative) depended on the structure and likely ionization of the particular compound of interest. Zwitterionic compounds were run in both negative and positive modes in separate runs. Precursor ion data was collected in both SWATH® Data-Independent Acquisition to scan all precursor masses between 100 and 1200 Da and multiple reaction monitoring (MRM) to monitor specific expected precursor ions based on compound formula. Ion spray voltage set at -4500 V and temperature set to 550 °C. The ion source, curtain, and collision (CAD) gas were set to 60 psi, 35

psi, and 10 psi, respectively. The collision energy was set to -5 V and the declustering potential to -20 V, both with no spread. For collection of MS/MS fragmentation data, SWATH® scanning was conducted with the mass range dependent on the precursor mass, as all fragments are expected to be lower in mass. The collision energy was -35 V for negative mode and +35 V in positive mode, with 30 V spread for each mode. The instrument was tuned prior to all analytical runs and mass calibrated every 5 injections using SCIEX Calibration Solution. When multiple compounds were acquired in one run, each sample was separated by a double blank, containing just methanol and water, to ensure that there was no carryover between library acquisitions.

Spectra were viewed and verified in SCIEX Explorer (Figure 3.12). The desired peak matching the known precursor mass was highlighted in the chromatogram for that mass and the fragmentation spectrum for that peak were displayed. For neat standards, spectra were verified using the Certificate of Analysis. For compounds with spectra published in literature, spectra were verified by confirming that the detected masses matched previously published spectra or mass transitions. After the spectra were verified, subtraction of background noise from each peak was performed in SCIEX PeakView. Library entries were created for individual compounds, including the compound name (the acronym previously created for the XIC list), compound structure, neutral formula, precursor mass, collision energy used in acquisition, and collision energy spread used in acquisition.

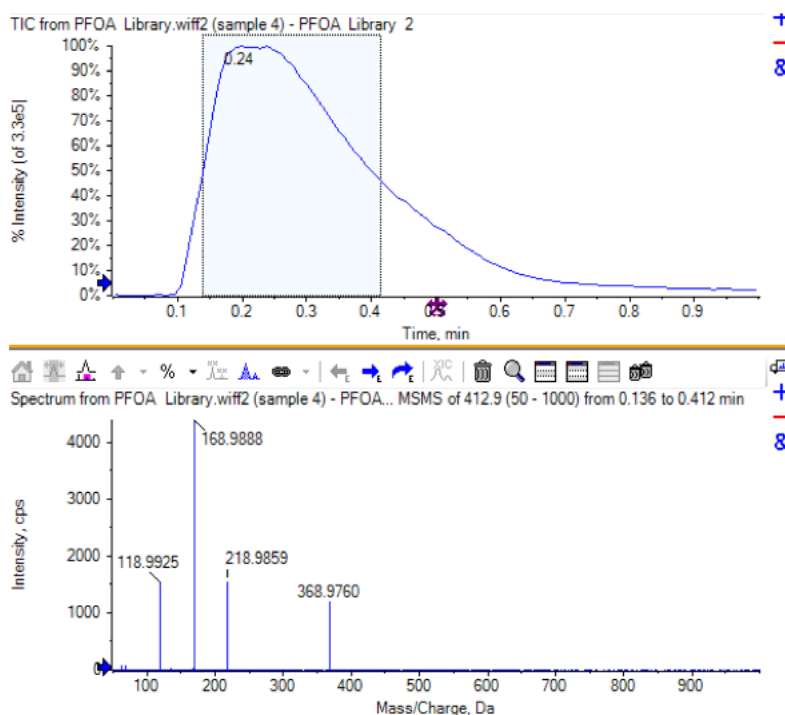


Figure 3.12. Screenshot of spectrum viewing and verification in SCIEX Explorer during acquisition process.

HRMS Library Database in SCIEX LibraryView. Files for spectra created in SCIEX Peakview were added to a SCIEX LibraryView database for use in suspect screening analysis of environmental samples. Figure 3.13 shows an example of data entered that can be found by looking up a specific compound in the LibraryView database. Library entries can be browsed and edited in LibraryView, and the LibraryView database can be referenced by the SCIEX OS data analysis software (SCIEX OS Analyst) to allow suspect screening of acquired sample data.

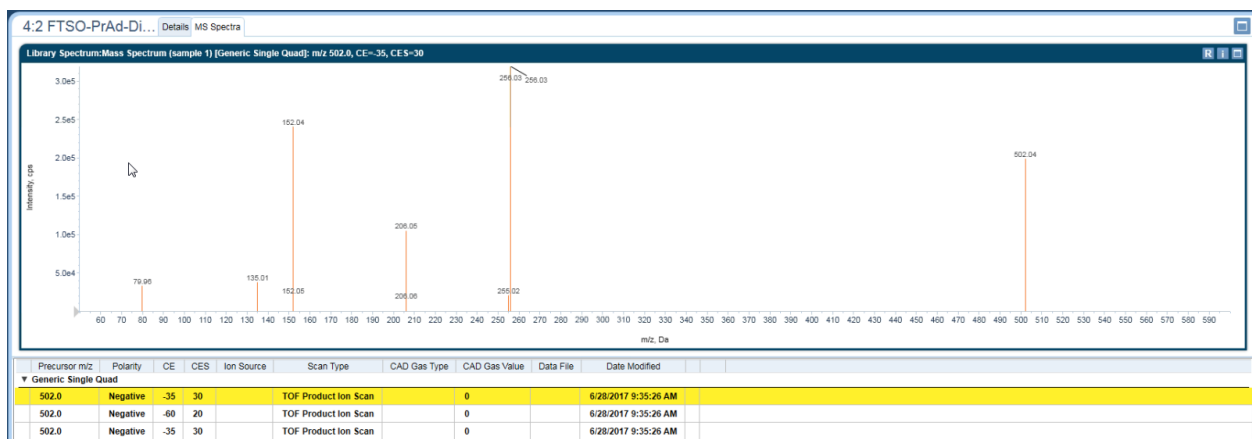


Figure 3.13. Screenshot of LibraryView spectrum entry for an example compound, 4:2 FTSO-PrAd-DiMePrS (4:2 fluorotelomer sulfinyl ethyl amide trimethyl sulfonic acid 1,1-dimethyl ethyl sulfonate)

Applying the XIC List and HRMS Library to a Suspect Screening Workflow. To identify AFFF-associated PFAS in environmental samples, samples were generally acquired using the same LC method described above for acquisition of spectra, with some modifications depending on sample matrix. QTOF-MS data was collected via SWATH® Data-Independent Acquisition as mentioned above, but with no MRM for targeted precursors.

A suspect screening method was created in SCIEX Analyst to screen samples for all masses included in the XIC list, and to evaluate the fragmentation spectra of all detected compounds for matching of spectral patterns to those in the HRMS Library. For samples run in negative ESI, samples were screened for the deprotonated molecular ion for all compounds in the XIC list amenable to negative ionization (902 compounds). For samples run in positive ESI, samples were screened for the protonated molecular ion for all compounds amenable to positive ionization (716 compounds). In both modes, an XIC window of 0.008 – 0.01 Da is generally used, along with a signal:noise threshold of 10:1 and baseline subtraction over 2 minutes. HRMS library searching was done using a mass error threshold of 0.1 Da for the precursor ion and 0.4 Da for the product ion, and an intensity threshold of 5% of the highest peak in the MS/MS spectrum (all fragments below this intensity are ignored). While these parameters are generally used, they may be modified depending on the characteristics of a particular sample set. However, they are kept constant for any group of samples being analyzed and compared to each other.

This processing method allows for peak identification with two levels of confidence (Figure 3.14): XIC match (only matched to a mass in the XIC list) and HRMS Library match (fragmentation matches data collected in the library). XIC matches were defined as compounds with accurate mass measurement of the precursor ion within 5 ppm and isotopic pattern differences < 10%. A compound designated as an XIC match has been matched based only on mass and formula information, and so is generally associated with a Schymanski confidence Level 4 (*Unequivocal molecular formula*; Schymanski et al., 2014). This could be raised to a Level 3 (*Tentative candidates based on structure*) if structural information can be gleaned from the MS/MS fragmentation. HRMS Library matches were defined as compounds with precursor ion mass measurement within 10 ppm and isotopic pattern differences < 20%, as well as a Library Purity Score above 70%. Library Purity Score is calculated by an algorithm in the SCIEX Analyst software based on the quality of match between the library and experimental MS/MS spectra (both presence/absence of expected fragments and relative fragment abundance are evaluated). HRMS Library matches are associated with a Schymanski confidence Level 2 (*Probable structure by library spectrum match*). This is the highest confidence level for compound identification that is possible without a reference standard.

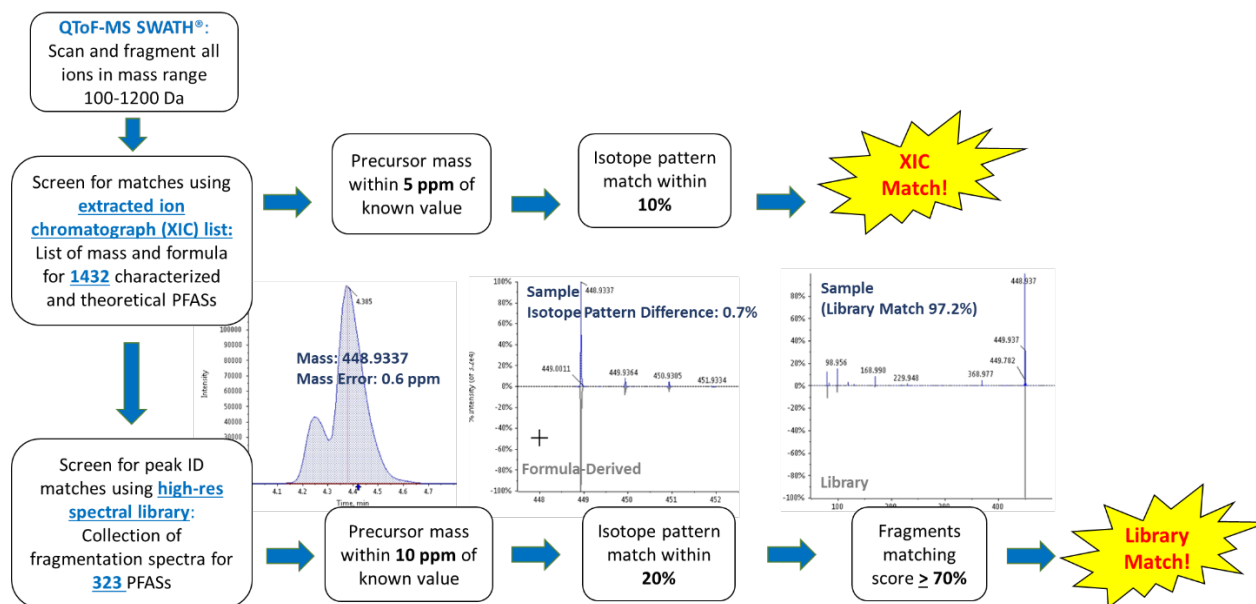


Figure 3.14. Suspect screening workflow to identify XIC and HRMS Library matches in sample data acquired via QToF-MS SWATH®

R Script for Data Post-Processing. Data were exported from SCIEX OS and parsed using an R script (R v 3.4.3) to identify MS/MS library and XIC list matches and produce spreadsheets containing all peak areas for XIC and library matches in all samples to facilitate data interpretation and visualization. The script also produces lists of all compounds found in a dataset and their frequency of detection as HRMS Library matches or XIC matches. The R script also flags XIC matches for which isomers exist in the XIC list, as these are not differentiable without structural

information. All possible isomers are listed for each compound in the sheet of XIC matches. Additionally, all XIC matches for which HRMS library data exist, but no library match was found, are flagged. In the future, additional features will be added to this script to further expedite data post-processing, including automatic blank censoring and treatment of sample replicates.

4.0 Results and Discussion

4.1. Screening of Commercially Available Anodes for Treatment of PFOA and PFOS

Anode screening experiments using the various mixed metal oxide (MMO) anodes were, in summary, ineffective for treating PFOA and PFOS. The best initial results (Exp. 1) were obtained using the Ti/RuO₂ (Grade 1) anode in a divided EC cell configuration, where PFOS decreases under applied current conditions (Figure 4.1.1) were greater than those in the no-current controls. However, as shown in Figure 4.1.1, subsequent experiments showed that PFOS removal compared to the controls was negligible. Thus, any activity of these MMO anodes with respect to PFOS removal were very short-lived.

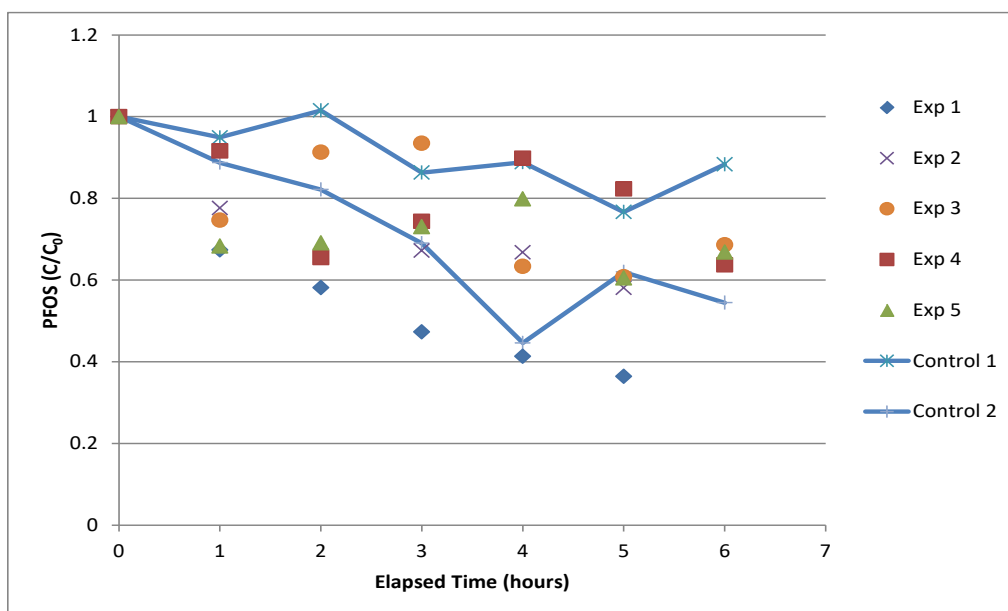


Figure 4.1.1. PFOS removal during electrochemical treatment using a Ti/RuO₂ (Grade 1) anode. While the initial Exp. 1 showed that PFOS removal relative to the no-current controls, subsequent experiments indicated that PFOS removal compared to the controls was negligible. The EC cell was operated in divided configuration, at 10 mA/cm² and a final pH of 2.

Using the Ti/SnO₂-F anodes, both divided and undivided electrochemical cell experiments with PFOA yielded little defluorination. Results from these experiments are summarized as follows:

- The Ti/SnO₂-F anodes prepared at the Colorado School of Mines had extremely low electrical conductivity. This prevented application of sufficient current density. Even after using an extended treatment duration (to, in part, account for the low amount of current we were able to apply), only trace fluoride generation was observed.

- The Ti/SnO₂-F anodes prepared at the commercial electrode facility were sufficiently conductive, comparable to the previous MMO anodes we have tested. However, no fluoride generation was observed in the divided electrochemical cell configuration, and only trace fluoride generation was observed in the undivided cell configuration. A palladium-doped Ti/SnO₂-F anode produced similar results as the non-palladium doped anode.
- An additional set of experiments was performed at high voltage (30V compared to the 11V typically used in the experiments). This high voltage experiment did not result in any appreciable increase in PFOA defluorination (Figure 4.1.2).
- While perchlorate formation was minimal to below detection in all experiments, substantial (>10 mg/L) levels of chlorate were formed

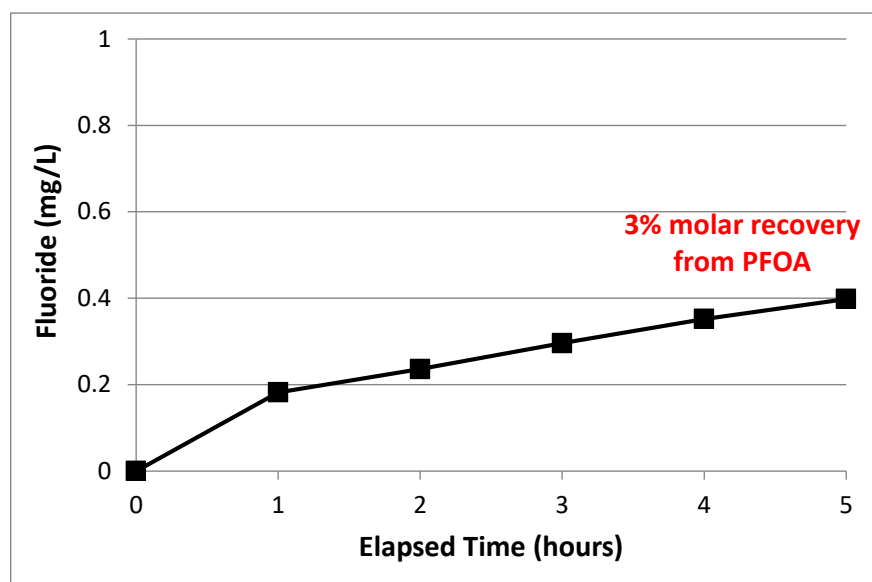


Figure 4.1.2. Fluoride generation from 20 mg/L PFOA in an undivided EC cell using Ti/SnO₂-F anodes prepared at the commercial electrode facility. The EC system was operated at 30 mA/cm² and approximately 30V.

Based on the less-than-promising results from these initial screening tests with MMO anodes, future testing focused on the use of commercially available BDD anodes. As discussed in detail in Section 4.2, results from the BDD anodes showed much greater promise than those obtained from the MMO anodes.

4.2 Electrochemical Experiments using Boron-Doped Diamond (BDD) Anodes

4.2.1 Initial Testing Using PFOA and PFOS

4.2.1.1 PFAS Removal and Defluorination

Figure 4.2.1 shows electrochemical treatment of PFOA (15 mg/L initial concentration) observed at three applied current densities in the absence and presence of chloride ions at ambient temperature. Cell voltages ranged from approximately 4.6 V (lowest current density) to 12 V (highest current density). The corresponding fluoride generation for these same experiments, plotted as the fluoride generated relative to the total fluorine initially present on PFOA, also is shown in Figure 4.2.1 PFOA removal was well-described by a first-order rate law, as indicated by the regression parameters shown in Table 4.2.1. Rates of PFOA removal and defluorination increased with increasing applied current density, indicating that observed PFOA treatment rates were current-controlled at the electrodes rather than by aqueous mass transfer controlled processes (Buxton et al., 1988; Chiu and Reinhard, 1995). The increase in the PFOA transformation rate constant (Table 4.2.1) was approximately proportional to the increase in current density. In the current-free control experiments, PFOA losses were less than 15%; these losses likely were the result of adsorption to electrochemical system components. During reactions, solution temperature increased slightly ($\leq 2^{\circ}\text{C}$ for the lower 2 current densities, $\leq 7^{\circ}\text{C}$ for the highest current density) due to resistive heating, and pH decreased to values as low as pH 4.

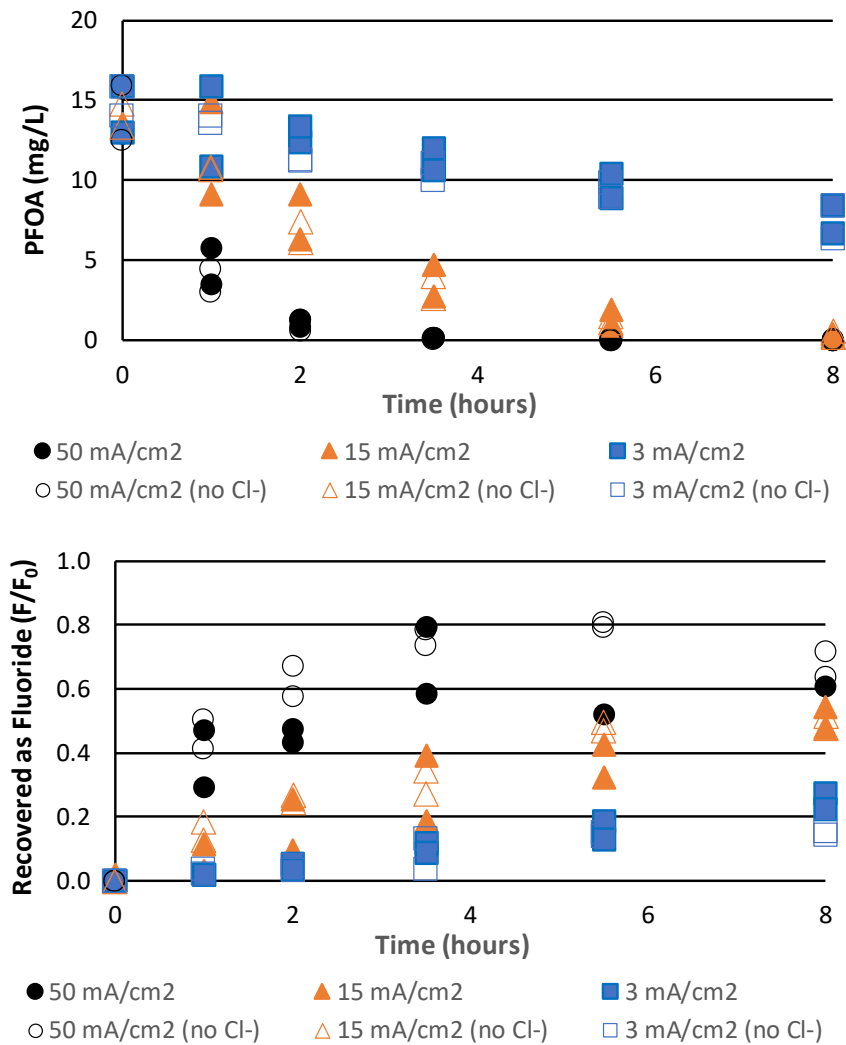


Figure 4.2.1. PFOA removal (top) and fluoride generation (bottom) versus time as a function of applied current density and with/without chloride present. Electrolyte solution consisted of 1500 mg/L Na₂SO₄, and (if added) 167 mg/L NaCl. Voltages ranged from 4.6 V (3 mA/cm²) to 12 V (50 mA/cm²). Duplicate results are shown. First order PFOA transformation rate constants regressed to the data are provided in Table 4.2.1.

Table 4.2.1. First order transformation rate constants determined during electrochemical testing of PFOA and PFOS using a BDD anode. PFHpS and PFHxS were present as low level impurities in the PFOS solution.

PFAS	C_{init} (mg/L)	Applied Current Density (mA/cm²)	Water Matrix^b	First-order transformation rate constant (h⁻¹)^a
PFOA	15	3	Na ₂ SO ₄	0.091 ± 0.0008 (0.86)
			NaCl + Na ₂ SO ₄	0.074 ± 0.0052 (0.95)
PFOA	15	15	Na ₂ SO ₄	0.37 ± 0.020 (0.98)
			NaCl + Na ₂ SO ₄	0.41 ± 0.012 (0.99)
			groundwater	0.33 ± 0.017 (0.99)
PFOA	15	50	Na ₂ SO ₄	1.4 ± 0.027 (0.99)
			NaCl + Na ₂ SO ₄	1.2 ± 0.047 (0.99)
PFOA	0.3	15	Na ₂ SO ₄	0.33 ± 0.019 (0.97)
			NaCl + Na ₂ SO ₄	0.34 ± 0.020 (0.97)
			groundwater	0.49 ± 0.056 (0.97)
PFOS	10	50	NaCl + Na ₂ SO ₄	0.37 ± 0.017 (0.99)
PFOS	0.6	15	Na ₂ SO ₄	0.12 ± 0.016 (0.46)
			NaCl + Na ₂ SO ₄	0.13 ± 0.017 (0.63)
			groundwater	0.041 ± 0.012 (0.33)
PFHpS	1	50	NaCl + Na ₂ SO ₄	0.25 ± 0.015 (0.97)
PFHxS	1	50	NaCl + Na ₂ SO ₄	0.11 ± 0.0098 (0.89)

^a ± values indicate the standard error. R² values are shown in parentheses. No rate constant measured for PFOS at a current density of 3 mA/cm² because only a very weakly decreasing trend in PFOS concentration was observed.

^b Electrolyte solutions prepared with 1500 mg/L Na₂SO₄ and (when added) 167 mg/L NaCl. Groundwater composition listed in Table 3.1.

The results shown in Figure 4.2.1 and Table 4.2.1 indicate that chloride had a minimal effect on the observed PFOA and PFOS transformation rate constants and defluorination. Chloride oxidation, which resulted in perchlorate formation, is facilitated by surface reactions on BDD anodes (Field, et al., 2013). The minimal impacts of chloride on PFOA oxidation suggests minimal competition between PFOA and chloride (or chloro-oxyanion intermediates) for available reaction on the BDD anode surface, at least for the concentrations and reaction conditions examined.

Several studies (e.g., (Buxton, et al., 1988)) have shown that PFOA oxidation via electrochemical treatment proceeds via a stepwise mechanism in which C-C bond cleavage occurs between the carbon chain and the carboxylate group, coupled with F⁻ elimination. This process is repeated, resulting in the intermediate generation of shorter-chain perfluorocarboxylic acids. Consistent with this mechanism, low concentrations of shorter chain perfluorinated carboxylates were observed (perfluorobutanoic acid, perfluoropentanoic acid, perfluorohexanoic acid, and perfluoroheptanoic acid), but at net concentrations $\leq 25\%$ of the total fluorine balance at all times during the experiments. Experiments performed at low current density generally showed the greatest abundance of the perfluorinated intermediate products, and the generation of these short chain carboxylic acids was up to 50% greater in the presence of chloride. The increased formation of intermediate transformation products in the presence of chloride may be due to increased surface competition between chlorine species and the perfluorocarboxylic acid intermediates as chain length gets shorter, or due to consumption of hydroxyl radicals by chlorine species. Total F molar balances (quantified PFASs + fluoride) ranged from 60 to 98% by the end of the experiments, with greater recoveries generally attained for the lower current densities. Perchlorate was generated in all experiments where the electrolyte contained chloride, with perchlorate concentrations ranging from approximately 50 mg/L (18% of the chloride present converted) in the lowest current density experiments to over 250 mg/L (88% of the chloride converted) in the highest current density experiments.

PFOA and PFOS removal for both the 50 mA/cm² and 3 mA/cm² applied current densities in the presence of chloride are shown in Figure 4.2.2; the PFOA and PFOS first-order transformation rate constants are shown in Table 4.2.1. PFOA and PFOS experiments were performed separately to distinguish fluoride generation for each compound. In general, PFOS was defluorinated more slowly than PFOA, with measured rate constants for oxidation of the former being roughly one third of the latter at comparable conditions; Zhuo et al. (Houtz, et al., 2013) also showed that PFOS was less reactive than PFOA during electrochemical treatment using BDD anodes. Unlike PFOA, no generation of shorter chain perfluorinated sulfonates or carboxylates was observed during PFOS, consistent with findings reported by Carter and Farrell (Bruton and Sedlak, 2017) who also reported that changes in TOC and PFOS tracked closely to one another during treatment, a finding that suggests that anodic oxidation leads to rapid mineralization. This contrasts with Zhuo et al. (Houtz, et al., 2013), who showed that BDD treatment of PFOS resulted in the generation of short chain perfluorocarboxylate intermediates. The reason for these contrasting observations is not readily explained, but may be due to the current densities at which the experiments were performed. These differences also may be due to the type of BDD anode used, as BDD performance can be impacted by the nature of the surface coating.

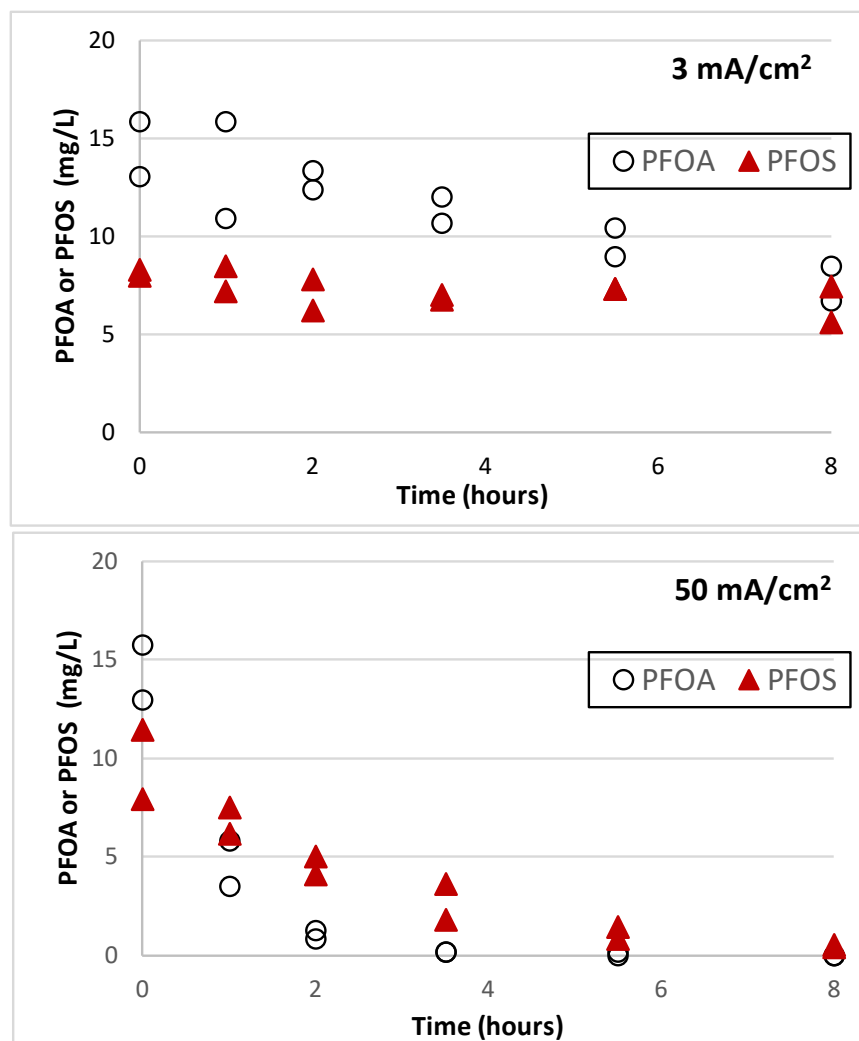


Figure 4.2.2. PFOA and PFOS removal at 3 mA/cm² (top) and 50 mA/cm² (bottom) in chloride-containing electrolyte.

The PFOS electrolyte solution contained approximately 1 mg/L each of perfluoroheptane sulfonate (PFHpS) and perfluorohexane sulfonate (PFHxS); these compounds were present as impurities within the PFOS reagent. Both PFHpS and PFHxS were removed at a current density of 50 mA/cm², with measured first-order rate constants provided in Table 4.1. The observed rate constants decreased with decreasing chain length for PFOS through PFHxS, consistent with the observations of others (Dinglasan, et al., 2004; Houtz, et al., 2013). No PFHxS or PFHpS removal (<10% decrease over time) was observed at a current density of 3 mA/cm². Smaller (n<6) chain perfluorosulfonates remained below the LOQs for all experiments, and no generation of perfluorinated carboxylates was observed. The observation that the first order degradation rate constant showed a decreasing trend in the perfluorinated chain length (Table 4.2.1) for the

perfluorinated sulfonates is consistent with a surface-controlled reaction due to sorption on the anode, as sorption is expected to decrease with decreasing perfluorinated chain length.

4.2.1.2 PFOA and PFOS Removal at Environmentally Relevant Concentrations

Using an applied current density of 15 mA/cm² with a mixture of low concentration PFOA and PFOS (approximately 0.3 and 0.6 mg/L, respectively), first-order PFOA and PFOS transformation rate constants were determined at these much lower and more environmentally relevant concentrations; regression parameters are provided in Table 4.2.1. Consistent with the results observed in experiments using the higher PFAS concentrations experiments, chloride had minimal effects on PFOA and PFOS removal, and the measured first-order rate constant for PFOA at low concentration in the presence of PFOS ($0.33 \pm 0.019 \text{ h}^{-1}$) was nearly equal to the first-order rate constant for PFOA at elevated concentration ($0.37 \pm 0.020 \text{ h}^{-1}$). Also, similar to results obtained at elevated PFAS concentrations, PFOA removal was greater than that of PFOS removal. The exception was that, at a current density of 15 mA/cm², PFOS removal was not well described by first-order kinetics, with $R^2 < 0.65$. The failure of the first order model is not readily explained, but may be due to the lack of sufficient electrode potential at the lower current densities. As shown in Table 4.1, PFOS mass removal was not significantly impacted by the presence of chloride.

Generation of shorter chain perfluorocarboxylates and removal of shorter chain perfluorosulfonates were not affected by the presence of chloride, similar to findings for the high PFOA concentration results obtained under similar operating conditions. Although the low initial concentrations of PFOA and PFOS used in these experiments prevented quantification of fluoride ion release, ion chromatograms did show small unquantifiable peaks corresponding to the elution time of fluoride that increased in size throughout the duration of the experiment.

4.2.1.3. Oxidant generation and mechanistic insights

Generation of solution phase oxidants (H₂O₂ and active chlorine species) in the absence and presence of chloride is shown in Figure 4.2.3 The quantity of generated oxidants increased with increasing current density, and oxidant generation nearly doubled in the presence of chloride.

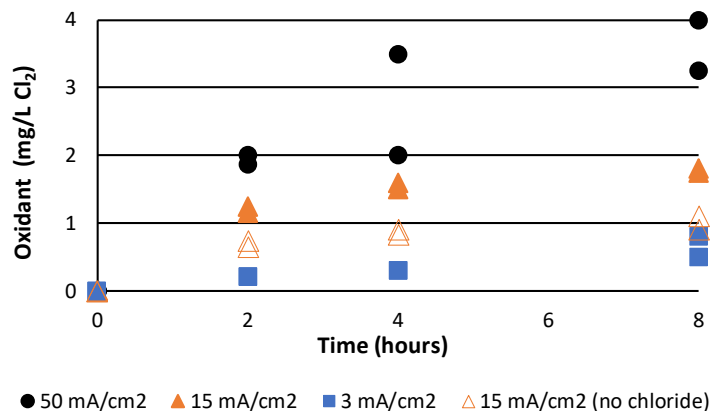


Figure 4.2.3. Oxidant generation, measured via the DPD method, during the electrochemical experiments at different applied current densities, and in the presence of chloride (sodium sulfate present in all experiments).

Experiments performed in the presence of TBA, which will scavenge hydroxyl radicals in bulk solution (i.e., hydroxyl radicals not sorbed to the BDD surface), did not result in any decrease in PFOA or PFOS removal, or in the generation of shorter chained transformation products. TBA concentrations decreased from 100 mg/L to approximately 3 mg/L within 4 h, and to approximately 0.5 mg/L by the end of the 8 h experiment. This TBA removal suggests that substantial quantities of hydroxyl radicals were being scavenged, and/or that TBA was being removed via a direct electron transfer mechanism at the anode.

PFOA removal (15 mg/L initial concentration) was evaluated in a natural groundwater containing a number of known hydroxyl radical scavenging species including chloride, carbonate/bicarbonate, and dissolved organic matter (Table 3.1). The measured first order PFOA degradation rate constant in the groundwater ($0.33 \pm 0.017 \text{ h}^{-1}$) was nearly identical to that measured in electrolyte solutions at comparable conditions ($0.37 \pm 0.020 \text{ h}^{-1}$, but fluoride generation was 23% greater in the natural groundwater system. The increased fluoride generation in the natural groundwater system is not readily explained, but this result does point to the complexities in the defluorination behavior in the presence of a complex aqueous geochemistry.

The behavior of the shorter chain perfluorinated compounds in the natural groundwater was similar to that observed in electrolyte, with decreases in PFHxA and PFHpA observed by the final sampling event. Repeating the natural groundwater experiments with a low concentration mixture of PFOA and PFOS showed that PFOA removal was slightly faster ($0.49 \pm 0.056 \text{ h}^{-1}$) than that measured using higher PFOA concentrations in groundwater ($0.33 \pm 0.017 \text{ h}^{-1}$) or comparable PFOA concentration in model electrolyte solutions ($0.34 \pm 0.020 \text{ h}^{-1}$) (Table 4.2.1). Similar to results obtained in electrolyte, PFOS removal in natural groundwater at 15 mA/cm^2 was not well described by a first order model ($R^2 = 0.33$). Approximately 27% PFOS mass removal was observed in natural groundwater at a current density of 15 mA/cm^2 , which is just over half that observed in the electrolyte systems. These results indicate that natural groundwater does not have

major adverse impacts on electrochemical treatment of PFOA and PFOS compared to treatment observed in electrolyte.

The rate of chloride removal also was unaffected by the presence of the hydroxyl radical scavenger TBA. These results suggest that the oxidation rate of both chloride and the target perfluorinated compounds was controlled by direct electron transfer reaction on the BDD anode surface (Bruton and Sedlak, 2017; Buxton, et al., 1988; Houtz, et al., 2013; Li, et al., 2012), and was not affected by the presence of any oxidants generated by the BDD anode, including hydroxyl radicals.

4.2.1.4 Perchlorate mitigation

The generation of perchlorate during electrochemical treatment with BDD anodes is a significant obstacle for implementation of this remediation technology since most natural water sources contain appreciable chloride ion. Although operating conditions (e.g., applied current density) may provide marginal control of perchlorate generation, use of BDD anodes will result in perchlorate levels that far exceed regulatory levels if even a relatively small fraction of chloride is oxidized to perchlorate. To assess if biotic reduction of perchlorate in electrochemically oxidized water is plausible, preliminary experiments were conducted to evaluate the biological treatment of perchlorate in the electrochemically treated solutions. Results of the biological perchlorate treatment experiment conducted in sand columns (to simulate re-injection of PFAS-treated groundwater into aquifers, as summarized in Figure 4.2.4) are presented in Figure 4.2.5. Biological treatment yielded up to a 3-log decrease in perchlorate levels over the 9-day hydraulic residence time in the sand columns; chlorate concentrations in the effluent were below the analytical detection limit (0.2 mg/L). Decreases in both perchlorate and chlorate were accompanied by a proportional increase in chloride. The effectiveness of this preliminary treatment study suggests that a biological treatment to remove perchlorate, following electrochemical oxidation to treat PFAS, is plausible (despite the production of electrochemically generated microbial inhibitors such as Cl₂) and warrants further study.

Developed costs for coupled nanofiltration/electrochemical treatment provided in a recent publication by Soriano et al. (2019) (*Water Research*, doi: <https://doi.org/10.1016/j.watres.2019.114954>), and fluidized bed reactor costs developed as part of ESTCP Project ER-200829, clearly show that the costs associated with biological treatment of perchlorate would be small (less than 10%) compared to that of the electrochemical/nanofiltration treatment. Thus, while biological treatment of electrochemically generated perchlorate would increase the overall PFAS treatment cost, this additional cost would be marginal.

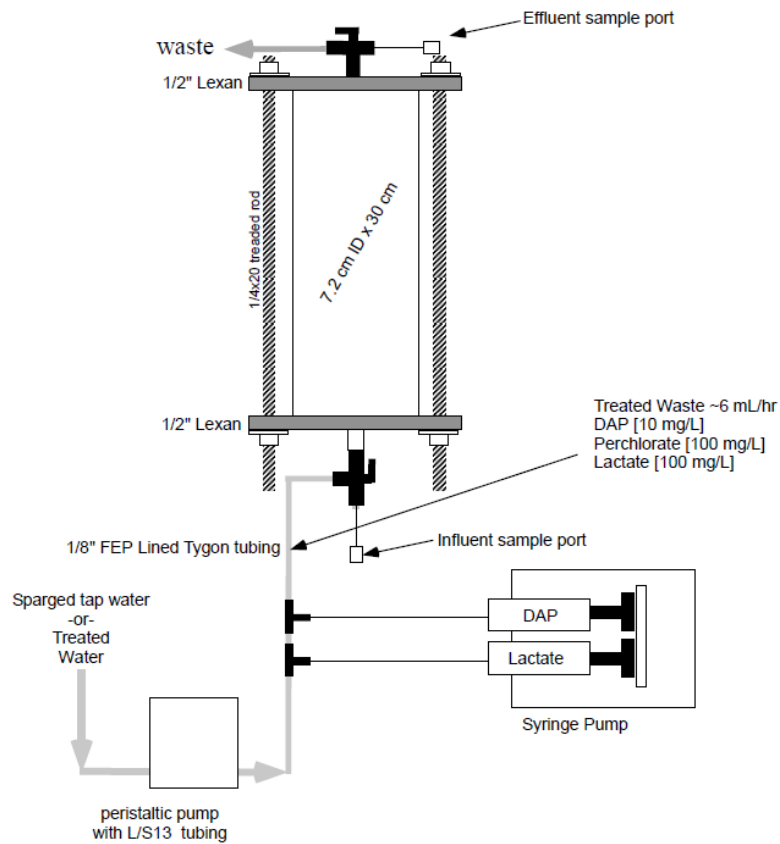


Figure 4.2.4. Biological treatment system to treat perchlorate in electrochemically treated water. DAP = diammonium phosphate. The hydraulic residence time through the sand columns was approximately 9 days.

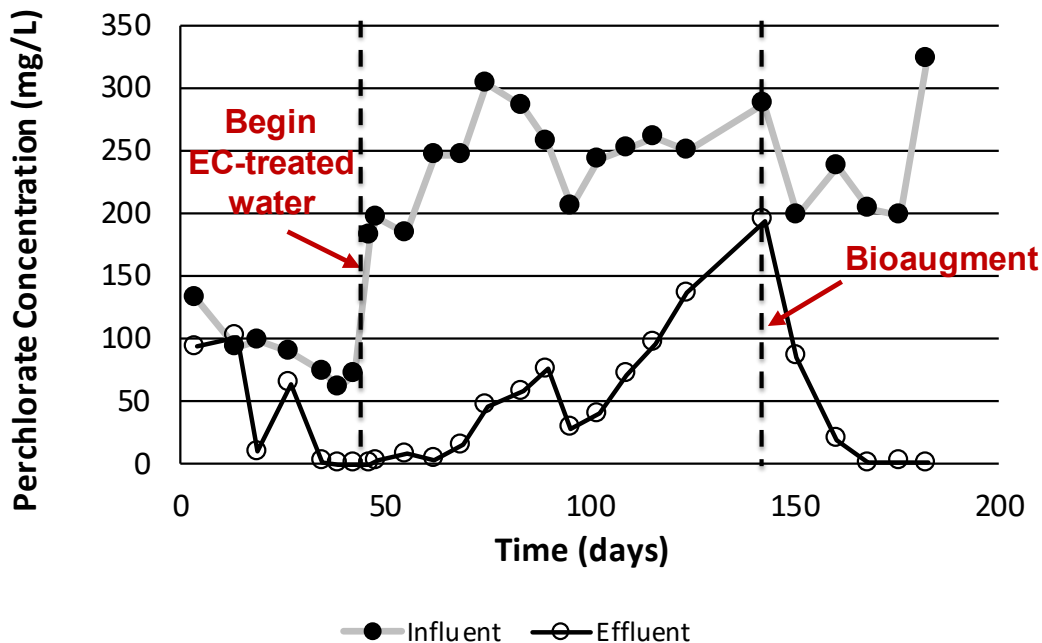


Figure 4.2.5. Influent and effluent perchlorate concentrations to the biological treatment column. Perchlorate influent varies due to the fact that the operating conditions (i.e., current density) varied for the electrochemically treated waters. The first vertical dashed line indicates when the influent was switched from deionized water amended with perchlorate to electrochemically treated water, and the second vertical dashed line indicates when bioaugmentation with *Azospira suillum* JPLRND (Sturchio et al., 2007; Farhan and Hatzinger, 2009) was performed.

4.2.1.5 Discussion and Application

Measured rate constants for PFOA and PFOS removal increased with increasing current density, suggesting that the observed reaction rates were surface controlled. Figure 4.2.6 shows the PFOA first order degradation rate constants as a function of current density. The first order transformation rate constants for chloride removal also are plotted in Figure 4.2.6. These data show that, consistent with a surface-controlled reaction, the first order rate constants for both chloride and PFOA removal are proportional to the applied current density. The rate constants for PFOA were within a factor of 2 but slightly greater than those determined for chloride, suggesting that PFOA had a greater affinity for the BDD surface than chloride, and/or was more rapidly oxidized than chloride at the BDD surface. While some studies have shown that the presence of chloride increases the rate of contaminant removal during BDD electrochemical oxidation (MacCrehan, et al., 1998; Marenich, et al., 2009) the presence of chloride (or subsequently, oxidized chlorine species) did not enhance the removal rate of PFOA or PFOS.

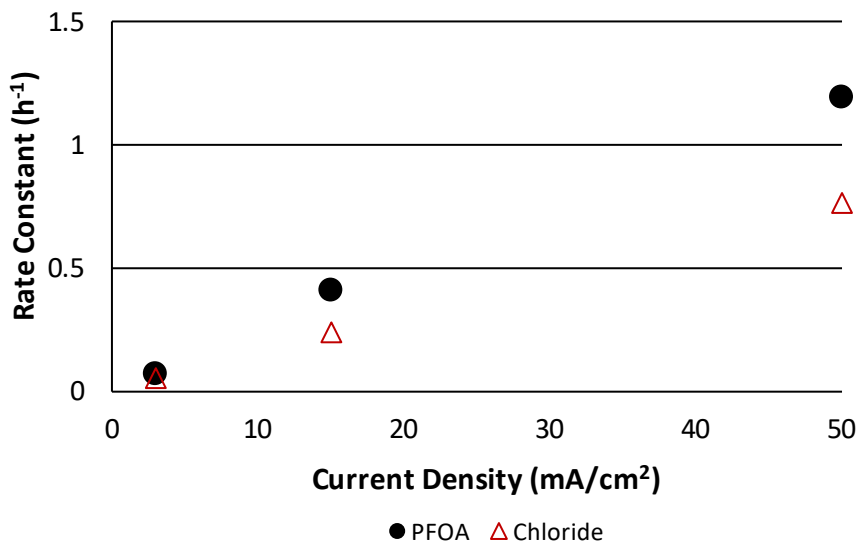


Figure 4.2.6. Degradation rate constants for PFOA and chloride during electrochemical treatment in electrolyte (1500 mg/L Na₂SO₄, 167 mg/L NaCl) as a function of the applied current density. Average of duplicate values shown.

While the generation of shorter-chain perfluorocarboxylates and fluoride accounted for up to 61% of the PFOA removed in the high current density experiments, and fluoride generation accounted for up to 75% of the PFOS removed in the high current density experiments, the fate of the remaining fluorine in both the PFOA and PFOS experiments was not determined. Fluorination of the anode surface may account for some of this loss (Buxton, et al., 1988). Previous electrochemical studies also have shown that volatile perfluorinated hydrocarbons (e.g., perfluorooctane) may have been generated (Baumgartner and McNeil, 2012) that could account for some of the discrepancy in mass balance. Alternatively, shorter chain non-volatile fluorinated byproducts which are not readily observed by LC-MS/MS are also likely forming during treatment.

The energy used by the electrochemical cell to attain an order of magnitude decrease in PFOA and PFOS at 50 mA/cm² was 180 W-h/L and 500 W-h/L, respectively. At an applied current density of 15 mA/cm², the energy demand for a 10-fold reduction in PFOA concentration was reduced to 110 W-h/L. Thus, the energy demand required for treatment is dependent, in part, upon the applied current density. The energy requirements increased with the applied current density, likely due to increased oxygen evolution that inhibited PFOA and PFOS oxidation.

The energy requirements for treating AFFF-impacted water are further discussed in Section 4.4.4.

4.2.2 Testing to Assess Electrochemical Treatment in the Presence of a Wide Range of PFAS

4.2.2.1 PFAS Composition in Model Groundwaters W1 and W2

PFAA concentrations in W1 and W2 are shown in Table 3.3.2. Suspect PFAS with an area response $>10^6$ present in W1 and W2 are summarized in Appendices A2 and A3, respectively; these appendices also identify PFAS that exhibited transient increases during electrochemical treatment. Compounds with perfluorinated chain lengths of $n=4$ through 6 typically were the most abundant species. Perfluorooctane sulfonamide ($n=8$), a potential precursor of PFOA and/or PFOS (Grimme, et al., 2011; Houtz, et al., 2013), was present in W1. Perfluoroalkane sulfonamides (FASAs) and perfluoroalkane sulfinates (PFASis), both of which have been identified as PFAA precursors (Houtz, et al., 2012; Hu, et al., 2016) also were present in W1.

W2 contained PFAS structures that generally were similar in structure to those identified in W1. However, compounds containing the sulfonated end groups of the non-fluorinated branches (e.g., S-OHPrAmPr-FQASA-OHPrS) were not detected in W1. Perfluorinated chain lengths of $n=4$ through 6 were the dominant species for these sulfonated sulfonamides. As with W1, FASAs (known PFAA precursors (Houtz, et al., 2013)), were also present in W2. For $n=5$ and 6, FASA levels showed area counts 10- to 100-times less than those for W1. For $n=4$ and 8, FASA levels were within a factor of 2 for both W1 and W2. These $n=8$ FASA levels, as well as the presence of $n=8$ compounds for both N-SPAmP-FASA and PFASA-PDA, suggest that W2 has similar or greater potential for formation of PFOA or PFOS from oxidative transformation of precursors as does W1. W2 did not contain any detectable PFASi's, another known class of PFAA precursors (Houtz, et al., 2012).

Figure 4.2.7 shows the fluorine content based on integrated area response for the precursors ($n=4$ through 8) present in untreated W1 and W2, and identified in Appendices A2 and A3. Based on Figure 4.2.7, W2 would be expected to produce a greater amount of PFAAs upon treatment via electrochemical oxidation, although this conclusion should be interpreted with caution as the response factors associated with W1 and W2 may differ.

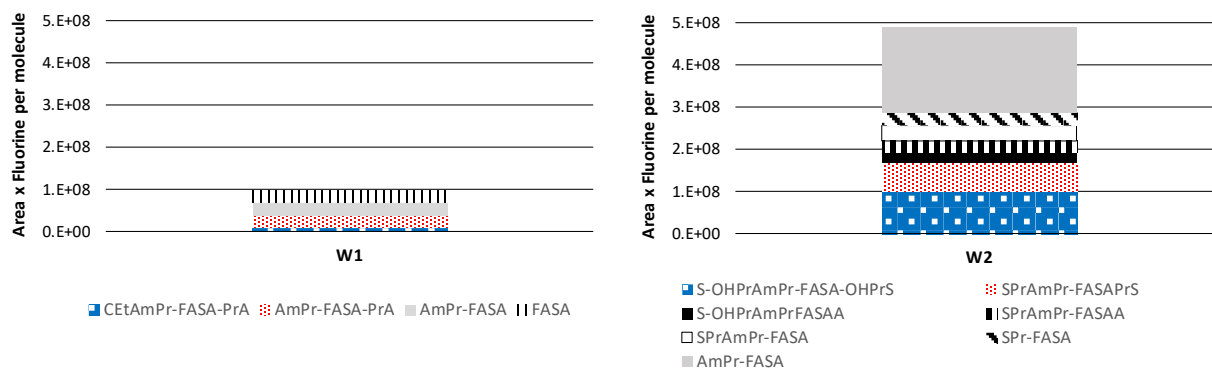


Figure 4.2.7. Semi-quantitative HRMS analysis used to estimate the fluorine in the predominant precursor compounds in W1 and W2. FASAs are not shown for W2 because the FASA values for W2 are only 5×10^6 .

The total oxidizable precursor (TOP) assay was used to assess PFAA transformation in W2. Results shown in Figure 4.2.8 indicate that PFAA formation was only observed in W1, and not W2. This result is surprising given the quantity of apparent PFAA precursors present in W2 relative to W1 shown in Figure 4.2.7. This apparent discrepancy highlights the importance of PFAS precursor structure (there are small differences in the structures of the “precursors” in W1 versus W2) and/or groundwater geochemical conditions in the fate of PFAS during oxidation.

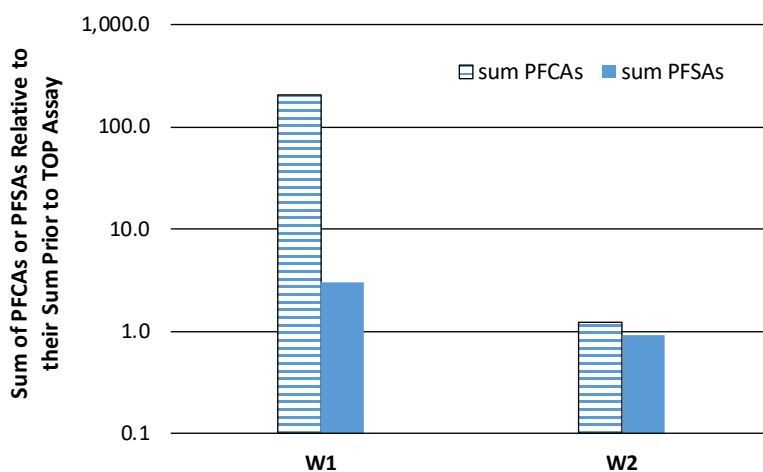


Figure 4.2.8. Total oxidizable precursor (TOP) assay results for W1 and W2. PFCAs increased nearly 200-times in W1 after performing the TOP assay, while no measurable increase in either PFCAs or PFASs were observed in W2.

4.2.2.2 PFAS Transformations during Electrochemical Treatment in Groundwater W1

At an applied current of 25 mA/cm², the applied voltage was 13 V for the W1 groundwater electrochemical experiments. The pH remained circumneutral, and a modest increase in temperature from 25 to 30 degrees C was observed.

Several of the suspected PFAA precursor compounds were rapidly removed in W1 (Figure 4.2.9), while others showed a transient increase followed by a decrease (Figure 4.2.10). The latter is indicative of oxidative formation followed by transformation, and is useful for insight into oxidation pathways. Transient PFCA increases were also observed in W1 during electrochemical treatment, but no transient increases in PFSAs were observed (Figure 4.2.11). The results shown in Figure 4.2.11 are consistent with the TOP assay results shown in Figure 4.2.8, and also with the results of Houtz and Sedlak. Fluoride generation also was observed, indicating that the PFAAs were defluorinated; additional discussion of the fluoride mass balance is provided in Section 4.2.2.4.

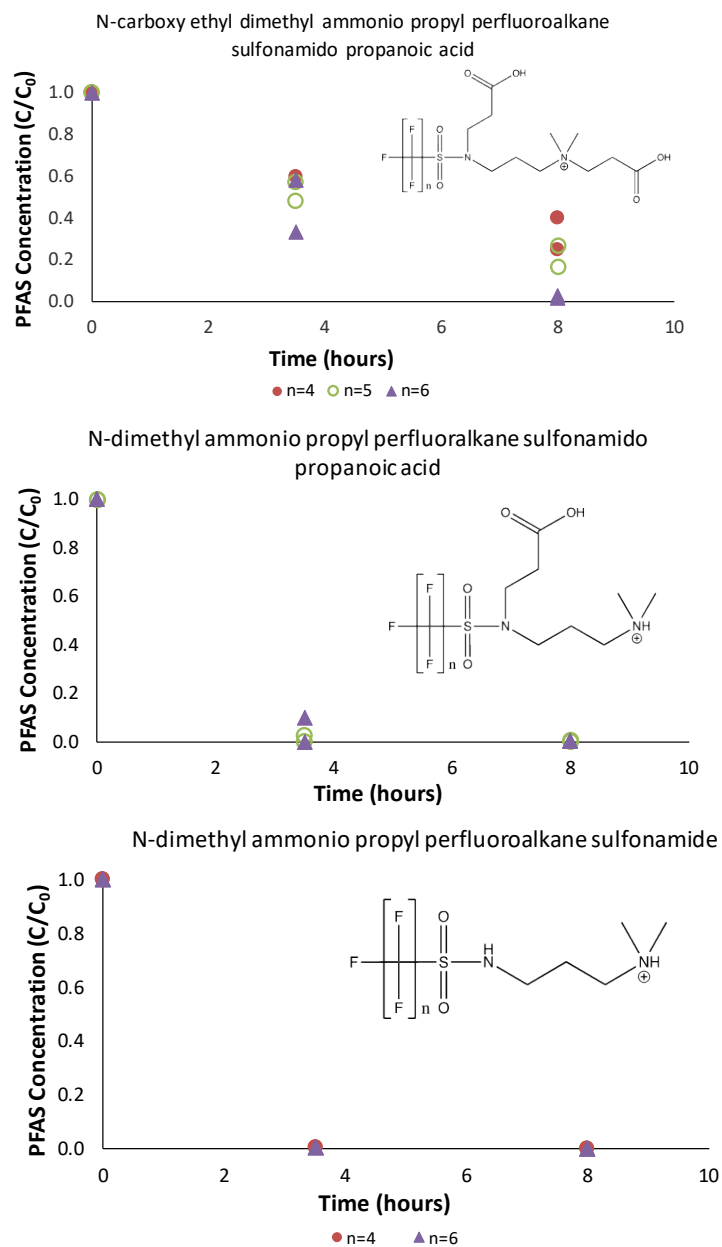


Figure 4.2.9. PFAS removal during electrochemical oxidation in W1. Values are normalized to no-current controls. Results of duplicate experiments are shown. n is the perfluoroalkyl chain length.

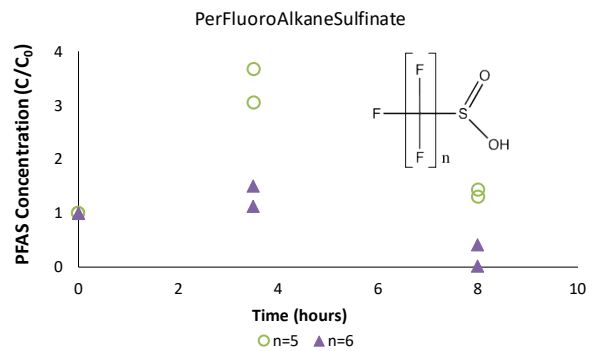
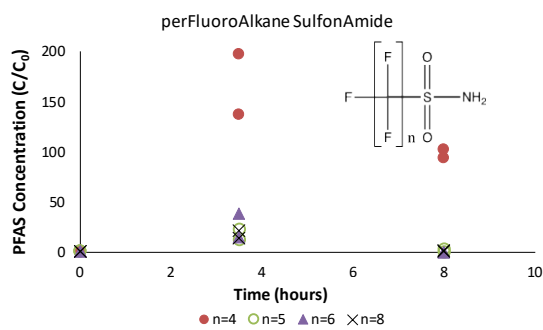
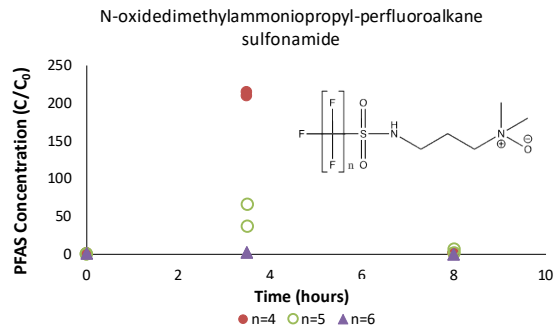
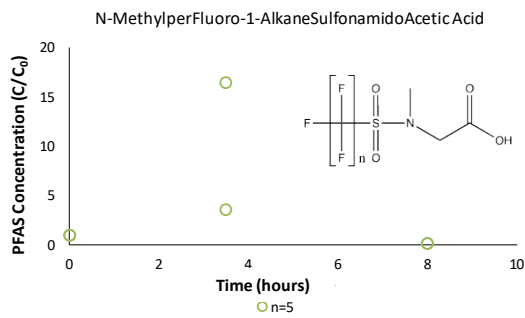


Figure 4.2.10. PFAS formation followed by removal during electrochemical oxidation in W1. Values are normalized to no-current controls. Results of duplicate experiments are shown. n is the perfluoroalkyl chain length.

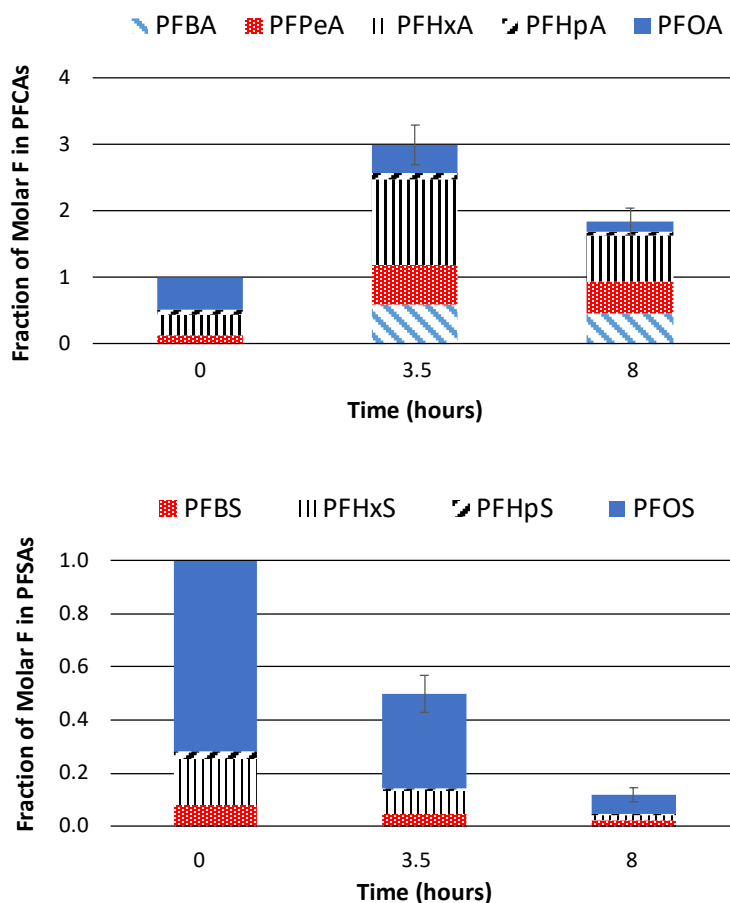


Figure 4.2.11. Fraction of the molar F concentration in the indicated PFAS relative to $t=0$ in PFCAs (top) and PFSAs (bottom) in W1 during electrochemical treatment. The applied current density was 25 mA/cm^2 . Average of duplicate experiments are shown. Error bars represent 95% confidence intervals on the sum of either the PFCAs or the PFSAs. PFBA= perfluorobutanoic acid, PFHxA=perfluorohexanoic acid, PFHpA = perfluoroheptanoic acid, PFOA=perfluorooctanoic acid. PFBS = perfluorobutane sulfonate, PFHxS = perfluorohexane sulfonate, PFHpS = perfluoroheptane sulfonate, PFOS = perfluorooctane.

The data presented in Figures 4.2.9. through 4.2.11 suggest that electrochemical oxidation proceeds through the pathway shown in Figure 4.12 for AFFF-spiked groundwater W1. All the intermediate species shown in Figure 4.2.12 were formed, and subsequently transformed, during electrochemical treatment. The formation of OAmPr-FASAs observed during electrochemical treatment is consistent with the oxidative formation of FASAs. Mejia-Avenidaño et al. (Hu, et al., 2016) have shown the formation of FASA from AmPr-FASAs. The formation of FASAi from FASAs also has been observed during aerobic biotransformation processes (Houtz, et al., 2012). However, the formation of PFCAs from sulfonamido precursors has only been observed through

abiotic pathways (Houtz and Sedlak, 2012; Plumlee et al., 2009), and not biotic pathways (Avendano and Liu, 2015; Rhoads et al., 2008). Houtz and Sedlak (2012) also have shown that abiotic oxidation of both MeFASAs and FASAs results in the formation of PFCAs, which is consistent with the oxidation pathway shown in Figure 4.2.12. Electrochemical oxidation of non-fluorine containing sulfonamides, with cleavage of the S-N bond, has been previously demonstrated (Fabińska et al., 2014). The unzipping and defluorination of PFAAs via electrochemical approaches have been well documented (Niu et al., 2013). Electrochemical dealkylation and amine oxidation for non-fluorine containing compounds also have been well documented (Adenier et al., 2004; Radjenovic et al., 2011).

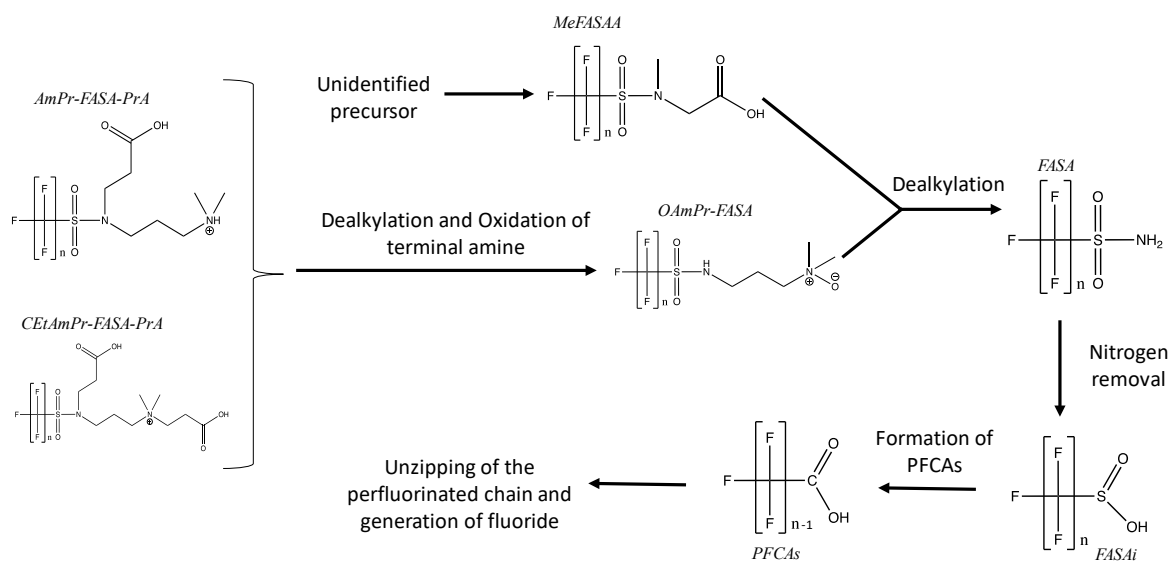


Figure 4.2.12. Oxidation pathway observed during electrochemical treatment of W1. Solid lines represent point to compounds that showed transient increase during electrochemical treatment.

4.2.2.3 PFAS Transformations during Electrochemical Treatment in Groundwater W2

At an applied current of 25 mA/cm², the applied voltage was 16 V for the W2 groundwater electrochemical experiments. The pH remained circumneutral, and a modest increase in temperature from 25 to 30 degrees C was observed.

Decreases in suspected PFAA precursors present in W2 are shown in Figure 4.2.13, and suspected PFAA precursors shown a transient increase followed by a decrease (FASAs (n=4 and n=6) and K-PFASs (n=2,3,4,6)) are shown in Figure 4.2.14. The transiently generated FASA levels

for n=4 and 6 were 10- to 100-times less than those for W1, and K-PFAS area counts were generally 3- to 10-times less than FASA area counts. In contrast to W1, electrochemical treatment of W2 groundwater yielded no transient increase in any PFAAs (Figure 4.2.16), but did yield a similar quantity of fluoride. An additional low current density (15 mA/cm²) with additional early-time sampling was performed for W2 to ensure that a large transient increase in PFAAs did not occur at early timepoints (t<3.5 hours).

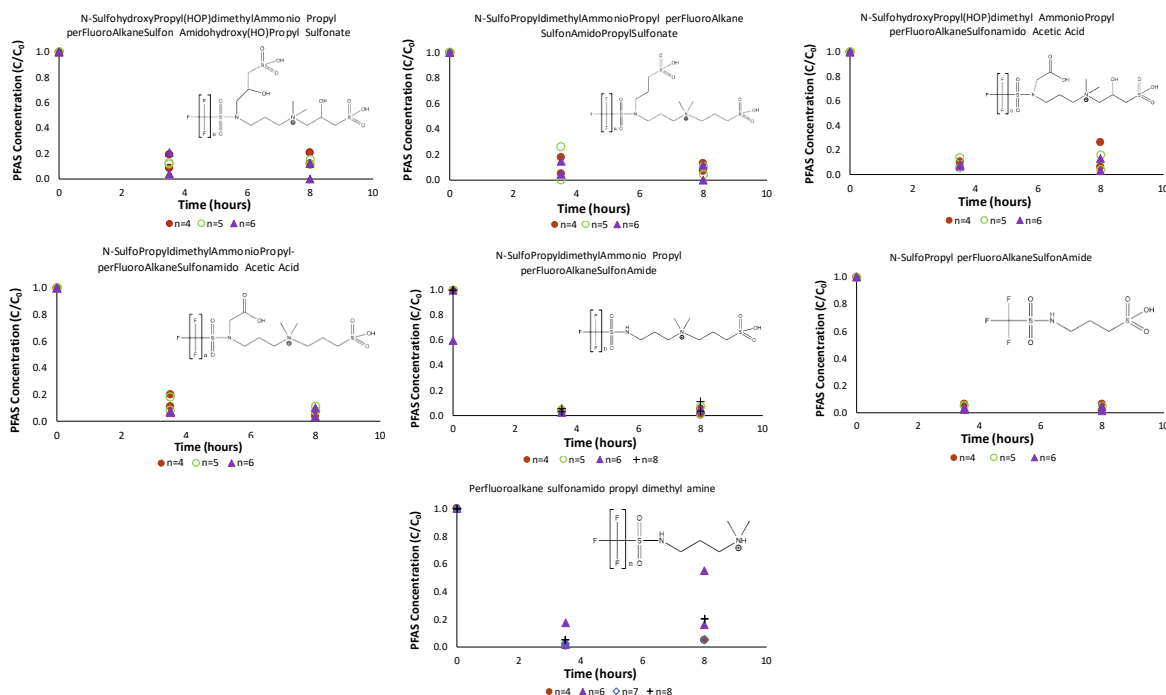


Figure 4.2.13. PFAS removal during electrochemical oxidation in W2. Values are normalized to no-current controls. Results of duplicate experiments are shown. n is the perfluoroalkyl chain length.

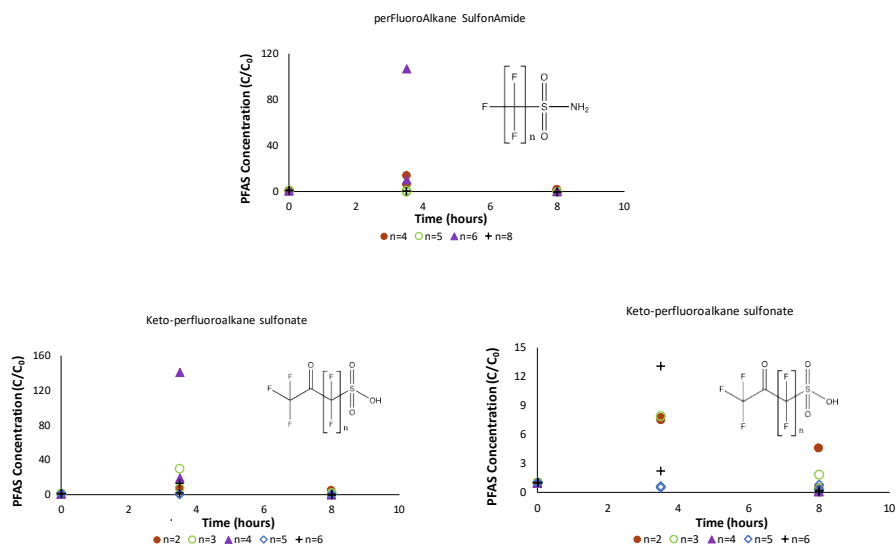


Figure 4.2.14. PFAS formation followed by removal during electrochemical oxidation in W2. Values are normalized to no-current controls. Results of duplicate experiments are shown. n is the perfluoroalkyl chain length.

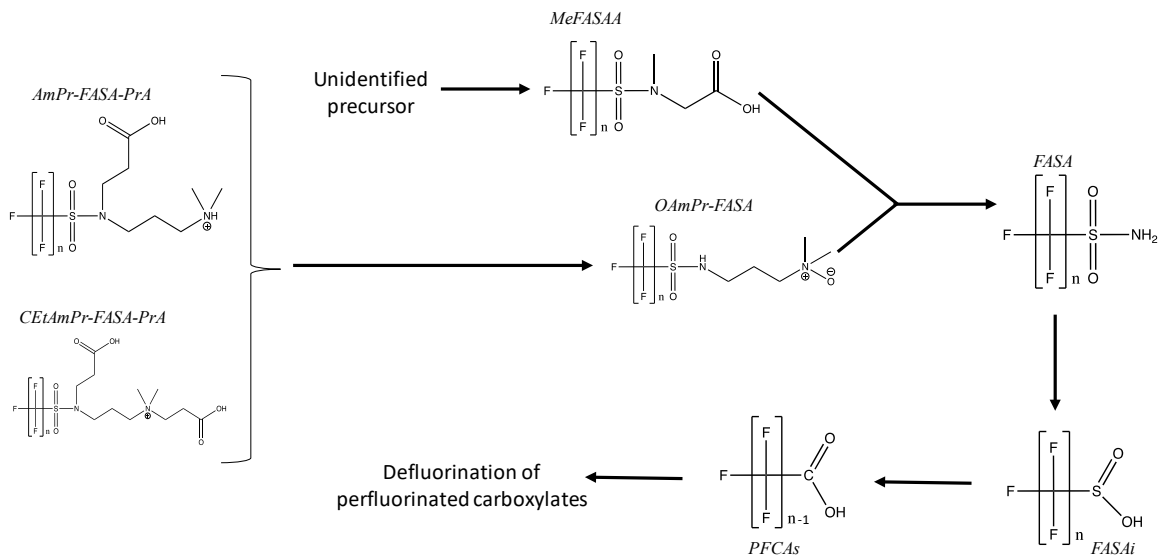


Figure 4.2.15. Proposed transformation pathway based on electrochemical treatment of W1. Solid lines represent point to compounds that showed transient increase during electrochemical treatment.

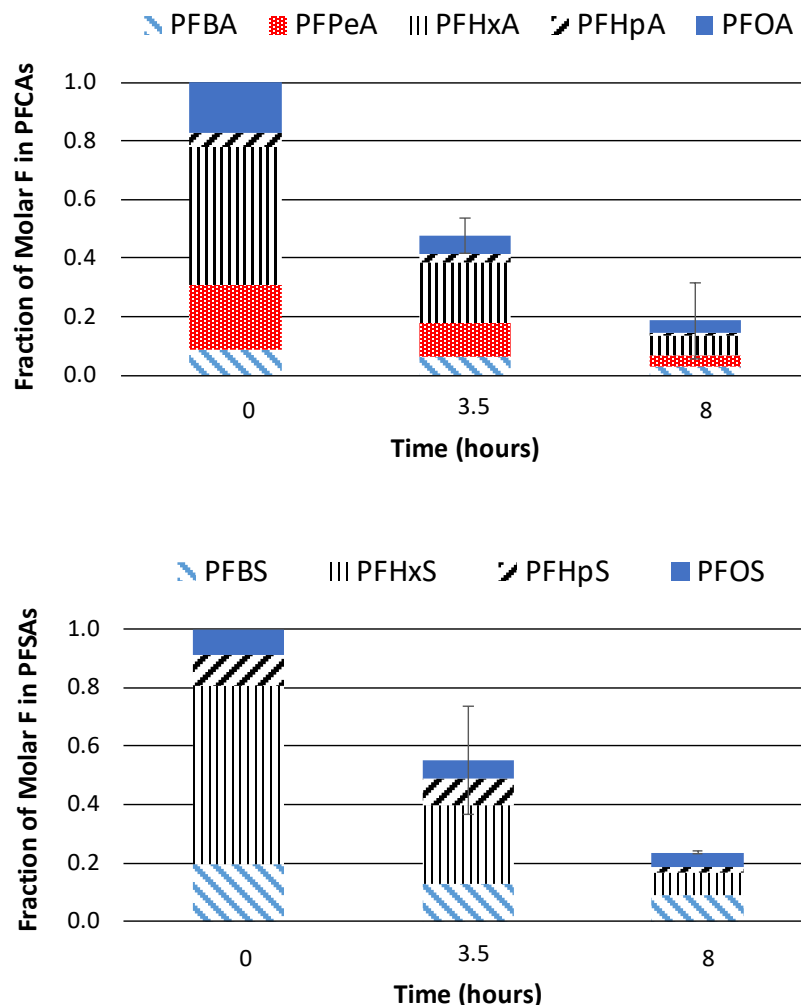


Figure 4.2.16. Fraction of the molar F concentration in the indicated PFAS relative to $t=0$ in PFCAs (top) and PFSAs (bottom) in W1 during electrochemical treatment. The applied current density was 25 mA/cm^2 . Average of duplicate experiments are shown. Error bars represent 95% confidence intervals on the sum of either the PFCAs or the PFSAs. PFBA= perfluorobutanoic acid, PFHxA=perfluorohexanoic acid, PFHpA = perfluoroheptanoic acid, PFOA=perfluorooctanoic acid. PFBS = perfluorobutane sulfonate, PFHxS = perfluorohexane sulfonate, PFHpS = perfluoroheptane sulfonate, PFOS = perfluorooctane.

The absence of transient PFAA increases in W2 during electrochemical oxidation is consistent with the results of the TOP assay, in which no PFAA formation was observed despite

the presence of several PFAS that would otherwise appear to be PFAA precursor compounds. Thus, the unexpected result that transient PFAA formation was not observed during the electrochemical experiments likely is the result of the nature of the PFAS associated with W2, and/or the groundwater geochemical conditions.

An additional set of experiments was performed to determine if either the slate difference in applied voltage (13V for W1 versus 16V for W2) or geochemical conditions (Table 3.2) were potentially responsible for the observed differences in transient PFAA formation between the two tested waters. Results showed that electrochemical testing of W1 at 16V of applied current (with an associated current density of 50 mA/cm²) were similar to the W1 experiments performed at low current density and voltage, in that transient formation of perfluorinated carboxylates was observed. Thus, the difference in behavior between W1 and W2 could not be explained by the differences in applied voltage. Likewise, the elevated sulfate levels in W2 were not responsible for the absence of transient PFAA formation, as transient formation of perfluorinated carboxylates was observed in an electrochemical experiments performed using 3M AFFF in a perchlorate electrolyte solution.

One plausible explanation for the fate of the suspected precursor compounds in W2 (e.g., S-OHPrAmPr-FASA-OHPrS, AmPr-FASA) is that the oxidation pathway for these compounds are substantially different than for the precursor compounds in W1; this explanation is consistent with the results of the TOP assay performed for W1 and W2. The formation of K-PFASs suggests that defluorination of the perfluoroalkyl chain occurs more readily for the PFASs in W2 than in W1, and that the subsequent transformation of K-PFASs yields organofluorine intermediates that are yet unidentified via HRMS (or below detection limits), ultimately generating fluoride. The PFAS transformation pathway in W2 is further explored in the following section by assessing the fluorine mass balance.

4.2.2.4 Evaluating the Fluorine Mass Balance during Electrochemical Treatment of W1 and W2

If only the PFAAs initially present in W1 and W2 were completely defluorinated, 0.28 and 0.35 mg/L of fluoride for W1 and W2, respectively, would be generated. Measured fluoride generation at the end of electrochemical treatment was approximately 3- to 4-times these values, indicating that F present in the non-target analytes provided the bulk of the fluorine for defluorination. It is interesting to note that the quantity of fluoride generation was similar for W1 and W2, despite the fact that the two water differed substantially in their TOP assay results (Figure 4.2.8), and despite the fact that W2 had substantially more suspected PFAA precursor compounds than W1 (Figure 4.2.7). It is hypothesized that this is due to the fact that the suspected PFAA precursor compounds in each of these water was oxidized via a different pathway.

Figure 4.2.17 shows the increases in F associated with fluoride and PFAA formation in W1 and W2 during electrochemical treatment. For W1, using the TOP assay as the basis for the fluorine mass balance (i.e., assuming all of the suspected precursors were converted to PFAAs), the fluorine mass balance for electrochemical treatment was approximately 71%. This fluorine mass balance

during electrochemical treatment is similar to that observed in single component PFAS electrochemical systems (PFOA or PFOS), and may represent losses due to formation of volatile fluorine species (Schaefer et al., 2015; 2017)

For W2, the increase in F shown in Figure 4.2.17 are due to fluoride generation only, as no PFAA formation was observed. The TOP assay results indicated that only 0.22 mg/L of fluoride could be generated during electrochemical treatment, which (base Figure 4.2.17) substantially underestimated the organic fluorine present. To assess the organic F initially present in the untreated (raw) water, total organic fluorine (TOF) analysis was performed on the W2 water by Leo Yeung using combustion analysis and ion chromatography. Results, shown in Figure 4.2.17, indicate that an excellent mass balance was obtained. The detect suspect analytes, TOF and electrochemical results confirm that the TOP assay failed to detect the majority of organic fluorine present in W2.

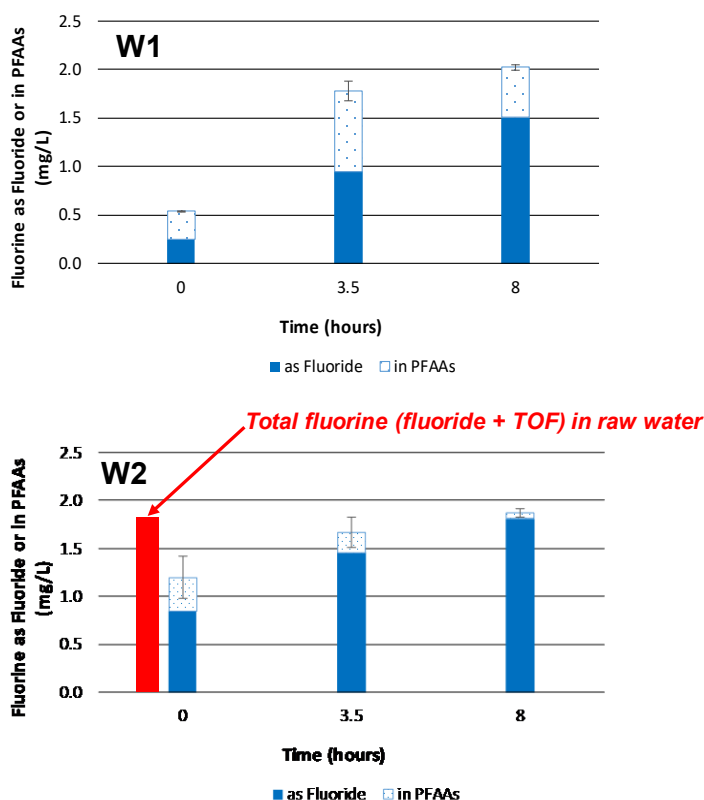


Figure 4.2.17. F generation as fluoride and in PFAAs during electrochemical treatment of W1 and W2. For W2, TOF analysis performed on the raw water confirmed that >90% of the fluorine mass balance was accounted for, and that >90% of the organic fluorine present was converted to fluoride during electrochemical treatment.

An additional 8-hour experiment was performed using W2 at an applied current density of 200 mA/cm². This test was performed to determine if additional defluorination (as evidenced by fluoride generation) would occur by increasing the applied current. Results showed that fluoride generation was essentially complete within the time period shown in Figure 4.2.17., consisted with the TOF data.

4.2.2.5 Electrochemical Defluorination Efficiency and Rate Constants

The dimensionless coulombic efficiency (CE) for electrochemical defluorination is calculated as follows (Bagastyo et al., 2012):

$$CE = FVe \frac{C_F}{At} \quad \text{Eq. 4.1}$$

where F is Faraday's Constant (94,486 C mol⁻¹), V is the batch volume (0.25 L), *e* is the number of electrons needed to generate fluoride (1 electron to cleave C-F bond is assumed). C_F is the measured fluoride generation (mol L⁻¹), A is the applied current (0.25A), and t is the time at the end of the 8 hour electrochemical experiment (s). The calculated values for the fluoride CE are 1.8 x 10⁻⁴ and 1.7 x 10⁻⁴ for W1 and W2, respectively. These extremely low CE values are due, in part, to the fact that additional electrons are needed to break bonds associated with the larger precursor compounds before defluorination occurs. The generation of anodic oxygen and oxidation of chloride are likely the most significant causes of these low CE values.

A current-normalized pseudo first order rate constant describing PFAS oxidation can be compared for different electrochemical treatment systems as follows:

$$k_n = \frac{kV}{C} \quad \text{Eq. 4.2}$$

where k_n is the current-normalized pseudo first order rate constant (L h⁻¹ A⁻¹), k is the regressed first order rate constant (h⁻¹), and C is the applied current (A). Calculated k_n values are provided in Table 4.2.2. A rate constant for PFOA in W1 for this study was not determined because the substantial generation of PFOA that occurred. The PFOA rate constant in W2 and in the sodium sulfate electrolyte were nearly identical. The PFOS rate constant in W1 and W2 differed by just under a factor of 3; it is unclear why the rate constant for PFOS showed this substantial difference between the two waters.

Table 4.2.2. Current-normalized pseudo first order rate constants as defined by Eq. 2. \pm values indicate the 95% confidence intervals from duplicate experiments; R^2 values are provided in parenthesis. A rate constant for PFOA in W1 is not provided due to the observed transient increase in PFOA.

Solution	Compound	Rate Constant ($L h^{-1} A^{-1}$)	Reference
W 1	PFOS	0.23 ± 0.056 (0.96)	Current study
W 2	PFOA	0.23 ± 0.084 (0.94)	Current study
	PFOS	0.084 ± 0.018 (0.94)	
Na ₂ SO ₄ Electrolyte	PFOA	0.24 ± 0.036 (0.93)	Current study

The energy per unit volume ($W\text{-h L}^{-1}$) applied over the 8-hour electrochemical treatment for W1 and W2, along with the corresponding change in PFAAs, is provided in Table 4.2.3. The relatively low removal of PFOS compared to PFHxS and PFHpS in W2 is surprising, as previous studies have shown that PFOS is removed more rapidly than shorter chained PFSAAs during electrochemical treatment (Niu et al., 2012). This observation suggests that low levels of PFOS were generated via precursors in W2 (but masked by the subsequent transformation of PFOS), and/or that components of the natural groundwater in W2 inhibit PFOS transformation. *It is important to note that for W1, the relationship between applied energy and perfluorinated carboxylate removal is masked by the oxidation of precursor compounds, which results in the formation of perfluorinated carboxylates.*

Table 4.2.3. Applied energy and percentage removal of PFAAs in W1 and W2. For PFHxA, PFPeA, and PFBA in W1, concentrations at the end of the experiment were greater than at the beginning due to precursor transformations.

W1

PFAS	% Removal	Energy (W-h/L)
PFOS	91	
PFHpS	94	
PFHxS	87	
PFBS	78	99
PFOA	71	
PFHpA	45	
PFHxA	(increase)	
PFPeA	(increase)	
PFBA	(increase)	

W2

PFAS	% Removal	Energy (W-h/L)
PFOS	40	
PFHpS	85	
PFHxS	89	
PFBS	63	136
PFOA	75	
PFHpA	59	
PFHxA	81	
PFPeA	67	
PFBA	57	

PFBA= perfluorobutanoic acid, PFPeA = perfluoropentanoic acid, PFHxA=perfluorohexanoic acid, PFHpA = perfluoroheptanoic acid, PFOA=perfluorooctanoic acid. PFBS = perfluorobutane sulfonate, PFHxS = perfluorohexane sulfonate, PFHpS = perfluoroheptane sulfonate, PFOS = perfluorooctane sulfonate.

4.2.3 Long-Term Electrochemical Testing

4.2.3.1 Electrochemical Performance and Fluorine Mass Balance

Figure 4.2.18 shows the removal of the perfluorinated carboxylates (PFCAs) and perfluorinated sulfonates (PFSAs), respectively, for each 24-hour batch cycle over the duration of the 21-day experiment. The long-chained PFAAs generally were removed more rapidly than the short-chained compounds. The exception was perfluorobutanoic acid (PFBA), which was removed more rapidly than perfluoropentanoic acid (PFPeA) during the first several days of treatment.

The rate of PFSAs and short-chained PFCAs began to decrease after the first 6 days, as indicated by their increasing values of C/C_0 . These increases were accompanied by an increase in applied voltage (from 15 to 21 V through 14 days). The final pH in the EC cell also increased from 7.0 to 7.9 over the first 14 days. In addition, the oxidative rate of chloride removal (forming chlorate and perchlorate) decrease over the first 14 days. Together, these data suggest that the overall electrochemical oxidation rate was decreasing in the system.

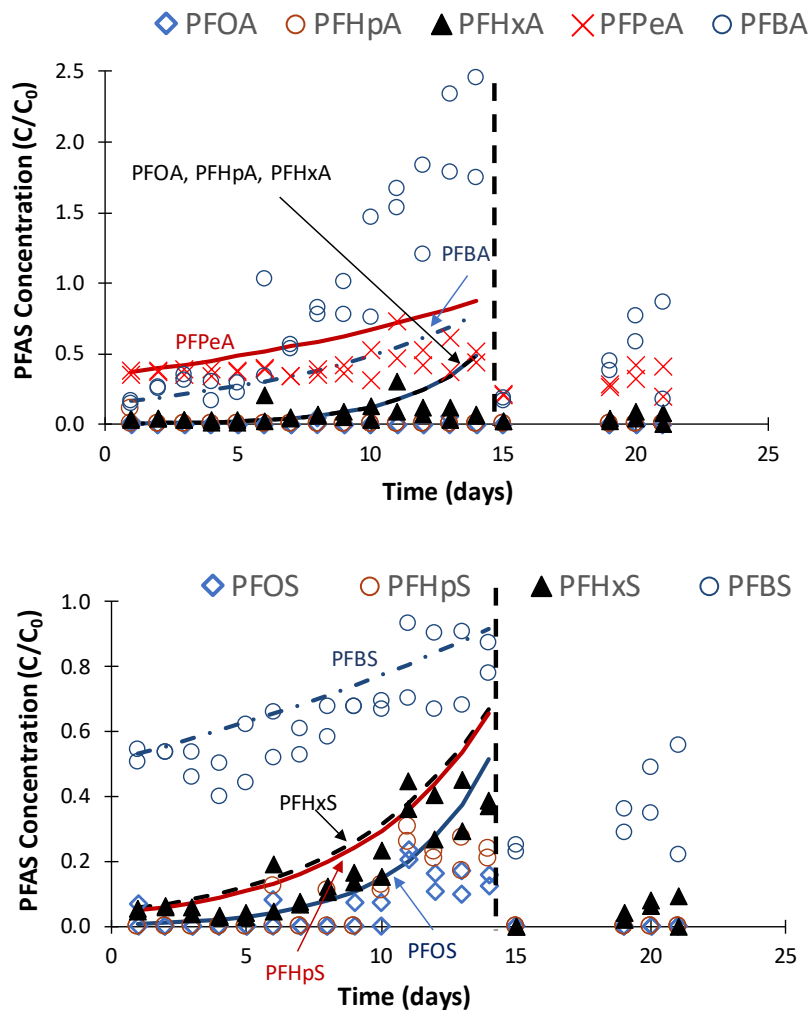


Figure 4.2.18. PFCAs (top) and PFSA (bottom) concentrations relative to the initial PFAS concentration measured at the end of each 24-hour EC batch treatment time. The observed first order PFAS transformation rate constant for the first day (k) was calculated as $\ln[c/c_0]/t$, where c_0 is the PFAS concentration at $t=0$ and c is the PFAS concentration at $t=24$ hours. t is the duration of each batch cycle (24 hours). The solid and dashed lines show the predicted change in PFAS relative concentration (C/C_0) assuming a first order model where the rate constants decrease at the same rate as the chloride rates constant shown in Figure 4.2.21 For PFOA, PFHpA, and PFHxA, the lines showing the predicted values overlap. The prediction for PFBA is poor due to generation of PFBA. The vertical dashed line shows when the system was shut-down for scale removal.

The EC system was disassembled after day 14, and substantial accumulation of scale (calcium and magnesium scale based upon analysis using HACH Method 8030) was observed near the cathode and along the screen that separated the electrodes. A 20% sulfuric acid solution was used to remove the scale. Upon restarting the system, a decrease in voltage to near the original levels was observed, and PFAA removal rates returned to near those observed during the initial days of operation. Over the last few days of the experiment, PFAA concentrations again began to increase, likely due to the same scaling issues previously described.

Results clearly show substantial removal of both PFCAs and PFSA's at day 1 (Figure 4.2.19), with no measurable accumulation of shorter-chained PFAAs, which is consistent with previous observations discussed in Section 4.1 and 4.2. However, at day 14, when EC system performance had deteriorated due to scale accumulation, PFAA concentrations in the EC treated water had substantially increased from those observed at day 0, as PFAA removal had decreased by approximately 20%. The generation of PFBA also accompanied this decrease in performance due to the scaling.

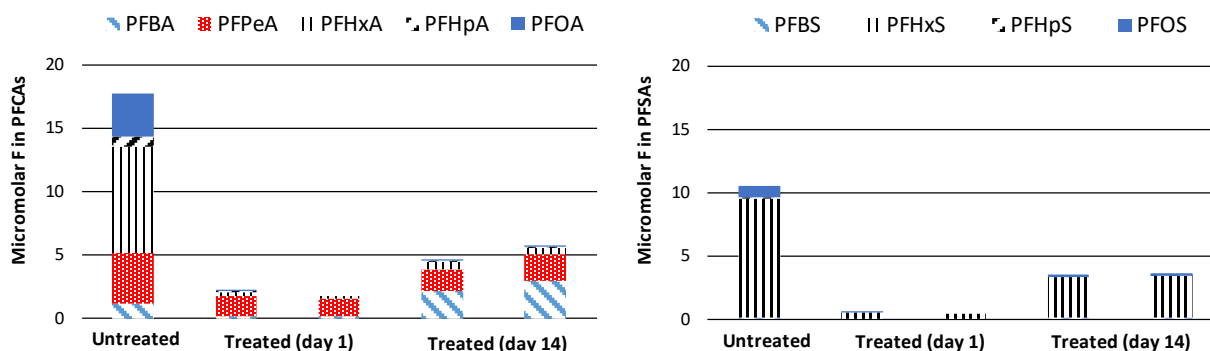


Figure 4.2.19. Removal of PFAAs at Day 1 compared to Day 14. Formation of PFBA is clearly observed, and micromolar F levels in PFBA at Day 14 increase from the untreated (raw water) condition. Duplicate results for Days 1 and 14 are shown.

The fluoride generation resulting from EC oxidation of the PFASs is shown in Figure 4.2.20. The fluoride present in the PFAAs in the untreated water can only account for up to approximately 28 μM of F. Thus, fluoride generation in excess of this likely was due to the electrochemical oxidation of PFAA precursors such as N-SulfohydroxyPropyl dimethylammonio propyl perfluorohexane sulfonamido hydroxypropyl sulfonate that has been identified in this groundwater during prior testing (Section 4.2). Fluoride generation shown in Figure 4.20 decreased between 40 and 60% over the first 14 days of treatment, which is greater than the 20% decrease in PFAA removal (Figure 4.2.19) observed over this same time period. These results suggest that the

relatively large decrease in defluorination was primarily attributable to a decrease in the oxidation/defluorination of the suspected PFAA precursors, and that the slow fouling of the EC system due to scaling had a greater adverse effect on the polyfluoroalkyl compounds than on the PFAAs.

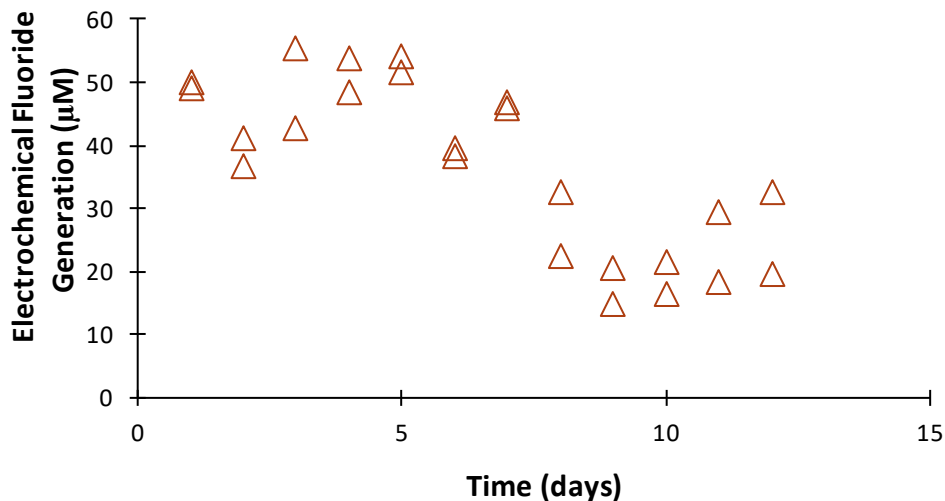


Figure 4.2.20. F removed as fluoride from PFAS. Based on the PFAAs present in the untreated water, approximately 28 μM of fluoride was present.

4.2.3.2 Electrochemical Oxidation Treatment Kinetics & Mass Transfer

Chloride was oxidized during the electrochemical treatment experiment, forming perchlorate. Up to 525 mg/L of perchlorate was generated on day 1. Perchlorate generation decreased as the oxidative activity of the system decreased (presumably due to the previously described scaling) over the first 14 days of operation. Assuming first order kinetics for the oxidation of chloride to perchlorate, the change in the first order rate constant describing the oxidation of chloride to perchlorate over the first 14 days is shown in Figure 4.2.21. As shown in Figure 4.2.21, the decrease in the first order rate constant over time was well described by a linear model, and likely was due to diminished contact with the electrodes in the cell due to the scale formation.

It is reasonable to assume that the decrease in chloride oxidation to perchlorate is proportional to the decrease in oxidation of the PFAAs. This is because chloride electrochemical

oxidation, like that of PFAAs, is initiated by an anodic surface reaction (Polcaro et al. 2009). Assuming that the electrochemical oxidation of PFAAs can also be reasonably described by a first order reaction (Urriaga et al. 2015, Schaefer et al. 2017), the decreasing trend in the first-order rate constant shown in Figure 4.2.21 can be applied to the electrochemical oxidation of the PFAAs. The solid and dashed curves in Figure 4.2.18 show that the decreases in PFAA oxidation correspond to that observed for the decreased oxidation of chloride to perchlorate, and therefore is consistent with a decrease in the anodic surface reaction rate due to the presence of the scale. The notable exception in Figure 4.2.18 is PFBA. PFBA is poorly described by the model due to the generation of PFBA, as discussed in Section 4.2.3.1.

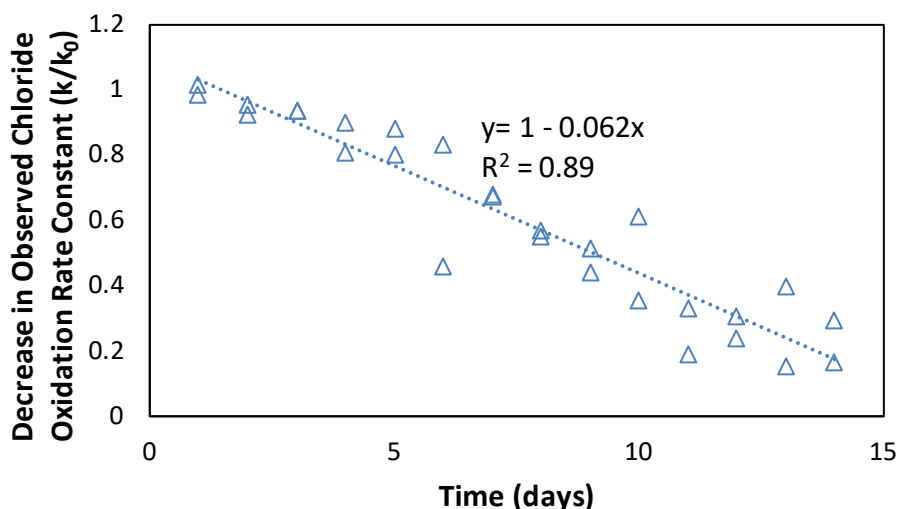


Figure 4.4.21. The decrease in the first order rate constant describing chloride removal (via electrochemical oxidation) relative to the chloride oxidation rate constant observed on day 1. This decrease was reasonably described by a linear model. This linear model with regressed fit (dashed line) is shown in the figure.

4.2.4 Testing Evaluating alternate Anode Materials and Electrochemical Cell Configurations

4.2.4.1 Divided Electrochemical Cell

Experiments performed using groundwater W2 showed that there was no measurable transformation of PFAA precursors (as evidenced by PFAA formation) during cathodic treatment. Results for PFOA and PFOS in groundwater W2 are shown Figures 4.2.22 and 4.2.23, respectively. Similar results were obtained for the synthetic groundwater spiked with 3M AFFF

(Figures 4.2.24 and 4.2.25). For both W2 and the AFFF-spiked synthetic groundwater, review of the suspect analyte data indicated that no transformation of any of the potential PFAA precursors occurred during cathodic treatment, which is consistent with the results shown in Figures 4.2.22 through 4.2.25. Thus, cathodic treatment (for the conditions used in this study) did not facilitate overall PFAS treatment.

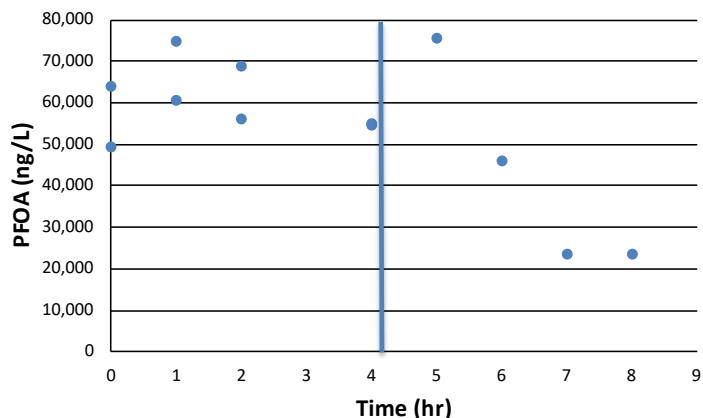


Figure 4.2.22. Using groundwater W2, PFOA concentrations in a divided electrochemical cell using sequential cathodic-anodic treatment. The vertical line indicates the transition from cathodic to anodic treatment. The applied current density was 25 mA/cm², and the applied voltage during cathodic treatment as approximately 12 V.

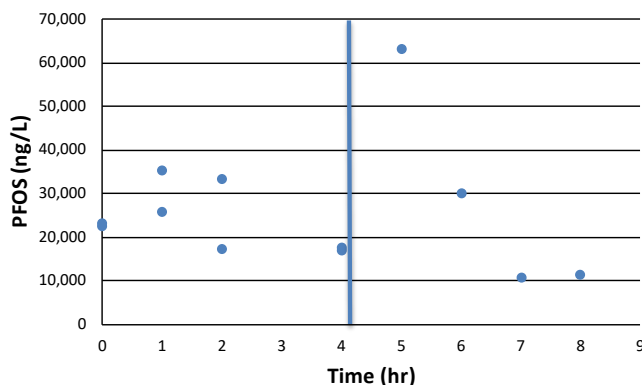


Figure 4.2.23. Using groundwater W2, PFOS concentrations in a divided electrochemical cell using sequential cathodic-anodic treatment. The vertical line indicates the transition from cathodic to anodic treatment. The applied current density was 25 mA/cm², and the applied voltage during cathodic treatment as approximately 12 V.

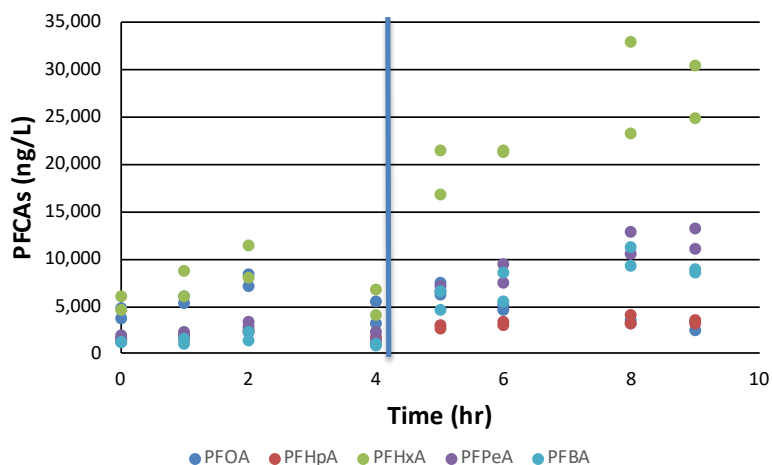


Figure 4.2.24. Using groundwater synthetic groundwater spiked with 3M AFFF, perfluorinated carboxylate concentrations showed no indication of formation or removal during cathodic treatment, but did show indications of formation (from oxidation of PFAA precursors) during anodic treatment. The vertical line indicates the transition from cathodic to anodic treatment. The applied current density was 25 mA/cm².

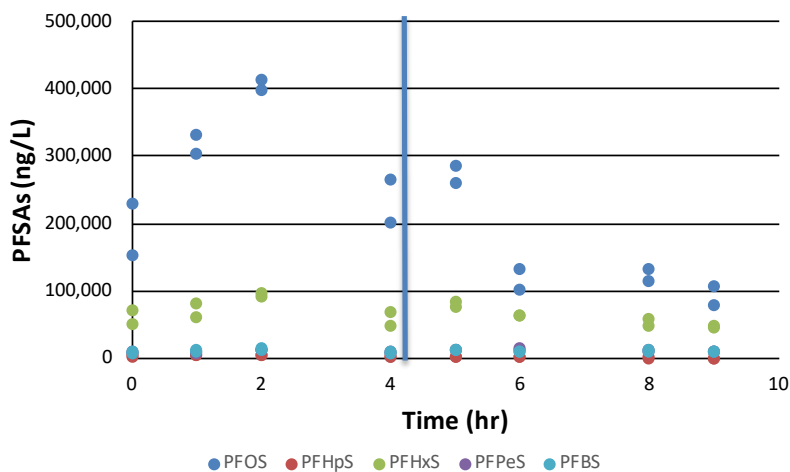


Figure 4.2.25. Using groundwater synthetic groundwater spiked with 3M AFFF, perfluorinated sulfonate concentrations showed no indication of formation or removal during cathodic treatment, but did show indications of removal during anodic treatment. The vertical line indicates the transition from cathodic to anodic treatment. The applied current density was 25 mA/cm².

4.2.4.2 Nitrogen-doped tetrahedral amorphous carbon (ta-C:N) electrodes

Nitrogen-doped tetrahedral amorphous carbon (ta-C:N) were manufactured by Fraunhofer for use as cathodes in undivided cell EC experiments. Ir/RuO₂ electrodes were used as the anodes, with 25 mA/cm² applied current. The W2 (Ellsworth AFB) groundwater was used in the testing. Results showed substantial decreases for nearly all the PFCAs and PFSA's examined. No fluoride generation was measured, but the relatively low PFAS levels in the groundwater may have masked the fluoride generation. Additional experiments with elevated levels (20 mg/L) of PFOS in sulfate electrolyte and an applied current density of 25 mA/cm² were subsequently tested. No measurable (<1 mg/L) fluoride detected. Thus, the ta-C:N electrodes were not effective for PFOS defluorination under the conditions of this study.

4.3 B₁₂-Catalyzed Reduction

Initial experiments tested the defluorination of PFMe₂OA (**1**; *See Table 3.4.1 and Figure 4.3.2 for names and structures relating to numbers referenced*), a well-defined branched structure, at rate-optimized reaction conditions reported previously (pH 9.0 and 70°C) (Ochoa-Herrera et al., 2008). Defluorination was evaluated by the concentration ratio of released F⁻ ions to the F initially present in the PFAS substrate. Significant defluorination occurred only in the presence of both Ti^{III} and B₁₂ (Figure 4.3.1). Figure 4.3.2 shows that a maximum of 85% defluorination from **1** was achieved in 7 d. Because LC-QToF-MS analysis indicated complete degradation of **1**, this high defluorination ratio corresponds to an average of sixteen of the nineteen F atoms within the PFMe₂OA structure being released as F⁻. According to the mechanisms proposed for Co-catalyzed dehalogenation reactions (X = Cl and Br), Ti^{III} reduces the Co^{III} in B₁₂ to Co^I, which then interacts with either the carbon or halide (X) to cleave the C-X bonds (Chiu and Reinhard, 1995; Kliegman and McNeill, 2008; Payne et al., 2015). Assuming a similar mechanism for the defluorination reactions, the turnover number (TON) for each Co center is estimated to be 6.5 for the reaction with **1**, demonstrating the catalytic nature of reaction. The TON could be further increased for at least 10 times (i.e., TON=65) because elevating the concentration of **1** from 0.1 mM to 1.0 mM still achieved the same defluorination ratio. The reaction slowed at room temperature (21 ± 2°C), but still resulted in at least 44% defluorination within 8 mo (Figure 4.3.2), suggesting the potential for slow defluorination of branched PFAS in low redox potential natural environments, where microorganisms employ B₁₂ for dechlorination (Men et al., 2013).

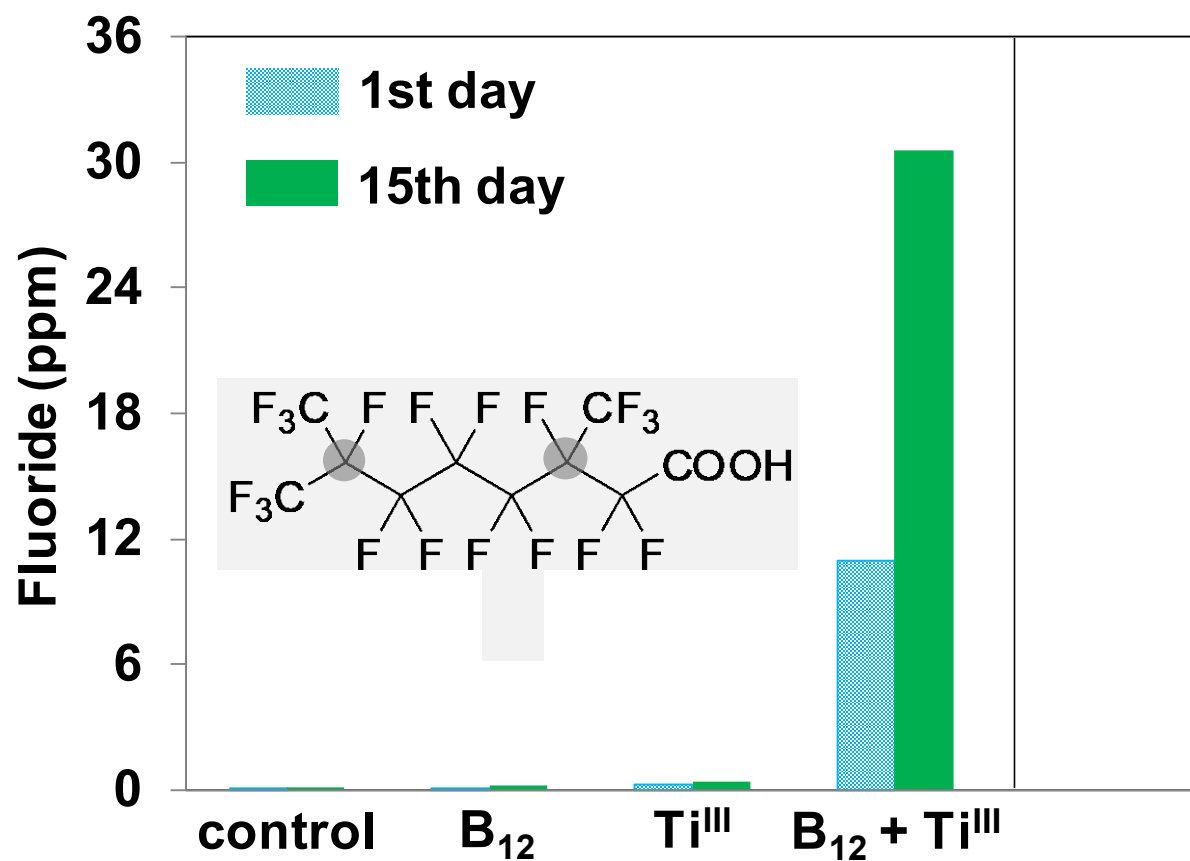


Figure 4.3.1. Defluorination of **1** under different conditions. Reaction conditions for “B₁₂ + Ti^{III}”: PFMe₂OA (0.1 mM), B₁₂ (0.25 mM), Ti^{III} citrate (~36 mM), and carbonate buffer (~40 mM) in water; pH 9.0; 70°C.

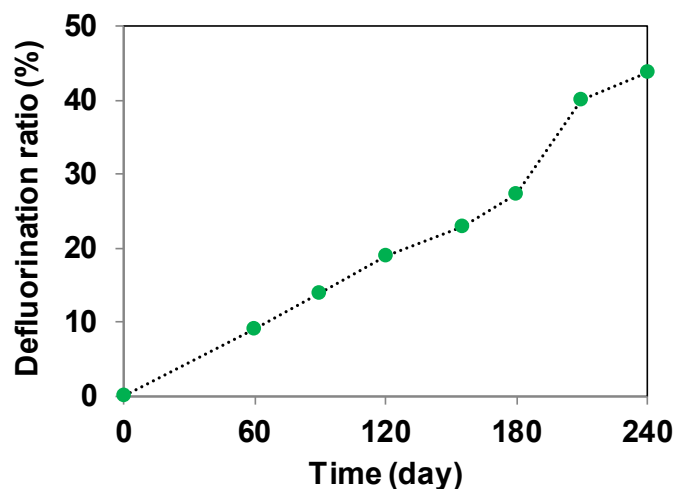


Figure 4.3.2. Defluorination of **1** at room temperature ($21 \pm 2^\circ\text{C}$). Reaction conditions: PFMe₂OA (0.1 mM), B₁₂ (0.25 mM), Ti^{III} citrate (~36 mM), and carbonate buffer (~40 mM) in water; pH 9.0. The reactor was occasionally stirred. After 8 months, the mixture turned into a “wet cake” due to the continuous precipitation of dark blue solids. In comparison, the lack of B₁₂ and Ti^{III} citrate in the aqueous solution of **1** resulted in negligible defluorination at room temperature for over 5 months.

To elucidate the relationship between PFAS structure and susceptibility to B₁₂-catalyzed defluorination, commercially available PFAS with different “branched structures” were reacted with B₁₂ and Ti^{III} (Figure 4.3.3). It was soon realized that a simple classification as “branched” was insufficient as a predictor for susceptibility to defluorination. For example, a branched fluorotelomer acid **4** (Figure 4.3.3d) released negligible F⁻ under the same reaction condition as **1**. In stark contrast, replacing the -CH₂-CH₂- moiety within the fluorotelomer structure with -CF=CF- (**2**) led to the rapid and complete degradation of the parent compound within 1 day and a maximum of 91% defluorination (an average of eight of the nine C-F bonds cleaved in each molecule, Figure 4.3.3b). Cyclic **3** is a carboxylic acid analog of PFECHS. It contains one branched carbon with two -CF₂- and a -COOH neighbors. The parent compound was partially degraded (70%), and the F⁻ release from **3** corresponded to an average of three out of eleven F atoms in each molecule (Figure 4.3.3c). In comparison, negligible F⁻ release was observed from the cyclic amine **6**, in which the N atom can be considered as a “branched” point. Negligible F⁻ release was observed for the perfluoroalkyl ether compound **5** possessing two branched carbons. Hence, it can be inferred that the local chemical environment surrounding the tertiary C-F is critical to their reactivity with B₁₂. No appreciable defluorination was observed in experiments with the linear PFOA (**7**) and several shorter chain linear acids lacking branched carbon atoms (CF₃SO₃H, CF₃COOH, and CF₃CF₂COOH). LC-QToF-MS analysis showed no significant degradation of **7** for up to 30 days.

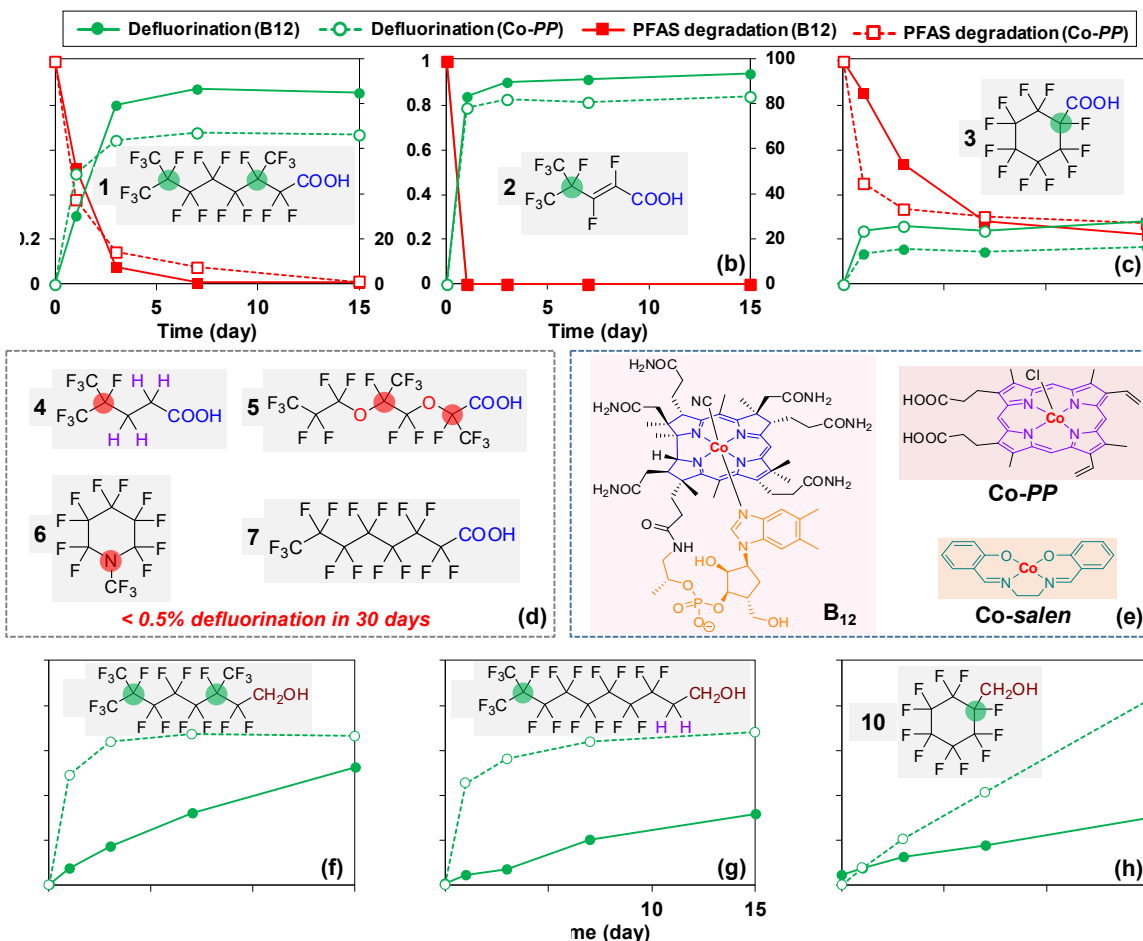


Figure 4.3.3. Degradation and defluorination for each PFAS with cobalt catalysts shown in (e). Branches that are effective and ineffective in promoting defluorination are highlighted in green and red, respectively. Reaction conditions: PFAS (0.1 mM), Co catalyst (0.25 mM), Ti^{III} citrate (~36 mM), and carbonate buffer (~40 mM) in water; pH 9.0; 70°C.

In comparison to the carboxylic acid 1, B_{12} -catalyzed F^- release was much slower for the analogous telomer alcohol structure 8 (Figure 4.3.3f versus 3a), and the F^- release from alcohol 9, with only one branched carbon, was even slower (Figure 4.3.2g). The comparison between cyclic 3 and 10 also shows much slower defluorination from the telomer alcohol than from the carboxylic acid (Figure 4.3.2h versus 2c). Degradation of alcohols in aqueous solution was not readily observed by LC-QToF-MS. Reactions with these alcohols were also conducted with variable headspace volumes (e.g., 9 mL liquid + 0 mL headspace versus 2 mL liquid + 7 mL headspace in the sealed 9-mL bottles). All conditions yielded similar defluorination results, excluding the possibility that the slower defluorination resulted from volatilization of alcohol substrates into the headspace.

Calculated C–F bond dissociation energies (BDEs) provide further insights into mechanisms for the *initial* step of defluorination. As shown in Figure 4.3.4, the general order of C–F BDEs is tertiary < secondary < primary. The lowest secondary C–F bond BDE (451.9 kJ mol^{-1}) in the 2-position of 7 can be attributed to its proximity to $-\text{COOH}$. In 1, 8 and 9, secondary

C–F bonds adjacent to branched carbons have even lower BDEs (414.2 to 431.0 kJ mol⁻¹). Importantly, BDEs for tertiary C–F bonds within the structures for which defluorination was observed (compound 1–3 and 8–10) range from 364.4 to 431.0 kJ mol⁻¹, whereas higher BDEs ranging from 431.4 to 443.9 kJ mol⁻¹ were found in the two branched structures with no defluorination (4 and 5). The higher BDEs for those tertiary C–F bonds are due to the presence of relatively weak electron-withdrawing hydrocarbon and oxo moieties nearby. We propose that the initial defluorination steps occur at tertiary C–F bonds with low BDEs. Such weak bonds can dissociate upon interaction with Co^I. A Comparison of the three non-cyclic structures 1, 8, and 9 suggests a rough correlation between the BDEs of the tertiary C–F bonds (1 < 8 < 9) and the reaction rates of defluorination (1 > 8 > 9). Comparison of the cyclic 3 and 10 reveals a similar trend.

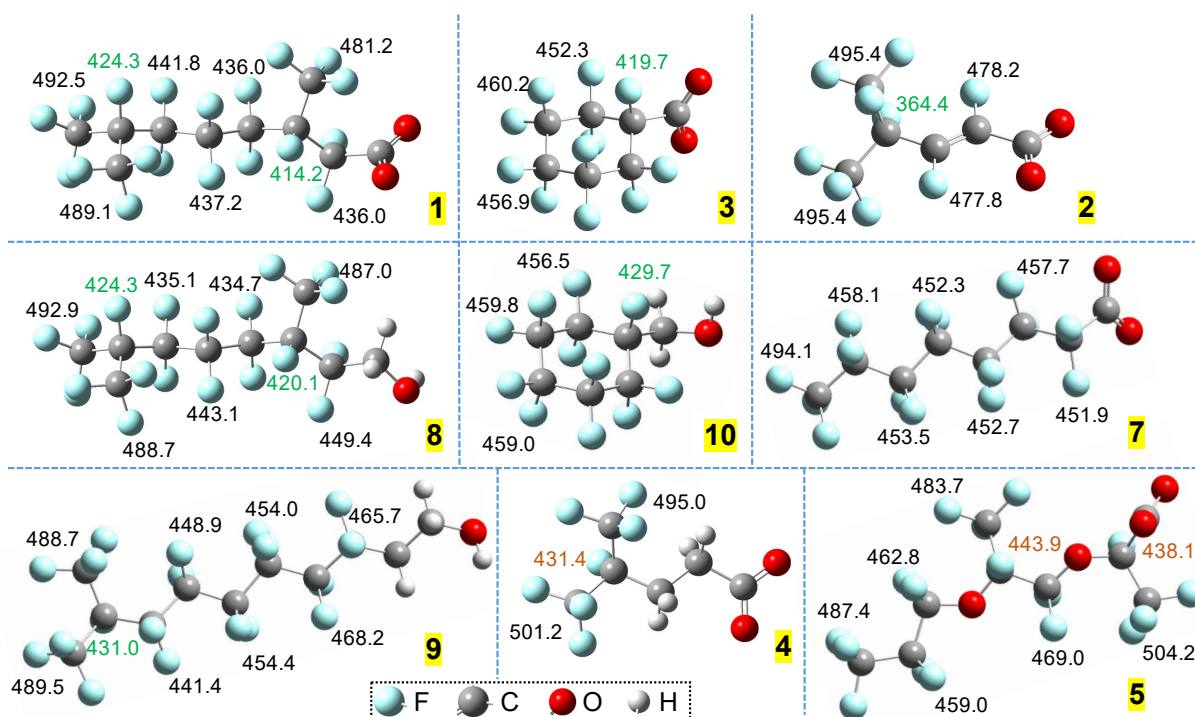


Figure 4.3.4 Calculated bond dissociation energies (in kJ mol⁻¹) at B3LYP/6-311+G(2d,2p)/SMD level of theory (BDEs) of C–F bonds. The displayed terminal group with two C=O bonds represent charge-delocalized –COO⁻ anion.

Compound 2 has two sp² C–F bonds with high BDEs (478.2 and 477.8 kJ mol⁻¹) and exhibited rapid and extensive defluorination. In comparison to 1, the presence of sp² C–F bonds seems to promote defluorination. The bonding with the C=C double bond significantly weakens the tertiary C–F bond (364.4 kJ mol⁻¹, the lowest BDE among all structures). Similar results have been reported by Im et al., who reported B₁₂-catalyzed defluorination of the only sp² C–F in the refrigerant HFO-1234yf (H₂C=CF–CF₃) yielding H₂C=CH–CF₃, and further defluorination of one sp³ C–F in H₂C=CH–CF₃ yielding H₂C=CH–CF₂H (Im et al., 2014). Additionally, sp² C–F bonds can be cleaved with H₂ gas and a Rh/Al₂O₃ catalyst while sp³ C–F bonds cannot (Baumgartner

and McNeill, 2012; Yu and Chiu, 2014). Defluorination involving unsaturated bonds probably follows reaction mechanisms similar to the Co-catalyzed dechlorination of chlorinated ethenes (Kliegman and McNeill, 2008). Future studies are necessary for mechanistic elucidation.

In addition, the close BDE values for the two tertiary C–F bonds in 9 and 4 (431.0 versus 431.4 kJ mol⁻¹) suggest that the neighboring atoms are also critical to initiate defluorination reactions. The experimental results described above indicate that, B₁₂-catalyzed defluorination requires a tertiary C–F branch surrounded by either three fluorinated carbons or two fluorinated carbons plus one carboxyl group. If one surrounding atom is changed to hydrocarbon or oxygen, the defluorination reaction cannot be initiated. Since typical ether compounds synthesized from C3 building blocks (e.g., the two shown in Figure 4.3.5) do not contain the susceptible C4 branched structure, they are expected to be recalcitrant toward B₁₂-catalyzed defluorination.

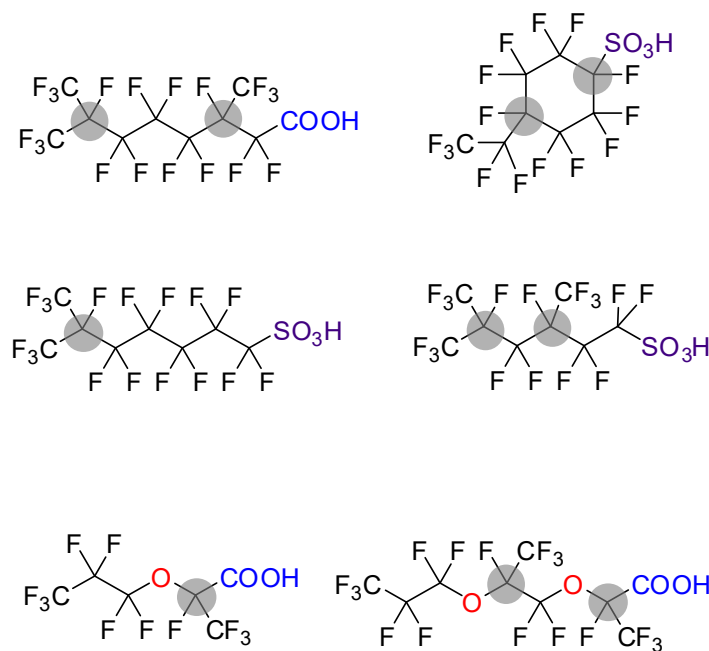


Figure 4.3.5 Examples of branched PFASs detected in the environment. Branched carbons are highlighted in grey.

It is important to emphasize that BDEs of the parent PFASs can only be used to interpret the *initiation* of defluorination reactions. For example, the experimental data for 1 suggests that, among the sixteen F⁻ released per 1, at least six derived from primary C–F bonds with high BDEs ranging from 481.2 to 492.5 kJ mol⁻¹. In contrast, although the linear 7 contains twelve secondary C–F bonds with BDEs ranging from 451.9 to 458.1 kJ mol⁻¹, no defluorination was observed.

These results collectively indicate that B₁₂-catalyzed defluorination reactions are initiated at tertiary C–F bonds with suitable local chemical environments.

Defluorination intermediates or end products were not observed by LC–QToF-MS (like those reported by Park et al. on branched PFOS isomers) (Park et al., 2017). One probable reason for the lack of observed products could be that, the fragmentation of PFASs during reaction led to the loss of ionizable groups (e.g., –COO[–]) that enable MS detection. We emphasize that the actual reaction mechanisms for the multiple step reactions are complicated because the interpretation goes beyond prediction with C–F bond BDEs of the parent structures. For example, the cyclic 3 does not contain any primary C–F bonds, but the defluorination ratio observed was much lower than that for 1, which contains nine primary C–F bonds. Furthermore, if F is replaced by H during defluorination, BDEs of the adjacent C–F bonds in the resulting structures are mostly elevated or unchanged (Figure 4.3.6), and this would appear to inhibit subsequent defluorination by the same mechanism. However, based on the unsaturated intermediate structures proposed by Park et al., other mechanisms such as HF elimination might be involved in further defluorination (Park et al., 2017). As discussed earlier for compound 2 and HFO-1234yf, the presence of C=C bonds could promote defluorination (Im et al., 2014). Clear mechanistic elucidation requires further experiments with more model compounds and theoretical calculations.

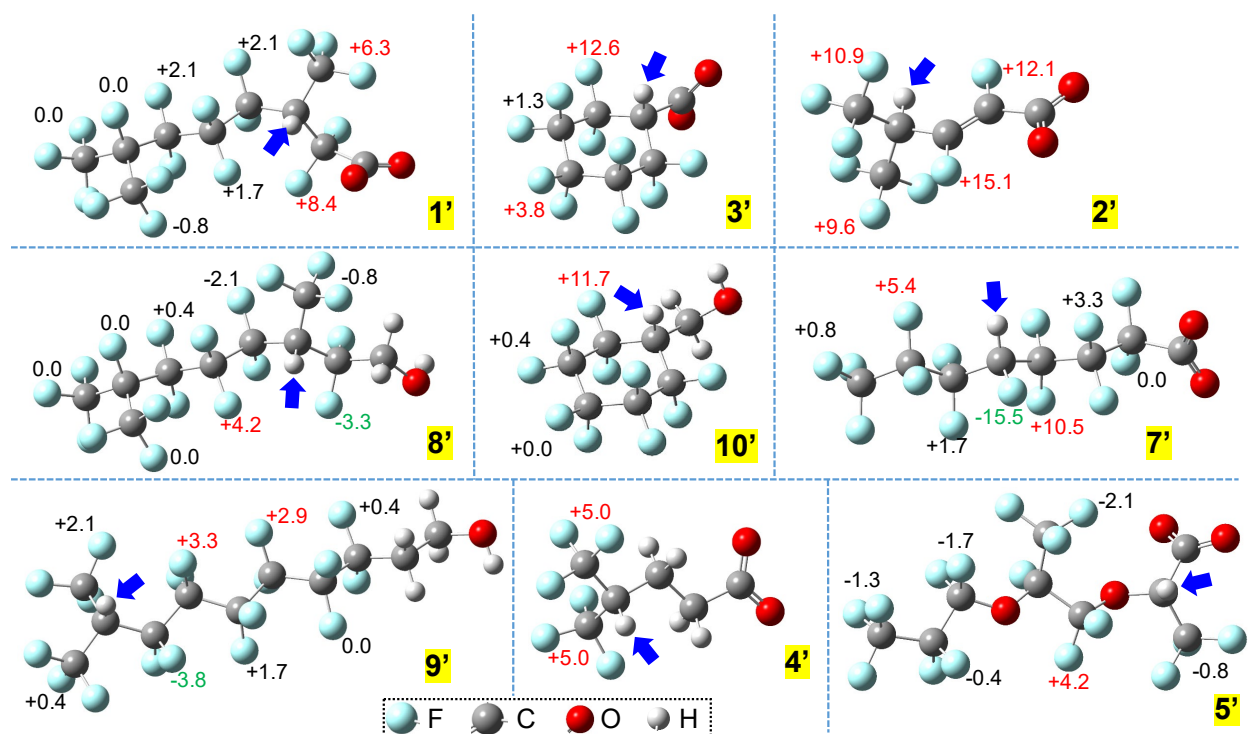


Figure 4.3.6 Change of individual C–F bond BDEs (in kJ mol^{-1}) upon the weakest C–F being replaced by a C–H (indicated by a blue arrow). BDEs were calculated at B3LYP/6-311+G(2d,2p)/SMD level of theory. The displayed terminal group with two C=O bonds represent charge-delocalized –COO[–] anion. Significant BDE changes (i.e., $>2.1 \text{ kcal mol}^{-1}$ or $>0.5 \text{ kcal mol}^{-1}$) are highlighted in red for increase and in green for decrease.

A protoporphyrin-coordinated complex, Co-PP (Figure 4.3.2e), exhibited higher initial rate of defluorination than B₁₂ for most PFASs (Yonetani et al., 1974). This trend is apparent for the three examined alcohols (Figure 4.3.2f–h). For 1, although the maximum defluorination by Co-PP (an average of thirteen of nineteen C–F bonds cleaved) was lower than by B₁₂, defluorination by Co-PP in the 1st day was higher than by B₁₂ (Figure 4.3.2a). For 3, Co-PP was superior to B₁₂ in both initial reaction rate and the maximum defluorination ratio (Figure 4.3.2c). Thus, the two Co complexes demonstrate selectivity toward specific PFAS structures. As with B₁₂, structures 4 to 7 (Figure 4.3.2d) were not reactive with Co-PP.

The difference between Co-PP and B₁₂ might be attributed to two factors. First, the lack of axial benzimidazole lower ligand as in B₁₂ may allow faster electron transfer from Ti^{III} to the Co^{III} precursor to form the reactive Co^I (Lexa and Saveant, 1983). Second, the porphyrin ligand has one more bridging carbon than corrin, and the π -electron resonance is circular. Thus, the N₄ ligand cavity size, ring flexibility, and electronic effects in Co-PP are all different from B₁₂, thus influencing the defluorination activity (Rovira et al., 2001). An N₂O₂-coordinated Co complex with a bis(salicylidene)ethylenediamine ligand (Co-salen, Figure 4.3.2e), inorganic CoCl₂, and Co₃O₄ nanopowder did not show any defluorination activity, suggesting again the critical role of the Co-coordinating ligand in defluorination activity. Systematic investigations are required to probe the effect of ligands. Nevertheless, the above results have clearly shown that even the highly recalcitrant primary *sp*³ C–F bonds in PFASs could be cleaved by natural and artificial N₄-coordinated cobalt species.

Although branched structures containing tertiary C–F bonds with low BDEs are subject to Co-catalyzed defluorination, it is worth mentioning that at ambient temperature the branched PFASs would still be relatively recalcitrant in the environment. Results from this project will be valuable in two aspects of environmental research. First, rational molecular design may be applied to develop more readily degradable PFAS and Co catalysts that are active for the rapid and complete defluorination in both natural and engineered systems. On the other hand, caution should also be taken as branched PFAS may be reactive in cells, tissues, and organs where B₁₂ or other catalytic metal species are present.

4.4 UV-Sulfite Reduction

4.4.1 Objectives

The final strategy examined for treatment of PFAS in AFFF-impacted groundwater was the application of UV-sulfite to produce hydrated electrons, e_{aq}^- , that can initiate reductive transformation of wide ranging PFAS structures. Experimental work first focused on studying PFAS present in AFFF that was spiked into buffered laboratory solution. This was done to (i) better understand the transformation of individual PFAS during treatment of AFFF-impacted water mixtures, (ii) provide insights into how PFAS structural features influence reactivity with hydrated electrons, and (iii) support the further development of a practical UV-sulfite technology for remediation of AFFF-impacted groundwater sources. This work was aided by the development of high resolution LC-QTOF-MS that enables tracking the evolution of a broad range of PFAS during reactions, including both targeted analysis (i.e., direct quantification with reference standards) and suspect screening analysis (i.e., semi-quantitative analysis of mass spectral intensities); fluoride release was also monitored as a measure of PFAS mineralization. By first examining AFFF mixtures in the absence of complicating geochemical factors, we could better understand the PFAS-specific factors influencing reactions. Building on these findings, we then extended our studies to include AFFF-impacted groundwater sources collected from DoD facilities or nearby to DoD facilities.

4.4.2 AFFF test mixture

The composition of the AFFF was first characterized, and a summary of the targeted analysis is provided in Table 4.4.1. Fifteen out of the 44 compounds were detected, including 7 perfluoroalkyl sulfonates (3C - 9C), 5 perfluoroalkyl carboxylates (4C - 8C), and 3 fluorotelomer sulfonates (FTSs) (6C - 10C). Analysis indicates that the PFAS in the targeted list account for 37% of the total fluorine content of the AFFF determined by F-NMR analysis. The presence of fluorotelomer sulfonates was somewhat unexpected since the bottle was labelled 1999 era 3M Lightwater Alcohol Resistant (AR)-AFFF, but AFFF manufactured by 3M used an electrochemical fluorination process that produces PFAS with perfluorinated carbon chains that varied by $-CF_2-$ units and does not yield fluorotelomers (Moody and Field, 2000; Place and Field, 2012). Fluorotelomers are produced via an alternative telomerization manufacturing process which yields polyfluorinated carbon chains that differ by the number $-C_2F_4-$ units (Moody and Field, 2000; Place and Field, 2012). Thus, the mixture used in experiments is likely a mixture of AFFF sources. The total organic carbon (TOC) measurement of the AFFF stock was $147 \text{ g-C}\cdot\text{L}^{-1}$ which originates from hydrocarbon surfactant and organic solvent components in addition to PFAS. The PFAS themselves are not accurately measured by the TOC method (Moody and Field, 2000). 9.7 g/L total fluorine was measured by ^{19}F NMR.

Table 4.4.1. Measured concentrations of PFAS from the target analyte list of 44 compounds after dilution 1-to-60,000, and following application of the TOP assay.

PFAS	Chain-length	After TOP assay oxidation	
		AFFF diluted (1-to-60,000) ($\mu\text{g}\cdot\text{L}^{-1}$)	AFFF diluted (1-to-60,000) ($\mu\text{g}\cdot\text{L}^{-1}$)
PFNS	9C	0.246 \pm 0.121	0.122 \pm 0.055
PFOS	8C	69.5 \pm 13.9	45.0 \pm 4.4
PFHpS	7C	1.20 \pm 0.28	1.15 \pm 0.35
PFHxS	6C	12.4 \pm 1.2	14.5 \pm 0.9
PFPeS	5C	3.55 \pm 0.50	2.30 \pm 0.08
PFBS	4C	1.48 \pm 0.44	2.00 \pm 0.10
PFPrS	3C	0.494 \pm 0.216	1.01 \pm 0.08
PFOA	8C	0.728 \pm 0.097	6.58 \pm 0.29
PFHpA	7C	0.296 \pm 0.026	12.3 \pm 1.0
PFHxA	6C	1.78 \pm 0.98	50.7 \pm 3.3
PFPeA	5C	0.374 \pm 0.147	33.0 \pm 1.8
PFBA	4C	0.457 \pm 0.268	24.4 \pm 0.4
8:2 FTS	10C	0.146 \pm 0.073	NA \pm NA
6:2 FTS	8C	0.424 \pm 0.196	NA \pm NA
4:2 FTS	6C	0.029 \pm 0.012	NA \pm NA

Results of a TOP assay indicate that PFCA concentrations increased by large amounts following exposure to hydroxyl radicals generated by heat-activation of persulfate. Individual PFCAs increased in concentration 9- to 88-fold, generating 123 $\mu\text{g}/\text{L}$ of additional PFCAs compared to the raw AFFF. This finding shows that PFAA precursors compose a large portion of the total PFAS present in the AFFF when compared with individual PFSA and PFCA, e.g., PFOS ($69 \pm 14 \mu\text{g}\cdot\text{L}^{-1}$) and PFOA ($0.73 \pm 0.10 \mu\text{g}\cdot\text{L}^{-1}$). In addition, these findings show that >50% of total fluorine originates from such precursors. Degradation of the FTSs (8:2 fluorotelomer sulfonate (8:2 FTS), 6:2 fluorotelomer sulfonate (6:2 FTS), and 4:2 fluorotelomer sulfonate (4:2 FTS)—known PFAA precursors) below detection levels in oxidized solutions further validates completion of the assay. However, because the total concentration of PFAA precursors in the AFFF solution was unknown, it was not possible to determine complete oxidation. Thus, results from this modified TOP assay may actually underestimate total PFAA precursors, further highlighting their significance. We also mention here that PFNS (perfluorononane sulfonate, 9C), PFOS (8C), and perfluoropentane sulfonate (PFPeS, 5C) concentrations dropped by 35-50% in the TOP assay samples. This is similar to findings reported previously, which were attributed to sorption or other physical phenomenon in the reactor bottles (Bruton and Sedlak, 2017). Significant increases in PFCA concentrations (1.5- to 31-fold) were also observed in UV-only reactor controls. This led to an additional 16 $\mu\text{g}\cdot\text{L}^{-1}$ of PFCAs compared to the control. This adds further support to the conclusion that the AFFF possessed high concentrations of PFAA precursors.

LC-QTOF-MS suspect screening analysis showed a wide diversity of structures beyond those included in the targeted analyte list (Table 4.4.2). These include 48 unique structures initially reported in or inferred from other work (Ahrens et al., 2009; Allred et al., 2015; Backe et al., 2013; Baduel et al., 2017; Barzen-Hanson et al., 2017; D'Agostino and Mabury, 2014; Dinglasan et al., 2004; Field et al., 2003; Kissa, 2001; Liu et al., 2015; Moe et al., 2012; Moody and Field, 1999; Nguyen et al., 2011; Place and Field, 2012; Tseng et al., 2014; Weiner et al., 2013). The 48 can be

separated into 7 different PFAS superclasses: (1) PFAAs, (2) FTSs and fluorotelomer carboxylic acids (FTCAs), (3) cyclic and unsaturated PFAAs, (4) perfluorinated amides, (5) FTS and FTCA derivatives, (6) substituted PFAA derivatives, and (7) sulfonamide precursors.

Table 4.4.2. PFAS detected by suspect screening analysis.

Super Class	Class Acronym	Structure	Compound Acronym
PFAAs	PFCA		PFBA (n = 3) PFPeA (n = 4) PFHxA (n = 5) PFHpA (n = 6) PFOA (n = 7) PFPrS (n = 2) PFBS (n = 3) PFPeS (n = 4) PFHxS (n = 5) PFHpS (n = 6) PFOS (n = 7) PFNS (n = 8)
	PFSA		
FTSs and FTAs	X:3 FTCA		6:3 FTCA (n = 5)
	X:2 FTS		4:2 FTS (n = 3) 6:2 FTS (n = 5) 8:2 FTS (n = 7)
Unsaturated PFAAs	H-UPFSA		H-UPFHxS (n = 2) H-UPFOS (n = 4) H-UPFHp-O/OH H-UPFN-O/OH H-UPFUd-O/OH
	H-UPFA-O/OH	No confirmed structure (Liu et al., 2015)	
Perfluorinated Amide	MeEtCMeAmPr-FAAd		MeEtCMeAmPr-FPeAd (n = 4)
FTS and FTA Derivatives	X:2 FTSO-PrAd-DiMePrS		6:2 FTSO-PrAd-DiMePrS (n = 5) 8:2 FTSO-PrAd-DiMePrS (n = 7)
	X:3 K-FTTh-K-EtOH		7:3 K-FTTh-K-EtOH (n = 6) 8:3 K-FTTh-K-EtOH (n = 7) 9:3 K-FTTh-K-EtOH (n = 8) 11:3 K-FTTh-K-EtOH (n = 10)
	X:3 K-FTTh-K-OH-PrA		3:3 K-FTTh-K-OH-PrA (n = 2) 5:3 K-FTTh-K-OH-PrA (n = 4) 7:3 K-FTTh-K-OH-PrA (n = 6)
Substituted PFAA Derivatives	X:2 FTSA-PrAn		4:2 FTSA-PrAn (n = 3) 6:2 FTSA-PrAn (n = 5)
	H-PFSA		H-PFPPrS (n = 1) H-PFBS (n = 2) H-PFPeS (n = 3) H-PFOS (n = 6)
	X:1 PFSA		5:1 PFHxS (n = 4) 7:1 PFOS (n = 6)
Sulfonamide Precursors	AmPr-FASA		AmPr-FBSA (n = 3) AmPr-FPeSA (n = 4) AmPr-FHxSA (n = 5)
	MeFASAA		MeFETsAA (n = 1) MeFHxSAA (n = 5)

4.4.3 Photodegradation of PFAS in AFFF

Observed UV-sulfite timecourses for the PFAS measured during targeted analysis are shown in Figure 4.4.1. After 49 h of reaction, PFOS degraded by 98% and PFOA by 93%. Degradation of these two compounds in the AFFF are consistent with rates measured for each in single-solute experiments reported previously for UV-sulfite. While the reactions observed here were somewhat slow, they can readily be accelerated by applying higher power light sources (e.g., Gu and coworkers reported half lives of ~8.5 min (PFOS) and ~2.4 min (PFOA) when irradiating with a 250 W light source (Gu et al., 2017, 2016)). These results demonstrate that UV-sulfite can be effective for treating 8-carbon PFAAs, in agreement with earlier reports (Gu et al., 2017, 2016; Song et al., 2013). Further, we found that, in general, long-chain PFASs such as PFNS (9C), PFOS (8C) and perfluoroheptane sulfonate (PFHpS, 7C) can be readily degraded by UV-sulfite (Figure 4.4.1A). Of note, shorter-chain sulfonate analogues like PFHxS (6C), PFPeS (5C), perfluorobutane sulfonate (PFBS, 4C), and perfluoropropane sulfonate (PFPrS, 3C) appeared to initially increase in concentration from the values measured in the untreated AFFF. We hypothesized that the observed generation of these analytes was a product of reaction between e_{aq}^- and abundant precursors containing sulfonate structures. Perfluorohexane sulfonate (PFHxS, 6C) and perfluoropentanesulfonate (PFPeS, 5C) were degraded during treatment, but only after initially increasing in concentration during the first 5 h. In contrast, some of the shorter chain PFASs, most notably PFBS (4C) and PFPrS (3C), proved to be unreactive after increasing to their peak concentration values, in agreement with earlier reports showing that PFSA reactivity with e_{aq}^- decreases with decreasing chain length (4C - 8C) (Park et al., 2009).

In comparison to PFASs, PFCAs were found to degrade faster as shown in Figure 4.4.1B. Reactivity trends among the PFCAs show that, unlike PFASs, reactivity was invariant with chain length, also consistent with earlier reports from single-solute experiments (Park et al., 2009). Like the 3C - 6C PFASs, an increase in concentration of PFHpA (perfluoroheptanoic acid) was observed before being rapidly degraded.

Measured concentrations of the three FTSs (8:2 FTS, 6:2 FTS, and 4:2 FTS) on the target analyte list were initially $<0.5 \mu\text{g}\cdot\text{L}^{-1}$ in the unreacted AFFF (Table 4.4.1), but their concentrations increased more than 10-fold within the first 2 h of reaction (Figure 4.4.1C). Like some of the PFASs and PFHpA, FTS generation is believed to originate from the reaction between hydrated electrons and precursors that contain the FTS moiety. Single-solute reactions initiated with either PFOS or PFHxS showed no FTS generation, so reductive defluorination of PFAAs is not believed to be an important source for FTS and FTCA generation. In agreement with general trends already noted, the long-chain FTS (8:2 FTS) was found to be more reactive than the two shorter chain FTSs after reaching their maximum concentrations.

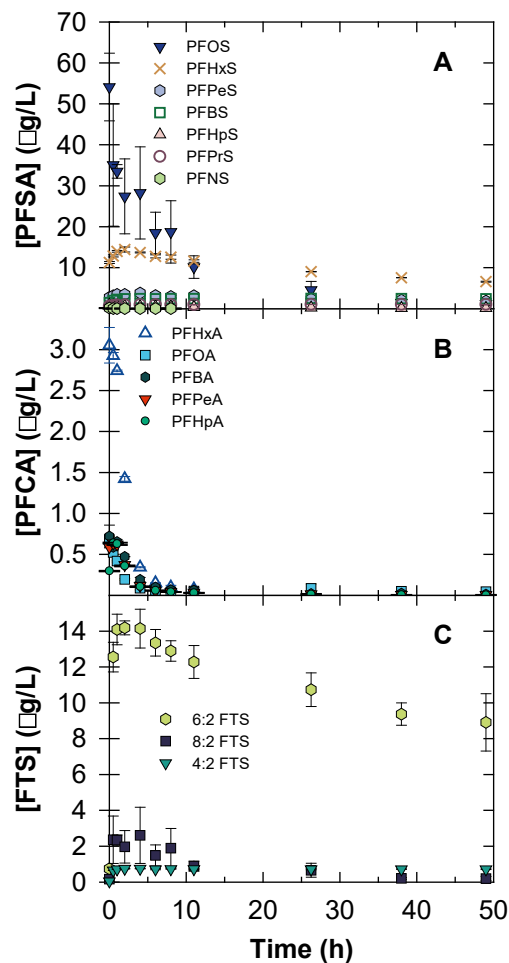


Figure 4.4.1. Reaction timecourses observed during UV-sulfite treatment of the targeted list PFAS within AFFF. (A) PFSA, (B) PFCAs, and (C) FTSs. Reaction conditions: AFFF diluted by 60,000 dilution, sulfite = 10 mM, bicarbonate buffer = 5 mM $\text{pH}_0 = 9.5$. Reactors were sparged with nitrogen gas before initiating reactions.

Analysis of fluoride ion release during reactions showed 53% of total fluorine in the AFFF was released as F^- following 49 h of UV-sulfite reaction (Figure 4.4.2). The fact that incomplete defluorination was observed is attributed to both unreactive PFAS, like the shorter-chain PFAS and FTSs, in the AFFF mixture, plus formation of similarly unreactive byproducts via transformation of structurally related precursors. Another possible contributor to the incomplete F^- generation is loss of fluorine to volatile byproducts that left solutions. However, we do not believe that this is a major source because GC-MS/MS analysis of the reactor headspace gases revealed minimal presence of such species.

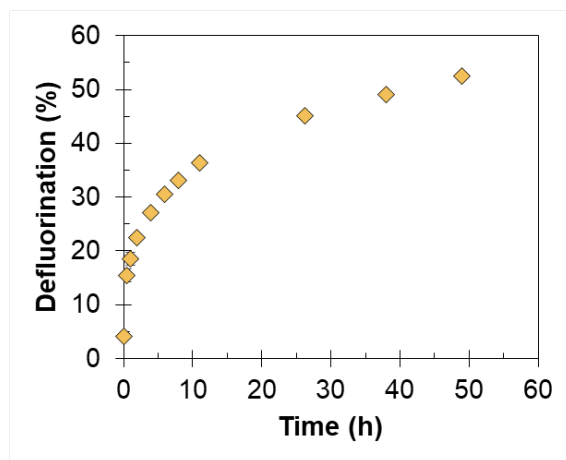


Figure 4.4.2. Observed defluorination of PFAS within AFFF during UV-sulfite treatment. Reaction conditions: AFFF diluted 60,000-fold, 10 mM sulfite, 5 mM sodium bicarbonate (pH 9.5), reactors were sparged with nitrogen gas.

Early tests showed that 10 mM sulfite was optimum for UV-sulfite treatment in the reactor configuration used in the study, data presented in Figures 4.4.1 and 4.4.2 were measured with this sulfite concentration. Figure 4.4.3 shows that reaction rates increased with increasing sulfite concentration, but approached a limiting value at higher concentrations. This is attributed to the fact that complete light absorption by the sensitizer occurs. After 11 h of reaction, the measured F^- release increased from 0.04 to 0.06 mg-F/L (23% to 34% defluorination) with increasing sulfite dose (1 to 10 mM). Previous work examining UV-sulfite treatment of PFOA alone reported increasing defluorination with increasing sulfite dose, but similar defluorination for both 10 mM and 20 mM sulfite doses (Song et al., 2013). Here, we also found little difference in fluoride ion release when treating with either 10 mM (0.059 mg-F·L⁻¹ after 11 hours) and 20 mM (0.056 mg-F·L⁻¹) sulfite. PFNS, PFOS, PFHpS, PFOA, PFHpA, PFHxA, PFPeA, and PFBA degradation increased with increasing sulfite dose. The longest-chain analogue, PFNS, was found to be completely degraded for sulfite doses ≥ 5 mM. Like the defluorination data, use of 20 mM sulfite did not greatly increase PFAS degradation compared to using 10 mM. For an effective UV path length of 2.85 cm, light absorption increased from 68% for 10 mM to 90% for 20 mM sulfite (Table 4.4.3), suggesting a diminishing return in hydrated electron production with increasing sulfite dose. Some of the PFAS, PFHpA, PFHxA, PFPeA, and PFBA, were not degraded when treating with only 1 mM sulfite, whereas PFHxS was only observed to degrade appreciably (albeit very slowly) when treating with 20 mM sulfite dose.

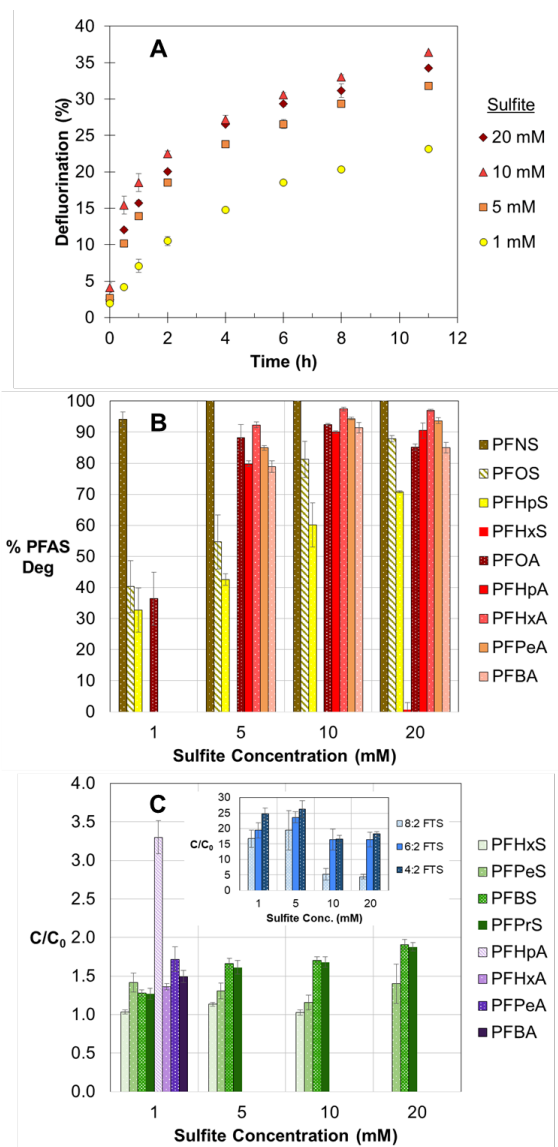


Figure 4.4.3. Influence of SO_3^{2-} concentration on (A) fluoride release, (B) PFAS degradation (%), and (C) PFAS generation ($C \cdot C_0^{-1}$) after reaction for 11 hours. Panel B is limited to only compounds that were degraded after an 11 h reaction period. Panel C is limited to only compounds that were generated after an 11 h reaction period. Reaction conditions: AFFF diluted by 60,000 dilution, sulfite = 1-20 mM, bicarbonate buffer = 5 mM $\text{pH}_0 = 9.5$. Reactors were sparged with nitrogen gas before initiating reactions.

Table 4.4.3 Optical properties of sulfite-containing solutions.

Sulfite (mM)	A _{254, 1 cm}	A _{254, Z_{eff}^a}	T _{254,z_{eff}^b}	% Light absorbed ^c
1	0.017	0.050	0.891	11
5	0.091	0.251	0.562	44
10	0.175	0.501	0.315	68
20	0.352	1.002	0.099	90

^aA₂₅₄ for a path length equal to the effective path length (i.e., Z_{eff} = 2.85 cm) and ε_{254,sulfite} = 17.6 M⁻¹·cm⁻¹.
^bTransmittance (i.e., 1/10^A) using A_{254,z_{eff}}. ^c100·(1 - T_{254,z_{eff}}).

Some of the PFCAs, PFHpA, PFHxA, PFPeA, and PFBA, were generated only when treating with 1 mM sulfite (Figure 4.4.3). This observation is similar to the UV-only control experiment where PFCA generation was observed (Table 4.4.4). Thus, it is likely that direct UV photolysis of AFFF components dominated under these conditions, leading to greater rates of PFCA generation than PFCA destruction. PFBS and PFPrS generation was observed to increase when treating with increasing concentrations of sulfite since more hydrated electrons were available to react with PFAA precursors that produce these PFAS. In comparison, PFHxS and PFPeS concentrations were unaffected by increasing sulfite dose. Generation of the fluorotelomer sulfonates (8:2 FTS, 6:2 FTS, and 4:2 FTS) increased a little when sulfite concentrations increased from 1 mM to 5 mM, but concentrations decreased at sulfite doses greater than 10 mM. This finding indicates that the additional hydrated electrons available at higher sulfite concentrations reacted with PFAA precursors to generate additional FTSs. The drop in FTS generation from 5 mM to sulfite concentrations exceeding 10 mM was possibly due to increased degradation of the FTS themselves (Figure 4.4.1C).

4.4.4 Suspect screening analysis

In addition to analysis of the target group of analytes, LC-QToF-MS was used to track the fate of a broader set of fluorochemical contaminants in AFFF. Both unreacted and UV-sulfite reacted samples were first subjected to comparison with a list of >300 suspect structures identified in recent discovery analyses. Figure 4.4.4 depicts a “bubble” plot showing collectively how chromatographic peaks detected within the full group of detected PFAS, including both the target and suspect screening lists provided in Tables 4.4.1 and 4.4.2, are affected by UV-sulfite reaction for 49 h. Each bubble plot arranges analytes by their chromatographic retention time (in min, x-axis) and their mass spectral mass-to-charge ratio (y-axis). The diameter of each “bubble” is then representative of the peak area measured for each analyte. The analytes are organized by super-classes listed in Table 4.4.2. Identified analytes whose peak areas exceeding the reporting threshold included 12 PFAAs, 4 FTSs and FTCAAs, 5 unsaturated PFAAs, 1 perfluorinated amide, 11 FTS and FTCA derivatives, 6 substituted PFAA derivatives, and 5 sulfonamide precursors. Comparison of the plots before and after reaction show an overall decrease in the mass of the monitored analytes (58% drop in total LC-QTOF-MS peak area). This finding does suggest a promising approach for treatment of PFAS-contaminated groundwater.

Table 4.4.4. Results of UV-only control reaction.^a

PFAS	t = 0 h		t = 49 h	
	Conc. ($\mu\text{g}\cdot\text{L}^{-1}$)		Conc. ($\mu\text{g}\cdot\text{L}^{-1}$)	
PFNS	0.133	\pm 0.013	0.170	\pm 0.032
PFOS	55.2	\pm 3.0	63.0	\pm 4.1
PFHpS	0.915	\pm 0.041	1.097	\pm 0.023
PFHxS	12.1	\pm 0.2	11.2	\pm 0.1
PFPeS	4.29	\pm 0.28	3.49	\pm 0.01
PFBS	1.25	\pm 0.01	1.23	\pm 0.001
PFPPrS	0.402	\pm 0.0004	0.388	\pm 0.006
PFOA	0.658	\pm 0.050	0.997	\pm 0.024
PFHpA	0.307	\pm 0.024	2.00	\pm 0.18
PFHxA	0.807	\pm 0.012	6.00	\pm 0.12
PFPeA	0.232	\pm 0.005	7.24	\pm 0.11
PFBA	0.191	\pm 0.0002	2.08	\pm 0.19
8:2 FTS	0.067	\pm 0.003	0.377	\pm 0.113
6:2 FTS	0.234	\pm 0.009	1.05	\pm 0.13
4:2 FTS	0.017	\pm 0.001	0.074	\pm 0.010

^aReaction conditions: $[\text{NaHCO}_3]_0 = 5 \text{ mM}$ ($\text{pH}_0 = 9.5$), reactors were sparged with $\text{N}_{2(\text{g})}$ for 1 h before reaction with 18 W UV LP Hg lamp. No sulfite was added to reactors.

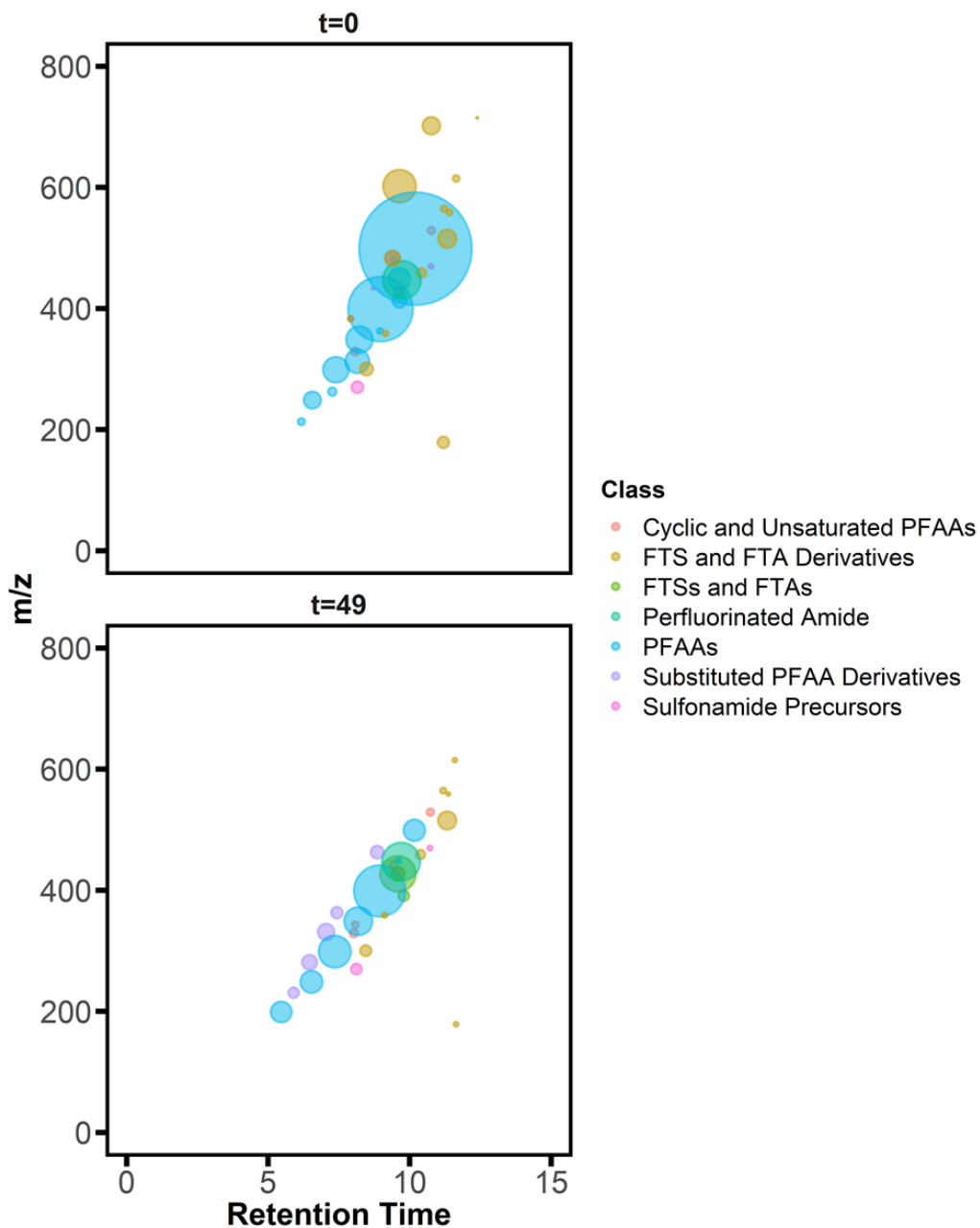


Figure 4.4.2. “Bubble” plots of PFAS in AFFF (A) before UV-sulfite treatment and (B) after 49 h of UV-sulfite reaction. PFAS with the highest summed area per superclass are presented. Bubbles signify individual PFAS and are organized by PFAS superclass indicated by color (see legend). The diameter of each bubble represents mass spec peak area, the x-axis values denotes the HPLC retention time of the analyte (also related to compound size), and the y-axis value denotes the mass-to-charge ratio of the analyte (related to molecular weight). Reaction conditions provided in Figure 4.4.1.

PFAAs were the dominant superclass in this AFFF mixture in terms of mass spec peak area, and PFOS was the most abundant PFAS within this group. As already discussed, PFCAs of all chain lengths (4 - 8C) and longer-chain PFASs (6 - 9C) were readily degraded during treatment, whereas shorter chain PFASs (2 - 5C) were much more recalcitrant.

Net generation of 6:3 FTCA, 6:2 FTS, and 4:2 FTS was observed during treatment, following the trends described earlier for 6:2 FTS and 4:2 FTS (Figure 4.4.1). Among these, 4:2 FTS concentration remained stable following an initial generation period during the first 2 h (note that peak areas showed degradation after generation due to lack of internal standard), whereas 6:3 FTCA and 6:2 FTS were observed to degrade after reaching a peak value. Compared to the PFAAs with the same carbon chain length, the FTCAs and FTSs were found to be generally less reactive.

FTS and FTCA derivative reactivity varied according to subclass. For the group X:3 K-FTTh-K-EtOH, degradation increased with increasing chain length (7:3 - 11:3). Long-chain X:2 FTSO-PrAd-DiMePrS derivatives (6:2, 8:2) were degraded within 49 h of UV-sulfite treatment, where longer-chain PFAS proved to be more reactive than short-chain homologues (Park et al., 2009). Similarly, shorter chain X:3 K-FTTh-K-OH-PrAs (3:3, 5:3) were unreactive, whereas a longer chain homologue (7:3) showed only 23% removal following reaction. The X:2 FTSA-PrAn class showed complete removal (4:2, 6:2). Formation of proton-substituted PFSA derivatives, initially absent in the unreacted AFFF, were observed to form as transient intermediates or stable endproducts, providing some evidence of defluorination occurring along the perfluoroalkyl chain. Stable short chain (3C - 5C) H-PFSA products formed following UV-sulfite reaction, whereas formation of the longer-chain H-PFOS during the first 4 h was followed by degradation to non-detect levels. 5:1 PFHxS and 7:1 PFOS in the X:1 PFSA class were also generated. Compared with the fully perfluorinated analogues, these structures were less reactive.

PFAS in the AmPr-FASA class (4C - 6C) were 99% removed within 49 h, whereas structures in the MeFASAA class were largely unreactive (removal <11% after t = 49 h). The additional N group in AmPr-FASA structures could contribute to its higher reactivity compared with MeFASAAs. A single perfluorinated amide was detected (MeEtCMeAmPr-FPeAd) and found to be unreactive during UV-sulfite treatment.

Six- and 8-carbon proton-substituted unsaturated perfluoroalkyl sulfonic acids (H-UPFSAs) were generated during treatment and were generally observed to be unreactive. Formation of such products may result from vicinal dehalogenation mechanisms initiated by hydrated electrons. The formation of UFTCAs from FTCAs through biodegradation of fluorotelomer alcohols (FTOHs) has previously been proposed (Washington et al., 2015).

4.4.5 Photoconversion of PFAA precursors

As discussed already, reaction timecourse data indicate formation of selected PFAAs and FTSs occurs during the initial stages of AFFF treatment. We hypothesize that these trends result from hydrated electron reactions that lead to cleavage of PFAA and FTS derivative structures. To test this hypothesis, a single-solute experiment was conducted using FOSAA (a sulfonamide

derivative PFAA precursor) as the starting reactant under identical experimental conditions as those presented in Figure 4.4.1. Results (Figure 4.4.3) for the first hour of reaction showed 42% degradation of FOSAA that yielded 22% PFOS, 14% PFOA, and 7% perfluorooctane sulfonamide (FOSA, 8C). *This confirms that PFSA formation can result from precursor reactions with hydrated electrons that are generated during UV-sulfite treatment.* This finding helps to explain the observed generation of PFSA and FTSA during treatment of AFFF mixtures.

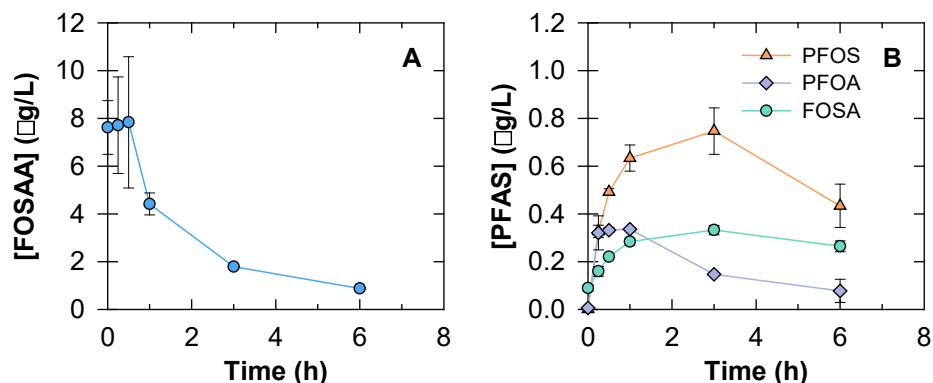


Figure 4.4.3. (A) Degradation of the PFSA derivative FOSAA by UV-sulfite treatment, and formation of PFOS, PFOA, and perfluorooctane sulfonamide (FOSA) (B). Yields of each product after 1 h were 22%, 14%, and 7% for PFOS, PFOA, and FOSA, respectively. Conditions: 10 µg/L FOSAA, 10 mM sulfite, 5 mM sodium bicarbonate (pH 9.5).

4.4.6 Volatile reaction products

GC-MS/MS analysis of reactor headspace was conducted in an attempt to identify any volatile transformation products during UV-sulfite treatment. SPME fibers were placed in the reactor headspace to collect and concentrate any volatile species. Qualitative trends showed very few gaseous byproducts, much less than were reported when potassium iodide was used as the UV sensitizer for hydrated electron generation. Park et al. detected 24 fluorinated gaseous byproducts (containing C, F) from UV-KI treatment of PFOS, 16 of which were also iodinated (containing C, F, I) (Park et al., 2009). In the same study, 9 fluorinated gaseous byproducts (C, F), 6 of which were also iodinated (C, F, I) were identified during reactions with PFOA (Park et al., 2009). In comparison, only 4 volatile fluorinated compounds (C, F) were detected during UV-sulfite treated AFFF solution (Figure 4.4.4). Both 8- and 10-carbon fluorotelomer alcohols (FTOHs) and 6- and 8-carbon polyfluorinated alkyl chains were detected in the photoreactor headspace following UV-sulfite treatment (not present in UV-only or dark control experiments). The lack of diversity in F-containing compounds during UV-sulfite treatment could be explained by radical coupling reactions between sulfite-derived radical intermediates and PFAS intermediates, which would

generate more polar/ionic products than comparable products formed by coupling with iodide-derived radicals.

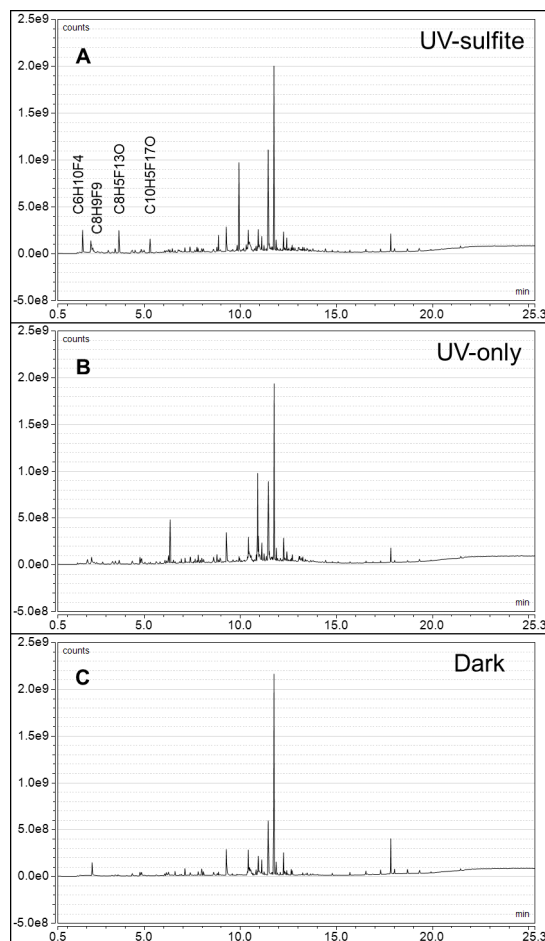


Figure 4.4.4. Analysis of volatile reaction products during UV-sulfite treatment of AFFF solutions. (GC-MS/MS total ion chromatograms). Gaseous products sorbed onto a PDMS/DVB SPME fiber after 2 h of reaction under (A) UV-sulfite reacted sample, (B) UV-only control, and (C) dark control sample. Reaction conditions: AFFF diluted 60,000-fold, 10 mM sulfite, 5 mM sodium bicarbonate (pH 9.5), anoxic.

4.4.7 Influence of AFFF matrix on PFAS degradation

Selected single-solute experiments were conducted to verify that other components within the AFFF mixture, including both PFAS and non-PFAS components (e.g., hydrocarbon surfactants, cosolvents), do not affect the kinetics of individual PFAS during UV-sulfite treatment. Results of these experiments are summarized in Figure 4.4.5. PFOS was readily degraded and ~98% removal was achieved in both the 60,000-fold diluted AFFF mixture and the single-solute experiment (Panel A). As a result, similar apparent first-order degradation rate constants (k_{obs})

were obtained (Panel D). For PFHxS, differing behavior is observed in that the initial increase in concentration observed during the first 2 h in AFFF reaction (attributed to precursor conversion reactions) does not occur in the single-solute experiment (because there are no precursors present in the reaction solution) (Panel B). However, after reaching maximum value, the timecourses for the PFHxS in AFFF and single-solute experiment parallel one another. As a result, the k_{obs} values determined for the decay portions of each timecourse are also comparable (Panel D).

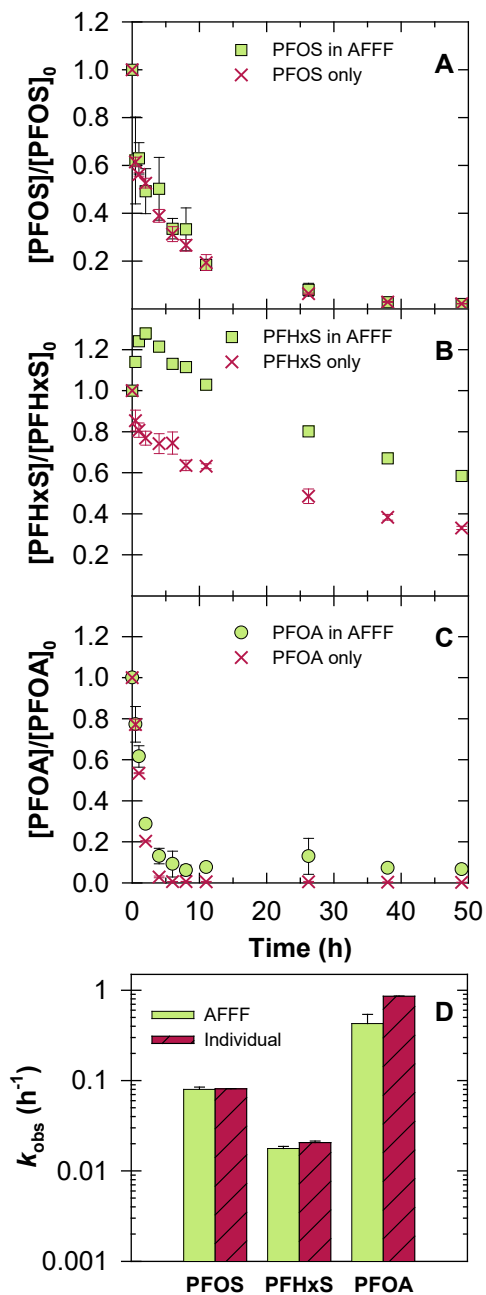


Figure 4.4.5. Changes in relative concentration of (A) PFOS, (B) PFHxS, and (C) PFOA measured in AFFF mixtures and in single-solute experiments. (D) Observed pseudo first-order degradation rate constants (k_{obs}). AFFF solution reaction conditions identical to those shown Figure 4.4.1. Single-solute experiment conditions: $[PFOS]_0 = [PFHxS]_0 = [PFOA]_0 = 10 \mu\text{g/L}$ 10 mM sulfite, 5 mM bicarbonate buffer (pH 9.5).

Results for PFOA were different from the perfluorinated sulfonates. The initial rate of decay was similar for both the single-solute experiment and AFFF (Figure 4.4.5C), although the k_{obs} values determined using data for the first 6 h of reaction differed by a factor of ~ 2 (Figure 4.4.5D). The lower apparent rate constant observed in the AFFF solution can be rationalized by the fact that in AFFF the observed decay trend represents a net balance between reactions leading to PFOA generation from PFAA precursors and PFOA degradation by reaction with hydrated electrons. It is worth recalling here that results from the TOP Assay (Table 4.4.1) indicated the presence of nearly 10 times higher concentration of PFOA precursors in AFFF than PFOA itself. Thus, even if only a small fraction of these precursors react with hydrated electrons for form PFOA, it could significantly retard the apparent rate of PFOA decomposition observed in the mixture. Furthermore, a “recalcitrant” residual of 8 - 16% of the initial PFOA concentration (40 - 84 $\text{ng}\cdot\text{L}^{-1}$) seems to persist in the AFFF solution for the full 49 h reaction despite the fact that $>90\%$ is degraded within first 6 h; for comparison, in the single-solute experiment, complete degradation of PFOA was observed with no detectable residual. Again, this residual concentration can be explained by the fact that a steady state PFOA concentration is being reached where rates of PFOA formation from precursors is balanced by reactions that degrade PFOA.

In summary, with certain exceptions, similarities between the k_{obs} measurements for individual PFAS in AFFF and single-solute experiments demonstrate that the mixture of other components in AFFF are not significant quenchers of hydrated electrons compared to the dominant background solution quenchers, i.e., H_2O ($k_{\text{eq-},\text{H}_2\text{O}} = 19 \text{ M}^{-1}\cdot\text{s}^{-1}$, $[\text{H}_2\text{O}] = 55.5 \text{ M}$) and H^+ ($k_{\text{eq-},\text{H}^+} = 2.8 \times 10^{10} \text{ M}^{-1}\cdot\text{s}^{-1}$) (Buxton et al., 1988).

4.4.8 Influence of PFAS structure on degradation rate constants

Concentration profiles observed for most of the target list structures (Figure 4.4.1) and the peak area profile of many of the suspect screening list structures followed a first-order rate law closely, enabling simple calculation of k_{obs} values using the full data sets. As discussed, some PFAS initially increased in concentration before reaching a peak value and then decaying with increasing reaction time. For these structures, k_{obs} was estimated using only the data points following the peak in concentration. Tables 4.4.5 and 4.4.6 summarize the apparent first-order rate constants (k_{obs} ; h^{-1}) for degradation of individual PFAS.

Table 4.4.5. Observed first-order degradation rate constants for PFAS on the target list.

PFAS	Chain-length	Linear k_{obs} (h^{-1})	Branched k_{obs} (h^{-1})
PFNS	9C	$1.71^a \pm 0.16$	---
PFOS	8C	0.080 ± 0.005	8^a
PFHpS	7C	0.043 ± 0.000	$> 2^a$
PFHxS	6C	$0.018^b \pm 0.001$	8^a
PFPeS	5C	$0.018^b \pm 0.002$	---
PFBS	4C	NA	---
PFPPrS	3C	NA	---
PFOA	8C	0.427 ± 0.114	$> 2^a$
PFHpA	7C	$0.440^b \pm 0.001$	$> 2^a$
PFHxA	6C	0.462 ± 0.003	---
PFPeA	5C	$0.432^b \pm 0.001$	---
PFBA	4C	0.306 ± 0.042	---
8:2 FTS	10C	$0.063^b \pm 0.005$	---
6:2 FTS	8C	$0.012^b \pm 0.001$	---
4:2 FTS	6C	NA	---

^aCalculated by the initial rate method using 2 points. ^bCalculated from the maximum formed concentration. NA indicates no degradation. No branched isomer observed if no value reported.

Table 4.4.6. Observed first-order degradation rate constants for PFAS on the suspect screening list.

Compound Acronym	k_{obs} (h^{-1})
6:3 FTCA	0.009 ^a ± 0.001
H-UPFHxS	NA
H-UPFOS	0.035 ^a ± 0.001
H-UPFHp-O/OH	NA
H-UPFN-O/OH	NA
H-UPFUd-O/OH	NA
MeEtCMeAmPr-FPeAd	NA
6:2 FTSO-PrAd-DiMePrS	3.22 ± 0.08
8:2 FTSO-PrAd-DiMePrS	2.74 ± 0.24
7:3 K-FTTh-K-EtOH	NA
8:3 K-FTTh-K-EtOH	NA
9:3 K-FTTh-K-EtOH	NA
11:3 K-FTTh-K-EtOH	NA
3:3 K-FTTh-K-OH-PrA	NA
5:3 K-FTTh-K-OH-PrA	NA
7:3 K-FTTh-K-OH-PrA	NA
4:2 FTSA-PrAn	0.103 ^a ± 0.008
6:2 FTSA-PrAn	0.114 ± 0.019
H-PFPrS	NA
H-PFBS	NA
H-PFPeS	NA
H-PFOS	0.051 ^a ± 0.003
5:1 PFHxS	NA
7:1 PFOS	0.015 ^a ± 0.003
AmPr-FBSA	0.103 ^a ± 0.008
AmPr-FPeSA	0.094 ± 0.008
AmPr-FHxSA	0.114 ± 0.019
MeFEtSAA	NA
MeFHxSAA	NA

^a Calculated from maximum concentration. NA indicates continuous PFAS generation or no statistically significant degradation throughout the reaction.

Evidence for both linear and branched isomers of selected PFAS, namely PFOS, PFHpS, PFHxS, PFOA, and PFHpA, was obtained from chromatographic separation, where two distinct peaks are observed, attributed to linear (larger peak) and branched isomers (smaller secondary peak) (Figure 4.4.6). The concentrations presented in Figure 4.4.1 were determined by collective integration of both peaks. However, these “total” concentration timecourses were not consistent with a first-order decay profile due to the rapid disappearance of the peaks associated with the branched isomers. Thus, branched versus linear isomers exhibit very different reactivity with hydrated electrons. Ochoa-Herrera reported similar isomer-dependent reactivity for PFOS reduction catalyzed by Vitamin B12 (Ochoa-Herrera et al., 2008). Separate analysis of the linear isomer peak areas show that degradation follow a first-order rate law, allowing for determination k_{obs} values. Separate rate constants, or lower-bound estimates, were determined for the branched

isomers. Eq 4.4.1 was used to determine the lower bound estimates for hydrated electron reactions with branched isomers of PFHpS, PFOA, and PFHpA since they were completely degraded before the first sample was collected after 30 min of reaction.

$$\frac{\Delta C}{\Delta t} = k_{obs} C_0 \quad (4.4.1)$$

where $\Delta C/\Delta t$ is the rate of PFAS decay calculated using the concentration change over the first 30 min, and C_0 is the initial concentration of the branched isomer in the unreacted AFFF mixture. Based on calculations using eq. 4.4.1, k_{obs} values for branched PFHpS, PFOA, and PFHpA were at least 2.0 h^{-1} .

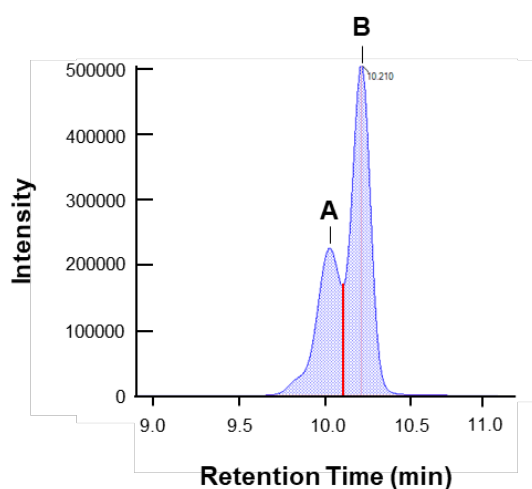


Figure 4.4.6. Chromatogram for the PFOS analyte in untreated ($t = 0 \text{ h}$) sample of UV-sulfite treatment of diluted AFFF. Reaction conditions were identical to Figure 4.4.1. Total PFOS was measured by integrating both the (A) branched and (B) linear isomer peaks. The red line represents the areas after integrating the (A) branched or (B) linear isomers individually.

Among PFASs, reactivity increases with chain length (Figure 4.4.7A). The measured value of k_{obs} for PFOS (8C) > PFHpS (7C) > PFHXs (6C) ~ PFPeS (5C). 96% of PFNS was degraded after 6 h of UV-sulfite reaction, but kinetics did not follow a first-order rate law. Though there was little difference between $k_{obs,PFHXs}$ (6C, 0.001 h^{-1}) and $k_{obs,PFPeS}$ (5C, 0.002 h^{-1}), no apparent degradation was observed for shorter chain lengths, i.e., $k_{obs,PFBS}$ (4C) and $k_{obs,PFPrS}$ (3C) (Figure 4.4.1A). Park et al. reported similar trends for UV-KI treatment, but $k_{obs,PFOS}$ was greater than $k_{obs,PFHXs}$ by only a factor of 2.5 (Park et al., 2009). The same study also found that $k_{obs,PFOS}$ was greater than $k_{obs,PFBS}$ by a factor of 7, whereas this study showed that PFBS was unreactive (Park et al., 2009). Similar rate constants were measured for PFCAs with chain length 4C - 8C ($0.30 - 0.46 \text{ h}^{-1}$) (Figure 5B). This trend is similar to data for UV-KI treatment (Park et al., 2009). Like PFASs, chain length heavily influence rate constants for degradation of FTS homologues. 8:2 FTS was more reactive than 6:2 FTS by a factor of 5 and 4:2 FTS showed no degradation.

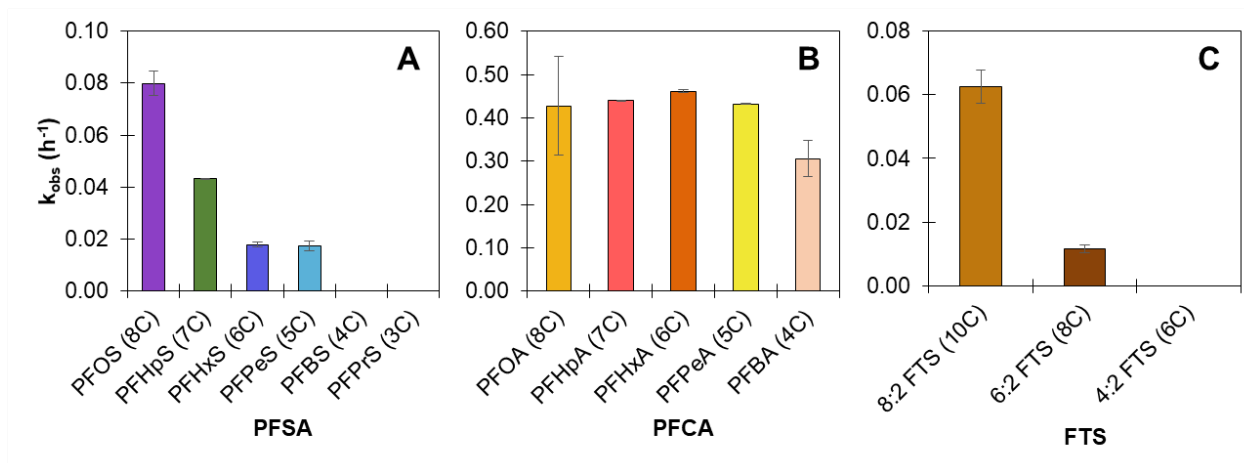


Figure 4.4.7. Observed rate constants for degradation of linear PFAS isomers: (A) PFSA, (B) PFCA, and (C) FTS in diluted AFFF during UV-sulfite treatment. Rate constants were calculated during the period of degradation. PFNS degradation did not follow first-order kinetics and is not shown. Reaction conditions identical to those in Figure 4.4.1.

Additionally, polyfluorinated PFAS appear to be more recalcitrant than perfluorinated PFAS of similar chain length. For example, comparing 8C perfluorinated sulfonate (PFOS, $k_{\text{obs,PFOS}} = 0.075 \text{ h}^{-1}$) with the polyfluorinated fluorotelomer sulfonate (6:2 FTS, $k_{\text{obs,6:2 FTS}} = 0.012 \text{ h}^{-1}$) shows that the former is more reactive by a factor of 7. This is particularly concerning considering the extensive FTS generation observed during the initial stages of UV-sulfite treatment.

Kinetic data clearly show that the branched isomers were much more reactive than the linear isomers, irrespective of chain length or head group. For example, the observed first-order rate constant for branched PFOS degradation ($k_{\text{obs,PFOS,branched}} = 7.9 \text{ h}^{-1}$) was nearly 100 times greater than linear PFOS ($k_{\text{obs,PFOS,linear}} = 0.08 \text{ h}^{-1}$). The branched isomer of PFHpS ($k_{\text{obs,PFHpS,branched}} > 2.0 \text{ h}^{-1}$) was at least 46 times more reactive than the linear isomer ($k_{\text{obs,PFHpS,linear}} = 0.04 \text{ h}^{-1}$). Others have shown that greater reactivity of the branched isomer is due to tertiary C-F bonds (Paul et al., 2004). It is also worth noting that despite the large difference in k_{obs} values among the linear PFSA isomers, the branched isomers appear similar in reactivity, suggesting a common reactive moiety (e.g., C-F bond at the branching carbon on the perfluoroalkyl chain).

Finally, PFAA precursors were generally found to be more reactive with hydrated electrons than the resulting products. While 3C - 6C PFSA and 6C - 8C FTSs were all generated as a result of hydrated electron reactions with PFAA precursors (Figure 4.4.1), first-order degradation rate constants measured for further reaction of the PFAAs were all $< 0.02 \text{ h}^{-1}$ (Figure 4.4.7C).

4.4.10 UV-Sulfite Treatment of AFFF-Impacted Groundwater

Groundwater water quality analysis. Water quality parameters for Ellsworth Air Force base groundwater (EAFB), Fountain (CO) groundwater (FGW), and Peterson Air Force base groundwater wells (MW 1-8, MW 2-3) are shown in Table 4.4.7.

Table 4.4.7. Water quality parameters in filtered groundwater samples.

Parameter	Ellsworth (EAFB)	Fountain (FGW)	Peterson (MW 1-8)	Peterson (MW 2-3)
Anions (mg/L)				
Fluoride	0.41	1.26	NA	0.20
Chloride	>100	>100	>100	>100
Nitrite	0.16	0.19	0.24	NA
Bromide	5.63	0.17	0.38	0.10
Nitrate	4.17	12.97	52.0	23.5
Sulfate	16.67	>100	>100	73.23
Organics (mg/L)				
TOC	22.71	2.42	3.74	1.75
TON	2.38	3.08	13.7	6.03
Absorbance				
A ₂₅₄	0.319	0.025	0.042	0.015
Metals/Elemental (mg/L)				
As	0.033	0.015	0.022	0.011
B	1.63	0.193	1.16	0.044
Ba	BDL	0.009	0.006	0.006
Ca	1.38	14.3	26.3	5.64
Cr	0.001	0.001	0.001	0.001
K	6.67	5.36	5.04	2.21
Li	0.174	0.039	0.020	0.018
Mg	61.2	21.4	29.6	3.2
Mo	0.010	0.011	0.003	0.004
Na	441	217	251	119
Ni	0.004	0.002	0.005	BDL
P	0.169	0.048	0.034	BDL
S	6.55	87.2	122	24.2
Se	0.020	0.011	BDL	BDL
Si	3.82	4.61	7.13	7.59
Sn	0.006	BDL	BDL	BDL
Sr	0.029	0.284	0.516	0.134
Zn	0.003	0.008	0.011	0.008

BDL = Below detection limit

Anion analysis showed that most of the anions were similar in concentration between the four groundwaters. All groundwaters had high chloride levels. Nitrate, a known e_{aq}^- scavenger, was particularly high in MW 1-8 and MW 2-3, both Peterson Air Force base groundwaters. FGW and MW 1-8 both showed high sulfate concentrations. TOC/TON analysis showed that EAFB has the highest TOC while MW 1-8 had the highest TON. Dissolved organic matter (DOM) contains

a light-absorbing fraction, which can explain why EAFB also had the highest absorbance at $\lambda = 254$ nm (A_{254}). Metals/elemental analysis showed that generally concentrations were consistent among the groundwaters. Na levels were high in all groundwaters. MW 1-8 had the highest Ca concentration.

PFAS degradation rate constants in Ellsworth Air Force base (EAFB) groundwater. Figure 4.4.8 shows first-order degradation rate constants calculated for PFASs in EAFB groundwater. Similar to AFFF solutions, reactivity of PFASs to UV-sulfite treatment increased with increasing chain-length and short-chained PFASs were the most recalcitrant. Also similar to AFFF solutions, PFCAs reactivity was not dependent on chain-length.

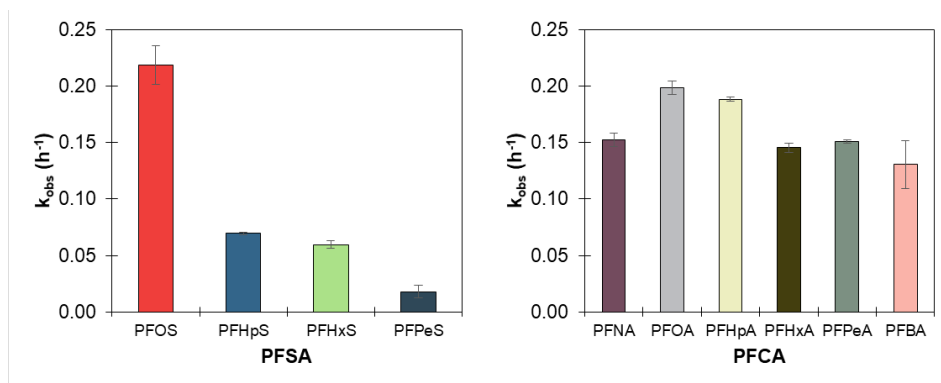


Figure 4.4.8. First-order degradation rate constants for targeted PFAS measured in Ellsworth Air Force Base groundwater. Reaction conditions: 575 mL groundwater ($0.7 \mu\text{m}$ GF filtered), $[\text{Na}_2\text{SO}_3]_0 = 10$ mM, $\text{pH}_0 = 9.5$, reactors were sparged with $\text{N}_{2(g)}$ for 1 h before reaction with 18 W UV LP Hg lamp.

There were detectable concentrations of 8:2 FTS ($0.6 \pm 0.1 \mu\text{g/L}$), 6:2 FTS ($65 \pm 3 \mu\text{g/L}$), and 4:2 FTS ($4.8 \pm 0.3 \mu\text{g/L}$) in EAFB groundwater. While 8:2 FTS showed 74% degradation after 24 h of UV-sulfite reaction, 6:2 FTS and 4:2 FTS were unreactive. Interestingly, generation of 6:2 fluorotelomer carboxylic acid (6:2 FTCA) was observed during UV-sulfite treatment. Generation of 6:2 FTCA could indicate that the FTCA is a transformation product of e_{aq}^- and precursors, similar to the generation of FTSS in dilute AFFF studies (Figure 4.4.1).

PFAS degradation rate constants in Peterson Air Force base groundwater from wells MW 1-8 and MW 2-3. Peterson Air Force base groundwater from well MW 1-8 followed PFAS reactivity trends found in EAFB and dilute AFFF experiments. PFSA reactivity increased with increasing chain-length and PFCA reactivity was independent of chain-length (Figure 4.4.10). Similarly, groundwater from well MW 2-3 also followed trends in EAFB dilute AFFF experiments. PFSA reactivity increased with increasing chain length (Figure 4.4.11).

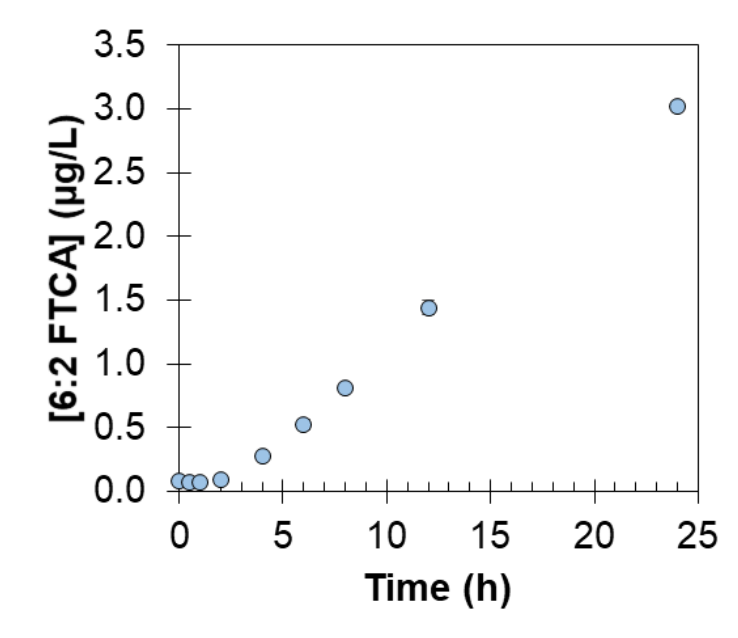


Figure 4.4.9. Concentration of 6:2 FTCA during UV-sulfite treatment. Reaction conditions identical to Figure 4.4.8.

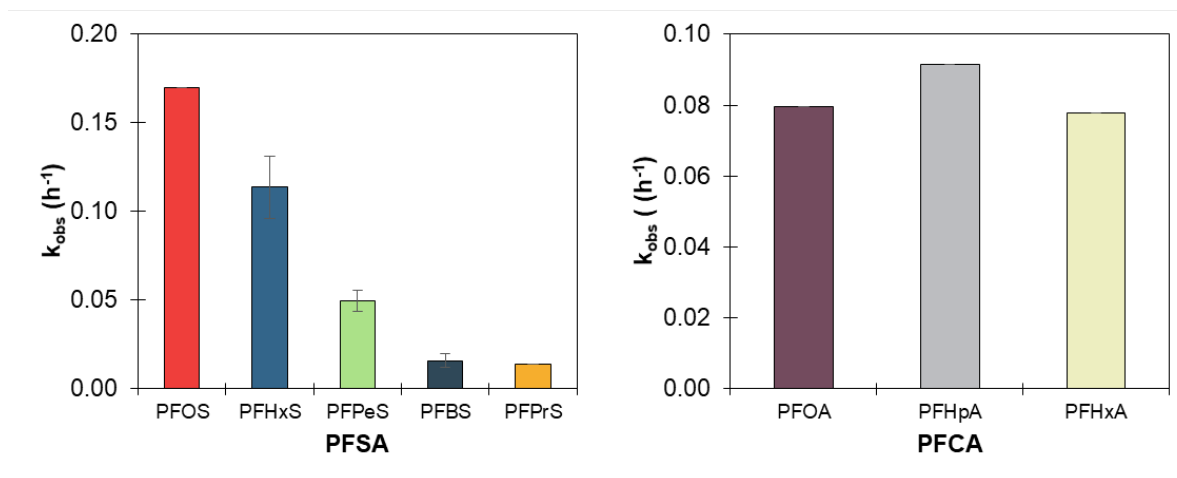


Figure 4.4.10. First-order degradation rate constants for targeted PFAS measured in Peterson Air Force Base groundwater from well MW 1-8. Reaction conditions: 575 mL groundwater (0.7 µm GF filtered), $[Na_2SO_3]_0 = 10$ mM, $pH_0 = 9.5$, reactors were sparged with $N_{2(g)}$ for 1 h before reaction with 18 W UV LP Hg lamp.

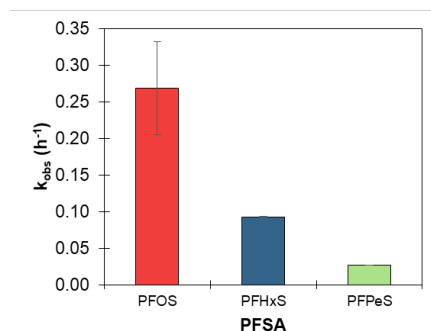


Figure 4.4.11. First-order degradation rate constants for targeted PFAS measured in Peterson Air Force Base groundwater from well MW 2-3. Reaction conditions: 575 mL groundwater ($0.7 \mu\text{m}$ GF filtered), $[\text{Na}_2\text{SO}_3]_0 = 10 \text{ mM}$, $\text{pH}_0 = 9.5$, reactors were sparged with $\text{N}_{2(g)}$ for 1 h before reaction with 18 W UV LP Hg lamp.

PFAS degradation rate constants in Fountain groundwater (FGW). Figure 4.4.12 shows the degradation of targeted PFASs during UV-sulfite treatment in Fountain groundwater. Unlike findings in EAFB, MW 1-8, MW 2-3 and AFFF solutions, PFHxS reactivity was similar to that of PFOS. Additionally, though PFOA, PFHpA, and PFHxA showed similar reactivity, PFPeA reactivity was lower.

Degradation rate constants measured in EAFB, MW 1-8, and MW 2-3 suggest that reactivity trends within the PFSA and PFCA classes in groundwater could be predicted from dilute AFFF experiments. However, reactivity trends for the PFSA and PFCA classes were different in FGW than the other groundwaters. This suggests that either (1) reactivity trends within PFAS classes will vary between different groundwaters or (2) conditions in FGW are unique and should be investigated further to elucidate mechanisms of PFAS transformation by e_{aq}^- .

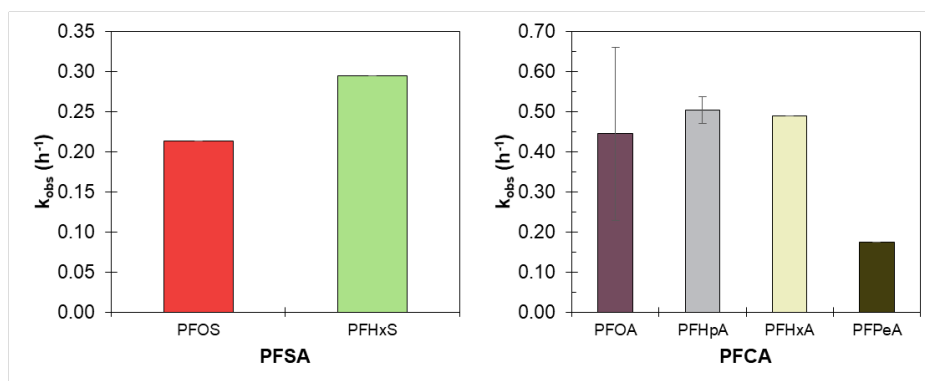


Figure 4.4.12. First-order degradation rate constants for targeted PFAS measured in Fountain groundwater. Reaction conditions: 575 mL groundwater ($0.7 \mu\text{m}$ GF filtered), $[\text{Na}_2\text{SO}_3]_0 = 10 \text{ mM}$, $\text{pH}_0 = 9.5$, reactors were sparged with $\text{N}_{2(g)}$ for 1 h before reaction with 18 W UV LP Hg lamp.

PFAS degradation rate constant comparison between different groundwaters. Figure 4.4.13 shows comparisons of observed PFAS first-order degradation rate constants (k_{obs}) between EAFB, FGW, MW 1-8, and MW 2-3.

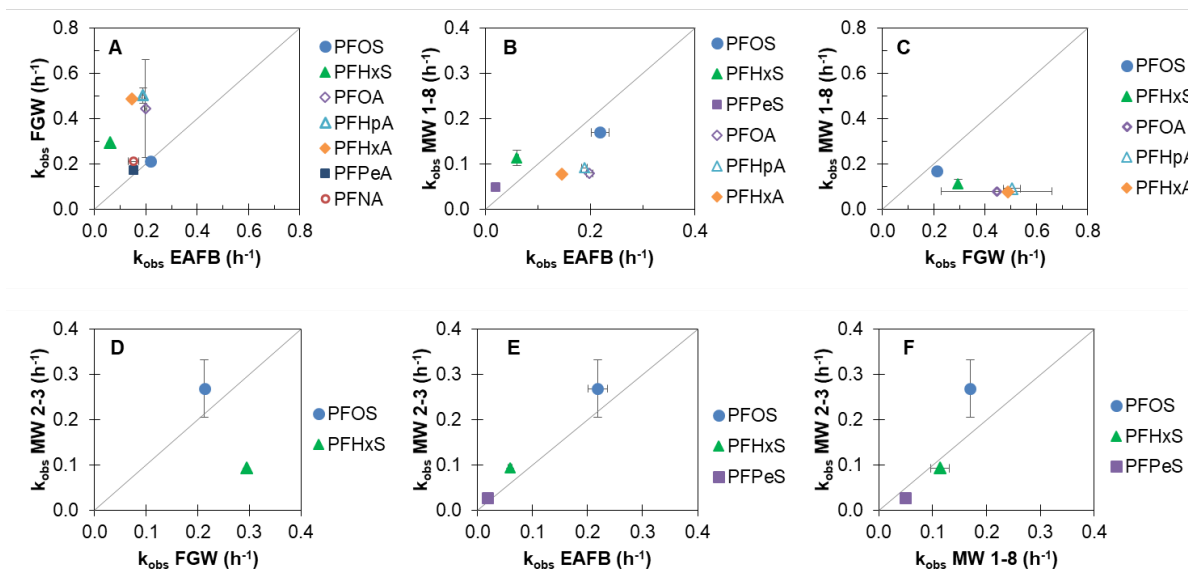


Figure 4.4.13. Comparison of observed first-order degradation rate constants (k_{obs} , h^{-1}) for PFASs in Ellsworth Air Force base groundwater (EAFB), Fountain groundwater (FGW), and Peterson Air Force base groundwater from two wells (MW 1-8, MW 2-3). A - F represent all combinations of comparisons for these 4 groundwaters. Each point represents a single PFAS where the x and y axis values correspond to the k_{obs} in each respective groundwater. The gray line (1:1) represents the case of equal reactivity for the two compared groundwaters.

Figures 4.4.13B, E, and F, show that MW 1-8, MW 2-3, and EAFB have points that lie near the 1:1 line indicating that PFAS reactivity in these 3 groundwaters is similar. However, Table 4.4.7 doesn't show any obvious similarities in any single water quality parameter between these 3 groundwaters. Thus, there may be a separate controlling factor that governs PFAS similar reactivity, such as having similar steady-state hydrated electron concentrations ($[e_{\text{aq}}^-]_{\text{ss}}$). Figures 4.4.13A and C, and D show that PFASs may be more reactive in FGW than in EAFB or MW 1-8.

PFAS degradation in background matrices with varying complexity. The reactivity of PFOS, PFHxS, and PFOA to UV-sulfite was compared in several matrices including groundwater, dilute AFFF, and single solute experiments. Figure 4.4.14 shows that PFOS showed enhanced reactivity in groundwaters. In the single solute experiment, PFOS showed lower reactivity and was comparable to the reactivity in AFFF experiments. Similarly, PFHxS showed higher reactivity in groundwater. These results suggest, PFSA reactivity may be enhanced in groundwaters. Enhanced PFOS reactivity has been shown in other work using KI as a e_{aq}^- photosensitizer while in the presence of natural organic matter (NOM) (Sun et al., 2017). Thus, NOM in groundwater could potentially enhance PFSA reactivity. In contrast, PFOA showed the highest degradation in the single solute experiment, and reactivity was diminished in both dilute AFFF and groundwater

experiments. Thus, PFAS reactivity in groundwater cannot be generalized across all compound classes. Results suggest the variation in reactivity caused by a different background water matrix could be dependent on the compound class.

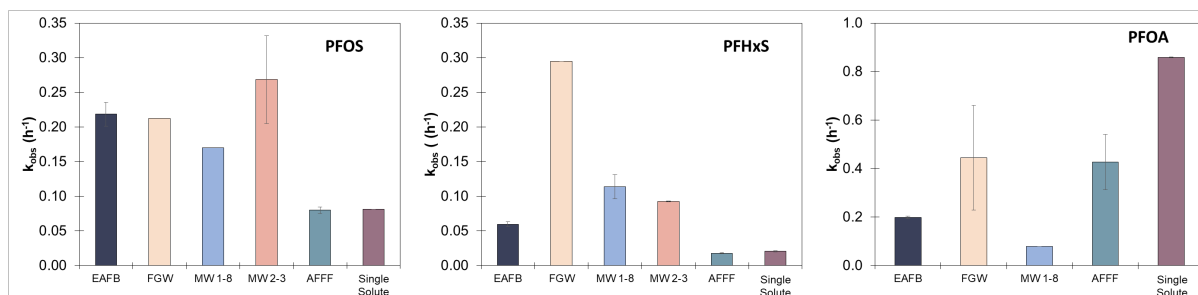


Figure 4.4.14. First-order degradation rate constants of PFOS, PFHxS, and PFOA in matrices varying in complexity, including: Ellsworth Air Force Base groundwater (EAFB), Fountain groundwater (FGW), Peterson Air Force Base groundwaters from two wells (MW 1-8, MW 2-3), dilute AFFF experiments (AFFF), and single solute experiments.

4.4.11 UV-Sulfite Energy Discussion

Energy is an important aspect of UV-sulfite treatment to consider. In AFFF solutions in this study (i.e., 18 W LP Hg UV lamp, 10 mM Na_2SO_3 , 575 mL treated water), 1-log removal of PFOS was achieved after ~ 24 h of irradiation—a $750 \text{ kWh}\cdot\text{m}^{-3}$ energy requirement. In contrast, the more reactive branched isomer of PFOS was removed after ~ 0.5 h of irradiation ($16 \text{ kWh}\cdot\text{m}^{-3}$)—a 50-fold lower energy requirement than total PFOS (linear + branched isomers). 1-log removal of PFOA was achieved after ~ 5 h of irradiation ($157 \text{ kWh}\cdot\text{m}^{-3}$). Though not as efficiently removed as the branched PFOS isomer alone, PFOA had 5-fold lower energy requirement than total PFOS. Other work investigating the removal of PFAS using UV-sulfite calculated energy requirements of $\sim 3250 \text{ kWh}\cdot\text{m}^{-3}$ for 1-log PFOS removal after ~ 20 min of irradiation (250 W HP Hg UV lamp, 10 mM Na_2SO_3 , 25 mL treated water) and $\sim 840 \text{ kWh}\cdot\text{m}^{-3}$ for 1-log PFOA removal after ~ 5 min of irradiation at similar reaction conditions (Gu et al., 2017, 2016). Thus, the application of methods involving photochemical destruction of high-energy C-F bonds in complex PFAS mixtures using sulfite photosensitizers will likely require considerable energy input. However, improvements to UV-sulfite treatment parameters could help considerably reduce energy consumption.

Though this study uses an 18 W LP Hg lamp, all 18 W of power are not directly converted into photons. Calculations converting photon flux (in photons·s⁻¹; $\lambda = 254$ nm) to power (in J·s⁻¹ = W) show that ~1 W originates from photons (i.e., ~5% lamp efficiency in photon production). If we consider only the power used to generate photons, 1-log removal of total PFOS and PFOA would require ~40 and ~10 kWh·m⁻³ of energy, respectively. Thus, as UV lamps become more efficient in photon generation, energy requirements could decrease by an order of magnitude. Improving e_{aq}⁻-generating sensitizers to more efficiently form e_{aq}⁻ with less energy input and increasing light absorption by optimizing reactor geometry could also increase PFAS degradation rates at a more reasonable energy consumption. Additionally, UV-sulfite processes could be designed to use light sources that yield greater light absorption within the sulfite absorption spectrum (i.e., lower wavelengths). This would increase e_{aq}⁻-generating efficiency by allowing for the use of lower sulfite concentrations which would in turn reduce e_{aq}⁻ scavenging by sulfite. Future changes to manufacturing processes that create more reactive branched PFAS isomers would also improve UV-sulfite efficiency.

4.5 PFAS Analytical Libraries

To date, we have built an XIC list containing 1432 compounds and an HRMS library containing 323 compounds. Some summary statistics for the databases are shown in Table 4.5.1.

Table 4.5.1. PFAS XIC list and HRMS library summary statistics

Classes in XIC list	130
Compounds in XIC list	1432
ESI- Amenable	902
ESI+ Amenable	716
Zwitterionic Compounds	227
Classes in library	74
Individual compounds in library	323
Compounds with ESI- Spectra	228
Compounds with ESI+ Spectra	138

Sharing of the XIC List Package. The Higgins laboratory has been disseminating the prepared XIC list to several other laboratories around the world along with auxiliary materials to assist users as a pilot project before making the resource more widely available. Auxiliary materials include a table containing an example structure for each compound group in the XIC list (Appendix A4), as well as a PowerPoint file explaining the naming convention used (Appendix A5). It also includes a shared spreadsheet where users can add information on additional compounds they would like to see added.

Sharing of the HRMS Library. The HRMS Library was built using SCIEX LibraryView and SCIEX PeakView software, and so is currently only shareable with other users who have access to this software and acquire data on SCIEX instruments. The library has been shared with other laboratories when possible, including Prof. Jennifer Field's laboratory at Oregon State University, Prof. Jochen Mueller's laboratory at the University of Queensland, and the Minnesota Department of Public Health.

Use of the XIC List and HRMS Library to Date. The XIC list and HRMS Library developed here are being used extensively by workers in the Higgins Laboratory, as well as their collaborators, in PFAS suspect screening workflows. These tools have led to a more streamlined workflow for identifying emerging PFASs of interest in a variety of matrices, including environmental and biological samples. Recent publications have used these tools to tentatively identify several groups of novel PFASs, including perfluoroalkyl sulfonamides, various substituted sulfonamides, and unsaturated and keto-perfluoroalkyl sulfonates, in AFFF-impacted groundwater (Murray et al., 2019; Xiao et al., 2017). The XIC list has also proven useful as a catalogue that links novel PFASs to their historical names, simplifying the process of understanding whether multiple papers are referring to the same compound using different nomenclature.

5.0 Conclusions and Implications for Future Research/Implementation

This project focused on PFAS transformation and defluorination via electrochemical oxidation on BDD anodes, catalytic reduction, and reduction in UV-sulfite systems. *Key findings from this research include the following:*

- B-12 catalyzed reduction was determined to be generally ineffective for treating PFAAs. Further research and/or alternate catalytic reductive approaches will be needed to advance this area of research.
- BDD anodes are effective for oxidatively defluorinating a wide range of PFAS in natural groundwater systems. The presence of hydroxyl radical-scavenging compounds that are likely to be in many of the treated waters (e.g., organic contaminants, chloride) are unlikely to have a substantial adverse impact on PFAS treatment
- Electrochemical oxidation of suspected PFAA precursors occurs relatively rapidly. However, oxidation of these compound may or may not result in the transient formation of PFAAs. The TOP assay may serve as a means to determine if such transient PFAA formation will occur.
- Fluorine mass balances between 70 and 80% were typically observed for PFAA electrochemical oxidation, and these losses have been attributed to volatilization of perfluorinated alkanes. Use of total organic fluorine analysis in an AFFF-impacted groundwater showed that that the fluorine mass balance was nearly 100%, with >90% of the fluorine in PFAS converted to fluoride.
- The TOP assay may not be a good indicator of the presence of polyfluorinated compounds in groundwater, as determined by a combination of semi-quantification of suspect analytes, total organic fluorine analysis, and measured fluoride generation during electrochemical treatment.
- Electrochemical oxidation of PFAS in water containing chloride will result in substantial generation of perchlorate. However, the electrochemically treated waters that contain this perchlorate are amenable to biotic reduction for removal of the perchlorate.
- Electrochemical treatment removes both long- and short-chained PFAS. The data shown in Figure 4.2.18 shows first order removal rate constants ranging from 0.23/hr for PFOA, to 0.028/hr for PFBS. While the kinetics are clearly slower for the shorter-chained compounds, this may be offset (in part) by less stringent regulatory levels that are currently in place for the shorter-chained compounds.
- Carbonate-based scaling at the cathode resulted in a substantial decreased PFAS removal after approximately 5 to 7 days. PFAS removal effectiveness was restored after acid cleaning of the cathode. Thus, for waters containing moderate to high hardness, routine cleaning of the cathode (via acid washing and/or polarity reversal) likely will be needed to maintain treatment effectiveness.

- UV-sulfite treatment shows promise, particularly for certain classes of PFAS compounds. However, energy demands for this technology may limit full-scale applications unless UV lamps are designed to focus energy in the sulfite-adsorbing wavelengths, and/or e_{aq}^- -generating sensitizers that are more energy efficient are developed.
- UV-sulfite treatment of polyfluorinated structures is much less effective than the corresponding perfluorinated structure. At the same time, polyfluorinated compounds can be transformed by advanced oxidation processes (AOPs) and activated persulfate oxidation processes to oxidize the polar headgroup and adjacent -CH₂- groups, forming a shorter chain perfluoroalkyl carboxylate structure. As we and others have observed, perfluoroalkyl carboxylates are highly reactive with UV-sulfite, regardless of chain length. Thus, we propose that a sequential treatment process involving application of AOP/activated persulfate followed by UV-sulfite might address polyfluorinated compounds in addition to perfluorinated compounds when present.
- Both the UV-sulfite and electrochemical oxidation technologies are more applicable to *ex situ* treatment than *in situ* treatment. Thus, future considerations of these technologies should focus on *ex situ* treatment. Comparison of costs and treatment effectiveness among the various emerging *ex situ* PFAS treatment technologies is needed to further evaluate the relative effectiveness of electrochemical and UV-based technologies.

This research project has provided for improved insight into the mechanisms and kinetics that govern PFAS transformation and defluorination during electrochemical oxidation, catalytic reduction, and UV-sulfite facilitated reduction in both ideal and complex water systems. Many of these insights (e.g., oxidation pathways, applicability of the TOP assay) have potential impacts in several on-going research projects related to PFAS treatment and environmental fate. While this research has yielded some important and exciting results, there remain many fundamental and applied questions that need to be addressed in future studies. These questions and issues include the following:

- *Does perchlorate generation during electrochemical treatment render this technology ineffective?* As discussed in Section 4.2.1.4, biological treatment to remove electrochemically generated perchlorate likely would result in only a marginal increase in the overall treatment cost. However, development of electrodes that mitigate perchlorate formation would likely improve the acceptance and potential commercial viability of this technology.
- *How feasible is long-term electrochemical treatment for removal of PFAS-impacted waters?* While electrochemical treatment of AFFF-impacted water over a 2 to 3 week period was assessed in this current study, assessment of treatment over a 3 to 6 month period is needed to more completely assess anode longevity and long-term PFAS defluorination rates.

More importantly, the costs of electrochemical treatment need to be further evaluated. In terms of energy demand (which corresponds to operating costs), EC treatment is 1 to 2 orders of magnitude greater than that typically needed for removal of organic contaminants,

but is less than many of the technologies currently being evaluated for PFAS treatment. Another important economic consideration is the capital costs associated with EC systems. While the EC systems studies herein are commercially produced and readily scalable, the elevated capital costs likely limit EC applications to relatively small and concentrated waste streams, such as concentrates from high pressure filtration, ion exchange regeneration fluids, or treatment of concentrated source materials.

- *How is electrochemical treatment impacted by elevated levels of salts (>0.1%) and/or other cosolvents that might be present when assessing treatment of PFAS concentrates?* Applications of electrochemical treatment will likely be limited to concentrated PFAS waste streams, such as concentrate from reverse osmosis or nanofiltration, or brines used to regenerate anion exchange resins used for PFAS treatment. Understanding and optimizing electrochemical performance in these waste streams, as is currently underway in ongoing SERDP Project ER18-1063, represents a critical data gap for this technology.
- *How can electrochemical treatment be applied within treatment trains to limit overall energy demand and costs?* Results from this study suggest that pre-oxidation of AFFF-impacted waters could result in transformation of PFAA precursors, and ultimately reduce the energy demands needed for treatment via electrochemical oxidation. Our results also suggest that, for water containing chloride, biotic treatment downstream of electrochemical oxidation could be an effective means to treat the electrochemically generated perchlorate. Recent studies further suggest that preconcentration of PFAS via high pressure filtration or use of anion exchange resins, followed by electrochemical treatment of the concentrates or regenerant brines, could result in effective PFAS treatment. Based on the findings presented in this current SERDP research effort, such approaches warrant further consideration and testing.

In addition, we recognize that developments are being made to these technologies, such as innovative electrode materials and systems, and alternate activation mechanisms for generation of hydrated electrons using UV systems. The approaches used to evaluate PFAS treatment herein can serve as both a guide and benchmark for evaluating these emerging technologies.

6.0 Literature Cited

1. United States Environmental Protection Agency (USEPA). Fact sheet: PFOA & PFOS drinking water health advisories, EPA 800-F-16-03 (2016).
2. Adenier, A.; Chehimi, M.M.; Gallardo, I.; Pinson, J.; Vilà, N., 2004. Electrochemical oxidation of aliphatic amines and their attachment to carbon and metal surfaces. *Langmuir*. 20, 8243-8253.
3. Ahrens, L.; Siebert, U.; Ebinghaus, R., 2009. Total body burden and tissue distribution of polyfluorinated compounds in harbor seals (*Phoca vitulina*) from the German Bight. *Mar. Pollut. Bull.* 58, 520–525.
4. Allred, B.M.; Lang, J.R.; Barlaz, M.A.; Field, J.A., 2015. Physical and Biological Release of Poly- and Perfluoroalkyl Substances (PFASs) from Municipal Solid Waste in Anaerobic Model Landfill Reactors. *Environ. Sci. Technol.* 49, 7648–7656.
5. Anderson, R.H.; Long, G.C.; Porter, R.C.; Anderson, J.K., 2016. Occurrence of select perfluoroalkyl substances at U.S. Air Force aqueous film-forming foam release sites other than fire-training areas: field-validation of critical fate and transport properties, *Chemosphere* 150, 678-685
6. Avendaño, S.M.; Liu, J., 2015. Production of PFOS from aerobic soil biotransformation of two perfluoroalkyl sulfonamide derivatives. *Chemosphere*. 119, 1084-1090.
7. Azizi, O.; Hubler, D.; Schrader, G.; Farrell, J.; Chaplin, B.P., 2011. Mechanism of perchlorate formation on boron-doped diamond film anodes, *Environ. Sci. Technol.* 45, 10582-10590.
8. Backe, W.J.; Day, T.C.; Field, J.A., 2013. Zwitterionic, Cationic, and Anionic Fluorinated Chemicals in Aqueous Film Forming Foam Formulations and Groundwater from U.S. Military Bases by Nonaqueous Large-Volume Injection HPLC-MS/MS. *Environ. Sci. Technol.* 47, 5226–5234.
9. Baduel, C.; Mueller, J.F.; Rotander, A.; Corfield, J.; Gomez-Ramos, M.-J., 2017. Discovery of novel per- and polyfluoroalkyl substances (PFASs) at a fire fighting training ground and preliminary investigation of their fate and mobility. *Chemosphere* 185, 1030–1038.
10. Bagastyo, A.Y.; Batstone, D.J.; Kristiana, I.; Gernjak, W.; Joll, C.; Radjenovic, J., 2012. Electrochemical oxidation of reverse osmosis concentrate on boron-doped diamond anodes at circumneutral and acidic pH. *Water Res.*, 46, 6104-6112.
11. Barzen-Hanson, K.A.; Field, J.A. 2015. Discovery and implications of C₂ and C₃ perfluoroalkyl sulfonates in aqueous film-forming foams and groundwater, *Environ. Sci. Technol. Lett.* 2, 95-99.
12. Barzen-Hanson, K.A.; Roberts, S.C.; Choyke, S.J.; Oetjen, K.; McAlees, A.; Riddell, N.; McCrindle, R.; Ferguson, P.L.; Higgins, C.P.; Field, J.A., 2017. Discovery of 40 classes

- of per- and polyfluoroalkyl substances in historical aqueous film-forming foams (AFFFs) and AFFF-impacted groundwater. *Environ. Sci. Technol.*, 51, 2047–2057.
13. Baumgartner, R.; McNeill, K., 2012. Hydrodefluorination and hydrogenation of fluorobenzene under mild aqueous conditions. *Environ. Sci. Technol.* 46, 10199–10205.
 14. Becke, A. D., 1993. Density-functional thermochemistry. III. The role of exact exchange. *J. Chem. Phys.* 98, 5648–5652.
 15. Bergmann, M.E.H.; Iourtchouk, T.; Schmidt, W.; Hartmann, J.; Fischer, M.; Nüsske, G.; Gerngroß, D. 2015. Laboratory- and technical –scale comparison of chlorate and perchlorate formation during drinking water electrolysis: a field study, *J. Appl. Electrochem.* 45, 765-778.
 16. Bergmann, M.E.H.; Rollin, J.; Iourtchouk, T., 2009. The occurrence of perchlorate during drinking water electrolysis using BDD anodes, *Electrochimica Acta* 54, 2102-2107.
 17. Bruton, T.A.; Sedlak, D.L., 2017. Treatment of Aqueous Film-Forming Foam by Heat-Activated Persulfate Under Conditions Representative of In Situ Chemical Oxidation. *Environ. Sci. Technol.*
 18. Buck, R. C.; Franklin, J.; Berger, U.; Conder, J. M.; Cousins, I. T.; Voogt, P. De; Jensen, A. A.; Kannan, K.; Mabury, S. A.; van Leeuwen, S. P. J., 2011. Perfluoroalkyl and polyfluoroalkyl substances in the environment: Terminology, classification, and origins. *Integr. Environ. Assess. Manag.*, 7, 513–541.
 19. Buxton, G.V.; Greenstock, C.L.; Helman, W.P., Ross, A.B., 1988. Critical Review of rate constants for reactions of hydrated electrons, hydrogen atoms and hydroxyl radicals ($\cdot\text{OH}/\cdot\text{O}^-$ in Aqueous Solution. *J. Phys. Chem. Ref. Data* 17, 513–886.
 20. Carter, K.E.; Farrell, J., 2008. Oxidative destruction of perfluorooctane sulfonate using boron-doped diamond film electrodes. *Environ. Sci. Technol.*, 42, 6111-6115.
 21. Chiu, P.-C.; Reinhard, M., 1995. Metallocoenzyme-mediated reductive transformation of carbon tetrachloride in titanium (III) citrate aqueous solution. *Environ. Sci. Technol.* 29, 595–603.
 22. Costa, C.R.; Montilla, F.; Morallón, E.; Olivi, P., 2009. Electrochemical oxidation of acid black 210 dye on the boron-doped diamond electrode in the presence of phosphate ions: effect of current density, pH, and chloride ions, *Electrochim. Acta* 54, 7048-7055.
 23. D’Agostino, L.A.; Mabury, S.A., 2014. Identification of Novel Fluorinated Surfactants in Aqueous Film Forming Foams and Commercial Surfactant Concentrates. *Environ. Sci. Technol.* 48, 121–129.
 24. Dinglasan, M.J.A.; Ye, Y.; Edwards, E.A.; Mabury, S.A., 2004. Fluorotelomer Alcohol Biodegradation Yields Poly- and Perfluorinated Acids. *Environ. Sci. Technol.* 38, 2857–2864.
 25. Donaghue, A.; Chaplin, B.P., 2013. Effect of select organic compounds on perchlorate formation at boron-doped diamond film anodes, *Environ. Sci. Technol.* 47, 12391–12399.

26. Enache, T.A.; Chiorcea-Paquim, A.-M.; Fatibelloe-Filho, O.; Oliveira-Brett, A.M., 2009. Hydroxyl radicals electrochemically generated in situ on a boron-doped diamond electrode, *Electrochem. Comm.* 11, 1342-1345.
27. Fabiańska, A.; Białk-Bielińska, A.; Stepnowski, P.; Stolte, S.; Siedlecka, E.M., 2014. Electrochemical degradation of sulfonamides at BDD electrode: Kinetics, reaction pathway and eco-toxicity evaluation. *J. Haz. Mater.*, 280, 579-587.
28. Farhan, Y.H.; Hatzinger, P.B., 2009. Modeling the biodegradation kinetics of perchlorate in the presence of oxygen and nitrate as competing electron receptors, *Biorem. J.* 13, 65-78.
29. Feng, W.; Deletic, A.; Wang, Z.; Zhang, X.; Gengenbach, T.; McCarthy, D.T., 2019. Electrochemical oxidation disinfects urban stormwater: Major disinfection mechanisms and longevity tests. *Sci. Total Environ.*, 646, 1440-1447.
30. Field, J.A.; Schultz, M.; Barofsky, D., 2003. Identifying Hydrocarbon and Fluorocarbon Surfactants in Specialty Chemical Formulations of Environmental Interest by Fast Atom Bombardment/Mass Spectrometry. *Chim. Int. J. Chem.* 57, 556–560.
31. Fogler, H.S., 2014. *Essentials of chemical reaction engineering*. Prentice Hall, Upper Saddle River, NJ.
32. Gomez-Ruiz, B.; Gómez-Lavín, S.; Diban, N.; Boiteux, V.; Colin, A.; Dauchy, X.; Urtiaga, A., 2017. Efficient electrochemical degradation of poly- and perfluoroalkyl substances (PFASs) from the effluents of an industrial wastewater treatment plant. *Chemical. Engin. J.*, 322, 196-204.
33. Grimme, S.; Ehrlich, S.; Goerigk, L., 2011. Effect of the damping function in dispersion corrected density functional theory. *J. Comput. Chem.* 32, 1456–1465.
34. Gu, Y.; Dong, W.; Luo, C.; LIU, T., 2016. Efficient Reductive Decomposition of Perfluorooctane Sulfonate in a High Photon Flux UV/Sulfite System. *Environ. Sci. Technol.* 50, 10554–10561.
35. Gu, Y.; Liu, T.; Zhang, Q.; Dong, W., 2017. Efficient decomposition of perfluorooctanoic acid by a high photon flux UV/sulfite process: Kinetics and associated toxicity. *Chem. Eng. J.* 326, 1125–1133.
36. Herbert, J.M.; Coons, M.P., 2017. The hydrated electron. *Annu. Rev. Phys. Chem.* 68, 447–472.
37. Houtz, E.F.; Higgins, C.P.; Field, J.A.; Sedlak, D.L., 2013. Persistence of Perfluoroalkyl Acid Precursors in AFFF-Impacted Groundwater and Soil. *Environ. Sci. Technol.* 47, 8187–8195.
38. Houtz, E.F.; Sedlak, D.L., 2012. Oxidative Conversion as a Means of Detecting Precursors to Perfluoroalkyl Acids in Urban Runoff. *Environ. Sci. Technol.* 46, 9342–9349.
39. Hu, X.C.; Andrews, D.Q.; Lindstrom, A.B.; Bruton, T.A.; Schaidler, L.A.; Grandjean, P.; Lohmann, R.; Carignan, C.C.; Blum, A.; Balan, S.A.; Higgins, C.P.; Sunderland, E.M., 2016. Detection of Poly- and Perfluoroalkyl Substances (PFASs) in U.S. Drinking Water

- Linked to Industrial Sites, Military Fire Training Areas, and Wastewater Treatment Plants. *Environ. Sci. Technol. Lett.* 3, 344–350.
40. Im, J.; Walshe-Langford, G. E.; Moon, J.-W.; Löffler, F. E., 2014. Environmental fate of the next generation refrigerant 2, 3, 3, 3- tetrafluoropropene (HFO-1234yf). *Environ. Sci. Technol.* 48, 13181–13187.
 41. Jeong, J.; Kim, C.; Yoon, J., 2009. The effect of electrode material on the generation of oxidants and microbial inactivation in the electrochemical disinfection process, *Water Res.* 43, 895-901.
 42. Kissa, E., 2001. *Fluorinated Surfactants and Repellents*. Marcel Dekker, Inc.: New York.
 43. Klassen, N.V.; Marchington, D.; McGowan, H.C.E., 1994. H₂O₂ Determination by the I₃- Method and by KMnO₄ Titration. *Anal. Chem.* 66, 2921–2925.
 44. Kliegman, S.; McNeill, K., 2008. Dechlorination of chloroethylenes by cob(I)alamin and cobalamin model complexes. *Dalton Trans.* 4191–4201.
 45. Krauss, M.; Singer, H.; Hollender, J., 2010. LC–high resolution MS in environmental analysis: from target screening to the identification of unknowns. *Anal. Bioanal. Chem.* 397, 943–951.
 46. Langlois, I.; Oehme, M., 2006. Structural identification of isomers present in technical perfluorooctane sulfonate by tandem mass spectrometry. *Rapid Commun. Mass Spectrom.* 20, 844–850.
 47. Lee, C.; Yang, W.; Parr, R. G., 1988. Development of the Colle-Salvetti correlation-energy formula into a functional of the electron density. *Phys. Rev. B: Condens. Matter Mater. Phys.* 37, 785–789.
 48. Lexa, D.; Saveant, J. M., 1983. The electrochemistry of vitamin B12. *Acc. Chem. Res.* 16, 235–243.
 49. Li, X.; Ma, J.; Liu, G.; Fang, J.; Yue, S.; Guan, Y.; Chen, L.; Liu, X., 2012. Efficient Reductive Dechlorination of Monochloroacetic Acid by Sulfite/UV Process. *Environ. Sci. Technol.* 46, 7342–7349.
 50. Liang, S.; Pierce Jr, R.D.; Lin, H.; Chiang, S.Y.; Huang, Q.J., 2018. Electrochemical oxidation of PFOA and PFOS in concentrated waste streams. *Remediation J.*, 28, 127-134.
 51. Lin, H.; Niu, J.; Liang, S.; Wang, C.; Wang, Y.; Jin, F.; Luo, Q.; Huang, Q., 2018. Development of macroporous Magnéli phase Ti₄O₇ ceramic materials: As an efficient anode for mineralization of poly-and perfluoroalkyl substances. *Chemical Engin. J.*, 354, 1058-1067.
 52. Liu, J.; Mejia Avendaño, S., 2013. Microbial degradation of polyfluoroalkyl chemicals in the environment: a review. *Environ. Int.* 61, 98–114.
 53. Liu, Y.; Pereira, A.D.S.; Martin, J.W., 2015. Discovery of C₅–C₁₇ Poly- and Perfluoroalkyl Substances in Water by In-Line SPE-HPLC-Orbitrap with In-Source Fragmentation Flagging. *Anal. Chem.* 87, 4260–4268.

54. MacCrehan, W.A.; Jensen, J.S.; Helz, G.R., 1998. Detection of Sewage Organic Chlorination Products That Are Resistant to Dechlorination with Sulfite. *Environ. Sci. Technol.* 32, 3640–3645.
55. Marenich, A. V.; Cramer, C. J.; Truhlar, D. G., 2009. Universal solvation model based on solute electron density and on a continuum model of the solvent defined by the bulk dielectric constant and atomic surface tensions. *J. Phys. Chem. B* 113, 6378–6396.
56. McGuire, M.E.; Schaefer, C.E.; Richards, T.; Backe, W.J.; Field, J.A.; Houtz, E.; Sedlak, D.L.; Guelfo, J. Wunsch, A.; Higgins, C.P. Evidence of remediation-induced alteration of subsurface poly- and perfluoroalkyl substance (PFAS) distribution at a former firefighter training area. *Environ. Sci. Technol.* 2014, 48, 6644-6652.
57. Mejia-Avenidaño, S.; Duy, S.V.; Sauvé, S.; Liu, J., 2016. Generation of perfluoroalkyl acids from aerobic biotransformation of quaternary ammonium polyfluoroalkyl surfactants. *Environ. Sci. Technol.*, 50, 9923-9932.
58. Men, Y.; Lee, P. K.; Harding, K. C.; Alvarez-Cohen, L., 2013. Characterization of four TCE-dechlorinating microbial enrichments grown with different cobalamin stress and methanogenic conditions. *Appl. Microbiol. Biotechnol.* 97, 6439–6450.
59. Merino, N.; Qu, Y.; Deeb, R. A.; Hawley, E. L.; Hoffmann, M. R.; Mahendra, S., 2016. Degradation and removal methods for perfluoroalkyl and polyfluoroalkyl substances in water. *Environ. Eng. Sci.* 33, 615–649.
60. Moe, M.K.; Huber, S.; Svenson, J.; Hagenaaars, A.; Pabon, M.; Trümper, M.; Berger, U.; Knapen, D.; Herzke, D., 2012. The structure of the fire fighting foam surfactant Forafac®1157 and its biological and photolytic transformation products. *Chemosphere* 89, 869–875.
61. Moody, C.A.; Field, J.A., 1999. Determination of Perfluorocarboxylates in Groundwater Impacted by Fire-Fighting Activity. *Environ. Sci. Technol.* 33, 2800–2806.
62. Moody, C.A.; Field, J.A., 2000. Perfluorinated Surfactants and the Environmental Implications of Their Use in Fire-Fighting Foams. *Environ. Sci. Technol.* 34, 3864–3870.
63. Moody, C.A.; Hebert, G.N.; Strauss, S.H.; Field, J.A., 2003. Occurrence and persistence of perfluorooctanesulfonate and other perfluorinated surfactants in groundwater at a fire-training area at Wurtsmith Air Force Base, Michigan, USA. *J. Environ. Monit.* 5, 341–345.
64. Murata, M.; Ivandini, T.A.; Shibata, M.; Nomura, S.; Fujishima, A.; Einaga, Y., 2008. Electrochemical detection of free chlorine at highly boron-doped diamond electrodes, *J. Electroanal. Chem.* 612, 29-36.
65. Murray, C. C.; Vatankhah, H.; McDonough, C. A.; Nickerson, A.; Hedtke, T. T.; Cath, T. Y.; Higgins, C. P.; Bellona, C. L., 2019. Removal of per- and polyfluoroalkyl substances using super-fine powder activated carbon and ceramic membrane filtration. *J. Hazard. Mater.* 366, 160–168.
66. Niu, J.; Lin, H.; Xu, J.; Wu, H.; Li, Y., 2012. Electrochemical mineralization of perfluorocarboxylic acids (PFCAs) by Ce-doped modified porous nanocrystalline PbO₂ film electrode. *Environ. Sci. Technol.* 46, 10191-10198.

67. Niu, J.; Lin, H.; Gong, C.; Sun, X., 2013. Theoretical and experimental insights into the electrochemical mineralization mechanism of perfluorooctanoic acid. *Environ. Sci. Technol.* 47, 14341-14349.
68. Niu, J.; Li, Y.; Shang, E.; Xu, Z.; Liu, J., 2016. Electrochemical oxidation of perfluorinated compounds in water. *Chemosphere* 146, 526-538.
69. Nguyen, V.T.; Reinhard, M.; Karina, G.Y.-H., 2011. Occurrence and source characterization of perfluorochemicals in an urban watershed. *Chemosphere* 82, 1277–1285.
70. Ochiai, T.; Iizuka, Y.; Nakata, K.; Murakami, T.; Tryk, D.A.; Fujishima, A.; Koide, Y.; Morito, Y., 2011. Efficient electrochemical decomposition of perfluorocarboxylic acids by the use of a boron-doped diamond electrode. *Diamond Related Mat.* 20, 64-67.
71. Ochoa-Herrera, V.; Sierra-Alvarez, R.; Somogyi, A.; Jacobsen, N.E.; Wysocki, V.H.; Field, J.A., 2008. Reductive Defluorination of Perfluorooctane Sulfonate. *Environ. Sci. Technol.* 42, 3260–3264.
72. Park, H.; Vecitis, C.D.; Cheng, J.; Choi, W.; Mader, B.T.; Hoffmann, M.R., 2009. Reductive Defluorination of Aqueous Perfluorinated Alkyl Surfactants: Effects of Ionic Headgroup and Chain Length. *J. Phys. Chem. A* 113, 690–696.
73. Park, H.; Vecitis, C.D.; Cheng, J.; Dalleska, N.F.; Mader, B.T.; Hoffmann, M.R., 2011. Reductive degradation of perfluoroalkyl compounds with aquated electrons generated from iodide photolysis at 254 nm. *Photochem. Photobiol. Sci.* 10, 1945–1953.
74. Park, S.; Lee, L.S.; Medina, V.F.; Zull, A.; Waisner, S., 2016. Heat-activated persulfate oxidation of PFOA, 6:2 fluorotelomer sulfonate, and PFOS under conditions suitable for in-situ groundwater remediation. *Chemosphere* 145, 376-383.
75. Park, S.; De Perre, C.; Lee, L. S., 2017. Alternate Reductants with VB12 to Transform C8 and C6 Perfluoroalkyl Sulfonates: Limitations and Insights into Isomer-Specific Transformation Rates, Products and Pathways. *Environ. Sci. Technol.* 51, 13869–13877.
76. Payne, K. A.; Quezada, C. P.; Fisher, K.; Dunstan, M. S.; Collins, F. A.; Sjuts, H.; Levy, C.; Hay, S.; Rigby, S. E.; Leys, D., 2015. Reductive dehalogenase structure suggests a mechanism for B12-dependent dehalogenation. *Nature* 517, 513.
77. Phillips, M. M.; Dinglasan-Panlilio, M. J. A.; Mabury, S. A.; Solomon, K. R.; Sibley, P. K., 2007. Fluorotelomer acids are more toxic than perfluorinated acids. *Environ. Sci. Technol.* 41, 7159–7163.
78. Place, B.J.; Field, J.A., 2012. Identification of Novel Fluorochemicals in Aqueous Film-Forming Foams Used by the US Military. *Environ. Sci. Technol.* 46, 7120–7127.
79. Plumlee, M.H.; McNeill, K., 2009. Reinard, M. Indirect photolysis of perfluorochemicals: hydroxyl radical-initiated oxidation of *n*-ethyl perfluorooctane sulfonamido acetate (*N*-EtFOSAA) and other perfluoroalkanesulfonamides. *Environ. Sci. Technol.* 43, 3662-3668.
80. Polcaro, A.M.; Vacca, A.; Mascia, M.; Palmas, S.; Ruiz, J.R., 2009. Electrochemical treatment of waters with BDD anodes: kinetics of the reactions involving chlorides. *J. App. Electrochem.*, 39, 2083-2092.

81. Qu, R.; Liu, J.; Li, C.; Wang, L.; Wang, Z.; Wu, J., 2016. Experimental and theoretical insights into the photochemical decomposition of environmentally persistent perfluorocarboxylic acids. *Water Res.* 104, 34–43.
82. Qu, Y.; Zhang, C.; Li, F.; Chen, J.; Zhou, Q., 2010. Photo-reductive defluorination of perfluorooctanoic acid in water. *Water Res.* 44, 2939–2947.
83. Radjenovic, J.; Escher, B.I.; Rabaey, K., 2011. Electrochemical degradation of the b-blocker metoprolol by Ti/Ru_{0.7}Ir_{0.3}O₂ and Ti/SnO₂-Sb electrodes. *Water Res.* 45, 3205-3214.
84. Rahn, R.O., 1997. Potassium Iodide as a Chemical Actinometer for 254 nm Radiation: Use of Iodate as an Electron Scavenger. *Photochem. Photobiol.* 66, 450–455.
85. Rajic, L.; Fallahpour, N.; Nazari, R.; Alshoawabkeh, A.N., 2015. Influence of humic substances on electrochemical degradation of trichloroethylene in limestone aquifers. *Electrochimica Acta* 181, 1123-129.
86. Rhoads, K.R.; Janssen, E.M.-L.; Luthy, R.G.; Criddle, C.S., 2008. Aerobic biotransformation and fate of n-ethyl perfluorooctane sulfonamidoethanol (n-EtFOSE) in activated sludge. *Environ. Sci. Technol.* 42, 2873-2878.
87. Rovira, C.; Kunc, K.; Hutter, J.; Parrinello, M., 2001. Structural and Electronic Properties of Co-corrole, Co-corrin, and Co-porphyrin. *Inorg. Chem.* 40, 11–17.
88. Schaefer, C.E.; Fuller, M.; Condee, C.; Lowey, J.; Hatzinger, P., 2007. Comparison of Biotic and Abiotic Treatment Approaches for the Co-mingled Perchlorate, Nitrate, and Nitramine Explosives in Groundwater. *J. Contam. Hydrol.* 89, 231-250.
89. Schaefer, C.E.; Andaya, C.; Urutiaga, A.; McKenzie, E.R.; Higgins, C.P., 2015. Electrochemical treatment of perfluorooctanoic acid (PFOA) and perfluorooctane sulfonic acid (PFOS) in groundwater impacted by aqueous film forming foams (AFFFs). *J. Haz. Mater.* 295, 170-175.
90. Schaefer, C.E.; Andaya, C.; Burant, A.; Condee, C.W.; Urutiaga, A.; Strathmann, T.J.; Higgins, C.P., 2017. Electrochemical treatment of perfluorooctanoic acid and perfluorooctane sulfonate: insights into mechanisms and application to groundwater treatment. *Chemical. Engin. J.* 317, 424-432.
91. Schaefer, C.E.; Choyke, S.; Ferguson, P.L.; Andaya, C.; Burant, A.; Maizel, A.; Strathmann, T.J.; Higgins, C.P., 2018. Electrochemical Transformations of Perfluoroalkyl Acid (PFAA) Precursors and PFAAs in Groundwater Impacted with Aqueous Film Forming Foams. *Environ. Sci. Technol.*, 52, 10689-10697.
92. Schmalz, V.; Dittmar, T.; Haaken, D.; Worch, E., 2009. Electrochemical disinfection of biologically treated wastewater from small treatment systems by using boron-doped diamond (BDD) electrodes. *Water Res.* 43, 5260-5266.
93. Schultz, M.M.; Barofsky, D.F.; J.A. Field, J.A., 2004. Quantitative determination of fluorotelomer sulfonates in groundwater by LC MS/MS. *Environ. Sci. Technol.* 38, 1828-1835.

94. Schymanski, E. L.; Jeon, J.; Gulde, R.; Fenner, K.; Ru, M.; Singer, H. P.; Hollender, J., 2014. Identifying Small Molecules via High Resolution Mass Spectrometry: Communicating Confidence. *Environ. Sci. Technol.* 48, 2097–2098.
95. Song, Z.; Tang, H.; Wang, N.; Zhu, L., 2013. Reductive defluorination of perfluorooctanoic acid by hydrated electrons in a sulfite-mediated UV photochemical system. *J. Hazard. Mater.* 262, 332–338.
96. Stephens, P.; Devlin, F.; Chabalowski, C.; Frisch, M. J., 1994. Ab initio calculation of vibrational absorption and circular dichroism spectra using density functional force fields. *J. Phys. Chem.* 98, 11623–11627.
97. Sturchio, N.C.; Böhlke, J.K.; Beloso Jr., A.D.; Streger, S.H.; Heraty, L.J.; Hatzinger, P.B., 2007. Oxygen and chlorine isotopic fractionation during perchlorate biodegradation: laboratory results and implications for forensics and natural attenuation studies. *Environ. Sci. Technol.* 41, 2796-2802.
98. Sun, Z.; Zhang, C.; Chen, P.; Zhou, Q.; Hoffmann, M.R., 2017. Impact of humic acid on the photoreductive degradation of perfluorooctane sulfonate (PFOS) by UV/Iodide process. *Water Research* 127, 50–58.
99. Sun, Z.; Zhang, C.; Xing, L.; Zhou, Q.; Dong, W.; Hoffmann, M.R., 2018. UV/Nitritotriacetic Acid Process as a Novel Strategy for Efficient Photoreductive Degradation of Perfluorooctanesulfonate. *Environ. Sci. Technol.*
100. Tian, H.; Gao, J.; Li, H.; Boyd, S.A.; Gu, C., 2016. Complete Defluorination of Perfluorinated Compounds by Hydrated Electrons Generated from 3-Indole-acetic-acid in Organomodified Montmorillonite. *Sci. Rep.* 6, 32949.
101. Trautmann, A.M.; Schell, H.; Schmidt, K.R.; Mangold, K.-M.; Tiehm, A., 2015. Electrochemical degradation of perfluoroalkyl and polyfluoroalkyl substances (PFASs) in groundwater. *Water Sci. Technol.* 143, 1569-1575.
102. Tseng, N.; Wang, N.; Szostek, B.; Mahendra, S.; 2014. Biotransformation of 6:2 Fluorotelomer Alcohol (6:2 FTOH) by a Wood-Rotting Fungus. *Environ. Sci. Technol.* 48, 4012–4020.
103. Urtiaga, A.; Fernandez-Gonzalez, C.; Gomez-Lavin, S.; Ortiz, I., 2015. Kinetics of the electrochemical mineralization of perfluorooctanoic acid on ultrananocrystalline boron doped conductive diamond electrodes. *Chemosphere* 129, 20-26.
104. Vecitis, C. D.; Park, H.; Chengm J.; Mader, B. T.; Hoffmann, M. R., 2009. Treatment technologies for aqueous perfluorooctanesulfonate (PFOS) and perfluorooctanoate (PFOA). *Front. Environ. Sci. Eng. China* 3, 129-151.
105. Vosko, S. H.; Wilk, L.; Nusair, M., 1980. Accurate spin-dependent electron liquid correlation energies for local spin density calculations: a critical analysis. *Can. J. Phys.* 58, 1200–1211.
106. Weiner, B.; Yeung, L.W.Y.; Marchington, E.B.; D'Agostino, L.A.; Mabury, S.A., 2013. Organic fluorine content in aqueous film forming foams (AFFFs) and biodegradation of the foam component 6 : 2 fluorotelomermercaptoalkylamido sulfonate (6 : 2 FTSAS). *Environ. Chem.* 10, 486–493.

107. Wu, M.; Zhao, G.; Li, M.; Liu, L.; Li, D., 2009. Applicability of boron-doped diamond electrode to the degradation of chloride-mediated and chloride-free wastewaters. *J. Haz. Mater.* 163, 26-31.
108. Xiao, X.; Ulrich, B. A.; Chen, B.; Higgins, C. P., 2017. Sorption of Poly- and Perfluoroalkyl Substances (PFASs) Relevant to Aqueous Film-Forming Foam (AFFF)-Impacted Groundwater by Biochars and Activated Carbon.
109. Yang, X.; Huang, J.; Zhang, K.; Yu, G.; Deng, S.; Wang, B., 2014. Stability of 6: 2 fluorotelomer sulfonate in advanced oxidation processes: degradation kinetics and pathway. *Environ. Sci. Pollution Resear.* 21, 4634-4642.
110. Yang, B.; Jiang, C.; Yu, G.; Deng, S.; Wu, J.; Zhang, H.; Zhuo, Q., 2015. Highly efficient electrochemical degradation of perfluorooctanoic acid (PFOA) by F-doped Ti/SnO₂ electrode. *J. Haz. Mater.* 299, 417-424.
111. Yonetani, T.; Yamamoto, H.; Woodrow, G. V., 1974. Studies on cobalt myoglobins and hemoglobins I. Preparation and optical properties of myoglobins and hemoglobins containing cobalt proto-, meso-, and deuteroporphyrins and thermodynamic characterization of their reversible oxygenation. *J. Biol. Chem.* 249, 682-690.
112. Yu, Y.-H.; Chiu, P. C., 2014. Kinetics and pathway of vinyl fluoride reduction over rhodium. *Environ. Sci. Technol. Lett.* 1, 448-452.
113. Zhuo, Q.; Deng, S.; Yang, B.; Huang, J.; Yu, G., 2011. Efficient electrochemical oxidation of perfluorooctanoate using a Ti/SnO₂-Sb-Bi anode. *Environ. Sci. Technol.* 45, 2973-2979.
114. Zhuo, Q.; Deng, S.; Yang, B.; Huang, J.; Wang, B.; Zhang, T.; Yu, G., 2012. Degradation of perfluorinated compounds on a boron-doped diamond electrode. *Electrochim. Acta.* 77, 17-22.

APPENDIX A: Supporting Data

Appendix A1: Analysis of Potential PFAA Precursors via High Resolution Mass Spectrometry (HRMS)

An aliquot of each samples was prepared with 10% Optima LCMS grade acetonitrile (Fisher Scientific) in a polypropylene auto-sampler vial. Chromatographic separation was performed at a flow rate of 0.3 mL/min and oven temperature of 30°C using a Dionex Ultimate 3000RS UHPLC system (Thermo Scientific) . A CTC Analytics PAL autosampler injected 5µL of sample on a 100mm x 2.1 mm Hypersil Gold C₁₈ column with a 1.9 µm particle size. The HPLC mobile phase consisted of HPLC grade water (A) and acetonitrile (B) for negative mode analysis, and 0.1% formic acid in water (A) and 0.1% formic acid in acetonitrile (B) for positive mode analysis. In both ionization modes, the chromatography gradient had initial composition of 5%B held for 2 minutes, increased to 56%B over 23 minutes, increased to 99%B over 5 minutes, held at 99%B for 5 minutes, then the composition returned to 5%B in 0.1 minutes and allowed to equilibrate for 5 minutes, for a total run time of 40 minutes. The first 1.5 minutes of the gradient were diverted to waste to prevent nonvolatile salts from contaminating the source. In addition, from 35-40 minutes the flow was diverted to waste during column equilibration.

Full scan MS detection was performed with an Orbitrap Fusion Lumos (Thermo Fisher Scientific, San Jose, CA) with resolution R=240000 at 200m/z, for m/z=150-2000 and max injection time of 50ms. Acquisition was performed with internal calibrant (EASY-IC) using electrospray ionization (ESI) in positive and negative modes with a spray voltage of +3.3 and -2.5 kV, respectively. The capillary temperature was 360°C, vaporizer temperature was 275°C, sheath gas flow at 40 arbitrary units, auxiliary gas flow at 12 arbitrary units. Acquisition was performed with peak apex detection and dynamic exclusion to ensure high quality spectra were acquired for each compound. High resolution Orbitrap MS/MS (resolution R=15000 at 200m/z) analysis consisted of high collision dissociation (HCD) =45±5% and collision induced dissociation (CID) = 35eV, AGC target =2.5e4, maximum injection time = 35 seconds, isolation window = 1.6 Da, cycle time = 1 second. An inclusion list and targeted MS/MS experiment were performed to obtain additional spectra for confirmation. Details of HRMS data analysis are provided in the supporting information.

HRMS Data Analysis.

The following references were used as a guide to identify features:

Loos, M., Singer, H. Nontargeted homologue series extraction from hyphenated high resolution mass spectrometry data. *J. Cheminformatics* **2017** 9, 12.

Loos, M., Singer, H. Nontargeted homologue series extraction from hyphenated high resolution mass spectrometry data. *J. Cheminformatics* **2017** 9, 12.

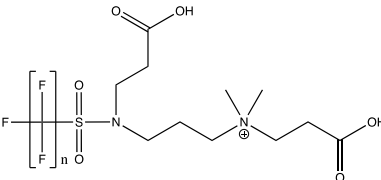
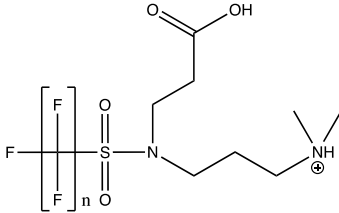
Dodder, N. G. and with code contributions from Mullen, K. M. OrgMassSpecR: Organic Mass Spectrometry. R package version 0.5–3. <http://CRAN.R-project.org/package=OrgMassSpecR>. **2017**

Schymanski, E. L.; Jeon, J.; Gulde, R.; Fenner, K.; Ruff, M.; Singer, H. P.; Hollender, J. Identifying Small Molecules via High Resolution Mass Spectrometry: Communicating Confidence. *Environ. Sci. Technol.* **2014**, 48, 2097–2098.

Feature detection, chromatographic alignment and isotope and adduct deconvolution was performed using the CompoundDiscoverer 2.1.0.401 SP1 (Thermo Scientific) software package. The resulting feature list included neutral molecular weight and retention time. Criteria to support a tentatively suspect identification included (1) exact mass match to screening list with less than 2ppm mass error, (2) occurrence of multiple masses in a homologue series, (3) expected retention time fluorocarbon chain number, (4) peak shape similarity within a homologue series, (5) homologue distribution using the R package “nontarget” (version 1.9, envipat version 2.2), and (6) spectra reference match. Reference spectra were acquired from an AFFF mixture by exact mass match of precursor ion to PFAS database and spectral similarity to MS2 found in literature. Similarity scores were calculated with a dot-product match using the R package “OrgMassSpecR” (version 0.5-3).

Appendix A2: Suspect Analytes Identified through HRMS

Table A2.1. PFASs identified through HRMS (excluding PFCAs and PFSA) in W1*.

Structure Class	Acronym	n	Molecular Formula	Theoretical Molecular Weight	Observed molecular weight	Mass error (ppm)
	CnEtAmPr-FASA-PrA	4	C15H21F9N2O6S	528.0976609	528.09818	-0.82
	N-carboxy ethyl dimethyl ammonio	5	C16H21F11N2O6S	578.0944673	578.09538	-1.58
	propyl perfluoroalkane sulfonamido propanoic acid	6	C17H21F13N2O6S	628.0912737	628.09203	-1.28
	n=4,5,6					
	CnAmPr-FASA-PrA	4	C12H17F9N2O4S	456.0765316	456.07677	-0.52
	N-dimethyl ammonio propyl perfluoroalkane sulfonamido propanoic acid	5	C13H17F11N2O4S	506.073338	506.07305	0.57
	n=4,5,6					
		6	C14H17F13N2O4S	556.0701444	556.07061	-0.84

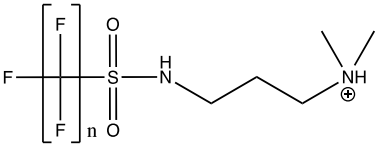
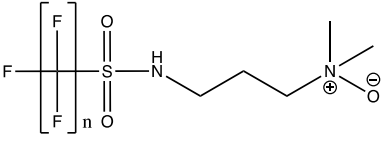
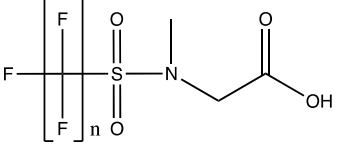
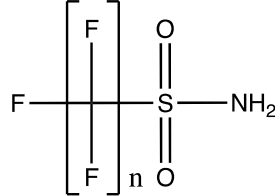
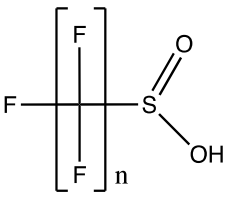
AmPr-FASA						
 n=4,5,6	N-dimethyl ammonio propyl perfluoroalkane sulfonamide	4	C9H13F9N2O2S	384.0554022	384.055245	0.41
		5	C10H13F11N2O2S	434.0522086	434.05225	-0.10
		6	C11H13F13N2O2S	484.049015	484.04933	-0.65
OAmPr-FASA**						
 n= <u>4</u> , <u>5</u> , <u>6</u>	N- oxidodimethylammoni opropyl- perfluoroalkanesulfona mide	<u>4</u>	C9H13F9N2O3S	400.0503168	400.05037	-0.13
		<u>5</u>	C10H13F11N2O3S	450.0471232	450.047105	0.04
		<u>6</u>	C11H13F13N2O3S	500.0439296	500.04433	-0.80

Table S1 (continued). PFASs identified through HRMS (excluding PFCAs and PFSA) in W1.*

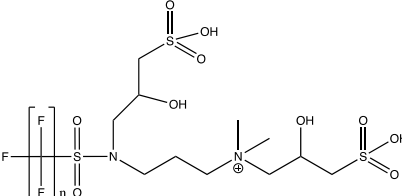
Structure Class	Acronym	n	Molecular Formula	Theoretical Molecular Weight	Observed molecular weight	Mass error (ppm)
-----------------	---------	---	-------------------	------------------------------	---------------------------	------------------

	MeFASAA**					
	N-	<u>4</u>	C7H6F9NO4S	370.9873822	370.98726	0.33
	MethylperFluoroAlkane	<u>5</u>	C8H6F11NO4S	420.9841886	420.98424	-0.12
	SulfonamidoAcetic Acid	6	C9H6F13NO4S	470.980995	470.981155	-0.34
n= <u>4,5,6</u>						
	FASA**			298.9662528		
	perFluoroAlkane	<u>4</u>	C4H2F9NO2S	348.9630592	298.966085	0.56
	SulfonAmide	<u>5</u>	C5H2F11NO2S	398.9598656	348.96294	0.34
		<u>6</u>	C6H2F13NO2S	498.9534784	398.959815	0.13
		<u>8</u>	C8H2F17NO2S		498.95376	0.23
n= <u>4,5,6,8</u>						
	PFASi**					
	PerFluoroAlkane	<u>5</u>	C5HF11O2S	333.9521602	333.952015	0.43
	Sulfinate	<u>6</u>	C6HF13O2S	383.9489666	383.94893	0.10
n= <u>5,6</u>						

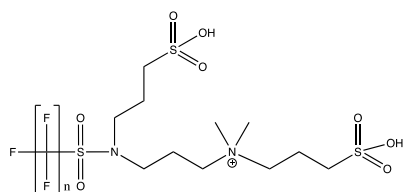
* Only compound classes identified with area counts of at least $\sim 10^6$ are listed, and/or compounds that showed a transient increase during electrochemical oxidation.

** Transient increase observed during electrochemical treatment for chain lengths that are underlined and in bold.

Table A2.2. PFASs identified through HRMS (excluding PFCAs and PFSAs) in W2*.

Structure Class	Acronym	n	Molecular Formula	Theoretical Molecular Weight	Observed molecular weight	Mass error (ppm)
 <p>n=4,5,6</p>	S-OHPrAmPr-FASA-OHPrS					
	N-Sulfohydroxypropyl dimethylAmmonio	4	C15H25F9N2O10S3	660.0527651	660.05146	1.97
	Propyl perFluoroAlkane	5	C16H25F11N2O10S3	710.0495716	710.04795	2.28
	Sulfonamido	5	C17H25F13N2O10S3	760.0463781	760.04713	-0.98
	hydroxypropyl Sulfonate	6				

SPrAmPr-FASAPrS

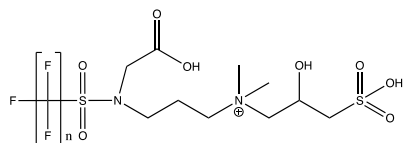


n=4,5,6

N-
SulfoPropyldimethylAm
monioPropyl
perFluoroAlkane
SulfonAmidoPropyl
Sulfonate

4	C15H25F9N2O8S3	628.0629358	628.0639	-1.53
5	C16H25O8S3N2F11	678.0597423	728.05822	-2.30
6	C17H25O8S3N2F13	728.0565488	728.0565488	-1.24

S-OHPrAmPr-FASAA

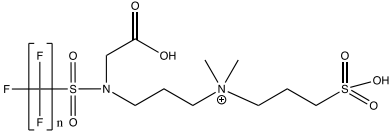
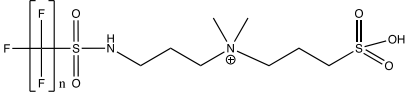


n=4,5,6

N-SulfohydroxyPropyl
dimethyl
AmmonioPropyl
perFluoroAlkaneSulfon
amido Acetic Acid

4	C14H21O8S2N2F9	580.05954	580.05954	-0.55
5	C15H21O8S2N2F11	630.05634	630.05634	-0.51
6	C16H21O8S2N2F13	680.05315	680.05315	-0.66

Table A2.2 (continued). PFASs identified through HRMS (excluding PFCAs and PFSAs) in W2.*

Structure Class	Acronym	n	Molecular Formula	Theoretical Molecular Weight	Observed molecular weight	Mass error (ppm)
SPrAmPr-FASAA						
 n=4,5,6	N- SulfoPropyl dimethylAm monioPropyl- perFluoroAlkaneSulfon amido Acetic Acid	4	C14H21O7S2N2F9	564.0646492	564.0646492	0.16
		5	C15H21O7S2N2F11	614.0614557	614.0614557	-0.64
		5	C16H21O7S2N2F13	664.0582622	664.0582622	-1.29
		6				
SPrAmPr-FASA						
 n=4,5,6,8	N-Sulfo Propyl dimethyl Ammonio Propyl perFluoroAlkaneSulfon amide	4	C12H19O5S2N2F9	506.0591698	506.0591698	0.73
		4	C13H19O5S2N2F11	556.0559763	556.0559763	-0.08
		5	C14H19O5S2N2F13	606.0527828	606.0527828	-0.79
		5	C16H19O5S2N2F17	706.0463958	706.0463958	-1.18
		6				
		8				

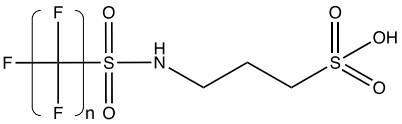
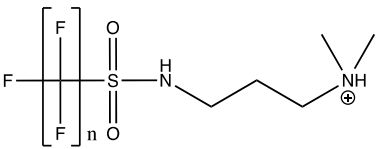
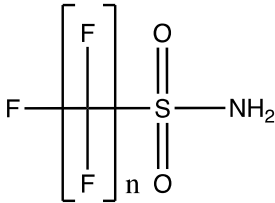
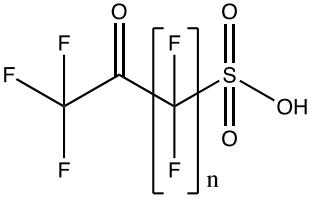
SPr-FASA						
						
	n=4,5,6	4	C7H8O5S2NF9	420.9700204	420.97013	-0.26
		5	C8H8O5S2NF11	470.9668269	470.9668269	-1.51
		6	C9H8O5S2NF13	520.9636334	520.96418	-1.05
AmPr-FASA						
						
	n=4,5,6,7,8	4	C9H13O2N2SF9	384.0554039	384.0554039	0.69
		5	C10H13O2N2SF11	434.0522104	434.0522104	0.72
		6	C11H13O2N2SF13	484.0490169	484.0490169	0.14
		7	C12H13O2N2SF15	534.0458234	534.0458234	-0.46
	8	C13H13O2N2SF17	584.0426299	584.0426299	-0.67	

Table A2.2 (continued). PFASs identified through HRMS (excluding PFCAs and PFSA) in W2.*

Structure Class	Acronym	n	Molecular Formula	Theoretical Molecular Weight	Observed molecular weight	Mass error (ppm)
FASA**						
 <p>n=<u>4</u>,<u>5</u>,<u>6</u>,<u>8</u></p>	perfluoroAlkane SulfonAmide	<u>4</u>	C4H2O2NSF9	298.9662544	298.9662544	0.55
		<u>5</u>	C5H2O2NSF11	348.9630609	348.9630609	0.38
		<u>6</u>	C6H2O2NSF13	398.9598674	398.9598674	0.04
		<u>8</u>	C8H2O2NSF17	498.9534804	498.9534804	2.35
		8				
K-PFAS**						
 <p>n=<u>2</u>,<u>3</u>,<u>4</u>,<u>5</u>,<u>6</u></p>	keto perfluoroalkane sulfonate	<u>2</u>	C4HO4SF7	277.9483782	277.9483782	-0.58
		<u>3</u>	C5HO4SF9	327.9451847	327.9451847	-0.53
		<u>4</u>	C6HO4SF11	377.9419912	377.9419	0.24
		<u>5</u>	C7HO4SF13	427.9387977	427.9387977	0.09
		<u>6</u>	C8HO4SF15	477.9356042	477.9356042	-1.37
		5				

* Only compound classes identified with area counts of at least $\sim 10^6$ are listed, and/or compounds that showed a transient increase during electrochemical oxidation.

** Transient increase observed during electrochemical treatment for chain lengths that are underlined and in bold.

Appendix A3: PFAS Suspect Analyte Identification Parameters

Table A3.1. Characteristic PFAS classes in W1 with molecular formula, precursor m/z , identification level of confidence and similarity score to reference MS2 spectra.

Compound Acronym	ESI mode	Molecular Formula	Precursor m/z	Collision Energy	Level of Confidence	Similarity Score
CEtAmPr-FASA-PrA	ESI(+)	C17H22F13N2O6S ⁺	629.0988	45	Reference Spectra Match	88.4%
AmPr-FASA-PrA	ESI(+)	C14H18F13N2O4S ⁺	557.0776	45	Reference Spectra Match	97.7%
AmPr-FASA	ESI(+)	C11H14F13N2O2S ⁺	485.0566	45	Reference Spectra Match	92.5%
	ESI(-)	C11H12F13N2O2S ⁻	483.0417	45	Reference Spectra Match	76%
CEtAmPr-FASA-PrA	ESI(+)	C11H14O3SN2F13 ⁺	501.0674	45	Reference Spectra Match	31.7%
MeFASAA	ESI(-)	C9H5O4NSF13 ⁻	469.7937	NA	Exact Mass Match	NA
FASA	ESI(-)	C6H192NSF13 ⁻	397.9523	45	Reference Spectra Match	99.8%
PFASi	ESI(-)	C6O2SF13 ⁻	382.9419	56	Reference Spectra Match	11.9%

Table A3.2. Characteristic PFAS classes in W2 with molecular formula, precursor m/z , identification level of confidence and similarity score to reference MS2 spectra.

Compound Acronym	ESI mode	Molecular Formula	Precursor Ion	Collision Energy	Level of Confidence	Similarity Score
S-OHPrAmPr-FASA-OHPrS	ESI(+)	C17H26O10S3N2F13 ⁺	761.0552	45	Reference Spectra Match	82.1%
	ESI(-)	C17H24O10S3N2F13 ⁻	759.0405	65	Reference Spectra Match	68.4%
SPrAmPr-FASAPrS	ESI(+)	C17H26O8S3N2F13 ⁺	729.0645	45	Reference Spectra Match	99.4%
	ESI(-)	C17H24O8S3N2F13 ⁻	727.0497	65	Reference Spectra Match	91.9%
S-OHPrAmPr-FASAA	ESI(+)	C14H22O8S2N2F9 ⁺	581.0634	45	Reference Spectra Match	99.8%
SPrAmPr-FASAA	ESI(+)	C16H22O7S2N2F13 ⁻	665.0655	45	Reference Spectra match	99.7%
	ESI(-)	C16H20O7S2N2F13 ⁻	663.0486	45	Reference Spectra match	99.5%
SPrAmPr-FASA	ESI(+)	C14H20O5S2N2F13 ⁺	607.0602	45	Reference Spectra Match	97.5%
	ESI(-)	C14H18O5S2N2F13 ⁻	605.0460	35	Reference Spectra Match	93.8%
SPr-FASA	ESI(-)	C9H7O5S2NF13 ⁻	519.9565	45	Reference Spectra Match	98.7%
AmPr-FASA	ESI(+)	C11H14F13N2O2S ⁺	485.0562	45	Reference Spectra Match	92.8%

Compound Acronym	ESI mode	Molecular Formula	Precursor Ion	Collision Energy	Level of Confidence	Similarity Score
	ESI(-)	C11H12F13N2O2S ⁻	483.0417	45	Reference Spectra Match	93.6%
FASA	ESI(-)	C6HO2NSF13 ⁻	397.9521	45	Reference Spectra Match	99.7%
K-PFAS	ESI(-)	C6O4SF11 ⁻	476.9284	45	Reference Spectra Match	69.0%

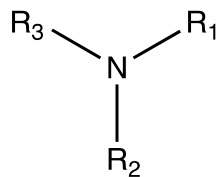
Appendix A4: PFAS Suspect Analyte Naming Rules

Carbon Chains:

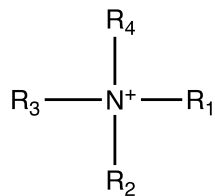
Me:	C ₁	Meth-
Et:	C ₂	Eth-
Pr:	C ₃	Prop-
B:	C ₄	But- (<i>Bu when terminal</i>)
Pe:	C ₅	Pent-
Hx:	C ₆	Hex-
Hp:	C ₇	Hept-
O:	C ₈	Oct-
N:	C ₉	Non-
D:	C ₁₀	Dec-
Ud:	C ₁₁	Undec-
Do:	C ₁₂	Dodec-
TrD:	C ₁₃	Tridec-
TeD:	C ₁₄	Tetradec-
PeD:	C ₁₅	Pentadec-
HxD:	C ₁₆	Hexadec-
HpD:	C ₁₇	Heptadec-
OD:	C ₁₈	Octadec-
Nd:	C ₁₉	Nonadec-

Substitution (R) Prefix:

	R ₁	
Di:	R ₂	Di-
T:	R ₃	Tri-
Te:	R ₄	Tetra-
Pe:	R ₅	Penta-
Hx:	R ₆	Hexa-
Hp:	R ₇	Hepta-
O:	R ₈	Octa-
N:	R ₉	Nona-
D:	R ₁₀	Deca-
Ud:	R ₁₁	Undeca-
Do:	R ₁₂	Dodeca-
TrD:	R ₁₃	Trideca-
TeD:	R ₁₄	Tetradeca-
PeD:	R ₁₅	Pentadeca-
HxD:	R ₁₆	Hexadeca-
HpD:	R ₁₇	Heptadeca-
OD:	R ₁₈	Octadeca-
Nd:	R ₁₉	Nonadeca-

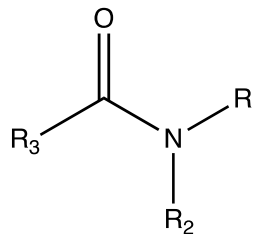


A (Amino)/An (Amine):
 Amino/Amine – unless terminal –
An; *A also used for "acid";*

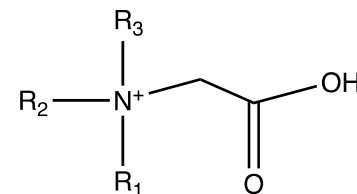


Am:
 Ammonio/Ammonium; assume dimethyl if no substituents mentioned (any unnamed substituents are Me)

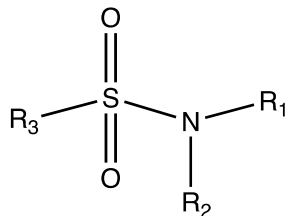
TAm:
 Trimethylammonio



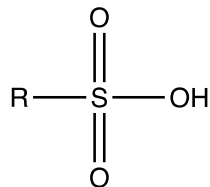
Ad:
 Amido/Amide;
 Ad Carbon is counted in chain-length



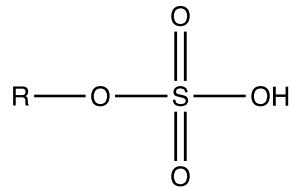
B:
 Betaine
 -- *used when terminal group*



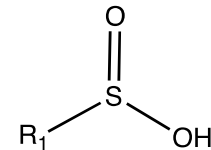
Sa or SA:
Sulfonamido/sulfonamide



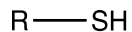
S:
Sulfonate/sulfo



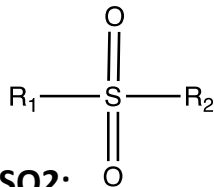
OS:
Sulfate



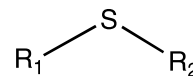
Si:
Sulfinate



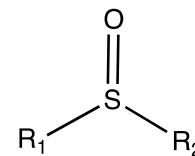
SH:
Thiol, except when S is
F-sub'd (pentaF-) → F5S



SO2:
Sulfonyl



Th:
Thia

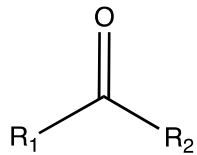
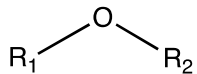


SO:
Sulfinyl

F5S:
Pentafluorosulfide

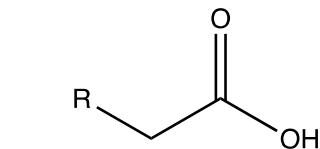
O:

Oxa-



K:

Keto-



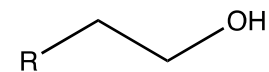
C (sub'd); A(end; acid)

Carboxy (substituent); -oic acid (end):

For **R=C₁**: carboxy ethyl (**CEt**); propanoic acid (**PrA**)

For **C₁**: Carboxy methyl (**CMe**) or Acetic Acid; **just A**

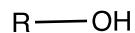
For fluorotelomer carboxylic acid → **FTCA**



EtOH:

Ethanol

(other chain numbers follow C chain nomenclature – MeOH; PrOH; HxOH)



OH:

Hydroxy



H:

Hydrido



Cl:

Chloro-

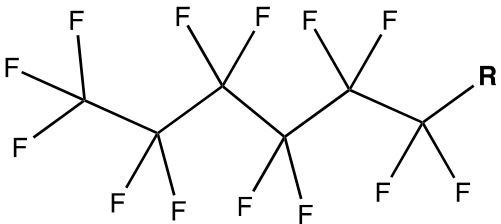
OCO:

Ester

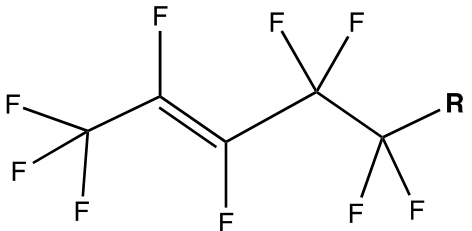
OCH:

Aldehyde

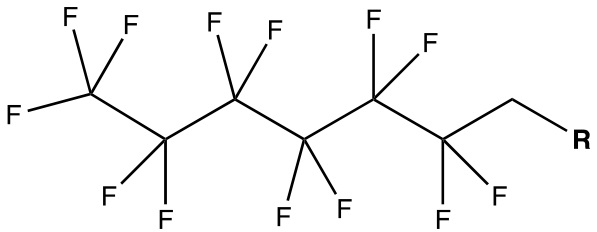
Handling Fluorinated Chains



F_n ; FHx
 Perfluorinated Carbon Chain,
 Length n ; Example: C_6 ; unless
 describes a PFOA, PFOS
 homolog, or sulfinate \rightarrow
PFHxS or **PFHxA**; **PFHxSi**



UF_n ; UFPe
 Unsaturated Perfluorinated
 Carbon Chain,
 Length n ; Example: C_5 ; unless
 describes a PFOA or PFOS
 homolog \rightarrow **UPFPeS** or **UPFPeA**
 Add C-chain number if know
 position, counting from R-end



$X:y F_n$; 6:1 FHx
 Perfluorinated and non-
 fluorinated carbon chain,
 Length n ; Example: C_6 ; unless
 describes a PFOA or PFOS
 homolog \rightarrow 6:1 **PFHxS** or 6:1
PFHxA

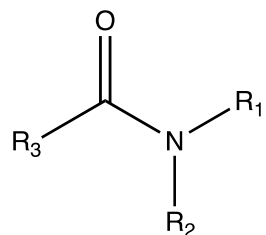
Cyclic: CHx

Exceptions/Notes

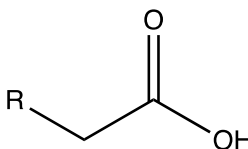
Dimethyl ammonio abbreviated as just Am: Assume methyl substitution unless otherwise stated. However, we will state when there's a terminal *trimethyl* ammonio, noted as TAm.

Dimethyl amino abbreviated as DiMeA; DiMeAn if terminal

Carboxylic acids and amides described by counting all carbons, but for carboxy- substituent don't account for surrounding carbons:

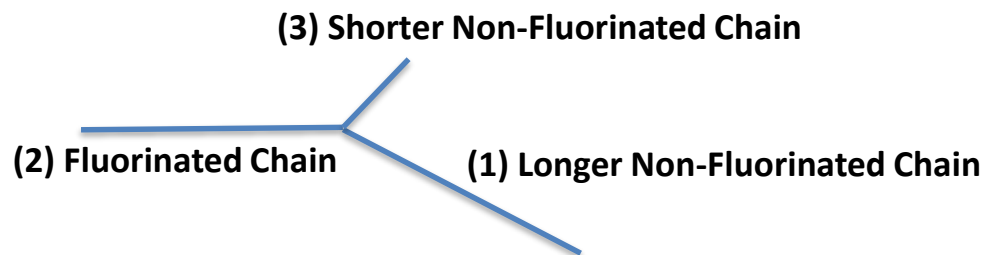


*If R₃ is C₂ chain,
propanamido*



*If R₃ is C₂ chain,
butanoic acid (terminal) or
carboxy propyl (CPr; non-
terminal)*

Naming Order

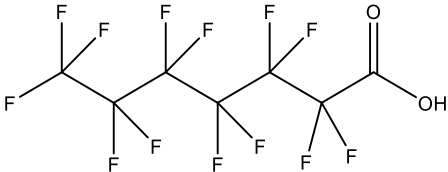
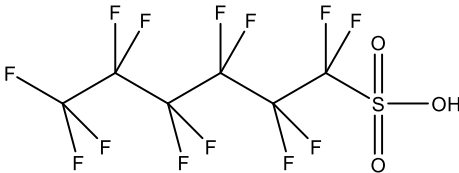
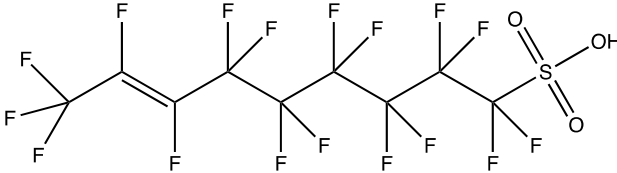
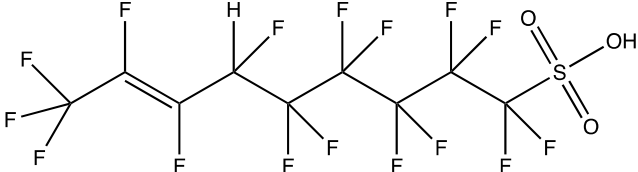


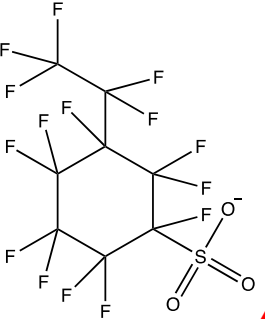
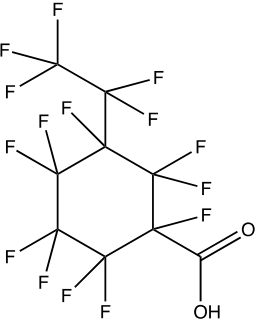
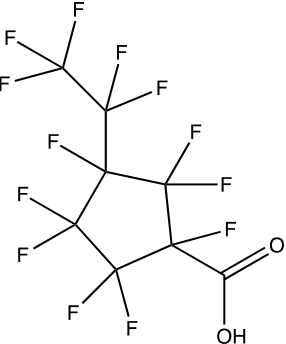
Generally 2-3 branches from central S or N functional group

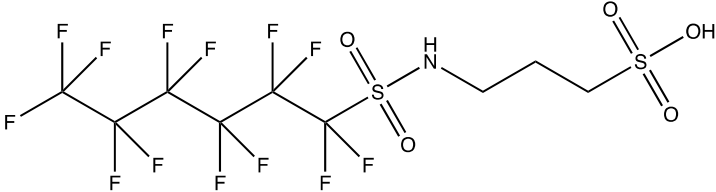
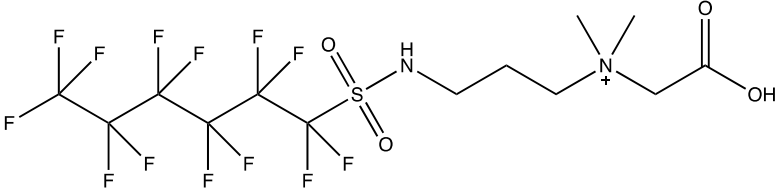
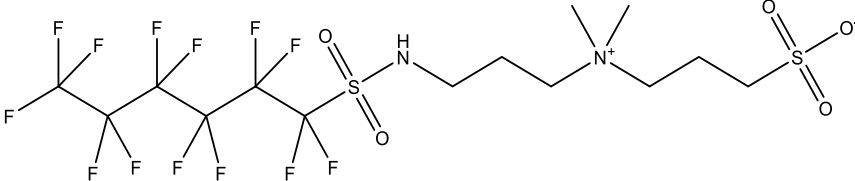
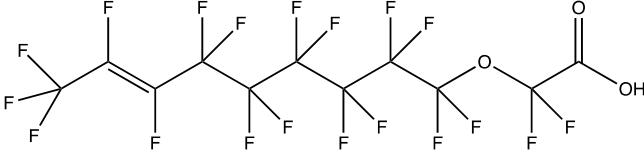
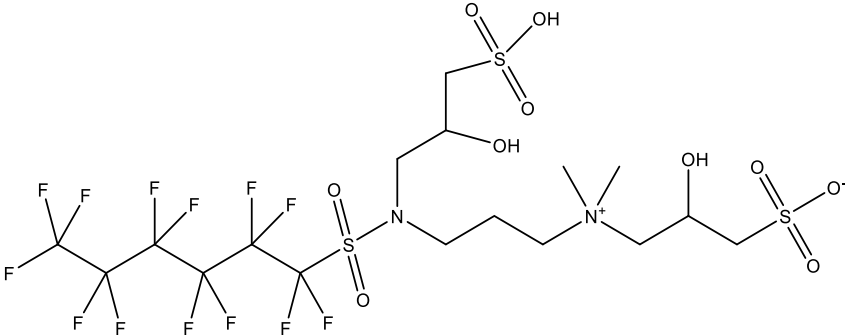
If fluorinated chain is:

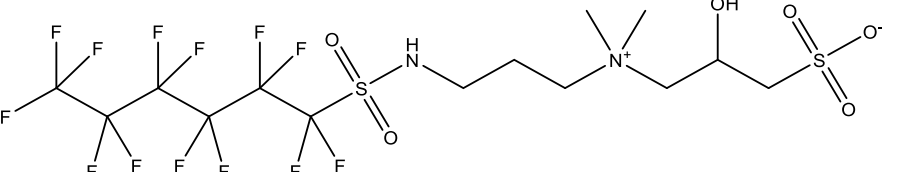
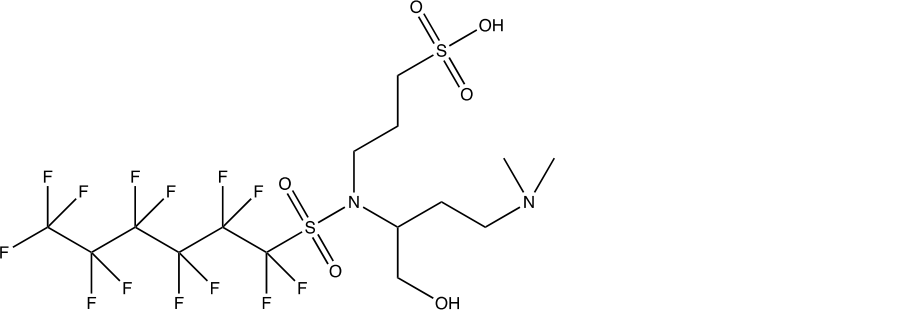
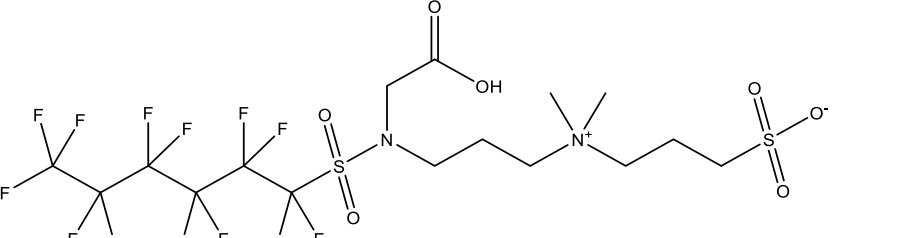
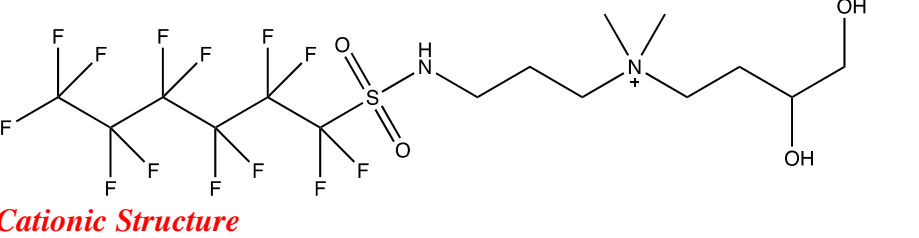
- Perfluorinated alkane with no non-fluorinated carbons: 1(out to in) → 2(out to in) → 3(in to out)
- Fluorotelomer chain (for example 6:2 FT): 2(out to in) → 1(in to out) → 3(in to out)
- Sulfonamido acetic acid (SAA) with (3) short alkyl chain: 3 → 2 → 1

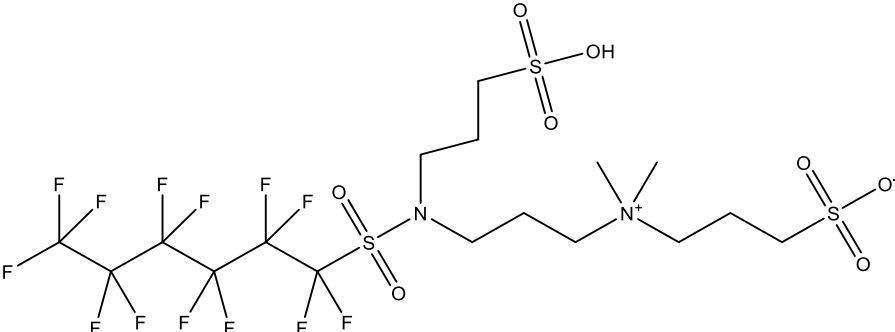
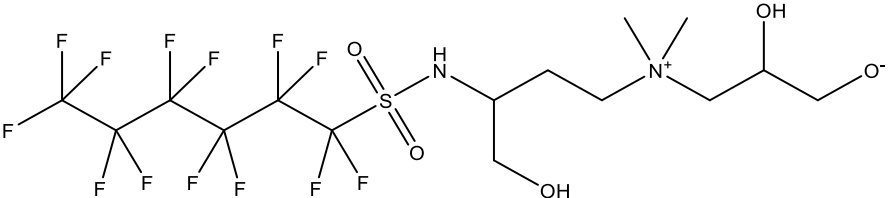
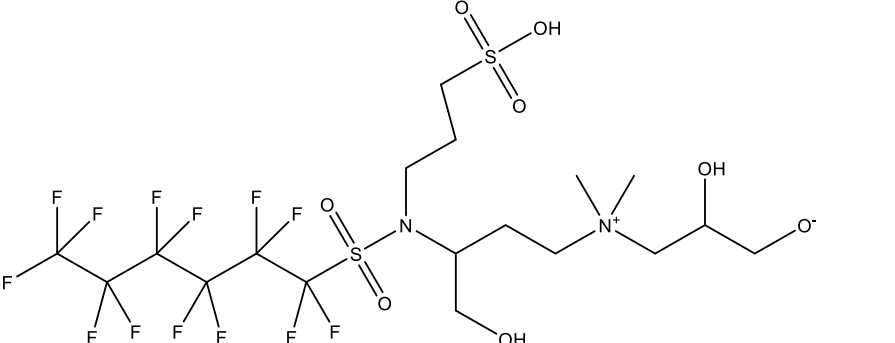
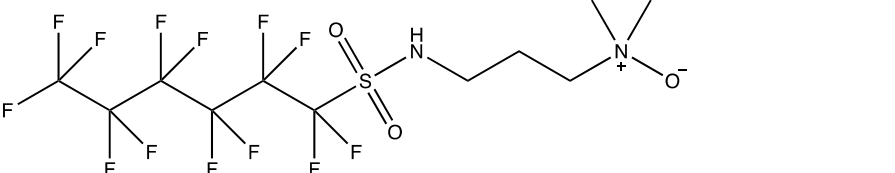
Appendix A5: PFAS Suspect Analyte Structures

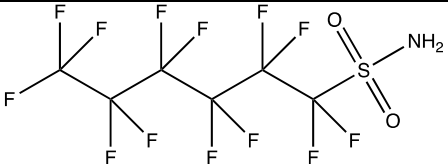
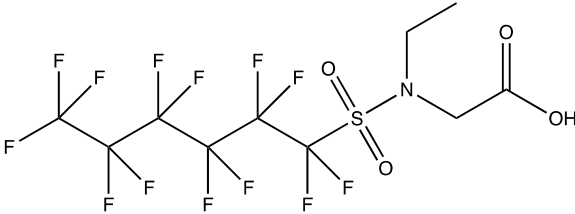
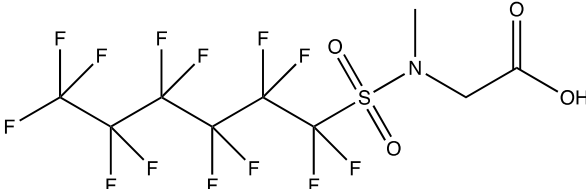
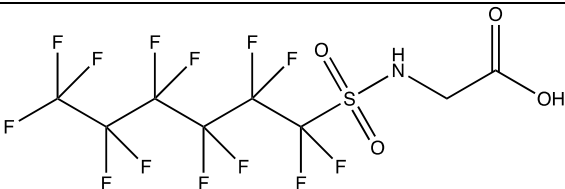
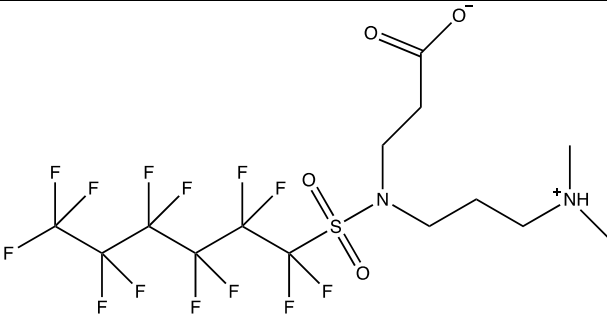
Name	Acronym; Formula; m/z	Structure
PFAAs		
Perfluoroheptanoic acid	PFHpA C7HO2F13 363.977	
Perfluorohexane sulfonate	PFHxS C6HO3SF13 399.944	
Cyclic and Unsaturated PFAAs		
Unsaturated perfluorononane sulfonate	UPFNS C9HO3SF17 511.938	
Hydrido-unsaturated perfluorononane sulfonate	H-UPFNS C9H2O3SF16 493.947	
perfluorohexane unsaturated ether/alcohol (-1F, +1H)	H-UPFHx-O/OH C6H2O2F10 279.995	No confirmed specific structure; Liu Table 1-4
perfluorohexane unsaturated chlorinated ether/alcohol (-1F, +1Cl)	Cl-PFHx-O/OH C6HOCIF10 313.956	No confirmed specific structure; Liu Table 1-5

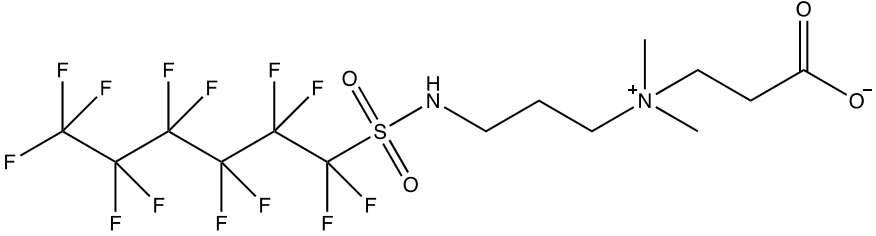
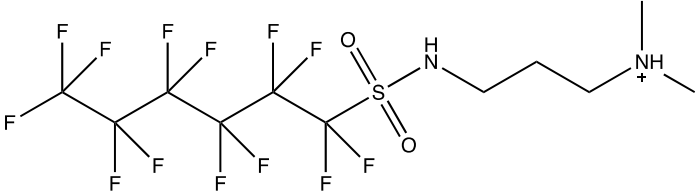
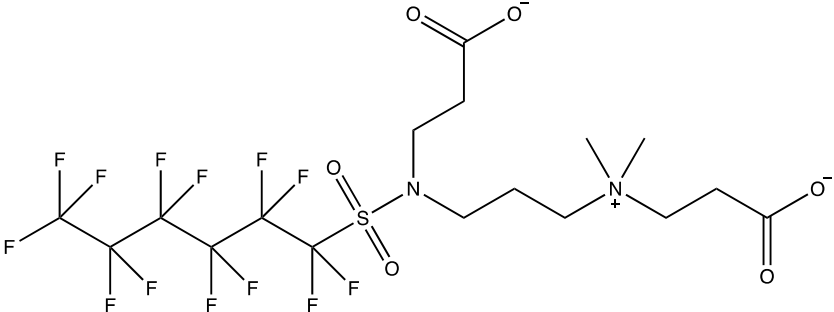
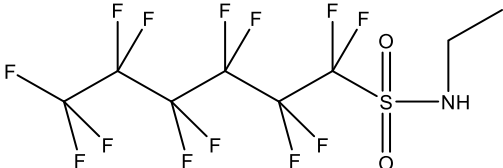
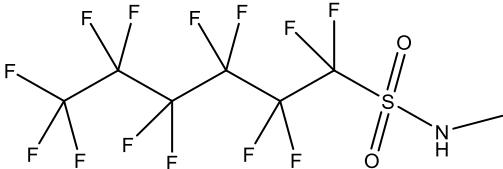
<p>perfluoro ethyl cyclohexane sulfonate</p>	<p>PFEtCH_xS C₈H₀SF₁₅ 461.941</p>	 <p><i>Anionic structure</i></p>
<p>perfluoro ethyl cyclohexane carboxylic acid</p>	<p>PFEtCH_xCA C₉H₀F₁₅ 425.974</p>	
<p>perfluoro ethyl cyclopentane carboxylic acid</p>	<p>PFEtCPeCA C₈H₀F₁₃ 375.977</p>	

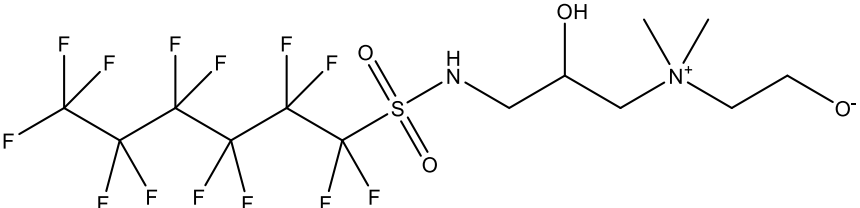
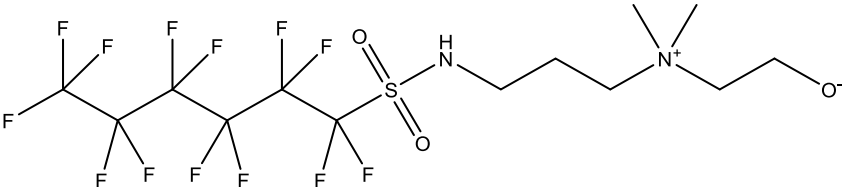
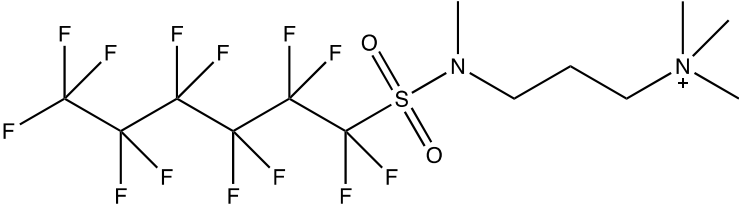
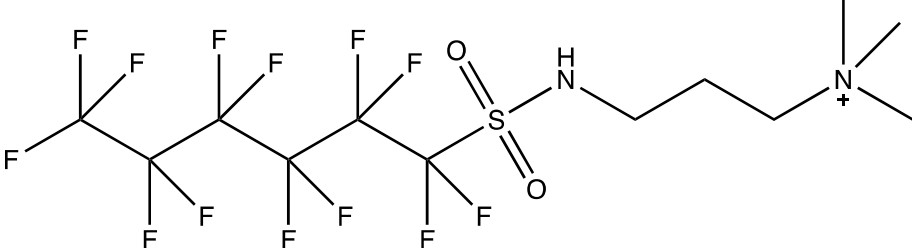
Sulfonamide Precursors		
N-sulfo propyl perfluorohexane sulfonamide	SPr-FHxSA C₉H₈O₅S₂NF₁₃ 520.964	
N-carboxy methyl dimethyl ammonio propyl-perfluorohexane sulfonamide	CMeAmPr-FHxSA C₁₃H₁₅O₄SN₂F₁₃ 542.055	 <i>Cationic structure</i>
N-sulfo propyl dimethyl ammonio propyl perfluorohexane sulfonamide	SPrAmPr-FHxSA C₁₄H₁₉O₅S₂N₂F₁₃ 606.053	
Oxa-unsaturated-perfluorododecanoic acid	O-U-PFDoA C₁₁H₀3F₁₉ 541.963	
N-sulfo hydroxy propyl dimethyl ammonio propyl perfluorohexane sulfonamido hydroxy propyl sulfonate	S-OHPrAmPr-FHxSA-OHPrS C₁₇H₂₅O₁₀S₃N₂F₁₃ 760.047	

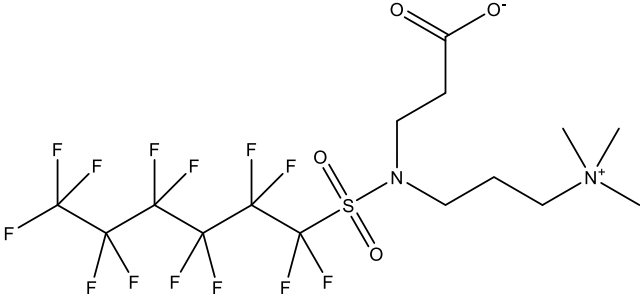
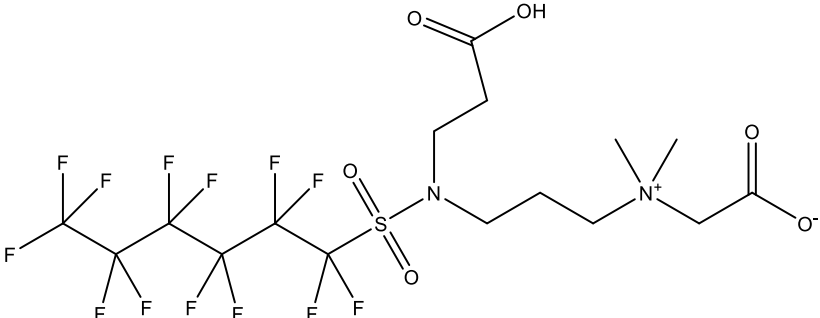
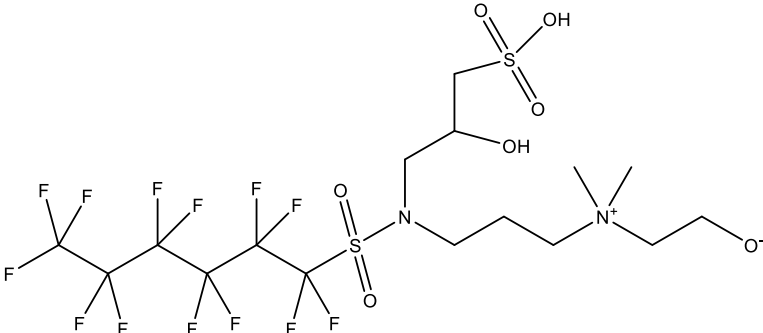
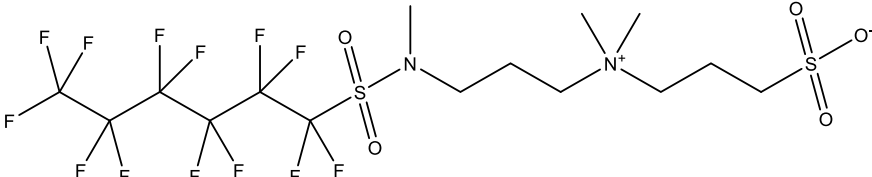
<p>N-sulfo hydroxypropyl dimethyl ammonio propyl perfluorohexane sulfonamide</p>	<p>S-OHPrAmPr-FHxSA C14H19O6S2N2F13 622.048</p>	
<p>N-dimethyl amino hydroxymethyl propyl-perfluorohexane sulfonamido propyl sulfonate</p>	<p>DiMeA-MeOHPr-FHxSAPrS C15H21O6S2N2F13 636.063895</p> <p><i>Isomeric class:</i> SPr-EtOHAm-Pr-FHxSA</p>	
<p>N-sulfo propyl dimethyl ammonio propyl-perfluorohexane sulfonamido acetic acid</p>	<p>SPrAmPr-FHxSAA C16H21O7S2N2F13 664.059</p>	
<p>N-dihydroxybutyl dimethyl ammonio propyl perfluorohexane sulfonamide</p>	<p>diOHBAmpPr-FHxSA C15H21O4SN2F13 572.102</p> <p><i>Isomeric Class:</i> EtOH-AmPr-FHxSA-EtOH</p>	<p><i>Cationic Structure</i></p> 

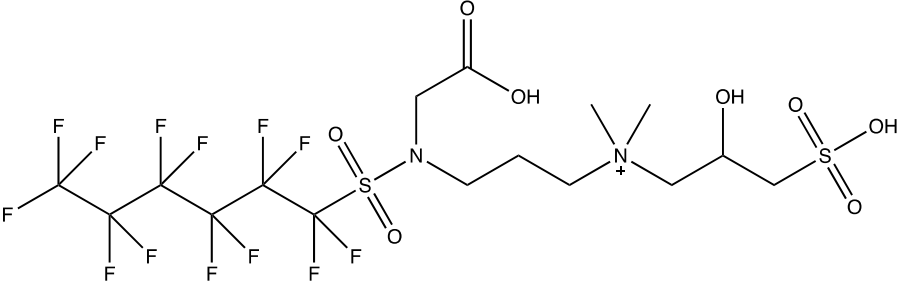
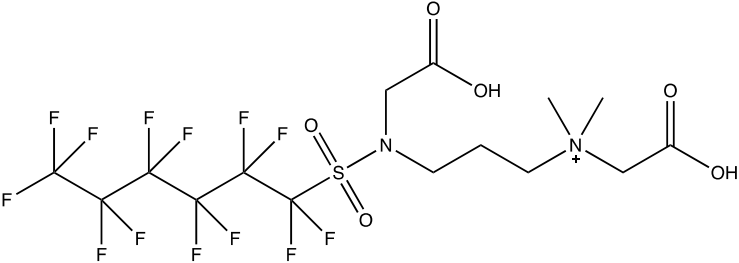
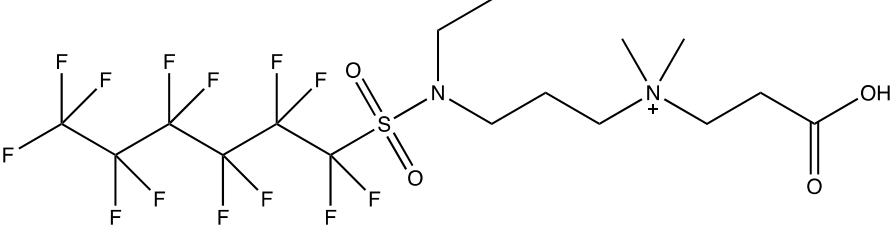
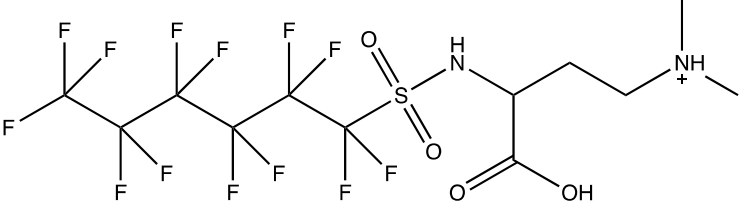
<p>N-sulfo propyl dimethyl ammonio propyl perfluorohexane sulfonamido propyl sulfonate</p>	<p>SPrAmPr-FHxSAPrS C17H25O8S3N2F13 728.057</p>	
<p>N-dihydroxy propyl dimethyl ammonio hydroxymethyl propyl perfluorohexane sulfonamide</p>	<p>diOHPrAm-MeOHPr-FHxSA C15H21O5SN2F13 588.097</p>	
<p>N-dihydroxy propyl dimethyl ammonio hydroxymethylpropyl-perfluorohexane sulfonamido propyl Sulfonate</p>	<p>diOHPrAm-MeOHPr-FHxSAPrS C18H27O8S2N2F13 710.101</p>	
<p>N-oxidedimethyl ammonio propyl-perfluorohexane sulfonamide</p>	<p>OAmPr-FHxSA C11H13O3SN2F13 500.044</p>	

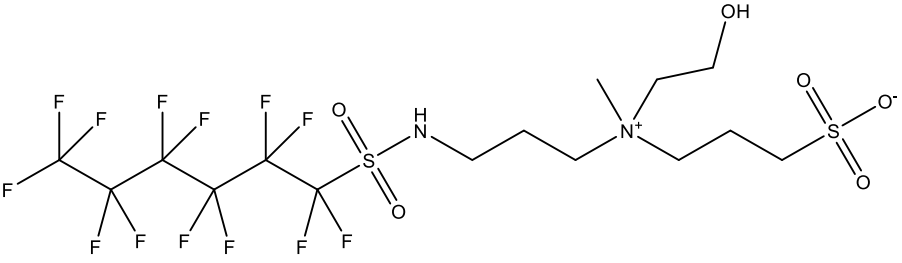
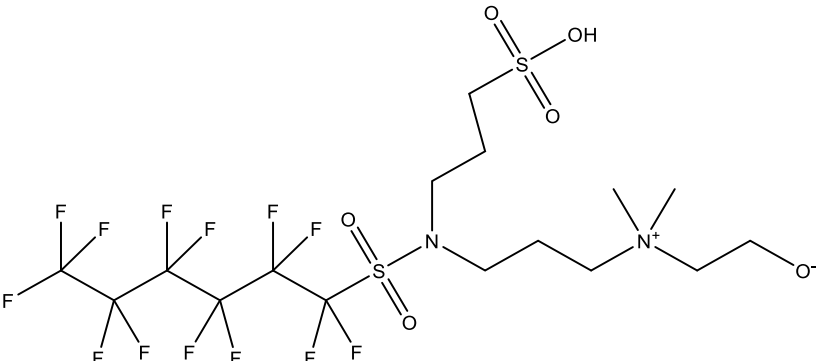
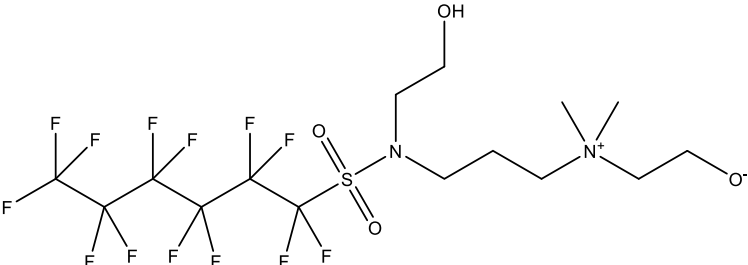
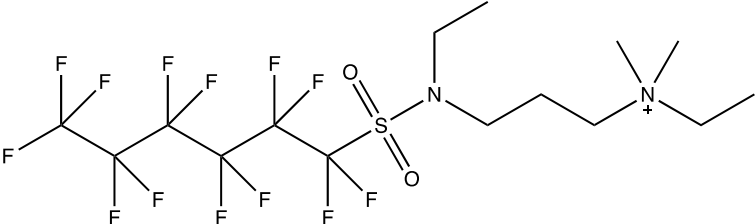
Perfluorohexane sulfonamide	FHxSA C6H2O2SNF13 398.960	
N-ethyl perfluorohexane sulfonamido acetic acid	EtFHxSAA C10H8O4SNF13 484.997	
N-methyl perfluorohexane sulfonamido acetic acid	MeFHxSAA C9H6O4SNF13 470.982	
perfluorohexane sulfonamido acetic acid	FHxSAA C8H4O4SNF13 456.9656	
N-dimethyl ammonio propyl perfluorohexane sulfonamide propanoic acid	AmPr-FHxSA-PrA C14H17O4SN2F13 556.071 <i>Isomeric Class:</i> CEtAmPr-FHxSA; 6:2 FTSA-Pr-MeAA	 Cationic Structure

<p>N-carboxy ethyl dimethyl ammonio propyl perfluorohexane sulfonamide</p>	<p>CEtAmPr-FHxSA C14H17O4SN2F13 556.071</p> <p><i>Isomeric Class:</i> AmPr-FHxSA-PrA; 6:2 FTSA-Pr-MeAA</p>	
<p>N-dimethyl ammonio propyl perfluorohexane sulfonamide</p>	<p>AmPr-FHxSA C11H13O2SN2F13 484.045</p> <p><i>Isomeric Class:</i> 6:2 FTSA-PrAn</p>	 <p>Cationic structure</p>
<p>N-carboxy ethyl dimethyl ammonio propyl perfluorohexane sulfonamido propanoic acid</p>	<p>CEtAmPr-FHxSA-PrA C17H21O6SN2F13 628.091825</p>	 <p>Anionic Structure</p>
<p>N-ethylperfluoro-1-hexane sulfonamide</p>	<p>EtFHxSA C8H6O2NSF13 426.992</p>	
<p>N-methyl perfluoro-1-hexane sulfonamide</p>	<p>MeFHxSA C7H4O2NSF13 412.9760</p>	

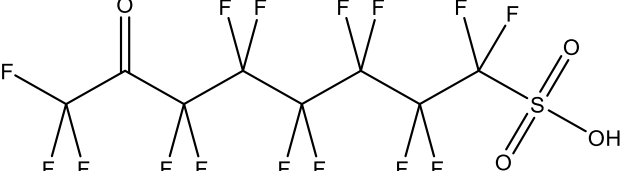
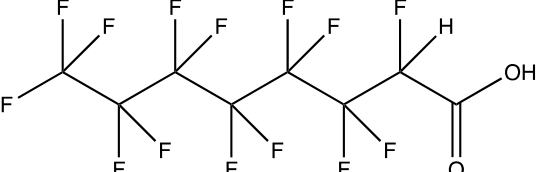
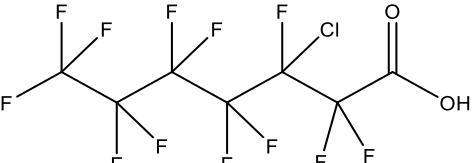
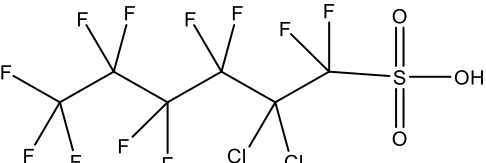
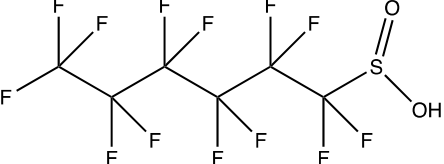
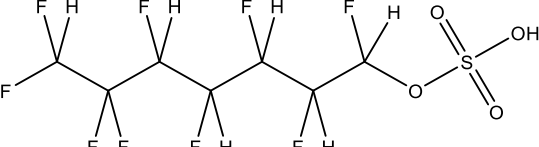
<p>N-hydroxyethyl dimethyl ammonio hydroxy propyl perfluorohexane sulfonamide</p>	<p>EtOH-Am-OHPr-FHxSA C13H17O4SN2F13 544.071</p>	
<p>N-hydroxyethyl dimethyl ammonio propyl perfluorohexane sulfonamide</p>	<p>EtOH-AmPr-FHxSA C13H17O3SN2F13 528.076</p>	
<p>N-trimethyl ammonio propyl N-methyl perfluorohexane sulfonamide</p>	<p>TAmPr-N-MeFHxSA C13H17O2SN2F13 512.081</p> <p><i>Isomeric Class:</i> 6:2 FTSAPr-DiMeAn</p>	 <p><i>Cationic structure</i></p>
<p>N-trimethyl ammonio propyl perfluorohexane sulfonamide</p>	<p>TAmPr-FHxSA C12H15O2SN2F13 498.065</p>	 <p><i>Cationic structure</i></p>

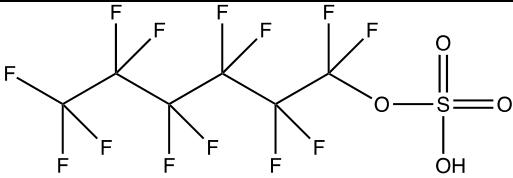
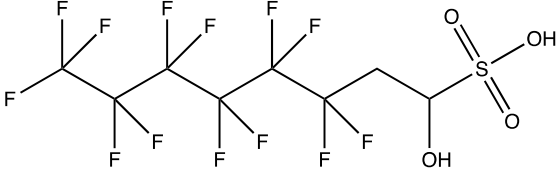
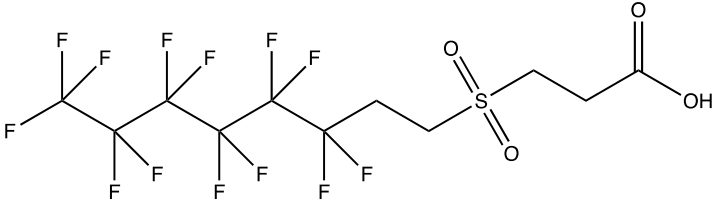
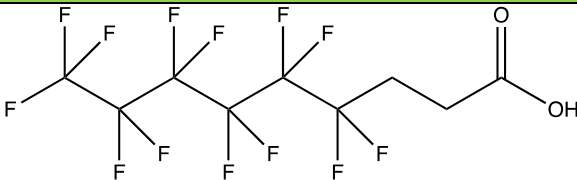
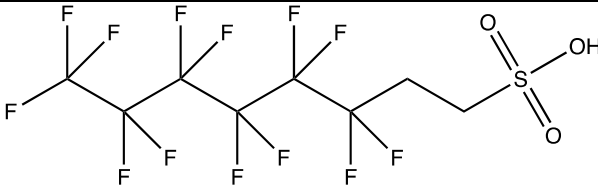
<p>N-trimethyl ammonio propyl perfluorohexyl sulfonamido propanoic acid</p>	<p>TAmPr-FHxSAPrA C15H19O4SN2F13 570.086</p>	
<p>N-carboxy methyl dimethyl ammonio propyl-perfluorohexyl sulfonamido propanoic acid</p>	<p>CMeAmPr- FHxSAPrA C16H19O6SN2F13 614.076</p>	
<p>N-hydroxyethyl dimethyl ammonio propyl perfluorohexane sulfonamido hydroxy propyl sulfonate</p>	<p>EtOH-AmPr-FHxSA- OHPrS C16H23O7S2N2F13 666.074</p>	
<p>N-sulfo propyl dimethyl ammonio propyl N-methyl perfluorohexane sulfonamide</p>	<p>SPrAmPr-N-Me- FHxSA C15H21O5S2N2F13 620.069</p>	

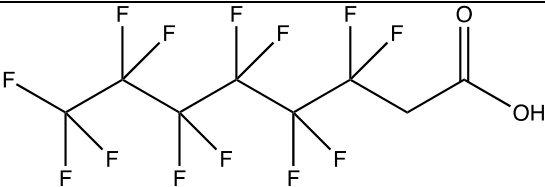
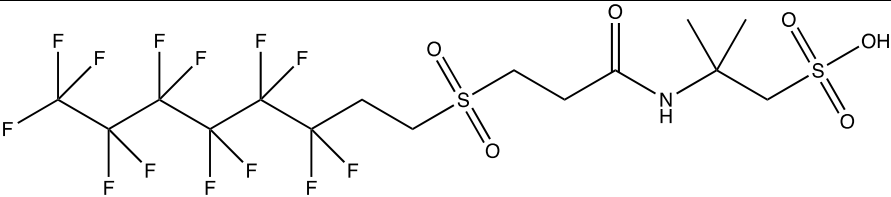
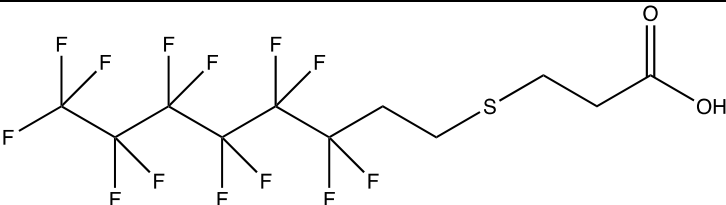
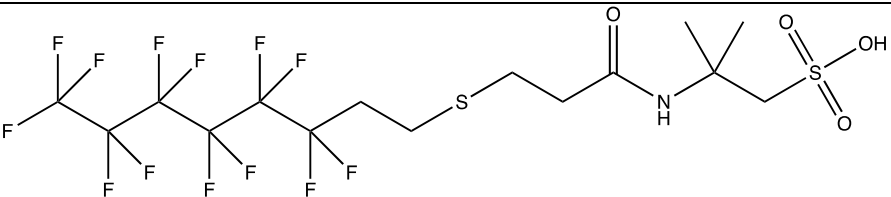
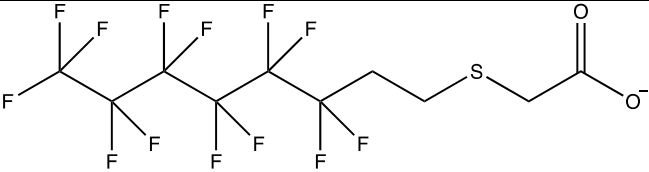
<p>N-sulfohydroxy propyl dimethyl ammonio propyl perfluorohexane sulfonamido acetic acid</p>	<p>S-OHPrAmPr- FHxSAA C₁₆H₂₁O₈S₂N₂F₁₃ 680.054</p>	 <p><i>Cationic structure</i></p>
<p>N-carboxy methyl dimethyl ammonio propyl- perfluorohexane sulfonamido acetic acid</p>	<p>CMeAmPr-FHxSAA C₁₅H₁₇O₆S₂N₂F₁₃ 600.060</p>	 <p><i>Cationic structure</i></p>
<p>N-carboxy ethyl dimethyl ammonio propyl-N-ethyl perfluorohexane sulfonamide</p>	<p>CEtAmPr-N-EtFHxSA C₁₆H₂₁O₄S₂N₂F₁₃ 584.102</p>	 <p><i>Cationic structure</i></p>
<p>N-dimethyl ammonio carboxy propyl- perfluorohexane sulfonamide</p>	<p>Am-CPr-FHxSA C₁₂H₁₃O₄S₂N₂F₁₃ 528.039</p>	 <p><i>Cationic structure</i></p>

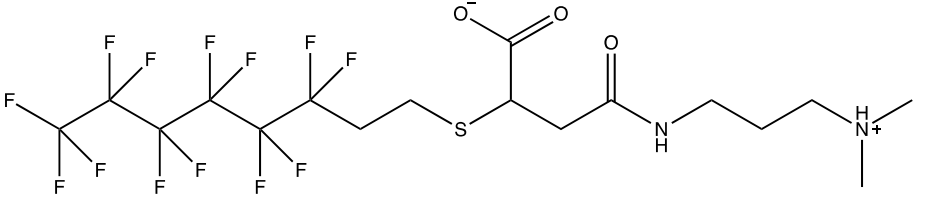
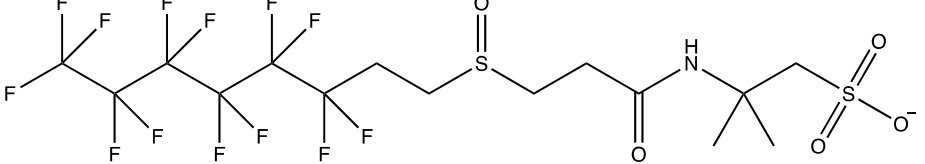
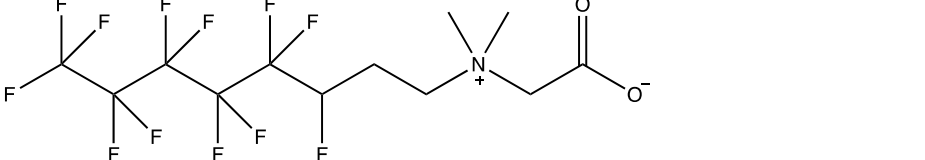
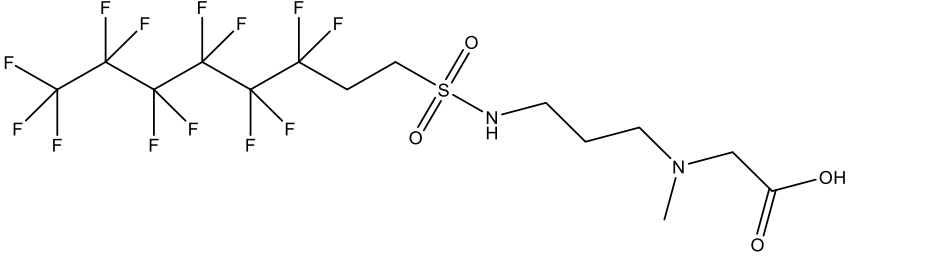
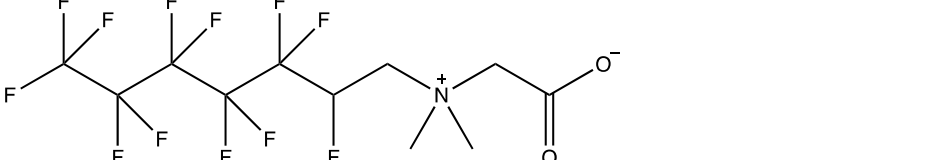
<p>N-sulfo propyl (hydroxyethyl methyl ammonio propyl perfluorohexane sulfonamide</p>	<p>SPr-EtOHAm-Pr-FHxSA C₁₅H₂₁O₆S₂N₂F₁₃ 636.064</p> <p><i>Isomeric Class:</i> DiMeA-MeOHPr-FHxSAPrS</p>	
<p>N-hydroxyethyl dimethyl ammonio propyl perfluorohexane sulfonamido propyl sulfonate</p>	<p>EtOH-AmPr-FHxSAPrS C₁₆H₂₃O₆S₂N₂F₁₃ 650.080</p>	
<p>N-hydroxyethyl dimethyl ammonio propyl perfluorohexane sulfonamido ethanol</p>	<p>EtOH-AmPr-FHxSA-EtOH C₁₅H₂₁O₄SN₂F₁₃ 572.102</p> <p><i>Isomeric Class:</i> diOHBAmPr-FHxSA</p>	
<p>N-ethyl dimethyl ammonio propyl perfluorohexane N-ethyl sulfonamide</p>	<p>EtAmPr-FHx-N-EtSA C₁₅H₂₁O₂SN₂F₁₃ 540.112</p> <p><i>Isomeric Class:</i> Barzen-Hanson Class 38</p>	 <p><i>Cationic Structure</i></p>

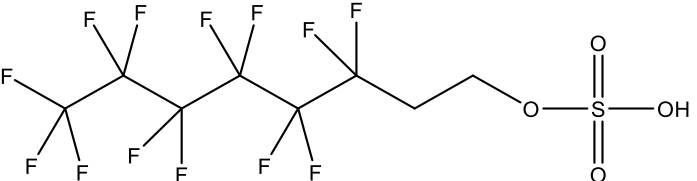
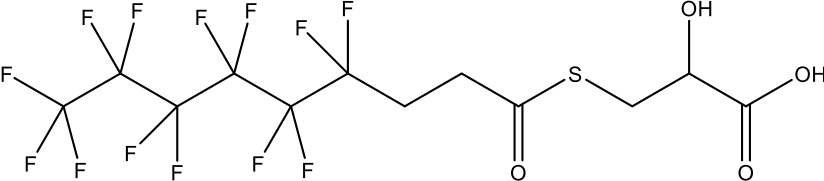
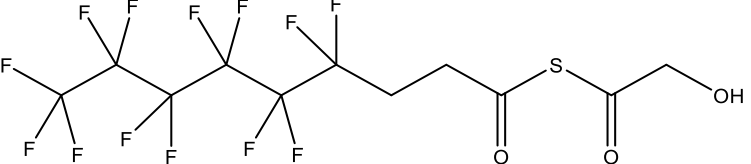
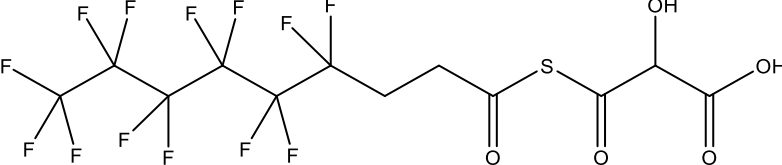
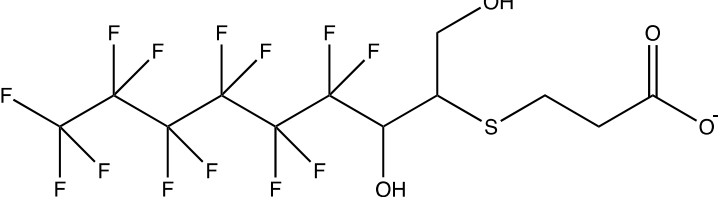
<i>Substituted PFAA Derivatives</i>		
Pentafluorosulfide-perfluorohexane sulfonate	F5S-PFH_xS C₆H₀S₂F₁₇ 507.910	
Pentafluorosulfide-perfluoroheptanoic acid	F5S-PFH_pA C₇H₀SF₁₇ 471.943	
Hydrido-perfluorooctane sulfonate	H-PFOS C₈H₂O₃SF₁₆ 481.947	
6:1 perfluoroheptane sulfonate	6:1 PFH_pS C₇H₃O₃SF₁₃ 413.960	
Chloro-perfluoroheptane sulfonate	Cl-PFH_pS C₇H₀S₃ClF₁₄ 465.912	
Oxa-perfluorooctane sulfonate	O-PFOS C₇H₀SF₁₅ 465.936	

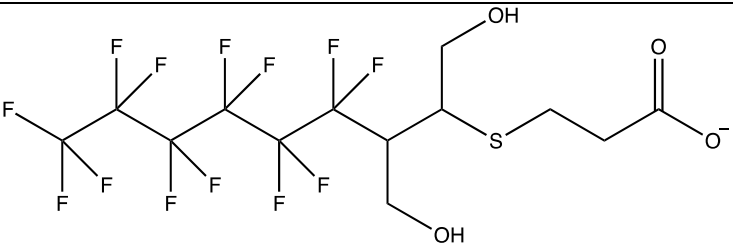
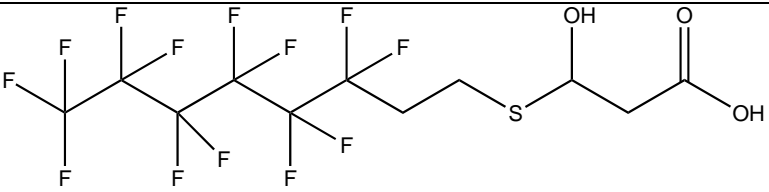
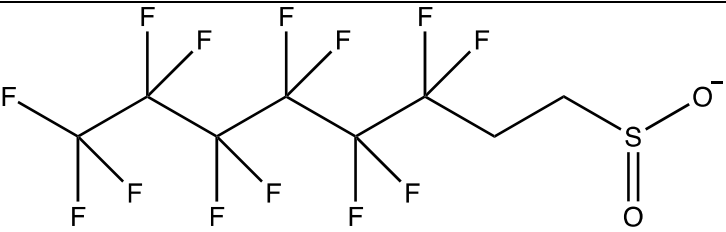
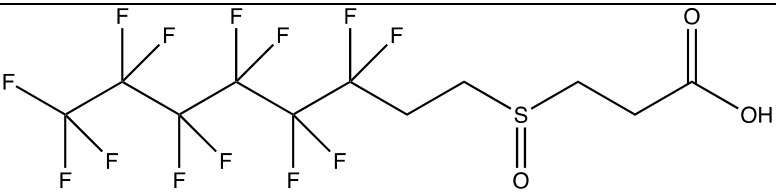
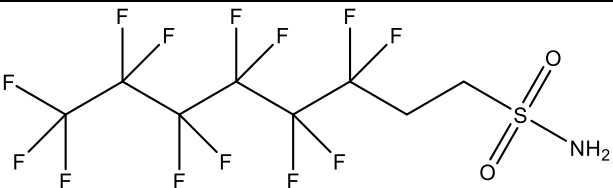
Keto-perfluorooctane sulfonate	K-PFOS C₈H₀O₄SF₁₅ 477.936	
Hydrido-perfluorooctanoic acid	H-PFOA C₈H₂O₂F₁₄ 395.984	
Chloro-perfluoroheptanoic acid	Cl-PFHpA C₇H₀ClF₁₂ 379.948	
Dichlorinated perfluorohexyl sulfonate	DiCl-PFHxS C₆H₀O₃SCl₂F₁₁ 431.885	
<i>PFSA Derivatives</i>		
Perfluorohexane sulfinic acid	PFH₆Si C₆H₀O₂SF₁₃ 383.9450	
Pentahydrido-fluoroheptane sulfate	PeH-FHpOS C₇H₆O₄SF₁₀ 375.983	

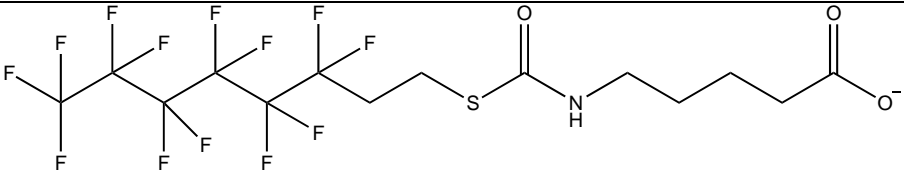
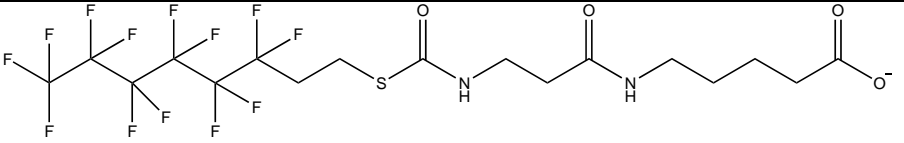
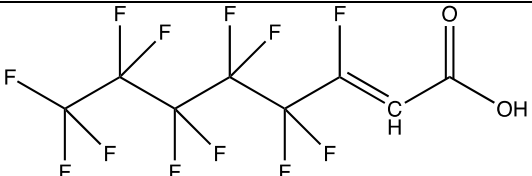
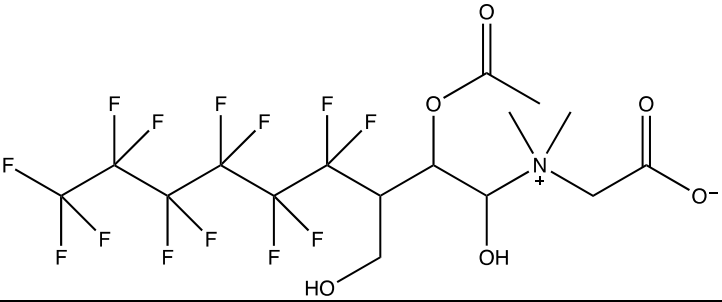
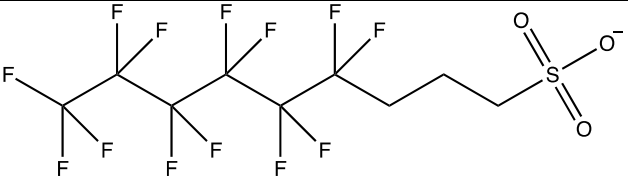
Perfluorohexane sulfate	PFHx-OS C6H04SF13 415.939	
Fluorotelomer Sulfonates/Sulfates		
1-hydroxy-6:2 fluorotelomer sulfonate	1OH-6:2 FTS C8H5O4SF13 443.971 <i>Isomeric Class:</i> 6:2 FTOS	
6:2 fluorotelomer sulfonyl propanoic acid	6:2 FTSO2PrA C11H9O4SF13 484.002	
FTSs and FTAs		
6:3 fluorotelomer carboxylic acid	6:3 FTCA C9H5O2F13 392.009	
6:2 fluorotelomer sulfonate	6:2 FTS C8H5O3SF13 427.976	

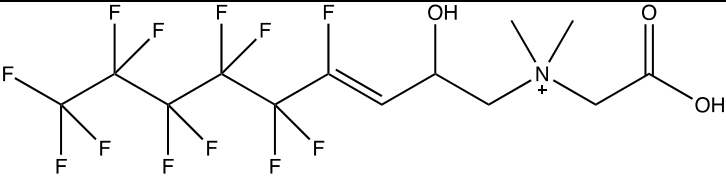
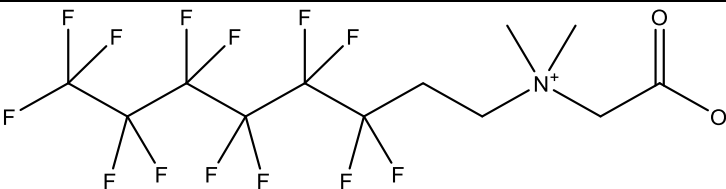
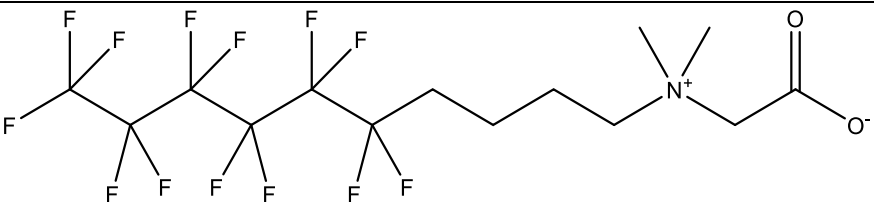
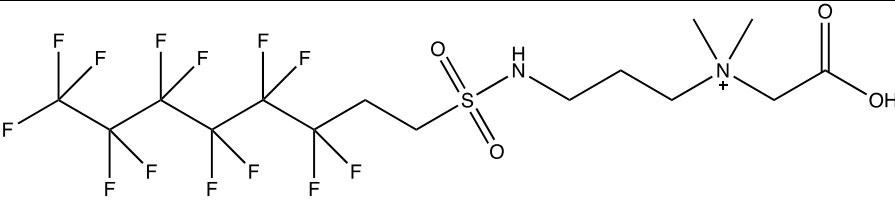
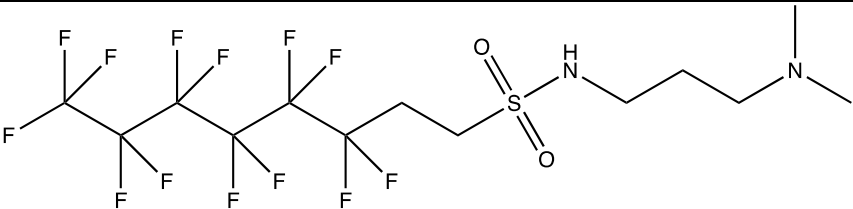
6:2 fluorotelomer carboxylic acid	6:2 FTCA C₈H₃O₂F₁₃ 377.993	
FTS and FTA Derivatives		
6:2 fluorotelomer sulfonyl propano amido-dimethyl ethyl sulfonate	6:2 FTSO₂PrAd-DiMeEtS C₁₅H₁₈O₆S₂NF₁₃ 619.037	
6:2 fluorotelomer thia propanoic acid	6:2 FTThPrA C₁₁H₉O₂SF₁₃ 452.012	
6:2 fluorotelomer thia propanoamido dimethyl ethyl sulfonate	6:2 FTTh-PrAd-DiMeEtS C₁₅H₁₈O₄S₂NF₁₃ 587.048	
6:2 fluorotelomer thia acetic acid	6:2 FTThA C₁₀H₇O₂SF₁₃ 437.996	 <p style="color: red; font-weight: bold; margin-top: 5px;">Anionic structure</p>

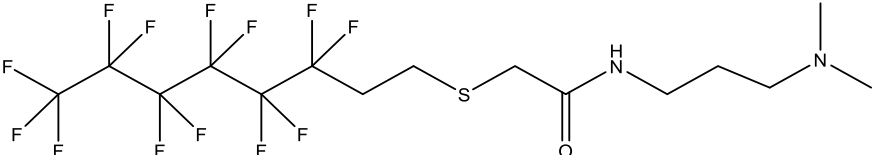
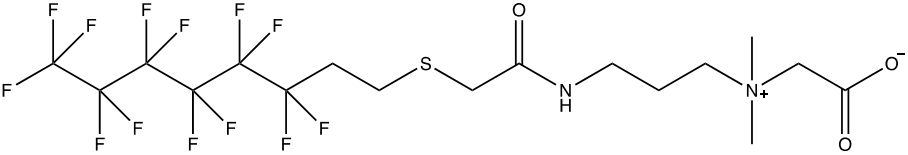
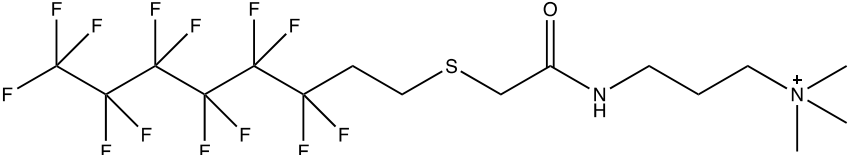
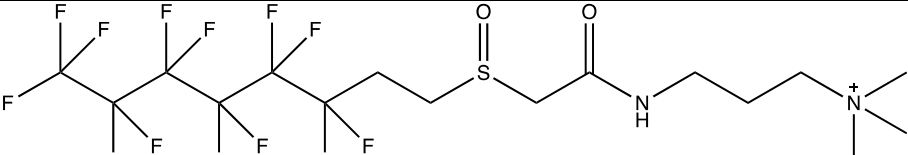
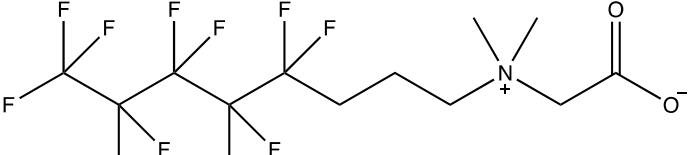
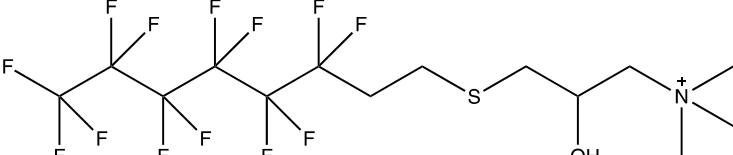
<p>6:2 fluorotelomer thia carboxy propanoamido propyl dimethyl ammonium</p>	<p>6:2 FTTh-CPrAd-PrAm C17H21O3SN2F13 580.107</p> <p><i>Isomeric Class:</i> 6:2 FTTh-EtAdPrB</p>	
<p>6:2 fluorotelomer sulfinyl propano amido dimethyl ethyl sulfonate</p>	<p>6:2 FTSO-PrAd-DiMePrS C15H18O5S2NF13 603.042</p>	 <p><i>Anionic structure</i></p>
<p>6:2 hydrido-fluorotelomer betaine</p>	<p>6:2 H-FTB C12H13O2NF12 431.076</p>	
<p>6:2 fluorotelomer sulfonamido propyl methyl amino acetic acid</p>	<p>6:2 FTSA-Pr-MeAA C14H17O4SN2F13 556.071</p> <p><i>Isomeric Class:</i> CEtAmPr-FHxSA; AmPr-FHxSA-PrA</p>	
<p>6:1 hydrido-fluorotelomer betaine</p>	<p>6:1 H-FTB C11H11O2NF12 417.060</p>	
<p>6:2 fluorotelomer ketone sulfonate*</p>	<p>6:2 FTKS C9H5O4SF13 455.971</p>	<p>Wellington – Tentative ID; structure not certain</p>

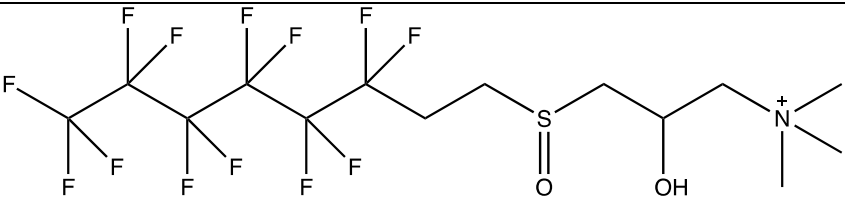
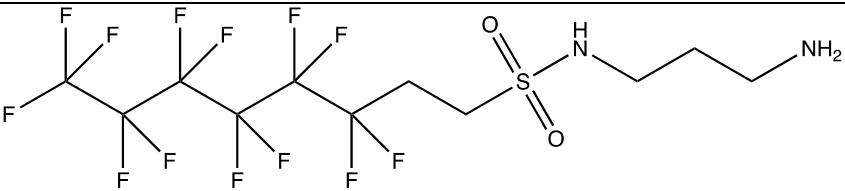
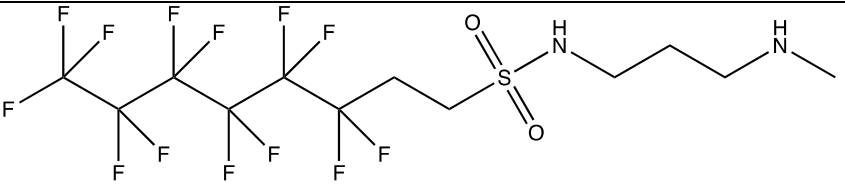
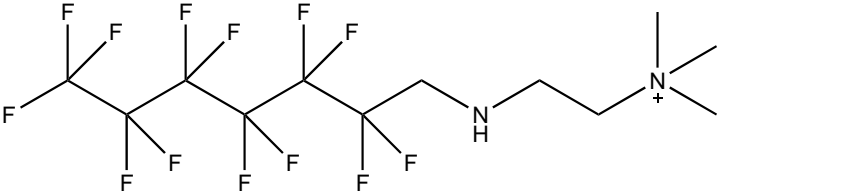
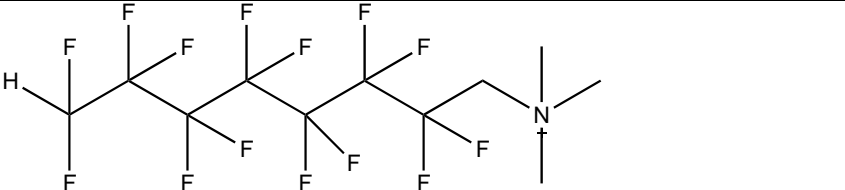
6:2 fluorotelomer sulfate	6:2 FTOS C₈H₅O₄SF₁₃ 443.971	
6:3 keto-fluorotelomer thia 2-hydroxy propanoic acid	6:3 K-FTTh-OH-PrA C₁₂H₉O₄SF₁₃ 496.002	
6:3 keto-fluorotelomer thia keto-ethanol	6:3 K-FTTh-K-EtOH C₁₁H₇O₃SF₁₃ 465.991	
6:3 keto-fluorotelomer thia keto 2-hydroxy propanoic acid	6:3 K-FTTh-K-OH-PrA C₁₂H₇O₅SF₁₃ 509.981	
6:2 1-hydroxy 2-hydroxymethyl fluorotelomer thia propanoic acid	6:2 OH-MeOH-FTTh-PrA C₁₂H₁₁O₄SF₁₃ 498.018	 <p><i>anionic structure</i></p>

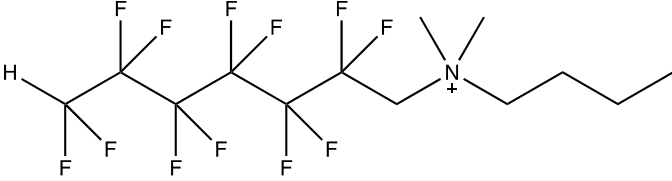
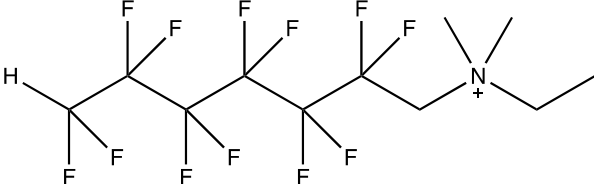
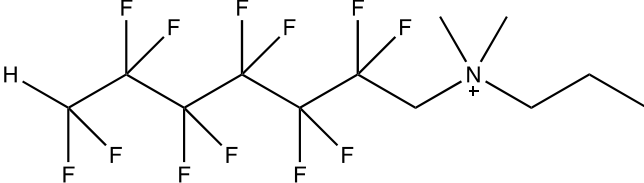
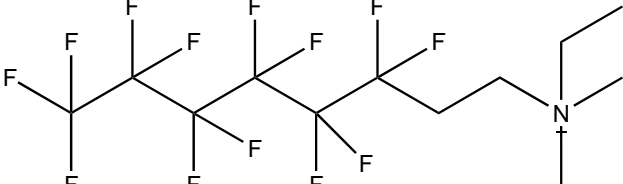
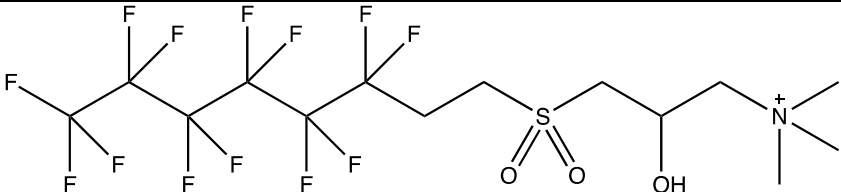
<p>6:2 1,2-di(hydroxymethyl) fluorotelomer thia propanoic acid</p>	<p>6:2 di(MeOH)-FTTh-PrA C13H13O4SF13 512.033</p>	 <p><i>anionic structure</i></p>
<p>6:2 fluorotelomer thia hydroxy propanoic acid</p>	<p>6:2 FTTh-OHPrA C11H9O3SF13 468.007</p> <p><i>Isomeric Class:</i> 6:2 FTSO-PrA</p>	
<p>6:2 fluorotelomer sulfinate</p>	<p>6:2 FTSi C8H5O2SF13 411.981</p>	 <p><i>Anionic structure</i></p>
<p>6:2 fluorotelomer sulfinyl propanoic acid</p>	<p>6:2 FTSO-PrA C11H9O3SF13 468.007</p> <p><i>Isomeric Class:</i> 6:2 FTTh-OHPrA</p>	
<p>6:2 fluorotelomer sulfonamide</p>	<p>6:2 FTSA C8H6O2SNF13 426.992</p>	

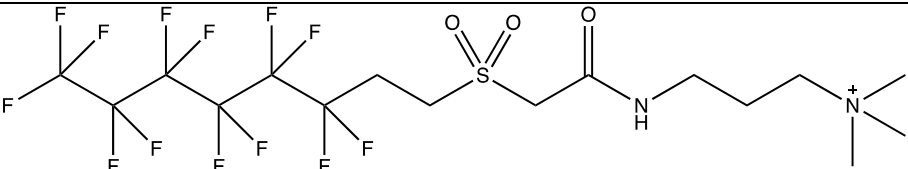
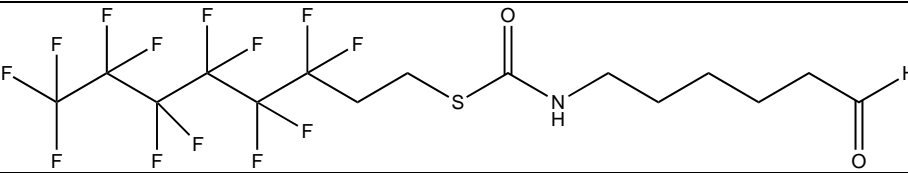
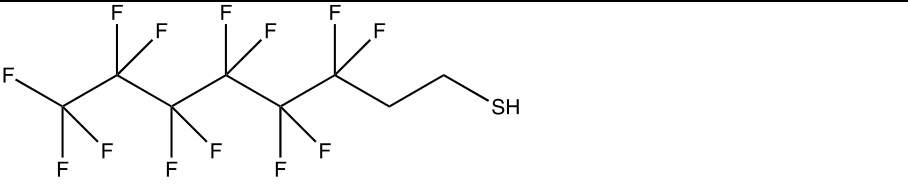
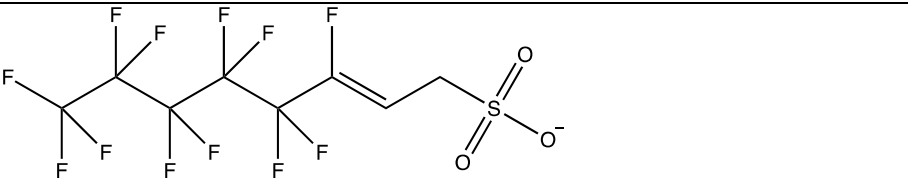
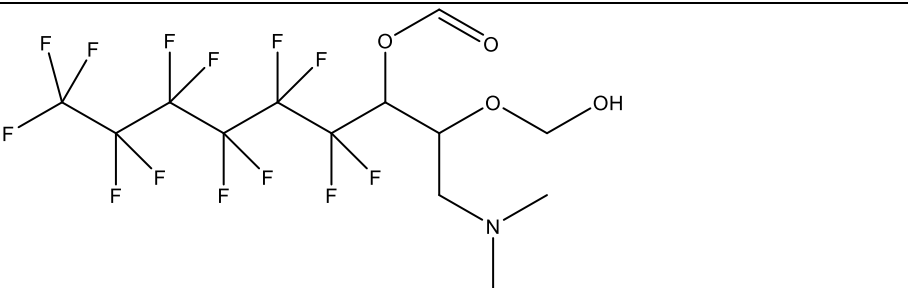
6:2 fluorotelomer thia amido pentanoic acid	6:2 FTTh-AdPeA C14H14O3SNF13 523.049	 <p><i>Anionic Structure</i></p>
6:2 fluorotelomer thia amido propano amido pentanoic acid	6:2 FTTh-AdPrAdPeA C17H19O4SN2F13 594.086	 <p><i>Anionic Structure</i></p>
6:2 unsaturated fluorotelomer carboxylic acid	6:2 UFTCA C8H2O2F12 357.987	
6:3 fluorotelomer 1-methanol, 2-methylester, 3-hydroxy betaine	6:3 MeOH-MeOCO-OH-FTB C16H18O6NF13 567.093	
6:3 fluorotelomer sulfonate	6:3 FTS C9H7O3SF13 441.991	 <p><i>Anionic Structure</i></p>

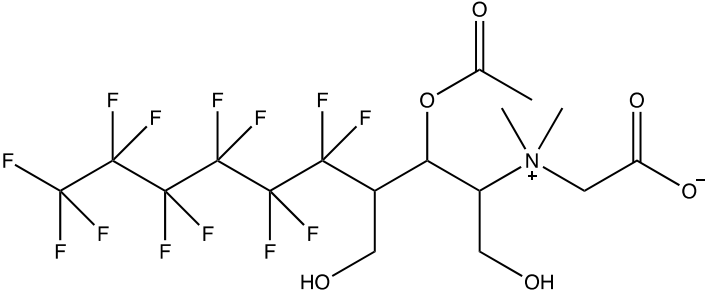
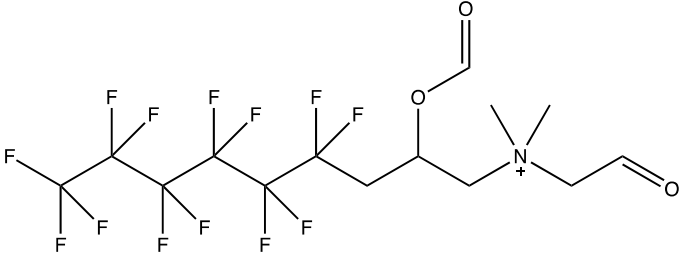
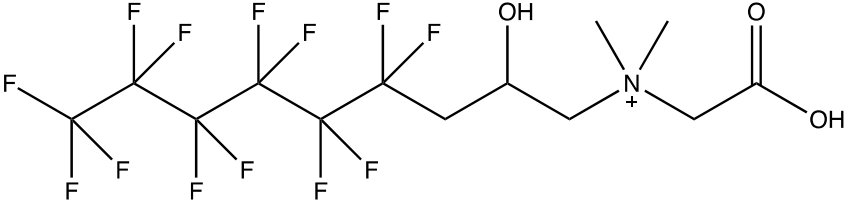
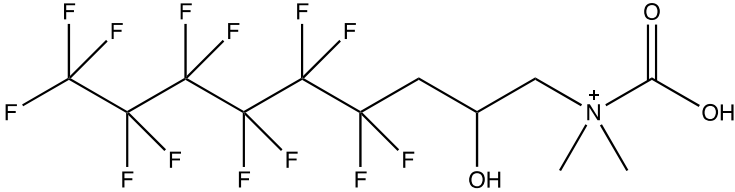
6:3 2-hydroxy unsaturated fluorotelomer betaine	6:3 OH-UFTB C13H13O3NF12 459.071	 <i>Cationic structure</i>
6:2 fluorotelomer betaine	6:2 FTB C12H12O2NF13 449.066	
6:4 fluorotelomer betaine	6:4 FTB C14H16O2NF13 477.098	
6:2 fluorotelomer sulfonamido propyl betaine	6:2 FTSA-PrB C15H19O4SN2F13 570.086 <i>Isomeric Class:</i> TAmPr-FHxSAPrA	 <i>Cationic structure</i>
6:2 fluorotelomer sulfonamido propyl dimethyl amine	6:2 FTSAPr-DiMeAn C13H17O2SN2F13 512.081 <i>Isomeric Class:</i> TAmPr-N-MeFHxSA	

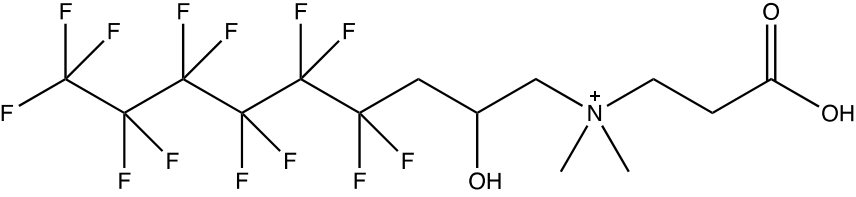
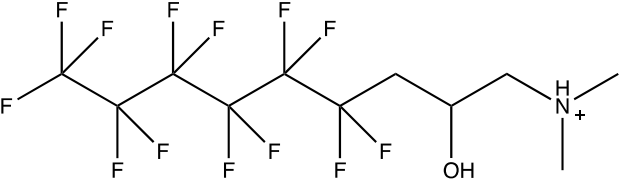
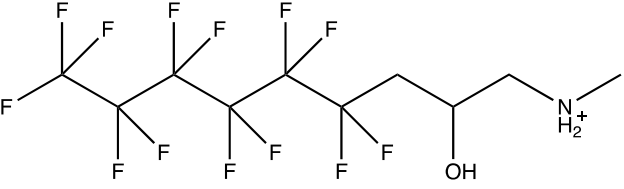
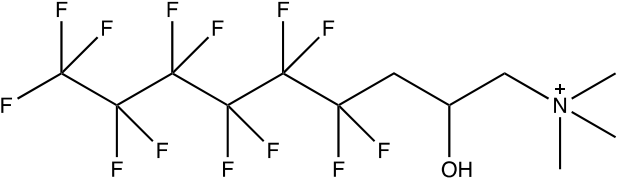
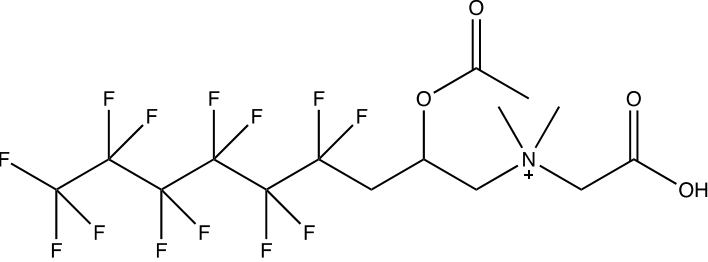
6:2 fluorotelomer thiaethanoamido propyl dimethyl ammonium	6:2 FTTh-EtAdPrAm C15H19OSN2F13 522.101	
6:2 fluorotelomer thiaethanoamido propyl betaine	6:2 FTTh-EtAdPrB C17H21O3SN2F13 580.107 <i>Isomeric Class:</i> 6:2 FTTh-CPrAd-PrAm	
6:2 fluorotelomer thiaethanoamido propyl trimethyl ammonium	6:2 FTTh-EtAdPrTAm C16H21OSN2F13 536.117	 <p><i>Cationic Structure</i></p>
6:2 fluorotelomer sulfinylethano amido propyl trimethyl ammonium	6:2 FTSO-EtAdPrTAm C16H21O2SN2F13 552.112	 <p><i>Cationic Structure</i></p>
5:3 fluorotelomer betaine	5:3 FTB C12H14O2NF11 413.085	
6:2 fluorotelomer thiahydroxypropyl trimethyl ammonium	6:2 FTTh-OHPrTAm C14H18OSNF13 495.091	 <p><i>Cationic structure</i></p>

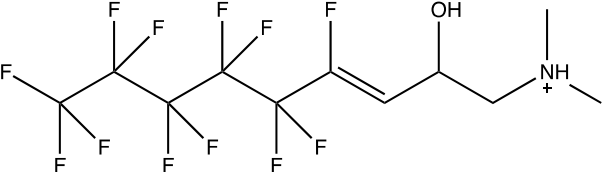
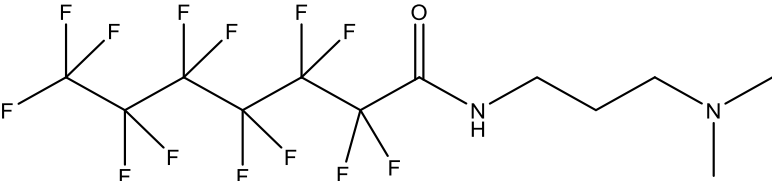
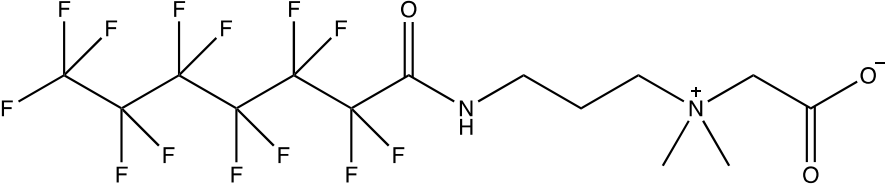
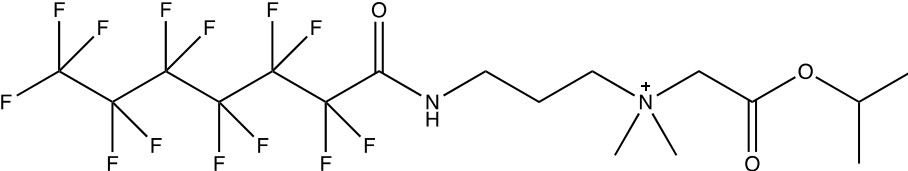
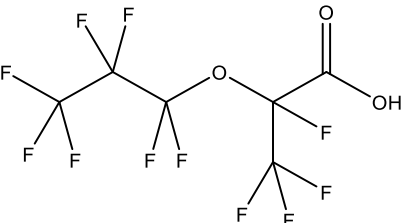
<p>6:2 fluorotelomer sulfinyl hydroxypropyl trimethyl ammonium</p>	<p>6:2 FTSO-OHPrTAm C14H18O2SNF13 511.086</p>	 <p><i>Cationic structure</i></p>
<p>6:2 fluorotelomer sulfonamido propyl amine</p>	<p>6:2 FTSA-PrAn C11H13O2SN2F13 484.050</p> <p><i>Isomeric Class:</i> AmPr-FHxSA</p>	
<p>6:2 fluorotelomer sulfonamido propyl methyl amine</p>	<p>6:2 FTSA-Pr-MeAn C12H15O2SN2F13 498.065</p> <p><i>Isomeric Class:</i> TAmPr-FHxSA</p>	
<p>6:1 fluorotelomer amino ethyl trimethyl ammonium</p>	<p>6:1 FTA-EtTAm C12H15N2F13 434.103</p>	 <p><i>Cationic Structure</i></p>
<p>7:1 hydrido-fluorotelomer trimethyl ammonium</p>	<p>7:1 H-FT-TAm C11H11NF14 423.067</p>	 <p><i>Cationic Structure</i></p>

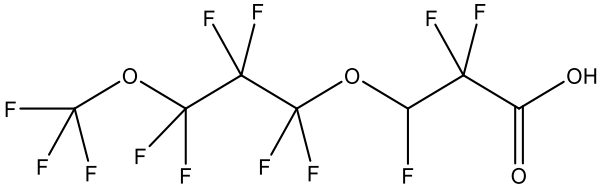
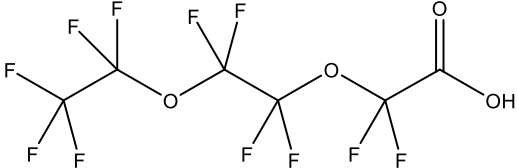
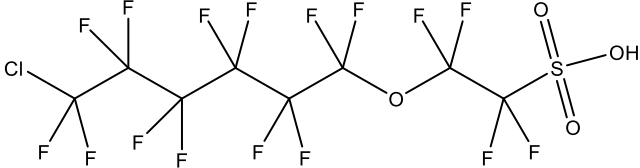
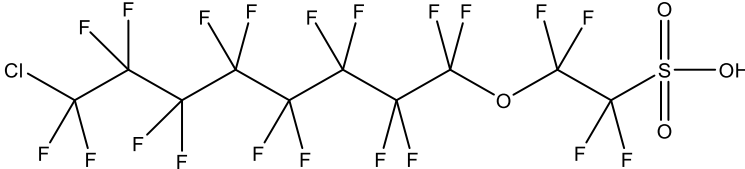
6:1 hydrido-fluorotelomer dimethyl ammonio butane	6:1 H-FT-AmBu C13H17NF12 415.117	 <p><i>Cationic Structure</i></p>
6:1 hydrido-fluorotelomer dimethyl ammonio ethane	6:1 H-FT-AmEt C11H13NF12 387.086	 <p><i>Cationic Structure</i></p>
6:1 hydrido-fluorotelomer dimethyl ammonio propane	6:1 H-FT-AmPr C12H15NF12 401.102	 <p><i>Cationic Structure</i></p>
6:2 fluorotelomer dimethyl ammonio ethane	6:2 FT-AmEt C12H14NF13 419.092	 <p><i>Cationic Structure</i></p>
6:2 fluorotelomer sulfonyl hydroxypropyl trimethyl ammonium	6:2 FTSO2-OHPrTAm C14H18O3SNF13 527.081	 <p><i>Cationic Structure</i></p>

<p>6:2 fluorotelomer sulfonyl ethano amido propyl trimethyl ammonium</p>	<p>6:2 FTSO₂-EtAdPrTAm C₁₆H₂₁O₃SN₂F₁₃ 568.107</p>	 <p><i>Cationic Structure</i></p>
<p>6:2 fluorotelomer thia amido hexyl aldehyde</p>	<p>6:2 FTTh-AdHxOCH C₁₅H₁₆O₂SNF₁₃ 521.070</p>	
<p>6:2 fluorotelomer thiol</p>	<p>6:2 FTSH C₈H₅SF₁₃ 379.991</p>	
<p>6:2 unsaturated fluorotelomer sulfonate</p>	<p>6:2 UFTS C₈H₄O₃SF₁₂ 407.970</p>	 <p><i>Anionic Structure</i></p>
<p>6:3 1-ester 2-oxa-methanol fluorotelomer dimethyl amine</p>	<p>6:3 OCO-OMeOH-FT-DiMeAn C₁₃H₁₄O₄NF₁₃ 495.072</p>	

<p>6:3 fluorotelomer 1,3-methanol, 2-methylester betaine</p>	<p>6:3 di(MeOH) MeOCO- FTB C17H20O6NF13 581.109</p>	
<p>6:3 2-ester fluorotelomer dimethylammonio ethano-ketone</p>	<p>6:3 OCO-FTAm-EtK C14H14O3NF13 491.077</p>	 <p><i>Cationic Structure</i></p>
<p>6:3 2-hydroxy fluorotelomer dimethylammonio ethanoic acid</p>	<p>6:3 OH-FTB C13H14O3NF13 479.077</p>	 <p><i>Cationic Structure</i></p>
<p>6:3 2-hydroxy fluorotelomer dimethylammonio carboxylic acid</p>	<p>6:3 OH-FTAmCA C12H12O3NF13 465.061</p>	 <p><i>Cationic Structure</i></p>

<p>6:3 2-hydroxy fluorotelomer dimethylammonio propanoic acid</p>	<p>6:3 OH-FTAm-PrA C14H16O3NF13 493.093</p>	 <p><i>Cationic Structure</i></p>
<p>6:3 2-hydroxy fluorotelomer dimethylamine</p>	<p>6:3 OH-FT-DiMeAn C11H12ONF13 421.072</p>	 <p><i>Cationic Structure</i></p>
<p>6:3 2-hydroxy fluorotelomer methylamine</p>	<p>6:3 OH-FT-MeAn C10H10ONF13 407.056</p>	 <p><i>Cationic Structure</i></p>
<p>6:3 2-hydroxy fluorotelomer trimethyl ammonium</p>	<p>6:3 OH-FT-Tam C12H14ONF13 435.087</p>	 <p><i>Cationic Structure</i></p>
<p>6:3 2-methylester-fluorotelomer betaine</p>	<p>6:3 MeOCO-FTB C15H16O4NF13 521.088</p>	 <p><i>Cationic Structure</i></p>

6:3 2-hydroxy unsaturated fluorotelomer dimethylamine	6:3 OH-UFT-DiMeAn C11H11ONF12 401.065	 <p><i>Cationic Structure</i></p>
Perfluorinated Amides		
N-dimethyl ammonio propyl perfluoroheptanoic amide	AmPr-FHpAd C12H13ON2F13 448.083	
N-betaine propyl perfluoroheptanoic amide	BPr-FHpAd C14H15O3N2F13 506.088	
N-methyl ethyl carboxy methyl dimethyl ammonio propyl perfluoroheptanoic amide	MeEtCMeAmPr-FHpAd C17H21O3N2F13 548.135	 <p><i>Cationic Structure</i></p>
Ether PFAAS		
Tetrafluoro-2-(heptafluoropropoxy)propanoic acid	HFPO-DA C6HO3F11 329.976	

3H-4,8-dioxa-perfluorononanoic acid	ADONA C7H2O4F12 377.977	
Perfluoroethoxy ethoxy acetate	PFEt-O-Ace C6H04F11 345.970	
9-Chloro-3-oxa-perfluorononane sulfonate	Cl-O-PFNS C8HO4SClF16 531.903	
11-Chloro-3-oxa-perfluoroundecane sulfonate	Cl-O-PFudS C10HO4SClF20 631.896	
C _n +10H ₁₈ O ₄ SN ₂ F _{2n+1}	C14H19O4SN2F9 482.091	No structure known – Barzen-Hansen Class 20
C _n +10H ₂₀ O ₇ SN ₂ F _{2n+1}	C13H21O7SN2F7 482.091	No structure known – Barzen-Hansen Class 20
C _n +8H ₁₅ O ₂ SN ₂ F _{2n+1}	C14H15O2SN2F13 522.065	No proposed structure in Barzen-Hansen Class 19
C _n +9H ₂₂ O ₂ SN ₂ F _{2n+1}	C15H21O2SN2F13 540.111614 <i>Isomeric Class:</i> EtAmPr-FHx-N-EtSA	No proposed structure in Barzen-Hansen; Class 38

APPENDIX B: LIST OF PUBLICATIONS

Schaefer, C.E., Andaya, C., Maizel, A., Higgins, C.P. “Assessing Continued Electrochemical Treatment of Groundwater Impacted by Aqueous Film-Forming Foams” *J. Environ. Eng.*, 145, 2019.

Schaefer, C.E., Choyke, S., Ferguson, P.L., Andaya, C., Burant, A., Maizel, A., Strathmann, T.J. and Higgins, C.P. “Electrochemical Transformations of Perfluoroalkyl Acid (PFAA) Precursors and PFAAs in Groundwater Impacted with Aqueous Film Forming Foams” *Environ. Sci. Technol.* 52, 10689-10697, 2018.

Liu, J., Van Hoomissen, D.J., Liu, T., Maizel, A., Huo, X., Fernández, S.R., Ren, C., Xiao, X., Fang, Y., Schaefer, C., Higgins, C.P., Vyas, S., Strathmann, T.J. “Reductive defluorination of branched per- and polyfluoroalkyl substances with cobalt complex catalysts” *Environ. Sci. Technol Letters* 5, 289-294, 2018.

Schaefer, C.E., Anadaya, C., Burant, A., Condee, C.W., Urtiaga, A., Strathmann, T.J., Higgins, C.P. “Electrochemical treatment of perfluorooctanoic acid and perfluorooctane sulfonate: insights into mechanisms and application to groundwater treatment”, *Chemical. Engin. J.* 317, 424-432, 2017.